Structural evolution of the Tenggol Arch and its implication for basement fracture patterns in the Malay Basin, Malaysia

Shahar, Suhaileen

STRUCTURAL EVOLUTION OF THE TENGGOL ARCH AND ITS IMPLICATIONS FOR BASEMENT FRACTURE PATTERNS IN THE MALAY BASIN, MALAYSIA.

By

Suhaileen Shahar

A thesis submitted in partial fulfillment of the degree of Master of Science

Department of Earth Sciences

University of Durham

2008

Declaration

The content of this thesis is the original work of the author and has not been previously published for a degree at this university or any other institution. The work of others is acknowledged throughout this thesis by reference.

Suhaileen Shahar
Department of Earth Science
University of Durham, England.

STRUCTURAL EVOLUTION OF THE TENGGOL ARCH AND ITS IMPLICATIONS FOR BASEMENT FRACTURE PATTERNS IN THE MALAY BASIN, MALAYSIA.

Suhaileen Shahar

Thesis submitted in partial fulfillment of the degree of Master of Science
University of Durham, 2008

The aim of this thesis is to evaluate the hydrocarbon potential of the Tenggol Arch, a basement high that forms part of the western margin of the Malay Basin, offshore peninsular Malaysia. Fractured crystalline basement rocks in this area have previously been identified as possible targets for hydrocarbon exploration, but, due to the lack of well data, little is known about the origin, distribution, geometry or hydrodynamic properties of these fractures. The first part of this study develops a new kinematic model to explain the tectonic evolution of the western Malay Basin, thereby providing a geological framework in which to understand the nature and timing of basement fracturing. The second part uses geophysical attribute analysis to better characterize the geometric properties of the basement fractures on the Tenggol Arch, and to discuss the implications of these findings for hydrocarbon exploration in this region.

The integration of previous published and unpublished research with offshore well data and new structural and stratigraphic interpretations of a 3D seismic dataset from the Tenggol Arch suggests that the pre-Tertiary to Late Oligocene history of the Malay Basin was characterized by basin opening during the Upper Cretaceous. This was followed by Paleocene to Late Oligocene NW-SE sinistral strike-slip and possible NE-SW extension. Previous workers have highlighted evidence for Late Miocene N-S shortening (E-W trending folds) in the north and centre of the Malay Basin contemporaneous with extension along NW-striking normal faults on the western margin of the Malay Basin and on the Tenggol Arch. This study has been able to reconcile these apparently conflicting observations by developing a model of Late Miocene/Pliocene dextral transtension. This new model has implications for geological risk evaluations of structural and fractured basement plays on the Tenggol Arch specifically and in the Malay Basin generally.

Geophysical attribute analysis of 3D seismic data over the basement complex on the upthrown fault block of the Tenggol Arch was able to identify deep-seated, well connected basement fracture sets. These fractures appear to be tectonic in origin. A set of east-striking fractures (similar to fracture trends mapped in the AU-1 exploration well) appears to be restricted to the shallowest sections of the basement and may represent a set of cooling joints within igneous rocks on the southern Tenggol Arch. However, attribute analysis alone is not sufficient to fully evaluate the hydrocarbon potential of fractured basement on the Tenggol Arch. New geological and petrophysical data (from new wells and further study of onshore analogues identified in this study) are required to mature the fractured basement play into potential drilling candidates.

ACKNOWLEDGEMENTS

I would like to thank the following companies and individuals for their support for the completion of this thesis:

1- Sincere thanks to the Management of PETRONAS for allowing to pursue this study and permission to use their data.

2- Sincere thanks to Dr Jonathan Imber for his role as supervisor and support throughout this study.

3- Special thanks to Prof. Holdsworth R.E. for his guidance and support throughout completion of this thesis.

3- Thank you to all individuals that help me through my stay in Durham.

Content

Declaration..... i
Abstract.....ii.
Acknowledgements iii
Contents.....iv
List of figures.....x

CHAPTER 1.....1
INTRODUCTION.....1
1.1 Exploration history and study objectives.....1
1.2 Introduction to the regional geology and tectonic setting of Southeast Asia..... 8
1.2.1 Pre-Cenozoic: Sibumasu and closure of paleo-Tethys.....8
1.2.2 Cenozoic tectonic framework.....10
1.3 Previous regional studies of the Malay Basin.....12
1.3.1 Malay Basin: Morphology and Basin History 1994).....12
1.3.2 Palynological Zonation (1996).....16
1.3.3 Integrated Regional Study (IRS) of Malay Basin (2005/2006).....18
1.3.4 Discussion and Conclusion.....24

CHAPTER 2.....28
Chapter Layout.....28
2.0 Malay Basin: Tectonic framework and basin origin.....30
2.1 Kinematics of offshore and onshore Peninsular Malaysia.....40
2.2 Stratigraphic correlation of the Tenggol Arch basement complex to onshore outcrop.....45
2.2.1a Malay Basin: Pre-Tertiary strata of the Western basin margin.....45
2.2.1b Malay Basin: Tertiary strata of Western basin margin.....49

2.2.2a Peninsular Malaysia: Paleozoic Continental Group.....59
2.2.2b Peninsular Malaysia: Permian to Triassic volcanic activity.....63
2.2.2c Peninsular Malaysia: Post-Triassic dykes and sills.....65
2.3 Summary.....66
2.4 Major structure in Peninsular Malaysia in relation to Tenggol Arch.....68
Peninsular Malaysia: Geological domains.....68
2.4.1 Geological setting of the West Domain.....70
2.4.2 Geological setting of the Central Domain..... 71
2.4.2a Bentong-Raub Suture zone 72
2.4.2b Bentong-Raub zone correlation to Bengkalis Trough, Sumatera.. 73
2.4.3 Geological setting of East and Southeast Domain.....77
2.4.4 Microcontinent rotation in Peninsular Malaysia.....78
2.5 Geological setting of Tenggol Arch 79
2.5.1 Pre-Tertiary deposition environment over Tenggol Arch.....79
2.5.2 Tertiary marine incursion in the region of the Tenggol Arch.....81
2.5.3 Pre-Cenozoic: Early structure of the Tenggol Arch.....82
2.5.4 Cenozoic: Regional compression and wrench modification.....84
2.6 Summary and Conclusions.....87

CHAPTER 3.....89
3.0 Study area and geophysical methods.....89
3.1 Database.....90
3.1.1 Seismic Data.....91
3.1.2 Seismic interpretation uncertainties.....96
3.2 The definition of seismic markers.....99
3.2.1 Top Basement seismic marker (Attachment 2).....100
3.2.2 Top Synrift seismic marker (Attachment 2).....102
3.2.2a Correlation of the Tenggol Arch Top Synrift marker with the Malay Basin.....102
3.2.3 Oligocene strata seismic marker (Attachment 2).....104
3.2.4 Intra-Miocene strata seismic markers.....105

3.2.5 Pliocene strata (Attachment 1).....106
3.3 Basis and methodology of seismic interpretation.....107
3.3.1 The basis of the time domain interpretation : The issue of velocity modelling.....108
3.3.2 Fault interpretation and structure mapping.....110
3.3.3 Geophysical attribute analysis.....115
3.4 Seismic facies interpretation 121
3.4.1 Objective.....121
3.4.2 Seismic characteristics and major facies.....122
3.4.3 Findings from seismic facies interpretation 123
3.4.3a Interpretation of azimuth mapping.....125
3.4.4 Basement complex seismic facies.....127
3.4.4.1 Volcanic, plutonic igneous facies.....127
3.4.4.2 Low grade metamorphic facies.....128
3.4.4.3 Carbonate facies.....128
3.4.5 Synrift, Late Oligocene and Early Miocene strata..... 129
3.4.5.1 Inline 5369 (M-2 well).....129
3.4.5.2 Inline 2629 (S-1 well).....130
3.4.5.3 Inline 2400 (S-5 well).....131
3.5 Discussion and Conclusion.....132

CHAPTER 4.....137
4.0 Geometry and kinematics of the Tenggol Fault, Tenggol Arch and Malay Basin.....137
4.1 Structure styles and fault patterns.....138
4.2 Fault throw profiles.....144
4.2.1 Top Basement fault throw profile.....145
4.2.2 Ta_6 fault throw profile.....149
4.2.3 Ta_3 and Ta_1 fault throw profiles.....150
4.2.4 Summary: fault geometry and throw profiles.....151
4.3 Isochore maps and Miocene basin evolution.....154

4.4 Structure and tectonic evolution of the Tenggol Arch and Malay Basin....159
4.4.1 Top Basement structure and pre-Oligocene structural evolution of the Tenggol Arch....159
4.4.2 Folding....163
4.4.3 Fault-related channel attributes....166
4.5 A Reassessment of the Miocene-Pliocene kinematics of the Malay Basin....170
4.5.1 Integrated Regional Study of the Malay Basin (2006)....170
4.5.2 Basis and hypothesis to be tested....171
4.5.3a Kinematic modeling: assumptions and methodology....174
4.5.3b Results and discussion....178
4.6 Miocene-Pliocene kinematics of the Tenggol Arch....182
4.7 Discussion: Structural Evolution of Tenggol Arch (Chronology)....183

CHAPTER 5....186
5.0 Antracking volume: Fracture interpretation....186
5.1 Onshore analogue: Structure style at Ulu Paka, Terengganu....187
5.2 Fault and fracture patterns of A-field, Tenggol Arch....189
5.2.1 Well data: AU-1 basement complex....190
5.3 Interpretation of the Antracking volume....193
5.3.1 Methodology: Comparison of fracture pattern from AU-1 FMI data to Antracking along the Tenggol Fault....193
5.3.2 Results from Antracking....196
5.4 Discussion and conclusions....204
5.4.1 Comparison of Antracking results with the regional kinematic history and stress orientations....204
5.4.2 Conclusions and implications for hydrocarbon exploration....206

CHAPTER 6....215
6.1 Petroleum conceptual model: Fractured Basement....215

6.1.1 Reservoir.....216
6.1.2 Trap.....219
6.1.3 Source rock and hydrocarbon migration.....220
6.1.4 Summary.....224

6.2 Conclusions.....225

REFERENCES.....234-254
TABLES
ATTACHMENT
APPENDIX

LIST OF FIGURES

Figure Page

1.1 Map showing location of Tenggol Arch and Malay Basin.....2

1.2 Schematic diagram of tectonic elements and structural domains of Malay Basin.....5

1.3 Interpreted igneous distribution offshore Peninsular Malaysia.....6

1.4 Example of fault shadow across Tenggol Fault.....7

1.5 Schematic diagram showing model of origin of Malaysian Terranes (IRS Malay Basin, 2005/06).....9

1.6a Tectonic framework of Southeast Asia during Cenozoic period (EPIC, 1994).....11

1.6b Tectonic elements of Malay Basin and South of Gulf of Thailand basin (Tapponnier, 1986).....13

1.6c Tectonic elements of Yinggehai Basin (Tjia, 1991).....13

1.7 Time structure map of the Late Middle Miocene of Malay Basin.....15

1.8 Stratigraphic scheme of Malay Basin after EPIC (1994) and PRSS (1996).....16

1.9 Evidence of first marine incursion in Malay Basin (PRSS, 1996/97).....18

2.1 Schematic diagram of "Malay Dome" of Cretaceous/ Late Cretaceous (Tjia, 1998b).....36

2.2 Time structure map of Top Basement marker on the Tenggol Arch.....41

2.3 Tectonic domains of Peninsular Malaysia and location of field stops (Tjia, 2005).....42

2.4a Seismic facies interpretation of the basement complex.....46

2.4b Seismic facies interpretation of Ta_5, Ta_6 and Synrift along Inline 2629.....48

2.4c Channel facies interpretation along Inline 4176.....51

2.4d Seismic facies interpretation along Inline 5369.....54

2.4e Seismic facies interpretation along Inline 2400.....55

2.5 Example of Pre-Tertiary continental deposits at Bukit Keluang, east coastline Peninsular Malaysia (Tjia, 2005).....61

2.6 Distribution of Mesozoic Igneous rocks in Peninsular Malaysia.....63

2.7 Schematic diagram showing Malaysian terrains as part of Sundaland, Sibumasu (Gondwana terrain) and Laurasia terrain (Tjia, 1989).....70

3.1 Figure showing 3D seismic basemap, wells location and 2D regional RC93_007 in the study area.....90

3.2a Seismic section (Trace 2705) showing example of interpretational uncertainties of the 3D seismic data.....92

3.2b Seismic section (Inline 5019) along dip-line of Tenggol Fault showing fault interpretation uncertainties encountered in this study.....93

3.2c General overview of geology along the footwall and hanging-wall of the Tenggol Fault based seismic sections (Trace 2215 and Trace 2715).....94

3.3a Figure showing 3D seismic acquisition sail-line directions along Tenggol Fault dip direction.....95

3.3b Figure showing (a) Time Slice at 2000ms (below Top Basement) indicates distinctive seismic facies between igneous and metamorphic rocks and (b) showing early interpretation of structure styles at A-field.....101

3.4 Azimuth map of Ta_6 surface showing rhomboidal-shaped patch of surface dipping North-Northeasterly on the hanging-wall of Tenggol-Fault.....114

3.5 Figure showing composite fault-line map (Top Basement to Ta_1 seismic markers).....111

3.6a Compilation of check-shots data from basement wells on Tenggol Arch shows generally consistent velocity range of basement with minor anomalies at well A-2 and S-2.....134

3.6b Time-depth plot from check-shots data shows normally distributed velocity ranges over Tenggol Arch reflected normal compaction and normally pressured area.....135

4.1 Time structure map of Top Basement marker on Tenggol Arch showing structure styles and faults orientations.....139

4.2 Time structure map of Ta_3 marker on Tenggol Arch showing structure styles and faults orientations.....140

4.3 Fault throw profile of the Top Basement marker along the Tenggol Fault.....140

4.4 Isochore map of Late Oligocene strata (Ta_6 to Top Basement maker) shows sediment depocentres in isolated basement lows.....142

4.5 Fault throw profile of the Ta_1 marker along the Tenggol Fault.....143

4.6 Seismic section (Inline 3552) along dip-direction of the Tenggol Fault shows presence of local reversed movement on observed along fault set8 at Top Basement marker.....146

4.7 Fault throw profile of the Ta_6 marker along the Tenggol Fault.....150

4.8 Fault throw profile of the Ta_3 marker along the Tenggol Fault.....151

4.9 Seismic section (Inline 3296) along dip-direction of the Tenggol Fault shows evidences of local reversal along fault set 10 at Ta _5 and Ta_6 markers.....153

4.10a Late Oligocene/Early Miocene sequence thickness profile along the Tenggol Fault shows similar thickness value across the fault towards north margin of the study area.....154

4.10b Middle Late Miocene sequence thickness profile along Tenggol Fault shows similar thickness distribution as Late Oligocene/Early Miocene 158

4.10c Late Miocene/Pliocene sequence thickness profile along Tenggol Fault indicates sudden increased in thickness on the hanging-wall near S-field (north).....159

4.11a Time structure map and schematic diagram of fault styles on the Top Basement.....160

4.11b Schematic diagram illustrating development of 'rhomboidal' pull-apart during sinistral strike-slip (after McClay & Bonora, 2001 and Mann, 2007).....162

4.12a Time structure map of Ta_3 showing gentle fold structure along N-NE striking antithetic faults.....164

4.12b Azimuth map of Ta_2 marker highlighted distinctively crescent-shaped sediment depocentres on the downthrown block of the N-NE striking antithetic fault suggested syn-depositional system.....165

4.12c Dip-line across Tenggol Fault showing folds from Ta_6 to Ta_3 seismic markers interpreted as inversion occurred post deposition of Ta_3.....167

14.12d Strike-line along hanging wall of Tenggol Fault showing gentle folding from Ta_6 to Ta_3 and fairly uniform similarly observed at dip-line.....168

4.13a Ta_3 channel facies (Middle Late Miocene) flowing along the ramp of antithetic faults of Tenggol Fault zone show evidence of syn-depositional system.....167

4.13b Channel facies on Ta_2 marker (Late Miocene/Pliocene) do not show any clear evidence of strike-slip displacement along the Tenggol Fault.....169

4.14a Schematic diagram of conceptual models of transtensional system (after N. De Paola et. al.; 2008) adapted on Tenggol Arch.....172

4.14b Depth structure map of Top Basement marker of Malay Basin were used as basis for quantification of kinematic modeling.....174

4.14c Schematic diagram of host rock's Poisson's ratio (v) to critical transport direction (α_c) adapted in Malay Basin and Tenggol Arch in determining wrench or extension dominated transtensional regime in/of the basin.....176

4.15a Depth structure map of Late Miocene/Pliocene of Malay Basin, shows misfits in structure styles in the central and northern Malay Basin (1) and Tenggol Arch (2) suggest transtension condition in Malay basin.....178

4.15b Interpretation of transtension in Tenggol Arch based fault styles on Top Basement marker.....182

5.1 Geological map of Ulu Paka, Terengganu showing example structure styles onshore east-coastline of Peninsular Malaysia within granitoids and metamorphic litho-type.....188

5.2 Schematic diagram of A-field (after 2004 FDP (Field Development Plan), PCSB) shows structure styles and fault orientation in comparison to Ulu Paka, Terengganu.....190

5.3 Time-Depth curve from AU-1 VSP (Vertical Seismic Profile) data shows clear indication of Top Basement marker from sudden increased in interval velocity circa 2480-2500mss.....191

5.4 Foliation and fracture orientations from manually interpreted FMI logs (Formation Micro Imager) of AU-1 well in basement section.....192

5.5a Comparison of vertical sections from Antracking™ volume and PSTM (Pre-Stack Time Migrated) volume over Tenggol Arch.....195

5.5b Horizon slices from the Antracking™ volume of basement complex.....197

5.6a Horizon slices from Atntracking™ volume of the basement complex on the foot-wall of the Tenggol Fault 198

5.6b (continuation) Horizon slices of basement Antracking™ volume on the foot-wall of the Tenggol Fault.....198

5.7 Horizon slice of Antracking™ at 150ms below Top Basement showing fracture orientations.....199

5.7a Horizon slice of Antracking™ at 150ms showing un-interpret and interpreted slices.....202

5.8 Horizon slice of Antracking™ at 200ms below Top Basement showing fracture orientations.....199

5.8a Horizon slice of Antracking™ at 200ms showing un-interpret vs interpreted slices.....202

5.9 Horizon slice of Antracking™ at 250ms below Top Basement showing fracture orientations.....200

5.10 Horizon slice of Antracking™ at 300ms below Top Basement showing fracture orientations.....200

5.11 Schematic diagram showing cumulative of fracture sets (Group set) distributions from 50ms to 300ms slices below Top Basement.....203

5.12 Geophysical attributes mapping of Top Basement marker at centre of Tenggol Fault zone 212

5.13 Geophysical attributes mapping of Top Basement marker at north of Tenggol Fault Zone.....213

6.1 Schematic diagram explaining the petroleum conceptual model of Tenggol Arch based on this study.....216

Structural evolution of the Tenggol Arch and its implications for basement fracture patterns in the Malay Basin

1.0 Introduction

1.1 Exploration History and Study Objectives

The Malay Basin is located in the Sundaland[1] region of offshore Peninsular Malaysia, to the south of the Gulf of Thailand (Figure 1.1). The basin covers an area of 90,000 km^2 with sediment thicknesses of more than 12km in the basin centre, gradually thinning southwards. The basin fill comprises inter-layered Tertiary sands and shales. Coal is extensive in the Middle Miocene strata, with some carbonate present as oolitic limestone along parts of the basin margin. Crystalline basement in the Malay Basin comprises igneous, metamorphic and carbonate rocks with age ranges from Jurassic (or older) to Cretaceous.

The first exploration activity took place in 1968 with the first concessions awarded to EPMI and Conoco. Since then, the main exploration targets have been Miocene siliciclastic strata, which are predominantly fluvial-channel plays of the lower coastal plain facies. The deepest play tested in the basin comprises a sequence of Upper Oligocene siliciclastic strata deposited in a marginal marine

[1] "Sundaland" refers to a continental platform in Southeast Asia encompassed by the Sumatera Trench towards Arakan-Yoma in the Himalaya and the Dangerous Zones, West of Borneo. The term Sundaland was first developed with reference to the floral and fauna distribution in the region and was later widely accepted in the geological literature (Figure 1.1) (Hutchinson, 1996, Tjia, 1998).

to inter deltaic environment. Primary well targets are mostly low-risk conventional plays characterized by four-way dip anticlines and combinations of stratigraphic and structural traps. These zones have proved to contain prolific hydrocarbon reserves and are still actively explored. Some fields are currently producing from these strata (Madon, Khalid Ngah et. al., 1999).

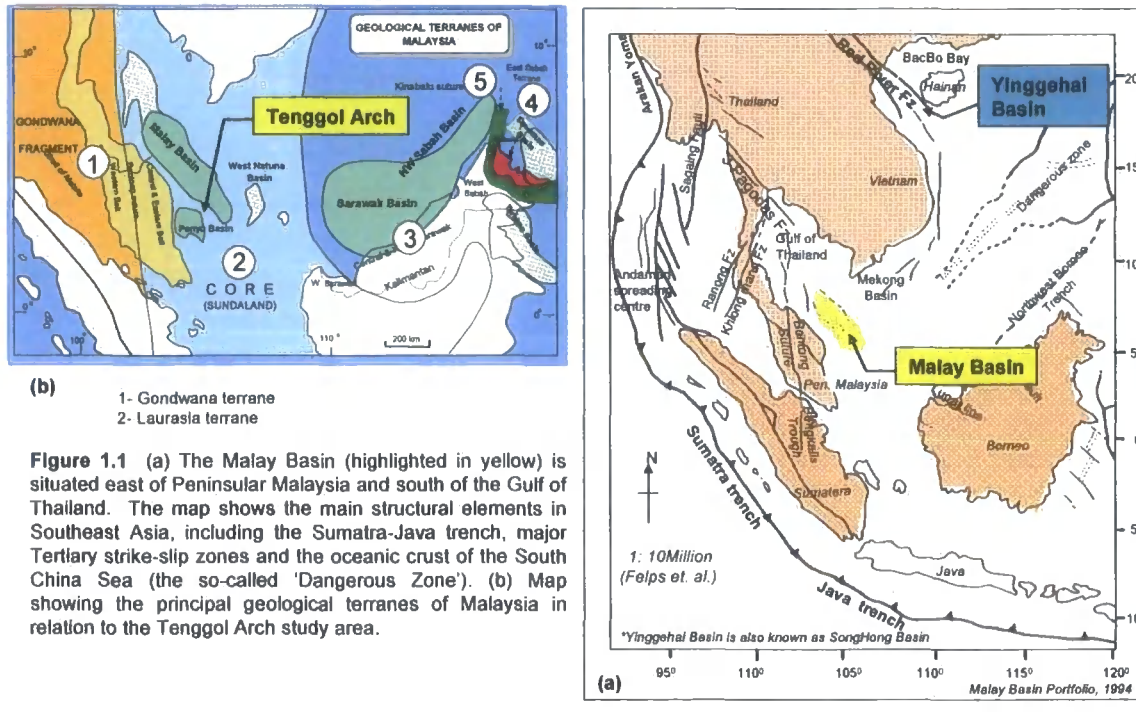

Figure 1.1 (a) The Malay Basin (highlighted in yellow) is situated east of Peninsular Malaysia and south of the Gulf of Thailand. The map shows the main structural elements in Southeast Asia, including the Sumatra-Java trench, major Tertiary strike-slip zones and the oceanic crust of the South China Sea (the so-called 'Dangerous Zone'). (b) Map showing the principal geological terranes of Malaysia in relation to the Tenggol Arch study area.

Since the 1980s, Petronas Carigali Sdn Bhd has actively explored the basin with basement rocks as one of the secondary objectives. Basement and deep wells have mostly been drilled along the basin margins where top basement occurs at shallow depths, between 1000 and 1500 ms two-way travel time (TWT) (circa 1000 to 2000 meters sub-sea). Although some wells have demonstrated the presence of hydrocarbon shows and oil stains in basement rocks, the play was

considered as being marginal and uneconomic due to high operational costs and its unknown reserve potential. In order to better estimate the petroleum potential of the basement play, a more rigorous geoscientific evaluation is required to constrain the geological uncertainties. This information will improve the basement play success ratio and could potentially enable the basement play to be considered as a primary drilling target in the future.

An improved geological understanding of the fracture network is of primary importance to the future success of the basement play. At present, the limited well control means that the fracture network characteristics are highly uncertain; in particular it is unclear whether the fractures provide a conduit for hydrocarbon migration, or whether the fractures are sealed, preventing hydrocarbons from migrating across the Tenggol Arch towards basement highs in the Western Zone (Figure 1.1). It is likely that the hydraulic properties of basement fractures depend on both the rock properties and on the tectonic evolution of the basin.

During the 2003/2004 exploration drilling campaign, an oil discovery was made within basement rocks, demonstrating the potential of the basement play as a working petroleum system. This discovery provided additional understanding of the basement play in the Malay Basin, providing a basis for further evaluation of this play as a future exploration target. Despite this discovery, very little is still known about the reservoir properties of the fractures such as their orientation, connectivity and density due to limited number of wells and uncertainties in

understanding the .regional structural evolution of the basement complex. This study therefore forms part of ongoing efforts by PETRONAS Carigali Sdn Bhd (PC*SB*) to further develop ideas arising from PETRONAS's benchmark 2005 regional study and to evaluate this play through an analysis of the 2004 3D seismic data, and information from recently drilled wells.

Current exploration and field development targets in the Malay Basin are mainly within the prolific Miocene section, whilst exploration targets within Late Oligocene strata are mostly limited to the basin margins (Appendix 1). Most economic conventional plays, (such as four-way dip anticlines, fault dependant structural plays and combined structural and stratigraphic traps), have been drilled and tested for hydrocarbons. The major fields within the above listed plays are mostly concentrated in the Central Zone, East Zone and footwall of the Western Zone (Figure 1.2). It is therefore the unconventional plays such as fractured basement and synrift sediments within the up-thrown fault blocks of Western Zone that remain under-evaluated.

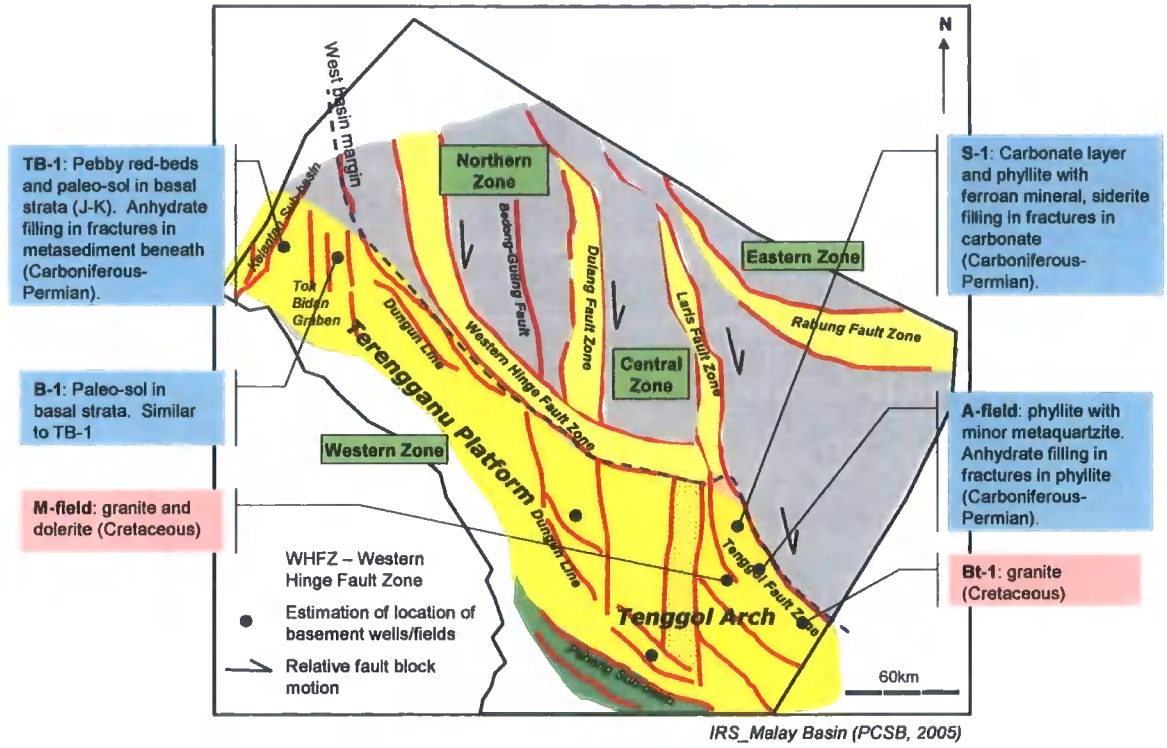

Figure 1.2 Schematic diagram showing the principal tectonic elements and structural domains ("Zones") of the Malay Basin. The structural elements have been identified at Top Basement level. The Top Basement structure map was itself derived from interpretations of 2D seismic data and regional Bouguer gravity anomalies. Blue dots show the approximate locations of wells or fields that penetrate basement within the Western Zone. The annotations for each well or field indicates the type and age of sampled basement rocks.

However, the development of a conceptual model for the fractured basement play requires integration of disparate datasets, including regional geological models, geophysical and petrophysical analyses, drilling results and measured production rates in basement fractured reservoirs. Lithological information concerning the basement complex within the Malay Basin and Tenggol Arch is limited, due to the paucity of wells that penetrate the basement (e.g. see Figure 1.3). Generally, the top basement seismic marker ranges from 1000ms to more than 3500ms in two-way time (circa 1500 to more than 3000 meters). Seismic resolution at top basement level is highly affected by overlying gas zones, whilst fault shadow zones along major faults cause seismic wave distortion, seismic

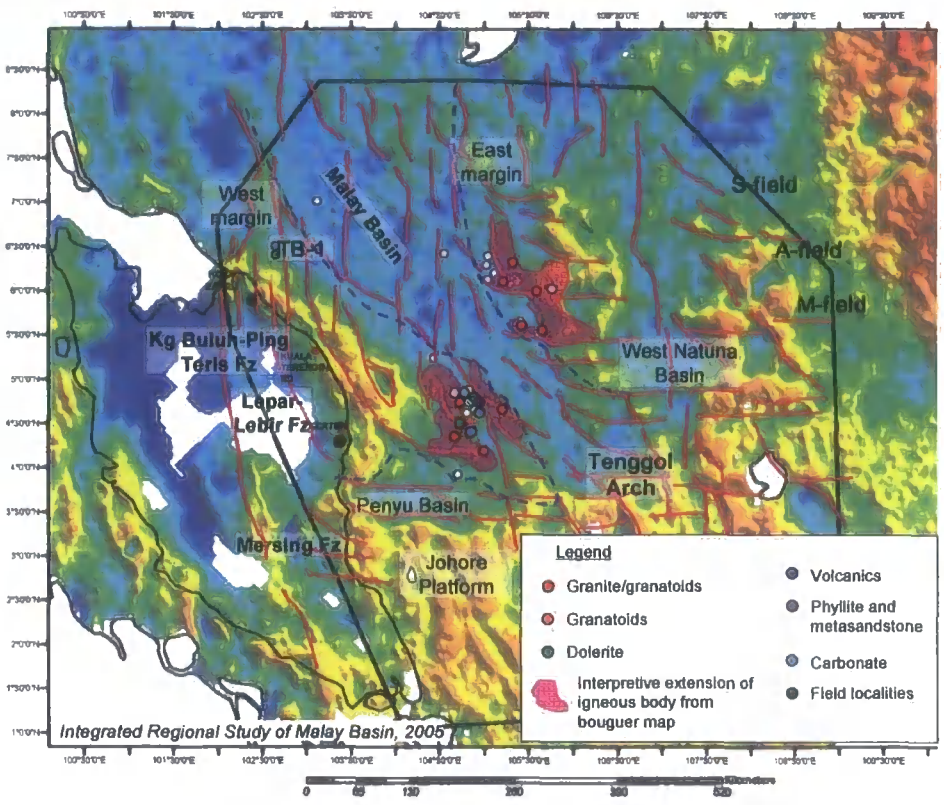

Figure 1.3 Bouguer anomaly map (GETECH, 2005) of Peninsular Malaysia and the Malay Basin with the locations of wells that penetrate basement (coloured dots; colours indicate basement lithology) superimposed. The extents of major sub-surface igneous bodies (pink) are shown, inferred from analysis of the Bouguer gravity anomalies. Onshore field localities with exposures of Paleozoic basement rocks are highlighted (black dots).

attenuation and amplitude absorption (Figure 1.4). The level of confidence of geophysical interpretations on the Top Basement marker therefore ranges from good at 1600ms to poor at approximately 2800ms and deeper.

This study has two main objectives. The first objective is to provide an overview of the regional geology of the Tenggol Arch – a basement high on the southern margin of the Malay Basin (Figure 1.2; Appendix 1) – which will improve understanding of the structural evolution and timing of tectonic events associated with the Tenggol Arch. The study will identify possible correlations between the Tenggol Arch basement complex and basement rocks exposed onshore in

Peninsular Malaysia to identify possible analogues that could be used as a basis for future detailed fracture characterization. Ultimately, the use of appropriate onshore analogues will be critical to properly evaluating the fractured basement play, in order to overcome the limitations inherent in offshore well and seismic data.

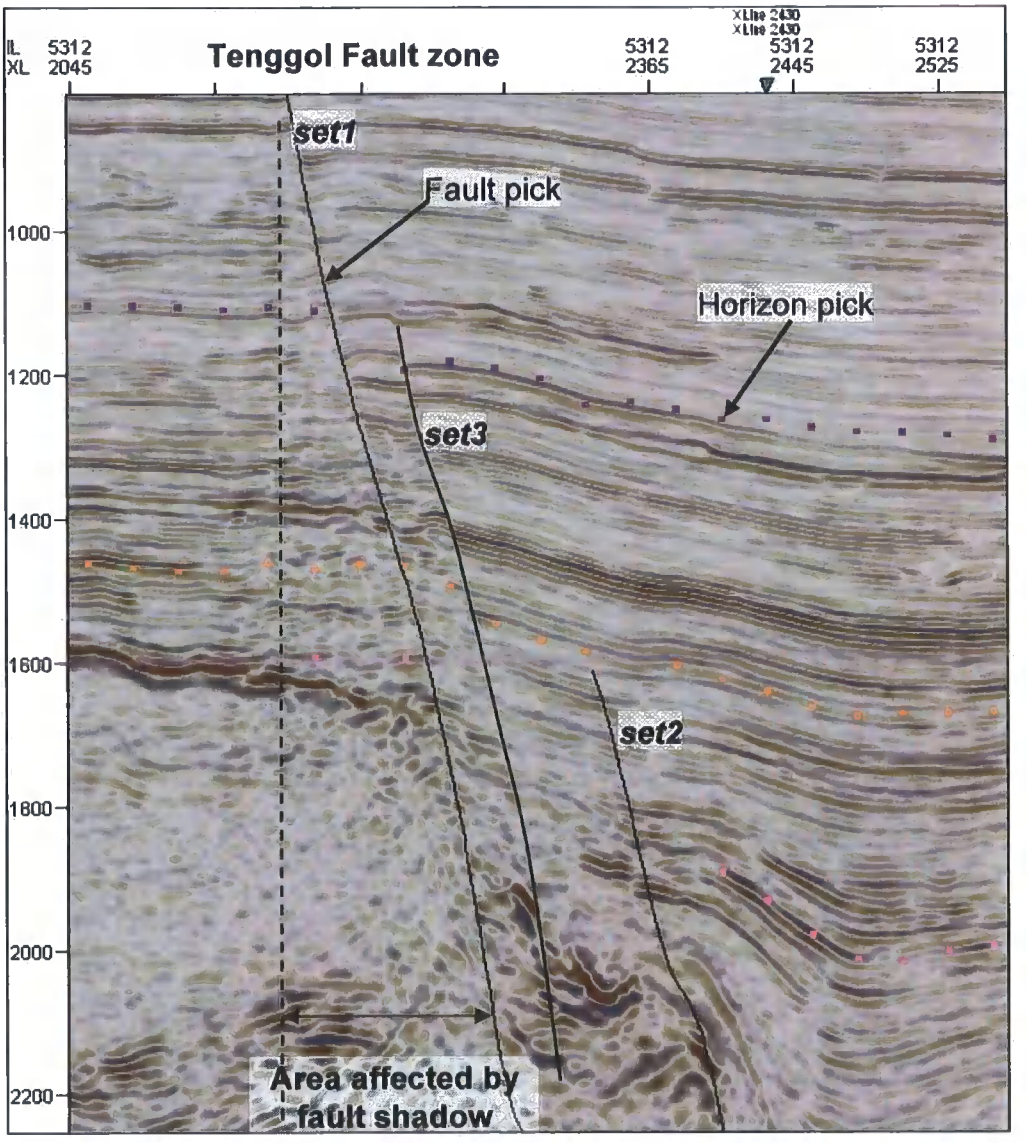

Figure 1.4 A typical 3D seismic line across the Tenggol Fault zone showing "fault shadow". The fault shadow effect increases the interpretational uncertainties within and adjacent to the fault zone.

The second phase of this project will identify and describe the faults, fractures and folds of the Tenggol Arch and Malay Basin, and discuss their relation to the regional tectonic and kinematic framework. A new kinematic model to explain the structural evolution of the Tenggol Arch will be developed to help interpret and evaluate regions where the seismic resolution deteriorates. The results of this study will provide a basis for further analysis of the fractured basement play as more basement wells and seismic data are acquired on the Tenggol Arch and the southern margin of the Malay Basin.

1.2 Introduction to the regional geology and tectonic setting of Southeast Asia

1.2.1 Pre-Cenozoic: Sibumasu & closure of paleo-Tethys

The pre-Cenozoic geology of Southeast Asia is dominated by structures associated with the closure of the paleo-Tethys ocean. This occurred as the Sibumasu crustal block advanced towards Indochina (e.g. Figure 1.5). The collision gave rise to the development of a north-south trending fault set (so-called "meridian faults") that are pervasive throughout Sundaland (Tjia, 1998a). The final closure of paleo-Tethys took place along the Bentong Suture Zone in

Peninsular Malaysia, and is interpreted to have occurred no later than the Middle Triassic (Tjia, 1989, Hutchinson, 1996). The Suture Zone is marked by a tectonic melange comprised of various marine and continental mega-olistoliths. Lithologies include chert, limestone, volcanic-tuffite and basalts of various different ages (Paleozoic-Mesozoic; Hutchinson, 1996; Tjia, 1987).

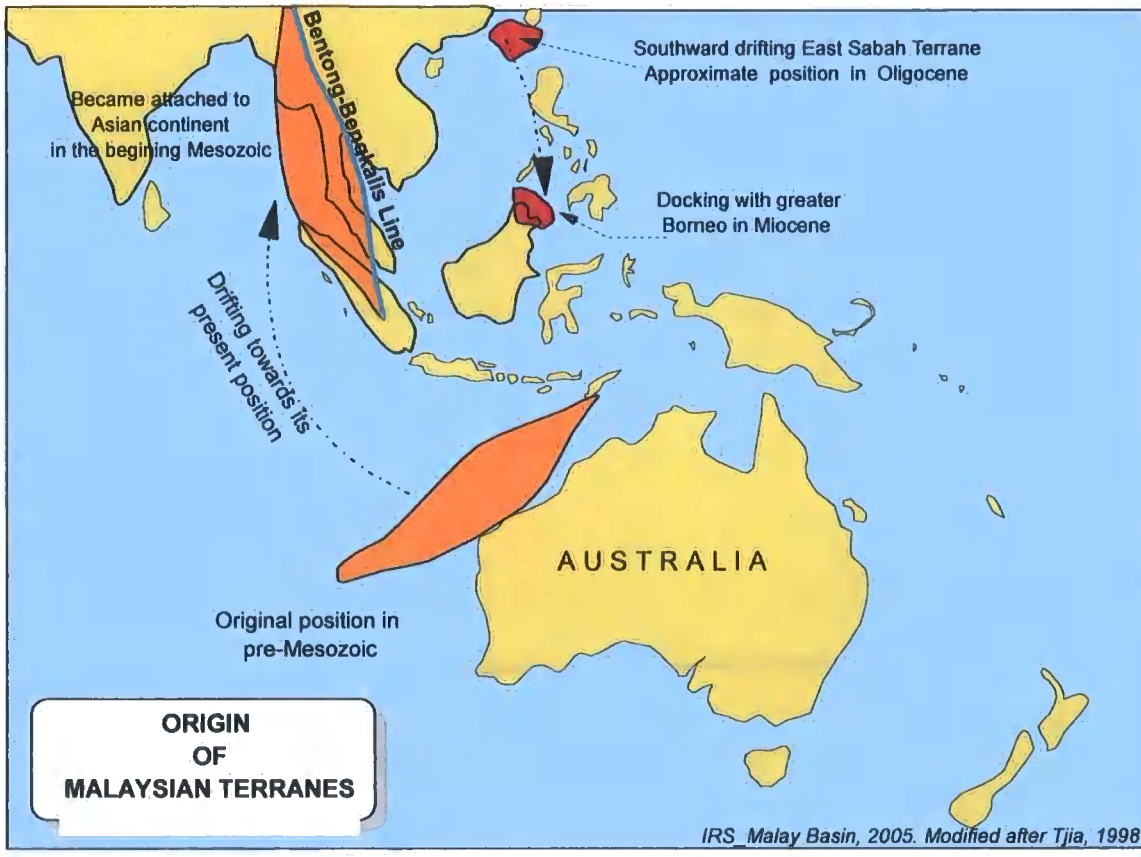

Figure 1.5 Schematic map showing the origin of pre-Early Paleozoic terranes that constitute the Malay peninsular and NE Borneo. The key point to note is that a microcontinent of Gondwanan origin (orange) drifted northwards colliding with a fragment of Laurasia, with final docking occuring along the Bentong-Bengaklis Line.

1.2.2 Cenozoic tectonic framework

Figure 1.6a is a schematic map showing the tectonic framework of the Malay Basin and its surrounding area. The area is bounded to the south and west by the Sumatra-Java Trench, which is a destructive plate boundary between the Australian and Eurasia Plates. The boundary continues northward along the western margin of the Andaman-Nicobar spreading center and towards Himalayas (Figure 1.6a). The plate boundary is still active due to the continued northward advancement of the Australian Plate towards the Eurasian Plate.

The Southeast Asia region is characterized by major northwest-southeast trending shear zones which extend northwards into Yunan and the Himalayas. Many researchers have suggested these shear zones developed due to "escape tectonics" whereby continental collision between India and Eurasia during the Late Eocene (Hutchinson, 1996, example from Xu et. al., 1985) caused lateral extrusion of the Southeast Asian continental crust, as predicted by analogue (plasticine) models of the collision zone (Tapponnier et al. 1986; Figure 1.5b). Numerous researchers have tested this model through field observations along these major shear zones (Leloup et. al., 2001, Harrison, 1992). The Three Pagodas, Wang Chao and Red River fault zones are examples of these structures that have particular relevance to this thesis. Specifically, the Red River Fault zone is believed to have controlled the development of the Yinggehai Basin

(Figure 1.6a), which has in turn been used as a natural analogue to explain the evolution of the Malay Basin (McAllister et. al, 1994[2])

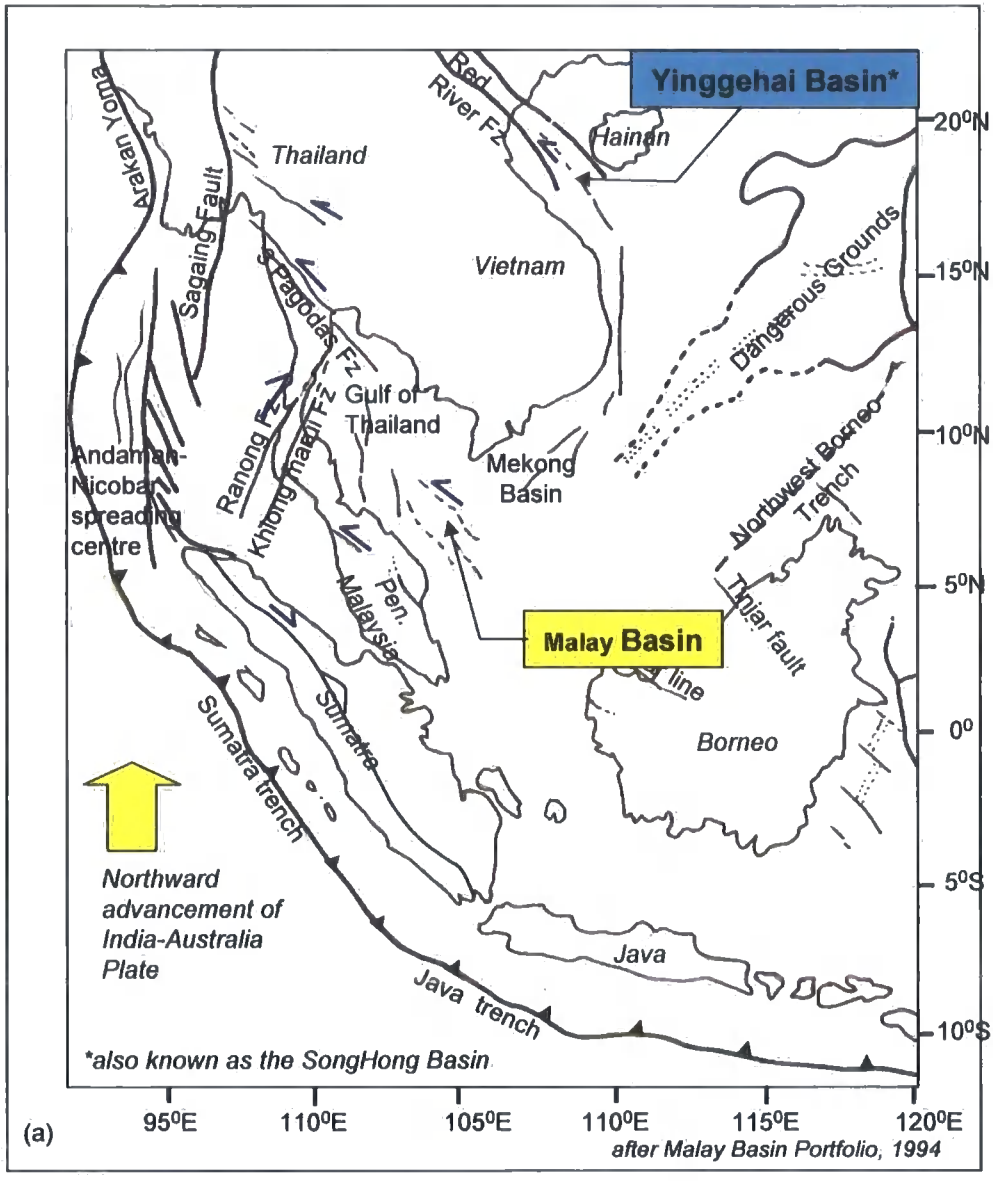

Figure 1.6a Schematic map showing the tectonic framework of SE Asia during the Cenozoic period. Note the major NW-trending strike-slip faults that are inferred to have been active during this period. Blue arrows show the relative slip sense. According to McAllister et al. (1994), the Malay and Yinggehai* basins are believed to have originated due to strike-slip along major shear zones.

[2] McAllister et. al, (1994) is an internal regional study which was partly carried-out by third parties (McAllister, Fairchild and Tahir) to generate Malay Basin's portfolios for investors and joint venture companies in the late 80s-early 90s. The study is a collaboration between PETRONAS and EPMI (Exxon Production Malaysia Inc) as major contributors in this project which was also known as EPIC project.

1.3 Previous regional studies of the Malay Basin

1.3.1 Malay Basin: Morphology and Basin History (1994)

A regional study of Malay Basin was carried out in 1994 by PETRONAS and EPMI (*Esso Production Malaysia Inc.*). The study area was mainly within the central and eastern parts of the basin, namely the PM5, PM8 and PM9 exploration blocks. This study was carried out by integrating 461 exploration and development wells and 13500 km of 2D seismic lines. The key objectives of this regional study were to develop an improved understanding of the geochemistry, geophysics and geology of the basin. In conjunction with this study, a chronostratigraphic scheme for the basin was developed in order to define the regional stratigraphic framework.

A working hypothesis, or tectonic model, to explain the opening of the Malay Basin was formulated based on the regional mapping undertaken during the 1994 study. The Malay Basin was interpreted as a back-arch basin related to the Sumatra-Java arch (Figure 1.6a). The study has suggested that the closest natural analogue to help understand the development of the Malay Basin is the Yingehai Basin of BacBo Bay (Figure 1.6c) based on similarities in basin geometry. This study assumed that the geometry and kinematics of the Malay Basin were controlled by deformation arising from the India–Asia. collision. Thus, the 1994 basin history and morphology study proposed that the Malay

Basin experienced a similar tectonic history as the Yingehai basin (Figure 1.6a). In particular, the opening of the Malay Basin was interpreted as a possible manifestation of sinistral strike slip motion along the Three Pagodas and Wang Chao Fault zones, which supposedly occurred during the Early Tertiary no later than Late Oligocene (Figure 1.6a and 1.6b). However, uncertainty about this working hypothesis remains, due to the lack of clear evidence for sinistral strike slip movements in the Malay Basin (cf. Shun et. al., 2003, Harrison et. al., 1992).

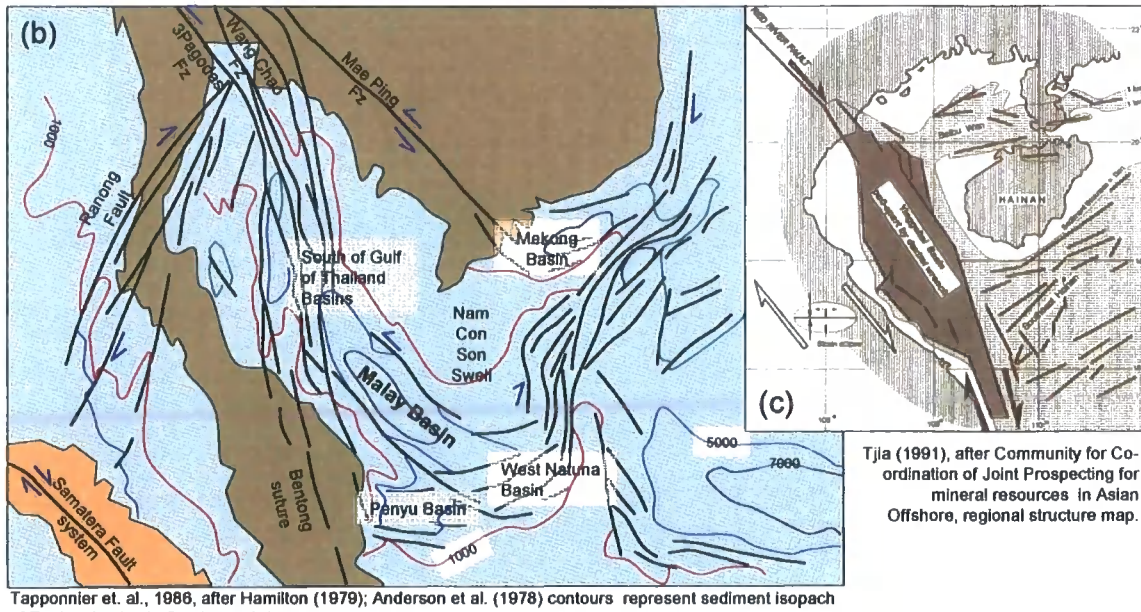

Tapponnier et. al., 1986, after Hamilton (1979); Anderson et al. (1978) contours represent sediment isopach of Tertiary basins in Southeast Asia.

Tjia (1991), after Community for Co-ordination of Joint Prospecting for mineral resources in Asian Offshore, regional structure map.

Figure 1.6 (b) Map showing the Malay and South Gulf of Thailand basins in the context of SE Asian extrusion tectonics as inferred by Tapponnier et al. (1986) & McAllister et al. (1994). The relative slip senses on major faults are shown by the blue arrows. The basins appear to be elongated parallel to the inferred offshore extension of the Three Pagodas and Wang Chao Faults. **(c)** Simplified map of the Yinggehai Basin (=*SongHong Basin*; Fig. 1.6a), which appears to be elongated parallel to the Red River Fault.

The 1994 regional study also involved reconnaissance work on the western margin of the Malay Basin to identify the exploration potential in this area utilizing sparse 2D seismic data. A major NNW- to NW-striking fault zone was identified along the western margin of Malay Basin, known as the Western Hinge Fault Zone (Figure 1.7). This Western Hinge Line separates the western margin from the basin centre and characteristically comprises a series of NNW- to NW-striking normal faults with fault planes dipping towards the east.

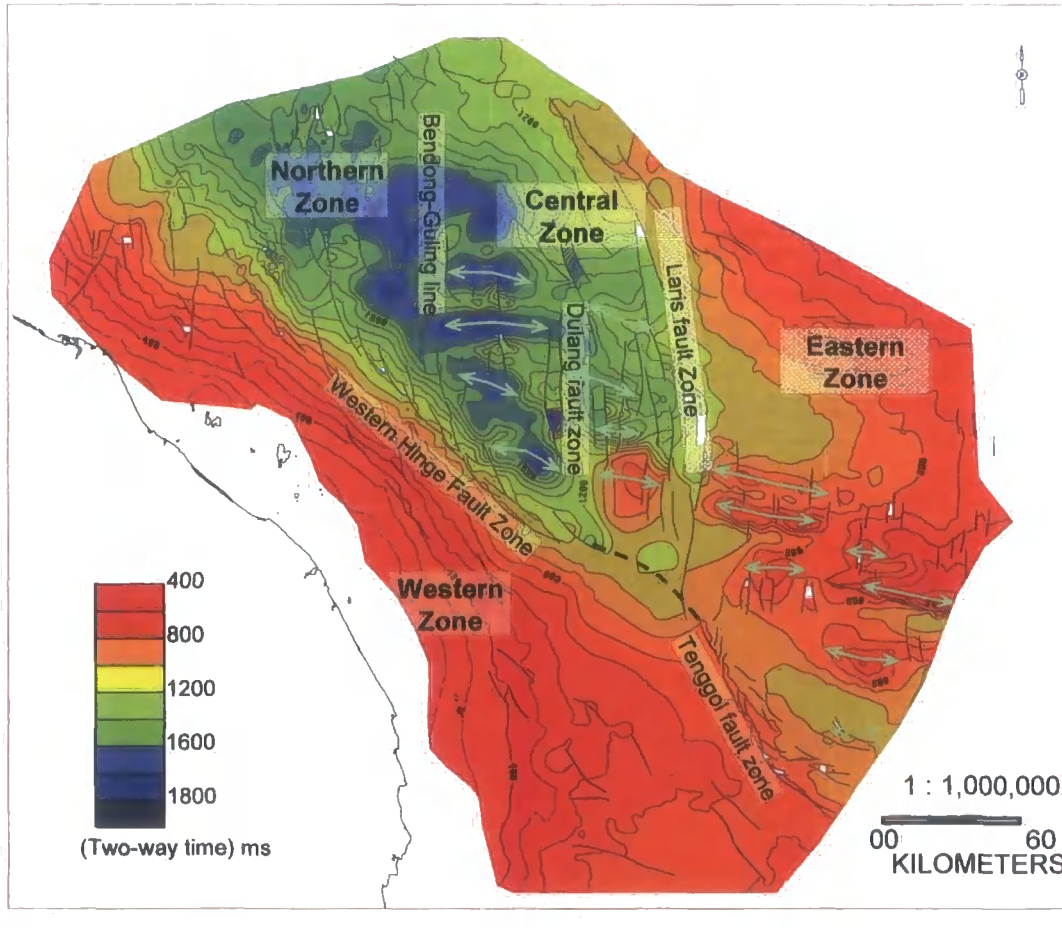

Figure 1.7 Time structure map of the Late Middle Miocene marker within the Malay Basin. Major faults within the Central Zone comprise en-echelon left-stepping segments. The Eastern and Central Zones are also characterised by numerous east-west trending folds (white arrows). The Western Zone is cut by mainly NW-SE trending faults.

During the 1994 study, regional geological markers were picked by identifying sequence boundaries and maximum flooding surfaces from gamma-ray log curves. These well markers were given an alphanumerical group name (Figure 1.8) and correlated with picks on the 2D seismic lines. Major well markers were used as a basis for interpreting basin-wide regional seismic markers. The regional well markers, known as "Group markers", were subsequently correlated with palynological zones in order to define the stratigraphic age and facies type of each group unit. The palynological zones, also known as "PR zones", were developed by *PETRONAS Research and Scientific Services* (PRSS) in 1996 and have been subsequently been applied throughout the basin ever since and are consistently identified in exploration wells.

In brief, the 1994 study suggested that shales of Late Miocene age, equivalent to Group E and F (Figure 1.8), contain one of the main source rocks in the central and northern parts of the Malay Basin. This shale unit is the primary source of oil accumulations in the Central, North and East zones of the Malay Basin. Shales of Late Oligocene to Middle Miocene strata (equivalent to Group K and Group L) were identified as potential source rocks in older strata (Figure 1.8). However, the possibility that intraformational shale can act as a potential *in-situ* source rock has not been ruled out.

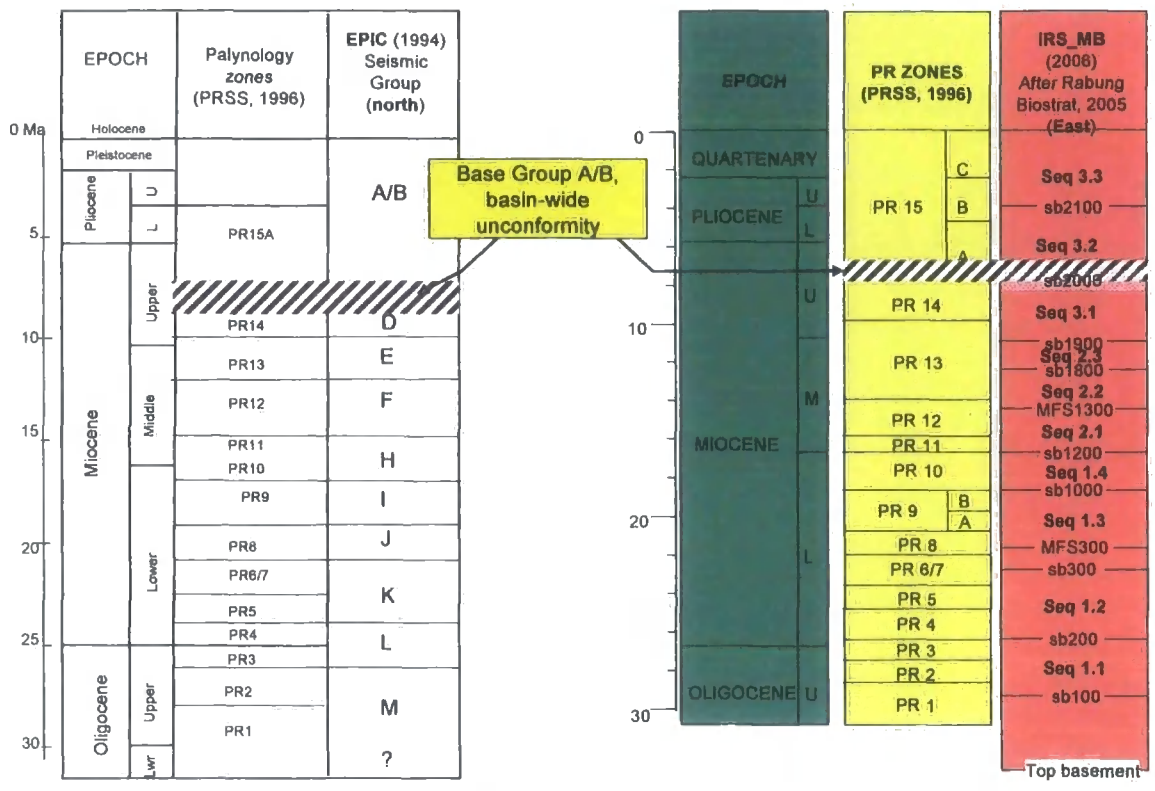

Figure 1.8 Stratigraphic charts for the Malay Basin showing (left) the Seismic Groups developed during the 1994 EPIC regional study and their correlation with the Palynology zones developed during the 1996 PRSS study. (Right) Correlation chart showing the Palynology zones alongside the regional sequence stratigraphic framework developed during the 2006 IRS study.

1.3.2 Palynological Zonation 1996

Extensive work was carried by PRSS in 1996 to determine the ages and facies types of the basin-wide Group markers by correlating them with palynological zones in the basin (Figure 1.9). The palynological scheme was developed using pollen and palynomorph samples taken from well-bore cores and well-bore cutting samples, which were derived mostly from PCSB exploration wells. The samples are derived predominantly from Miocene to Pliocene strata whilst older

strata, such as the Late Oligocene, appear to be barren of pollen and palynomorphs. This observation, together with the lithologies seen in / inferred from cutting samples, well core and log curves, led to the proposal that the Late Oligocene strata encountered in most wells located near to the basin centre were likely to be of continental origin. The Miocene samples mostly indicate fluvial coastal plain to near–shore depositional environments.

The oldest marker drilled was identified as Late Oligocene, and is known as Top Group L. The youngest unconformity was defined at Base Group A/B, and dated as Late Miocene/Pliocene. The study also confirmed that the Malay Basin comprises mostly Miocene infill with Late Oligocene sediments overlying the basement units along the basin margins. Thinning of sediment packages from the basin centre towards the basin flanks can be clearly be seen on the regional 2D seismic section shown in Appendix 2.

From the regional seismic sections, the deepest part of the Malay Basin is seen to contain up to 14 km of sedimentary infill (IRS Malay Basin, 2006). Unfortunately, no well has penetrated the oldest sequences and the sequence appears to be onlapping along the basin flanks at deeper levels (circa 3500ms) (Appendix 2 and 3). Thus, the stratigraphic age of the deeper sequence remains uncertain. However it has been inferred to be of Early Tertiary to Early to Middle Oligocene age. From seismic facies interpretation, i.e. by mapping seismic reflector characteristics laterally and vertically across strata, the basal strata were

interpreted to be broadly similar to shallower Late Oligocene facies. Therefore, the Malay Basin's basal strata possibly comprise of continental deposits of alluvial facies with an upper coastal plain fluvial to lacustrine setting.

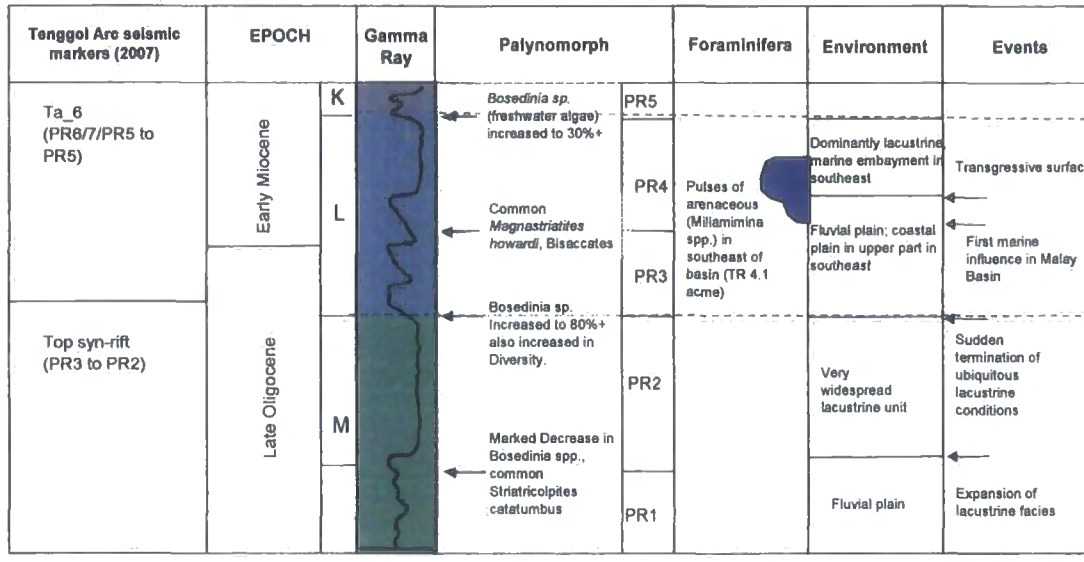

Modified after PRSS, 1996/97 with additions

Figure 1.9 Chart showing a typical gamma ray response and palynological and foraminiferal assemblages recovered from Late Oligocene to Early Miocene strata within the Malay Basin. A change from a lacustrine to a marine depositional environment has been inferred from the first appearance of arenaceous benthonic foraminifera. Seismic markers (Ta_6; Top syn-rift) mapped across the Tenggol Arch during the present study are shown for reference (Chapter 3).

1.3.3 Integrated Regional Study (IRS) of Malay Basin 2005/2006

An update on the regional study was carried out in 2005/2006 to further improve the geological understanding of the basin using newly acquired data, which included 2D seismic data of 1993 to 2000 vintage, some field-scale 3D seismic data and exploration wells drilled from 1997 to 2004. The two main objectives of

this study were: 1) to develop a structural and kinematic framework of the basin; and 2) to validate and update the existing stratigraphic framework.

Seismic sequence stratigraphic methods were used to develop consistent, basin-wide seismic markers and as basis for developing an updated stratigraphic and chronostratigraphic scheme for the basin. The seismic sequence stratigraphic markers, (known as "sb markers"), represent major sequence boundaries and have been interpreted based on reflector truncations and major unconformities observed in 1993 2D regional seismic lines. In order to define a consistent set of seismic markers[3] across the basin, the integrated regional study (IRS) did not attempt to tie *sb* (sequence boundary) markers to previously-defined Group units. However, *sb* markers have been calibrated to palynological zones (PR Zone) at well locations. Thus, an indirect comparison of *sb* markers to the Group units is available and is shown in Figure 1.8.

Based on this analysis, the first marine incursion is believed to have occurred along the south-southeast margin of the basin during the Late Oligocene (PRSS, 1997), where samples of benthonic foraminifera were identified in the *sb*100 shale unit. The sequence below *sb*100 was identified as being non-marine

[3] *markers*; *SB* markers were generated solely from seismic sequence stratigraphic interpretation of 1993-vintage regional 2D seismic lines (RC93). The markers were required due to a lack of basin-wide consistency in Group unit markers. The Group markers were developed from well gamma-ray logs and litho facies from cores and cuttings, mostly focusing in the basin centre and populated basin-wide using 2D seismic data of various vintages. As marker correlation continues westward towards the basin margins, they become less consistent, due to geophysical and geological factors. The geophysical factors are variations in the sample rate, amplitude and frequency spectrum from various processing centres. Geological factors include lateral displacement along major faults which cause changes in lithofacies as we cross major strike slip faults. Therefore at this stage it is critical to develop a set of markers that are stratigraphically consistent from one field to another and that can be related to Group units that can be applied basin-wide with high confidence.

clastic in origin, based on wells drilled into the top section of this sequence. Cutting samples indicate a lacustrine environment as shown in Figure 1.9 (PRSS, 1997, 2005). Laterally extensive coal beds occur mainly within the *sb*1200 to *sb*1800 sequence, consistent with deposition in a Lower Coastal Plain environment associated with an increase in relative mean sea level during the Middle Miocene (Morley, 2002).

The IRS study showed that the Malay Basin is compartmentalized by north-south trending basement-rooted fault zones in the central part of the basin and by predominantly NNW- to NW-striking faults in the West and South margin, contrary to the findings of the 1994 regional mapping. Based on these findings, four structural zones were defined based upon the dominant trend of the structural grain and play type. These four structure zones are known as the Eastern, Northern, Western and Central Zones (Figure 1.2).

The Eastern Zone comprises mainly east-west trending faults which are dominant at top basement level (Figure 1.3). Fault trace orientations change to pervasive NW-SE, North-South and some East-West trending faults towards the East margin in the Miocene to Pliocene sequences (Figure 1.3 and 1.7). The Northern and Central zones are characterized by north-south elongated sub-basins bounded by north-south trending faults (Figure 1.3). Both zones are characterised by East-West trending anticlines with predominant N- striking faults which are believed to have developed due to reactivation of basement faults.

The East-West trending anticlines are most clearly developed in the Central Zone, possibly due to the large sediment thicknesses in this zone. The Western Zone, which is the widest zone, encompasses the entire western margin of Malay Basin. The Tenggol Arch and Terengganu Platform are included in this zone, which runs northwest-southeast parallel to the eastern coastline of the Malaysian Peninsula and protruding into southeast margin the basin. The Western Zone comprises northwest-southeast and north-south trending faults, which are dominant in Miocene and younger strata. East-west trending faults are also present in the Western Zone but are found only locally within basement to Late Oligocene (sb100) strata. The Western Hinge Line can be clearly identified in seismic sections and on the Bouguer anomaly map. This lineament comprises numerous normal faults that downthrow towards the east and extend roughly 400 km from north to south along western basin margin (Figure 1.3).

Exploration targets in the Malay Basin are mostly within Late to Middle Miocene strata in the prolific Eastern and Central zones. Exploration activities in the Western Zone mostly focus on the hangingwall region of the Western Hinge Line, targeting clastic plays in Miocene to Late Oligocene strata. Exploration activities situated on the footwall of the Western Zone are geologically high-risk. Due to thinning of Tertiary strata towards the basin flank and indications of increasingly sand-prone strata (based on seismic reflector characteristics), there is a high probability that cap rocks are absent and/or that the region lies within a

hydrocarbon migration shadow. As a result, exploration activities have been less extensive in the footwall of the Western Hinge Line compared to the basin centre.

The structural and kinematic framework of the Malay Basin was developed by integrating interpretations of offshore 2D seismic, Bouguer gravity data, and satellite images of onshore Malaysia. The Southeast Asia extrusion tectonic model of Tapponnier et al. (1986) was adapted in IRS Malay Basin study in order to explain the kinematic evolution of the basin. Regional mapping identified possible evidence of strike-slip deformation, which apparently caused dextral displacement of Middle to Late Miocene strata. Left-stepping en-echelon faults were mapped along major lineaments such as the Western Hinge Line and the Laris Fault Zone (Figure 1.2 and 1.5). East-west trending anticlines, believed to have developed during structural inversion of sedimentary basins in the Middle to Late Miocene were also mapped within the Eastern, Central and Northern Zones. These observations are consistent with the tectonic and structural evolution of the Malay Basin as suggested by Khalid (1996). In this model, the east-west trending anticlines were attributed to lateral displacements and the growth of positive flower structures along the Laris Fault Zone during the Miocene (Figure 1.7). Although this evidence for Middle to Late Miocene strike-slip deformation can be mapped throughout the basin, evidence for a sinistral strike slip displacement in pre-Miocene strata, as suggested in the earlier 1994 regional study based on a comparison with the Yinggehai Basin (see section 1.2.1), could not be substantiated. Alternatively, Morley (2002) suggested that a left-stepping

fault pattern may also arise due to oblique extension. In this model, the regional extension is oblique to pre-existing structures within the basement giving rise to an en-echelon fault pattern within the shallow sequence. This alternative model has yet to be fully evaluated and will be tested further in the present study.

The major Laris Fault Zone (Figure 1.2) generally strikes N to NNW but gradually becomes more NW in the southern part of the Malay basin. The Laris Fault Zone can be clearly defined in seismic sections and appears to be formed from a series of steeply-dipping, basement-rooted faults with distinctive positive flower structures in Miocene strata (Appendix 1). Both the Laris Fault Zone and Western Hinge Line can be identified as prominent lineaments on the Bouguer gravity maps from the Malay Basin (Figure 1.3). This observation supports the idea that both the Laris Fault Zone and Western Hinge Line are basement-rooted, and potentially older than Late Oligocene (Khalid, 1996).

Peak regional compression in the Malay Basin was constrained to occur during the Miocene to Late Miocene (sb1900 to sb2000). This inference was based on observations of the youngest folded strata in the basin, which are mostly mapped within the Eastern Zone. Mapping of sb1900 and sb2000 shows prevalent east-west trending anticlines, which are predominant in the Eastern and Central Zones. These features were believed to have developed during Middle to Late Miocene inversion with peak compression during the Late Miocene. A key

conclusion of the present study is to suggest that these "inversion" structures in fact developed during Late Miocene wrench-dominated transtension (Chapter 4).

By contrast, the Tenggol Arch was characterized by active extension during the Late Middle Miocene. NNW- to NW-striking normal faults are prevalent and generally dip towards the east. Folding is restricted to within Middle to Late Miocene strata along Western Hinge Line, where fold axial traces are typically oriented parallel to fault planes. To summarize, folds in Western Zone are minimal and subtle in comparison to folds in the Central and Eastern Zones (Appendix 2). Moreover, folds in Western Zone have a NNW to northwest trend, whilst folds in Central and Northern Zone typically trend East-West.

1.3.4 Discussion and Conclusion

In summary, the 1994 study was focused on prolific zones situated mainly in the centre and along the Eastern margin of the Malay Basin. The study developed seismic and well markers which are consistent for the central basin and its eastern margin. However, as exploration efforts have expanded towards the western, southern and northern parts of the basin, correlation of well and seismic markers becomes more difficult and mis-ties more prominent. The miss-ties usually occurred as interpretation took place across various vintages of 2D seismic data.

The 2005 regional study attempted to tackle these correlation issues whilst investigating the remaining exploration potential in the basin. In the 2005 study, an alternative approach to understanding the structural and stratigraphic framework of the basin was required in order to develop new conceptual play models for the basin. This study identified the western margin as one of the best exploration targets in the Malay Basin and proposed that the remaining resource potential in the basin lies within unconventional fractured basement and syn-rift plays.

Observations from these previous regional studies have highlighted important issues regarding the structure and kinematics of the Western zone and Tenggol Arch. These include the possibility that the structural evolution of the Western zone was influenced by the mechanical heterogeneity of the basement complex – for example by structures inherited from the final closure of the paleo-Tethys ocean and docking of the Sibumasu microcontinent. Onshore peninsular Malaysia may provide an analogue for understanding the significance of these structures and the pre-Miocene structural evolution of the Western zone and Tenggol Arch. In addition, it may be possible to test the hypothesis that Miocene structures in the Western zone may have developed in response to extension oblique to these pre-existing basement fabrics – i.e. during transtension (Morley 2002; De Paola et al. 2005a, b). A further refinement of this idea is that the different structural geometries observed in the Western zone compared with the

basin centre may also have arisen due to lateral variations in the mechanical properties of basement and cover sequences and/or regional variations in the orientations of basement structures (De Paola 2005b; see Chapter 4).

To summarize, several issues need to be addressed in relation to the structural framework and kinematics of the Tenggol Arch. These are:

1) to identify the nature and timing of structural events on the Tenggol Arch and surrounding areas;

2) to identify pre-Cenozoic basement structures from surrounding areas (in particular, onshore Peninsular Malaysia); and

3) to identify any possible indicators that basement-influenced transtension and/or lithological variations could have played a major role in controlling deformation on the Tenggol Arch.

This study will address these issues by using a newly acquired 3D seismic dataset from the Tenggol Arch, integrated with existing findings from the 2005/2006 regional study of the Malay Basin.

In general, the thesis is organized as follows:

- Chapter 2: Tectonic and geological setting of Malay Basin and Peninsular Malaysia

- Chapter 3: Seismic study area and geophysical methods

- Chapter 4: Tenggol Arch – structural evolution and analysis of fault geometry and kinematics

- Chapter 5: Fracture interpretation from geophysical attribute mapping

- Chapter 6: Discussion and recommendations for future study

The next chapter will discuss the tectonic and geological setting of the Malay Basin and Peninsular Malaysia based on regional models from previous work.

Chapter Layout

In Chapter 1, I have introduced the tectonic framework of the Malay Basin, based on the results of previous regional studies of Sundaland. These working models were sufficient for frontier exploration activities during early 1990's. However, as exploration activities have continued, more geological and geophysical data have been acquired which have allowed the working model to be updated and refined. Updating the regional tectonic framework is a critical step in hydrocarbon exploration within the Malay Basin. Issues such as dry wells and new discoveries require a redefinition of the basin petroleum system conceptual model, a prerequisite for identifying unconventional plays. In this chapter, I discuss in more detail the evidence for wrench and extensional deformation in the Malay Basin offshore and onshore Peninsular Malaysia using published field-scale structural and stratigraphic evidence.

At present, there are two main end-member hypotheses used to explain the tectonic development of the Malay basin:

1) The Malay basin is a pull-apart formed due to extrusion of the Southeast Asian crust during India-Eurasia collision; and
2) The Malay basin initiated as a failed rift basin, which was modified during wrench deformation at a later stage.

A clearer understanding of the basin origin and tectonic framework will affect the evaluation and interpretation of fault and fracture geometries within the study area. This evaluation will in turn influence assessments of the reservoir and sealing potential of the fractured basement play. Thus the following chapter summarizes existing tectono-stratigraphic models to explain the development of the Tenggol Arch specifically and the Malay Basin in general highlighting any relevant geological evidence from onshore and offshore regions.

Geophysical data used in this study include 2D and 3D seismic data, Bouguer gravity anomaly maps from marine and airborne surveys acquired in 1995 and from more recently acquired airborne and satellite surveys carried out by Getech. Geological data from the basin comprises well data, which includes electrical logs and documented reports on biostratigraphic samples, well-bore core and cutting samples. The method used to interpret the tectono-stratigraphic framework of the Tenggol Arch involved identifying major sequence boundaries from seismic sections. The seismic markers were then correlated with the Malay Basin stratigraphic scheme for age calibration. A simplified table showing the stratigraphic scheme and chronostratigraphy of Malay Basin is shown in Appendix 1.

2.0 Malay Basin: tectonic framework and basin origin

The opening of Malay Basin is believed to be related to stretching of the Sundaland continental crust (Hutchinson, 1996), possibly associated with mantle plume activity in the region during Triassic to Late Cretaceous magmatism (Tjia, 1995). The crust of Sundaland is interpreted to be of continental origin based on similarities between continental rocks drilled in deep exploration wells (2300 m and deeper), and Paleozoic rocks of continental origin that crop out along the East domain of Peninsular Malaysia (Malaysia Geology & Mineral Resources Dept., Yew, 1985, 1995).

Four models, related to the crustal extrusion and/or failed rift hypotheses described above, have been proposed to explain the crustal stretching and opening of the Malay Basin:

Tapponnier et al. (1986):

Following the work of Tapponnier and co-workers, the opening of the Malay Basin has been interpreted by many authors to be related to the polyphase extrusion of Southeast Asia, resulting from the Indian plate colliding with Eurasia. The age of soft-collision of the Indian-Australian plate (e.g. Curray et. al., 1982 and Dewey et. al. 1989) occurred between Early Eocene to Middle Eocene times. Xu et. al. (1985) have suggested that the Late Eocene represented the hard collision of the Indian and Eurasian plates. The

plasticine model analogues used by Tapponnier et al. (1986) demonstrate the possible effects of India-Eurasia collision on the kinematics of the East and Southeast Asia regions. In this model, left-lateral displacements along major strike-slip fault zones (Figure 1.6b) throughout Sundaland are predicted during the Eocene. It has been proposed that relative left-lateral displacement of over a hundred kilometers occurred along the Three Pagodas Fault zone resulting in the opening of offshore pull-apart basins in the Gulf of Thailand and Malaysian peninsula regions (Figure 1.6b). The Yinggehai Basin[1], located to the east of the study area (in the Gulf of Tonkin, south of the China Shelf), has a superficially similar geometry to the Malay Basin. Both basins are narrow rifts with rhombic "pull-apart" geometries in map view (see Figure 1.6b and 1.6c).

Using this conceptual framework, the Malay Basin was interpreted as having developed as a pull-apart basin during movement along the offshore continuation of the Three Pagodas and Wang Chao Fault zones offshore into the Gulf of Thailand and South China Sea (Figure 1.6b). Therefore, the origin and general tectonic setting of the Malay Basin were interpreted to be similar to those of the Yinggehai Basin (McAllister et. al, 1994) (Figure 1.6a and Figure 1.6c). Nevertheless, Tapponnier et al. (1986) also highlighted the possibility that the orientations of the Tertiary basins in Sundaland were

[1] Yinggehai Basin is also known as Song Hong Basin in some literature (Phan Trung et. el., 1998) situated offshore Vietnam in BacBo Bay, east Vietnam sea.

inherited from the pre-rift structural fabric. However no further study has been carried-out to evaluate this possibility.

Hall (1998)

Hall (1998) summarizes the histories of major plate reorganizations in South East Asia using plate reconstruction modeling. This work suggests that the Malay Basin is most likely to have opened as a rift basin between 50 and 40Ma. The India and Australia plates became amalgamated (45 Ma) and continued to move northward, which resulted in the combined India-Australia plate colliding with Eurasia. The northward advancement of the India-Australian plate caused amalgamation of Gondwana fragments in the Southeast Asia region. The distribution and ages of these Gondwana fragments was one of the factors considered in this plate reconstruction, in addition to the onshore and offshore evidence. These fragments may possibly be contributing to the pre-rift structural fabric in Mesozoic or older formations. In his model, Hall (1998) concluded that the timing and causes of initial rifting in Sundaland were still uncertain due to poorly dated continental basement rock in this region. However, he also suggested that initial opening of the Sundaland rift-basins may also be consequences of oblique convergence or extension influenced by pre-rift structural fabrics, as also proposed by Hutchinson (1996).

The Late Eocene – Late Oligocene (30 to 20 Ma) was a very significant period in the development of Sundaland, as emphasized by Hall's (1998) reconstruction. During this period complex marginal basins and oceanic plate reorganization in Southeast Asia took place. Modeling by Hall indicates that major tectonic events took place in surrounding regions, such as along the margins of the Philippine-Caroline-Pacific oceanic plates and Australia-West Sulawesi margins, together with widening of the Fiji and Solomon Sea marginal basins. Geological evidence suggests that ophiolite emplacement in Sulawesi (e.g. Mubroto et. al. 1994; Hall, 1998) and activity along the Sorong strike-slip fault system in the New Guinea region at this time are likely to have been related to plate reorganization (Figure 1.6a).

Though the eastern margin of Southeast Asia was characterized by large-scale plate reorganization, the western margin, particularly along the Malay Basin and Tenggol Arch is characterized by a major unconformity dated as Late Oligocene from well-calibrated seismic sections. Regional basin mapping by the IRS Malay Basin 2005 study indicates that whilst the Late Oligocene unconformity is widely observed on regional seismic sections, it becomes less distinguishable towards the eastern flank of Malay Basin (Appendix 2). In other words, sequences above and below the unconformity surface gradually became more conformable towards the eastern flank of the Malay Basin. Based on this observation, the study has suggested that the basin was possibly tilted towards the east during Early Tertiary or Oligocene

times and has led to the interpretation that uplift of the basement complex particularly along western and south margin of Malay Basin gave rise to the Tenggol Arch (PETRONAS, 2006 (b)).

McAllister et al. (1994)

The Malay Basin portfolio[2] study (McAllister et. al., 1994) again suggested that the collision between the India-Australia plate and Eurasia during the Middle to Late Eocene played an important role in basin opening and strike-slip deformation throughout the Southeast Asia region. A working hypothesis to explain the opening of the Malay Basin was developed based on comparisons with the geology of the Yinggehai Basin, which lies to the northwest of the South China Sea (Figure 1.6a and Figure 1.6c). This basin is believed to be the offshore continuation of Red River Fault Zone. Cross-sections through the Malay Basin from the earlier EPIC study (Chapter 1) shows that the northwest-southeast trending basin has an asymmetric profile, characterized by a steeply-dipping southwestern margin and a slightly more gently dipping northeast flank (Appendix 1). Sinistral strike-slip faults associated with the Red River Fault Zone were thought to extend into the Yinggehai Basin. McAllister et al. (1984) therefore proposed that the Malay Basin formed as a pull-apart feature during sinistral strike-slip deformation related to lateral displacement of Peninsular Malaysia relative to Indochina along the Three Pagodas and Mae Ping Fault Zones (Figure 1.6b). Since this

[2] A portfolio study of Malay Basin (1994) was carried out to evaluate the exploration potential for business and shareholder purposes which was an in-house project operated by EPMI (Exxon-Production Malaysia Inc.).

proposal was made, no sinistral displacements with the magnitudes required by this model have been observed either in the onshore or offshore regions of Peninsular Malaysia.

Tjia, 1998

Tjia (1998) suggested that the opening of the Malay Basin occurred prior to Late Cretaceous magmatism in the region and has categorized it as a failed rift basin. He proposed that rifting of the Malay Basin was initiated by Mesozoic magmatism in Sundaland that was possibly related to a Cretaceous to Late Cretaceous mantle plume with a radius of ca. 500 km. The centre of the plume was interpreted as being situated to the south of the Tenggol Arch, from where three basins - Malay, Penyu and West Natuna - radiate outwards forming a 'triple junction' (Figure 2.1). Tjia proposed that to generate such a 'triple junction', the required large-scale tensile forces may have arisen from the updoming of continental crust above the mantle plume. The widespread development of Cretaceous igneous rocks in Sundaland (Figure 1.3), and high present-day heatflow measurements made in wells from the Tenggol Arch and southern margin of the Malay Basin lend some support to this hypothesis (Table 1; Madon, 1999; Hutchinson, 1996; Wan Ismail, 1984). High present-day heatflow is also observed in surrounding basins; for example, the Penyu Basin shows average of 38^0C/km and Tenggol Arch average present-day heatflow at 45.3^0C/km.

More recently, White (1992) concluded that magmatism was related to either subduction, rifting or thinning of the lithospheric mantle. The presence of high amplitude Bouguer anomalies over the Malay Basin (GETECH, 2005)

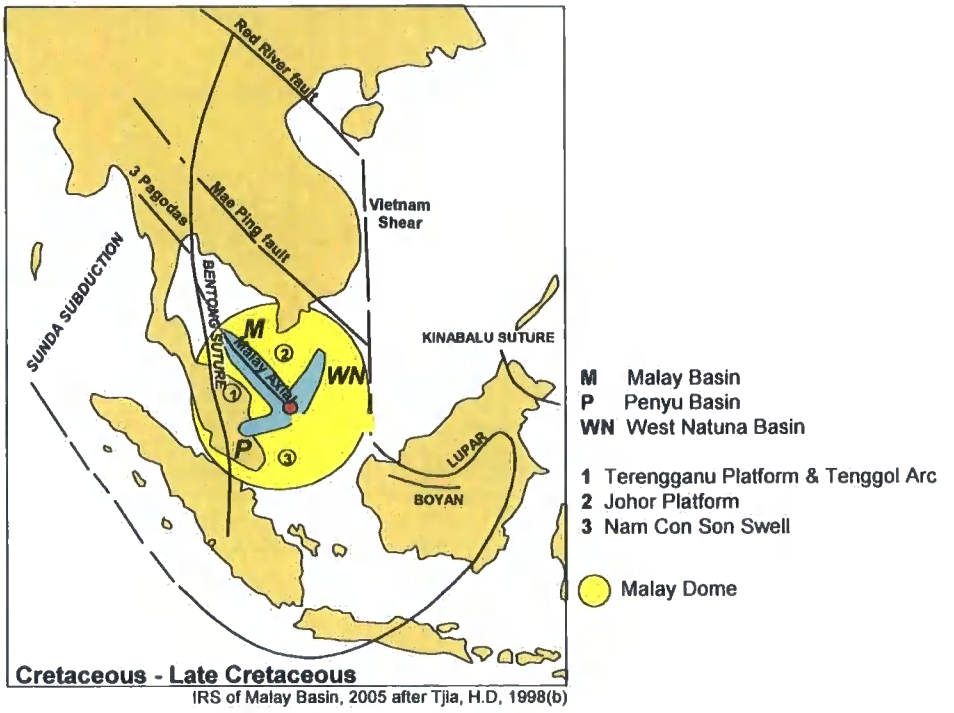

Figure 2.1 Simplified structural map of southeast Asia showing major faults (black lines) and the inferred extent of the c. 500km^2 "Malay Dome" (yellow), which is believed to have been generated by a Cretaceous to Late Cretaceous mantle plume. Thermal uplift is believed to have caused rifting in the Malay Basin (M), Penyu Basin (P) and West Natuna Basin (WN), centered upon a triple junction (red spot). Regions numbered 1,2 and 3 are present-day platforms (structural highs) that may be remnants of Malay Dome.

indicates thinning of the crust or shallowing of the Moho over Sundaland in general and specifically beneath the Malay Basin. These observations are also consistent with the possible presence of mantle plume in the region. Stretching of the continental crust in Sundaland initiated an extensional fault system that propagated as splays from the Three Pagodas and Wang Chao Fault zones (Figure 1.6b). Pre-existing structural fabrics, perhaps formed as a result of amalgamation of Gondwana fragments (see previous section; Hall,

1998), may have contributed to the NW-SE Malay Axial trend. Following Cretaceous to Late Cretaceous opening (rifting), the basin was interpreted by (Tjia, 2001) to have undergone wrench modification during Paleogene sinistral deformation and dextral modification during the Middle to Late Tertiary. This was followed by a second phase of dextral deformation during Late Tertiary to Pliocene times (Table 2a). These postulated wrench deformation events are consistent with evidence for strike-slip recorded along major strike-slip zones in Southeast Asia (Figure 1.6a) as suggested by Tapponnier (1986) and further discussed by Hutchinson (1996) and Hall (1998).

Onshore studies of the Three Pagodas Fault zone (3PFz) in north Thailand have identified three phases of fault slip: early sinistral motion, followed by dextral transtension and younger dextral transpression (Rhodes et al., 2004). Extensive argon dating of biotite grains preserved within the shear zone suggests that the earliest deformation probably occurred during the Eocene to Oligocene and Miocene (^{40}Ar-^{39}Ar age dating by Lacassin et. al. 1997). Morley (2004) used fission-track zircon ages to suggest that the earliest deformation along Red River Fault Zone occurred between 29.7 $\pm$ 1.4 Ma and 35.9 $\pm$ 1.3 Ma. Sedimentary strata that are displaced across the 3PFz constrain the youngest phase of deformation to be Holocene.

Onshore studies of deformation along the Red River shear zone have shown that sinistral deformation along this fault ceased during Early Miocene times (Harrison et al., 1992). This event was followed by dextral strike-slip around 5 or 5.5 Ma (Late Miocene to Pliocene). During this stage, dextral displacement was recorded by river offsets of approximately 25km in Yunan, China (Replumaz et al., 2001). Geological studies offshore East Vietnam have also suggested that dextral slip motion along the Red River shear zone may possibly have been related to sea floor spreading in the South China sea during 32 to 17 Ma (Lisa & Leloup et al.,2003; Replumaz & Lacassin et al.,2001).

Four key points are clear from the above listed models to explain the origin and tectonic framework of the Malay Basin. These are:

1) Extrusion tectonic of Southeast Asia likely plays an important role in basin opening across Sundaland during the Early Tertiary;

2) The amalgamation of Gondwana fragments due to the northward advance of the Australia-India plate during the Mesozoic or older (Hall, 1998) gave rise to deep-seated basement fabrics across Sundaland. This fabric appears to have influenced the later structural framework.

3) A mantle plume and/or mantle-related magmatic activity occurred across Sundaland during the Mesozoic and may have initiated rifting of the Malay Basin.

4) Geometric similarities between the Yinggehai and Malay basins suggest that the latter may also have originated as a pull-apart basin during dextral

deformation along the offshore continuations of the Three Pagodas-Wang Chao Fault zone.

Most models suggest that the Malay basin initiated during the Oligocene, this postdates the main phase of supposed extrusion tectonics in the Southeast Asia region (Tapponnier, 1986, McAllister, 1994, Hall, 1998). Although the Oligocene to Late Oligocene basal marker in Tertiary basins of neighboring areas, especially central and Gulf of Thailand basins, is widely recognized (Morley et. al., 2000), the equivalent marker in the Malay Basin appears highly localized along the western margin of the Malay Basin. In addition, heatflow measurements from wells in the Malay Basin indicate relatively high present-day heat-flow (Wan Ismail, 1984, Madon, 1997; Table 1). Analysis of the source rock geochemistry in the Malay Basin shows that the Early Miocene source rock (equivalent to mfs300) vitrinite reflectance indicates immature to early mature with (V_0) of 0.6 (Waples & Ramly, 1996). These observations suggested that opening of Malay Basin should pre-date the Late Oligocene. Thus Late Cretaceous or Paleogene opening are possible, perhaps as a consequence of mantle plume activity, as suggested by the 'Triple-junction' model of Tjia (1998).

However, basin-wide the oldest penetrated sediment proven in Malay Basin indicates age of Late Oligocene from biostratigraphy studies of wells drilled in the SE of the basin (PETRONAS, 1999). Hence, age of rifting or opening of Malay

Basin can still be interpreted as no younger than Late Oligocene, which is similar to other basins of Southeast Asia.

2.1 Kinematics of offshore & onshore Peninsular Malaysia

The Integrated Regional Study of Malay Basin (PETRONAS, 2006(b)) suggested that the east-west trending folds within Middle Late Miocene strata (sb1900 sequence) found in the central and eastern zones of the Malay Basin (Figure 1.7) represent the "peak compression" event. The folds are distributed within zones or blocks separated by major, basement-rooted north-south trending fault zones. These fault traces extend up into strata as shallow as the Upper Pliocene. NNW-striking faults, which include the Western Hinge Fault Zone (Figure1.7) run parallel to the present-day coastline and were interpreted as dextral strike-slip faults (PETRONAS, 200(b)). This interpretation was based on the recognition of supposed positive flower structures associated with the left-stepping en-echelon faults observed on structural maps of Miocene strata (Figure 1.7, Appendix 1). Dextral strike-slip was also interpreted to have occurred along the N-S trending Laris Fault zone (Appendix 1 and 2). A similar structural pattern can be observed throughout all of the Middle Miocene to Pliocene strata of the Malay Basin. In Oligocene and older strata, no clear indications of lateral displacement are observed in the basin centre, possibly due to over-printing of younger

deformation. However, the structural styles of basement relief on the Tenggol Arch and Terengganu Platform are thought by some workers (Liew, 1998, Tjia, 2001) to indicate possible evidence of both sinistral and dextral deformation, based on observations of rhomboidal shaped sub-basins on the basement highs (Figure 2.2).

Fieldwork along the east coast of the Malay peninsular (Figure 2.3) was carried out by Tjia (2005), following the exploration and appraisal campaign of basement wells drilled in late 2004 and early 2005. The objectives of this fieldwork were to establish possible stratigraphic and structural correlations between the basement complex offshore and onshore exposures of the pre-Tertiary basement. These

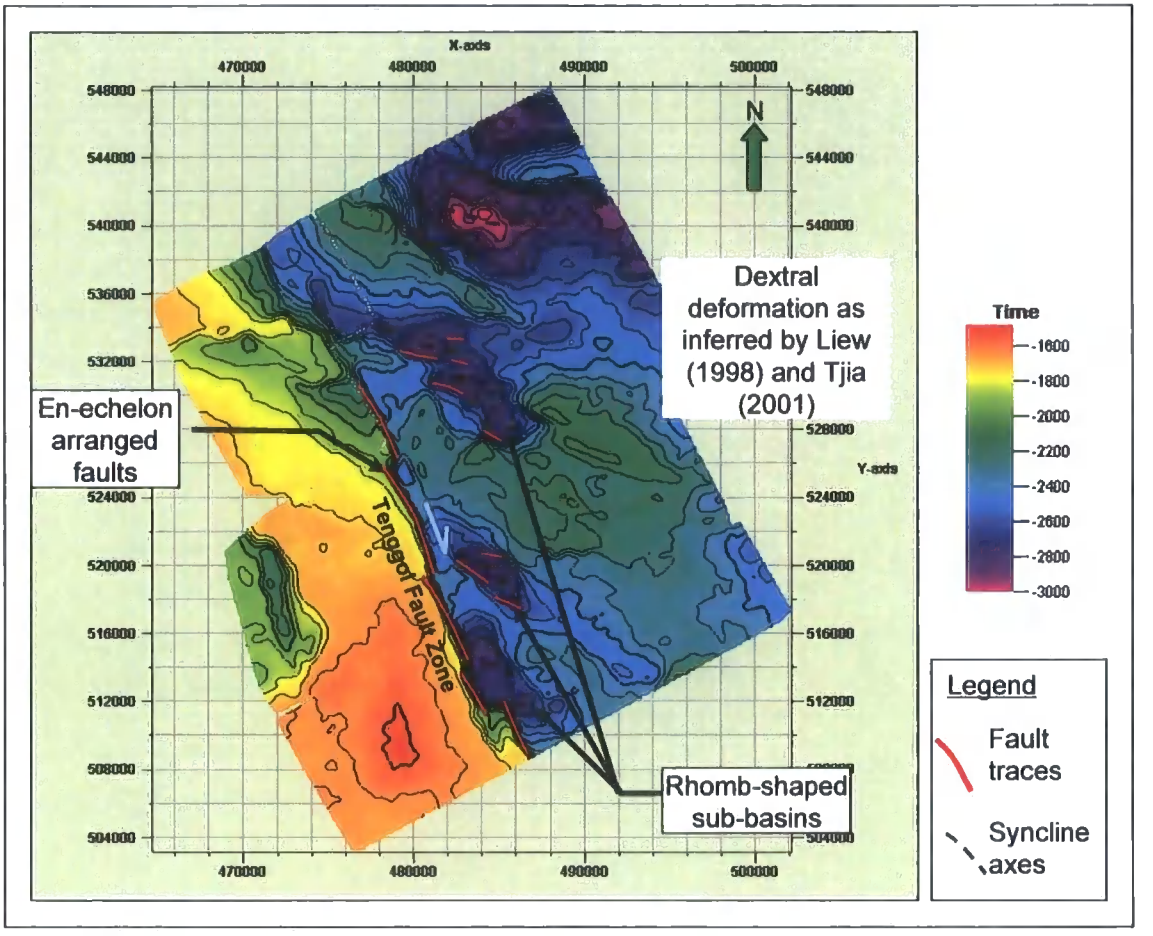

Figure 2.2 Time structure map of the Top Basement marker on the Tenggol Arch. Note the en-echelon NW-SE trending faults show right-stepping arrangements and rhomb-shaped sub-basins in the hanging-wall of NE-dipping Tenggol Fault zone.

correlations are important for the basement play evaluation because the complexity of the basement unit in the basin cannot be adequately sampled from sparse well data. This complexity includes highly variable lithologies, formation ages and structural patterns. K-Ar dating of igneous rock samples from the basement complex sampled in wells suggests that the rocks are of Jurassic to Cretaceous age (*Geological studies, unpublished*[3]).

[3] Geological studies of well core samples usually carried out by third party geological laboratory services and scientific researches for internal use only *(Robertson Research and Lab Services)*

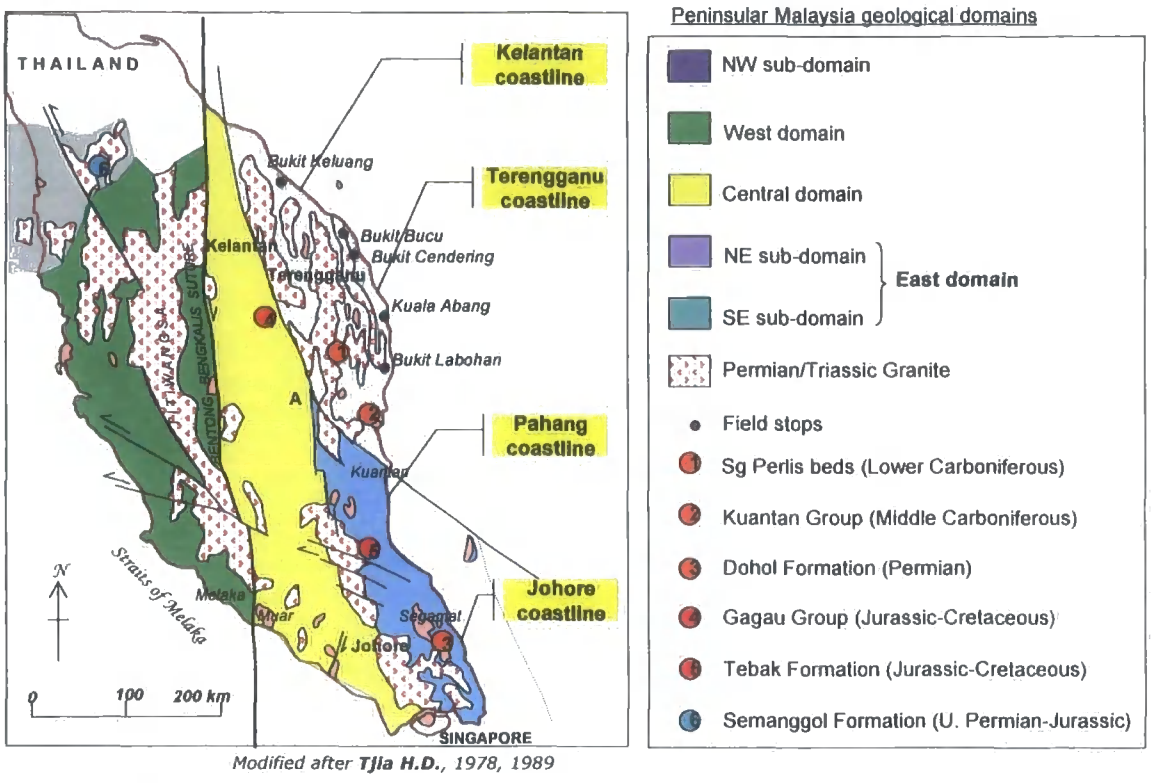

Modified after ***Tjia H.D.****, 1978, 1989*

Figure 2.3 Map showing the tectonic domains of Peninsular Malaysia. The locations of onshore field localities with good exposures of Paleozoic-Mesozoic basement rocks are highlighted.

The Top Basement structural pattern can be resolved using 3D seismic data designed for fractured basement targets, such as the 2004 Tenggol Arch 3D seismic survey which utilized 4.8 kilometer cable length with acquisition bins at 6.25 meter x 18.75 meter spacing (Appendix 4). The 2004 3D seismic is able to image structural patterns at the Top Basement marker with fair to good quality imaging between 1500 and 2500 ms (Attachment 1 and 2). However, detailed fracture interpretation requires post-processing of the data to remove residual noise related to stratigraphic dips and azimuth through structural smoothing. Fault traces are further enhanced by compensating PSTM with a variance cube,

producing an Antracking™ cube. Further discussion about structural mapping and the results of geophysical attribute analysis will be provided in Chapter 5. Despite using seismic data that has been optimized to image the basement, and the recent advances in geophysical analysis, the interpretation of basement fracture patterns remains problematic. Difficulties arise due to the loss of resolution at depth, which is caused in part by energy absorption due to the presence of high reflectivity surfaces in the shallow clastic sequence. Hence, to get a better picture of the structural framework of the Tenggol Arch, a useful strategy is to examine the equivalent onshore formations located along the eastern coastline of the Peninsular Malaysia.

One of the objectives of the Integrated Regional Study (PETRONAS, 2006 (b)) was to correlate major structural lineaments within the Malay Basin with those mapped onshore in Peninsular Malaysia. This was done using geophysical methods, mostly utilizing regional-scale data such as total magnetic intensity and Bouguer anomaly maps to evaluate the offshore area. Other regional scale data such as satellite images of Landsat and Radarsat were used to interpret the regional lineament pattern onshore peninsular (Attachment 4). However the geological significance of the mapped lineaments was unclear: the lineaments were possibly of structural, stratigraphic or superficial geomorphologic origin. Hence the likely origins of these lineaments were verified through cross-referencing to structural mapping by previous workers associated with local

universities, the governmental Institution of Mineralogy and Natural Resources and field work carried internally by the regional team.

The field work demonstrated that the N-S trending Kampung Buluh-Ping Teris fault zone that crops out in northern Peninsular Malaysia (Appendix 6) likely extends offshore into the Kelantan sub-basin. The NW-striking Lepar and Lebir Fault zones within the East Domain of Peninsular Malaysia (Figure 1.3) can be extended offshore into the Kuantan sub-basin, located south of the Tenggol Arch. In the southern part of the East Domain, the Mersing Fault zone displays lateral displacements that can be traced offshore towards the Johore Platform, located to the south of Penyu Basin based on gravity anomaly map (Figure 1.3).

It can be concluded that major structures in the East Domain of the peninsular can potentially serve as structural analogues for basement structures preserved on the Tenggol Arch and Terengganu Platform. Further analysis of these structural patterns and styles are therefore important to prove this idea. The following section examines, in turn, the pre-Tertiary and basement rocks of the Malay basin and the onshore Malay peninsular.

2.2 Stratigraphic correlation of the Tenggol Arch basement complex to onshore outcrop

2.2.1a Malay Basin: Pre-Tertiary Strata of the Western Basin Margin

The western margin of Malay Basin is defined by the Terengganu Platform, which runs parallel to the present-day coastline. The Tenggol Arch is a continuation of the Terengganu Platform and lies to the south of the western margin of the Malay Basin proper, protruding southeast and straddling the southern Malay Basin and the Penyu Basin (Figure 1.1). On the Tenggol Arch, the basement comprises mainly Pre-Tertiary units. These Pre-Tertiary rocks have been drilled between 2300m and 3000m deep by wells located on the basement high (Figure 1.3).

The Pre-Tertiary strata of the Tenggol Arch mainly comprise argillaceous metasediments, with some quartzitic metasandstone layers. Other lithologies include a crystalline unit of volcanic-plutonic igneous material and localized occurrences of recrystallised limestone to the north of the Tenggol Arch. The age of metamorphism is most likely to be related to regional magmatism during the Triassic to Cretaceous periods (Tjia, 1998, Hutchinson, 1996).

The top basement marker within the Malay Basin appears to be a major unconformity between Pre-Tertiary and Tertiary strata. The basement complex

was defined as any type of lithology which includes crystalline, metamorphic and clastic rocks with ages no younger than Late Cretaceous (PETRONAS, 2006 (b)). The top basement marker and underlying basement complex can be easily recognized in seismic sections (Figure 2.4a).

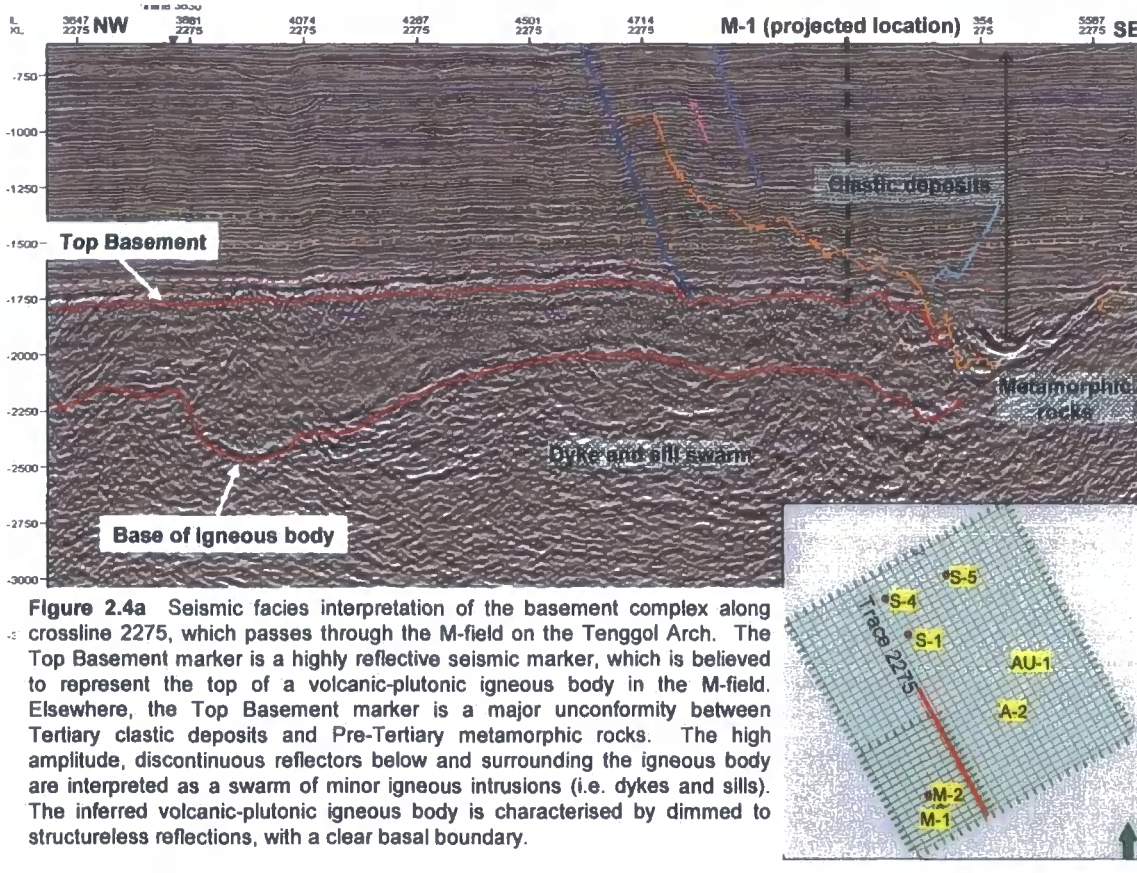

Figure 2.4a Seismic facies interpretation of the basement complex along crossline 2275, which passes through the M-field on the Tenggol Arch. The Top Basement marker is a highly reflective seismic marker, which is believed to represent the top of a volcanic-plutonic igneous body in the M-field. Elsewhere, the Top Basement marker is a major unconformity between Tertiary clastic deposits and Pre-Tertiary metamorphic rocks. The high amplitude, discontinuous reflectors below and surrounding the igneous body are interpreted as a swarm of minor igneous intrusions (i.e. dykes and sills). The inferred volcanic-plutonic igneous body is characterised by dimmed to structureless reflections, with a clear basal boundary.

K-Ar dating of basement igneous rocks was carried-out to determine the age of the basement complex on the Tenggol Arch. Ages range from Jurassic to Cretaceous/Upper Cretaceous. Radioactive dating of metasedimentary rocks indicates possible Cretaceous ages, but interpretation of the K-Ar ages is ambiguous due to feldspar alteration during metamorphism, i.e. these could date

metamorphism rather than depositional age. Correlations with argillaceous metasediments exposed onshore along the eastern coast of the Malay Peninsula could help to constrain the depositional age. Here, analysis of fossil assemblages suggests that the rocks were largely deposited during the Carboniferous (Appendix 9).

The age of carbonates within the basement complex on the Tenggol Arch is uncertain, although the limestone formation was interpreted as being of Pre-Tertiary age, based on the presence of a limestone layer below the Top Basement seismic marker near the S-field (Figure 2.4b). It therefore seems likely that the limestones on the Tenggol Arch are most likely to be equivalent to Paleozoic marine limestones in onshore Peninsular Malaysia (Panching Limestone). Localized feldspathic volcanics (i.e., extrusive igneous rocks) occur sporadically in the lower part of the sequence. These are similar to ignimbrites observed onshore along the east coastline of Johore.

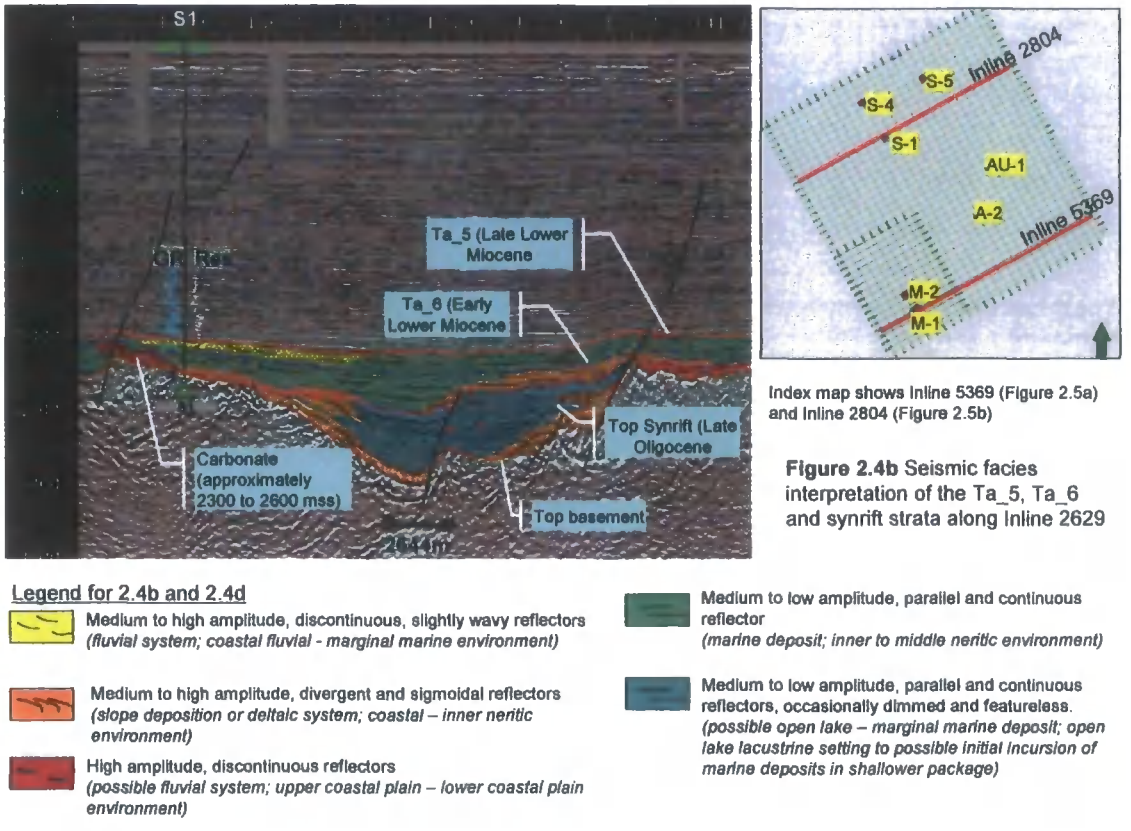

Figure 2.4b Seismic facies interpretation of the Ta_5, Ta_6 and synrift strata along Inline 2629

Continental deposits observed onshore (Attachment 5), such as the Gagau Group and Tebak Formation, crop out in the Eastern and Central Domains of the Malay peninsular. The Gagau Group, which is exposed at Gunung Gagau, Kelantan (Figure 2.3), comprises reddish conglomerates with subordinate sandstone, some siltstone, shale, occasional volcanics and rare thin lenses of coal (Rishworth, 1974, Khoo, 1983). The Tebak Formation is exposed at Gunung Belumut, Johore (Figure 2.3), where it predominantly comprises argillaceous rocks dated as Upper Jurassic to Lower Cretaceous and interpreted as continental deposits based on fossil plant assemblages (Table 3). Similar formations have been encountered near the bottom of the TB-1 well, northwest of

the Malay Basin (Lasmo Oil, 1971), and may be correlatives, although fossil evidence is lacking (Attachment 6).

It is also possible that the basal strata encountered within the TB-1 and B-1 wells are Late Oligocene/Early Miocene age as they are overlain by Middle Miocene rocks. This would require the basement in the western margin to have been elevated above mean sea level and exposed for a long period with very limited sediment deposition from some point following the Lower Cretaceous. Basal sequences drilled on the Tenggol Arch in the Lg-1 well (Figure 1.3) indicate possible Early Tertiary/Early Miocene continental sediment ages. Core samples recovered from the A-field and TB-1 wells reveal the presence of anhydrite infilling fractures (PETRONAS, 2006(b)). The anhydrate deposits may suggest semi-arid conditions at least on the western margin, or high hydrothermal activity during the Early Tertiary period.

2.2.1b Malay Basin: Tertiary Strata of Western Basin Margin

The Tertiary strata of the Western margin of the Malay basin can be divided into (1) an Early Tertiary sequence of synrift continental strata, (2) Oligocene to Early Miocene marginal marine to lower coastal plain strata and (3) Middle Miocene to Recent marine strata. The Tertiary strata that uncomformably overlie the Top Basement marker on the Western margin of the Malay Basin become

conformable towards the Eastern flank. A geo-seismic section across the Tenggol Arch shows wedge-shaped Miocene strata towards the basin flank (Appendix 2). This regional geoseismic section illustrates the stratigraphy of the basin, the generalized facies distribution and the basin geomorphology.

The Oligocene to Miocene sequence consists mostly of fluvial to coastal fluvial deposits of interbedded sand and shale with some occurrences of thin coal layers and lignified beds. These are considered to be the primary reservoir targets in the basin, hence interpretations of the Oligocene and Miocene sequence markers are robust and their stratigraphic ages have been established through analysis of microfossil and palynomorph data. The thickest sediment package comprises Miocene strata, which consists primarily of lower coastal plain to coastal fluvial marine deposits, with some thin layers of lignified siltstone and fine grained sandstone within the Middle to Middle Late Miocene sequence (Well Completion Reports, unpublished). Channel facies of the lower coastal plain are commonly found in Late Middle Miocene to Late Miocene strata and can be easily recognized on seismic sections (Figure 2.4c). A detailed discussion on seismic facies interpretation and interpretation of channelized features will be presented in Chapter 3.

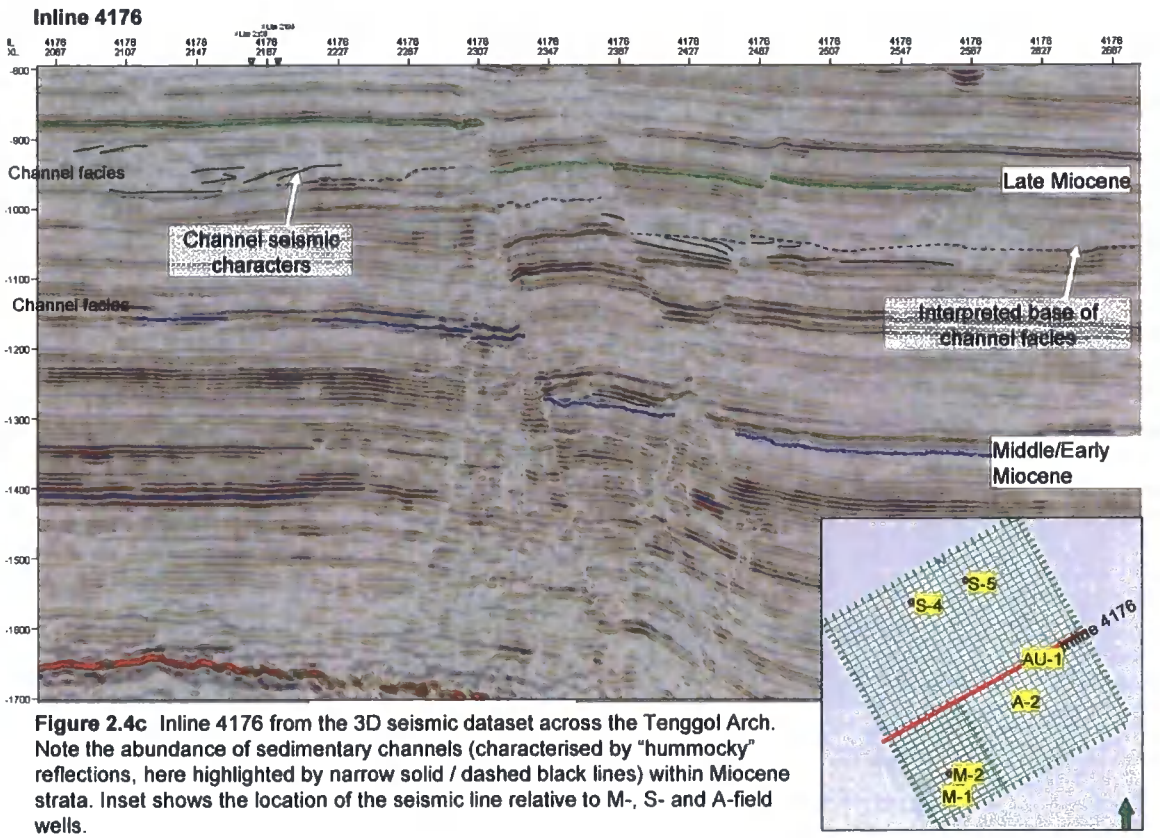

Figure 2.4c Inline 4176 from the 3D seismic dataset across the Tenggol Arch. Note the abundance of sedimentary channels (characterised by "hummocky" reflections, here highlighted by narrow solid / dashed black lines) within Miocene strata. Inset shows the location of the seismic line relative to M-, S- and A-field wells.

The oldest known sediments penetrated by wells along the Western margin are Late Oligocene. These rocks define the top of the Synrift sequence on the Tenggol Arch, and are equivalent to the sb100 marker in the Malay Basin proper. At the onset of rifting, sub-basins on the Tenggol Arch were initially filled by continental slope and alluvial deposits. The age ranges of the Synrift sequence are undefined due to the lack of fossils so far recovered from deep basement wells. The basal middle Tertiary unit is interpreted to be a transgressive package, as demonstrated by the low sand to shale ratio of this unit and the on-lapping nature of markers along the basin slope (Appendix 2). The first marine incursion occurred during the Early Miocene in the southern part of the Malay

Basin (Figure 1.9). The top of this transgressive marine sequence has been identified as Top Group L (EPIC seismic group, 1994) or mfs200 (PETRONAS, 2006 (b)) and is equivalent to the Ta_6 seismic marker on the Tenggol Arch (Attachment 3).

The top Synrift marker on the Tenggol Arch has been identified on the basis of its seismic reflector characteristics, following the methodology of Prosser (1993). A detailed description of the seismic markers will be presented in Chapter 3. The top Synrift seismic marker is equivalent to *sequence 1.1* identified by the regional stratigraphic scheme[4] applied to the centre of the Malay Basin. The top Synrift marker in the basin centre is equivalent to the sb50 regional marker as illustrated in Appendix 1. The sb50 marker was developed from a regional interpretation of 2D seismic lines, which suggests that, in general, the Malay Basin is characterized by several major transgressive sequences with progradational cycles of para-sequences. These cycles can be clearly observed in 2D regional seismic sections (Appendix 2).

The oldest seismic marker the Malay Basin is defined by the sb50 pick on regional seismic lines, this package abuts along the western margin, and gradually on-laps the eastern flank of the basin. The sb50 sequence has not been drilled, so there is no confirmation on the stratigraphic age. However based

[4] *Sequence 1.1* is defined by SB100 as the base of the sequence and SB200 as the top of the sequence (Attachment 3.2). *Sequence 1.1* is dated Late Oligocene can be correlated widely throughout the basin.

on seismic interpretation, it seems likely that the sb50 seismic marker should be no younger than Oligocene.

The sb100 regional marker (Late Oligocene) overlies sb50 in the basin centre and is, continuous onto the western flank of the Malay Basin. Thus, the sub-basins on the Tenggol Arch should be filled by Oligocene to Late Oligocene sediment. The top Synrift marker on the Tenggol Arch was defined as a maximum flooding surface and correlates with the initial post-rift marker interpreted throughout the Malay Basin.

Lower coastal plain to coastal fluvial deposits of Miocene to Pliocene age are conformable on the Top Synrift marker. This package consists mainly of inter-layered sandstone and shale sequences of fluvial and marginal marine origin. Localized thin coal layers and occasional lignified carbonaceous siltstone are present in the Middle to Late Miocene strata *(Well Completion Reports[5])*. Calcareous shale layers are common in this interval and usually occur in association with marginal marine siltstones and fine grained sandstones. The Miocene strata can be further subdivided by four major seismic stratigraphic sequence boundaries, namely Ta_6 (Early Miocene), Ta_5 (Early to Middle Miocene), Ta_4 (Middle Miocene) and Ta_3 (Late Middle Miocene) and Ta_2/Ta_1 (Late Miocene to Pliocene) (Figure 2.4d).

[5] Well Completion Reports- unpublished PETRONAS Carigali internal geological and well results documentation.

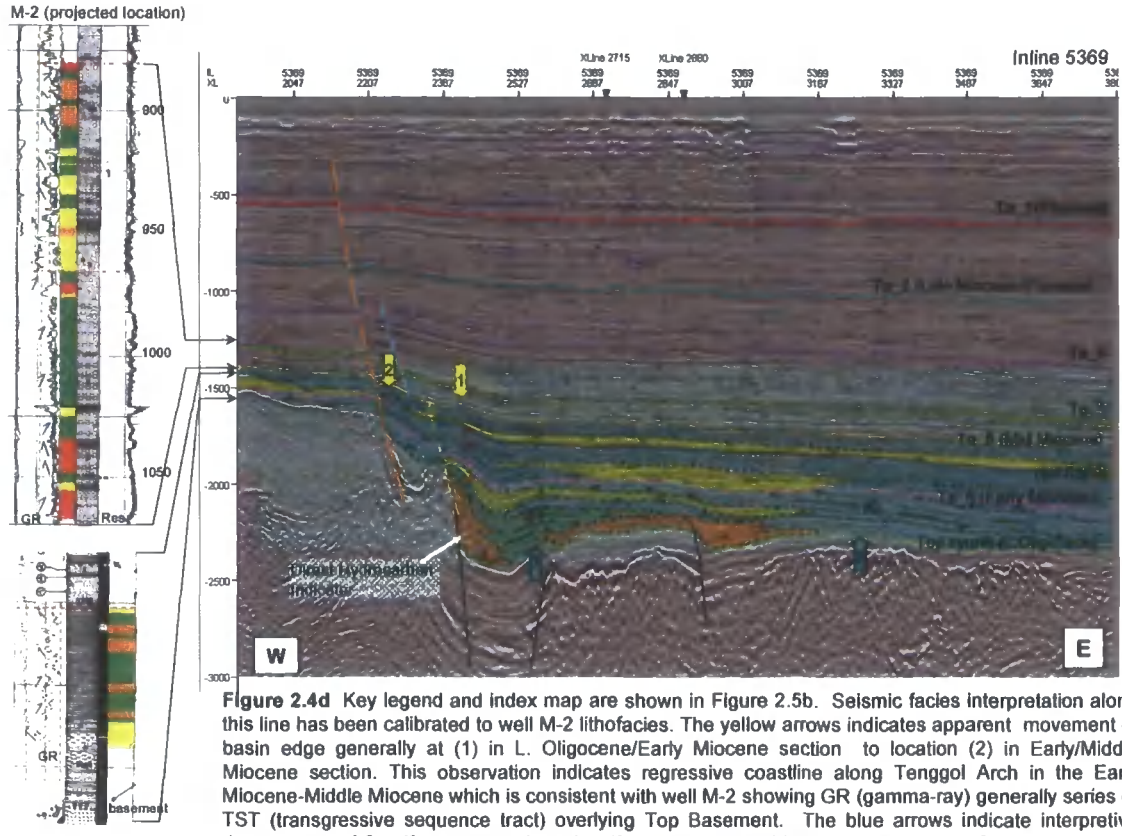

Figure 2.4d Key legend and index map are shown in Figure 2.5b. Seismic facies interpretation along this line has been calibrated to well M-2 lithofacies. The yellow arrows indicates apparent movement of basin edge generally at (1) in L. Oligocene/Early Miocene section to location (2) in Early/Middle Miocene section. This observation indicates regressive coastline along Tenggol Arch in the Early Miocene-Middle Miocene which is consistent with well M-2 showing GR (gamma-ray) generally series of TST (transgressive sequence tract) overlying Top Basement. The blue arrows indicate interpretive depocentres of Synrift sequence. Location (2) indicates possible later depocenters of synrift sequence based on seismic facies characters.

Isochore maps (discussed further in Chapter 4) show that the Synrift and Ta_6 sequences were deposited mostly in localized basement lows. Sediment provenance was mainly from local basement highs on the Tenggol Arch. An isochore map of the Ta_5 sequence shows a marked change in basin geometry and basement topography. During the Early Miocene, the basin appears to have widened, with sediment deposition focused along the southern margin of the Tenggol Arch and northward towards the centre of the Malay Basin proper.

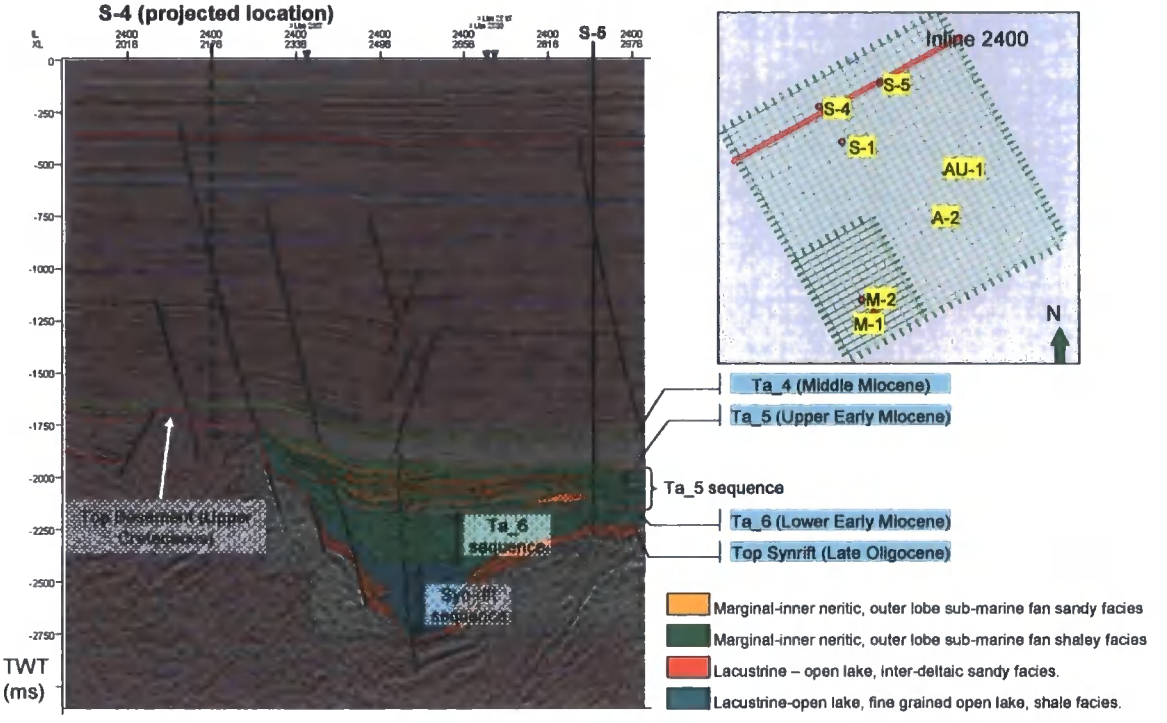

Figure 2.4e 3D seismic section (Inline 2400) through the S-field. Seismic facies analysis and well-calibrations show that the Early Miocene strata are characterised by marginal marine facies with open marine influences. A few faults appear to terminate above or below shale-prone strata within the Early Miocene Ta_5 sequence. The significance of this possible shale-rich "detachment" layer is discussed in the text. Inset shows the location of the seismic line relative to S-, A- and M-field wells.

During the Middle Miocene (i.e. during the deposition of the Ta_4 sequence), sediment deposition was mostly concentrated along the northern margin of the Tenggol Arch. This depositional pattern suggests that the Malay Basin was tilted to the north, which may have been caused by differential uplift of the basement over the Tenggol Arch. An isochore map of the Ta_3 sequence (Middle Late Miocene) shows that sediment deposition remained focused in the north. However, the Ta_4 thickness over the Tenggol Arch is fairly uniform, and is associated with an increasingly transgressive sequence from Middle Miocene (sb1300) to Pliocene/Recent times as concluded by the IRS Malay Basin study (PETRONAS, 2006(b)). This transgressive sequence is consistent with a

continuous rise in mean sea level in the region throughout the Cenozoic, as suggested by the global sea level curve model of Haq et. al (1987, 1992) (Appendix 1).

The Ta_2 (Late Miocene/Pliocene) sequence isochore map shows sediment deposition eastward along the hanging-wall of the Tenggol Fault zone. Changes in sediment depocentres observed from isochore maps can be interpreted as resulting from reorganization (i.e., uplift and structural inversion) of basement structures. Inverted basement structures have been identified along the Western Hinge Fault Zone, north of the Terengganu Platform and in some areas beyond the southern margin of the Malay Basin (IRS Malay Basin; PETRONAS, 2006(b)). This regional study also identified evidence of basin inversion during the Miocene, mostly between Middle Miocene (sb1000) and Late Middle Miocene (sb1900). The IRS Malay Basin study suggested that Miocene inversion resulted from regional compression caused by the extrusion of Southeast Asia (Tjia,1998b). The nature and significance of the supposed inversion event is considered further in Chapter 4.

Inverted structures at basement level were first identified in 2D seismic regional mapping (PCSB, 1995) as localized structures to the north of the Terengganu Platform. Similar structures were also identified in other parts of the platform and along the Western Hinge Fault Zone down to the southern margin of the Malay Basin in the 2005 regional mapping. However, no interpretation or further

discussion has been carried out to explain the possible causes of this inverted basement. However the 2005 regional study has identified the Western Zone as a prospect for further evaluation in hydrocarbon exploration and an evaluation of basement structures and inversion on the Tenggol Arch forms part of the present study.

The Ta_5 and Ta_6 intervals (Early to Middle Miocene strata), were identified as shale-prone sequences based on seismic facies analysis (Attachment 2) and well log (Figure 2.4d) interpretations. These intervals are characterized by low seismic amplitudes or dimmed features with occasional medium amplitudes. The Ta_5 and Ta_6 seismic facies is distinctively different from the younger Middle to Late Miocene strata. Seismic reflectors from the latter sequence show continuous, parallel to sub-parallel or divergent patterns, with clear on-lapping and truncation relationships (Attachment 2). Calibration with seismic facies logs has been carried out for these intervals (Appendix 3). It can be concluded that the Early Miocene strata (Ta_5 and Ta_6) comprise fluvial to deltaic sediments deposited in a marginal marine to inner neritic environment (Attachment 7 and Attachment 8).

The Ta_3 (Middle Late Miocene) strata display minimal variation in sediment thickness throughout the mapped area, even across faults as observed in isochore maps (Attachment 9 (d)). On seismic sections, the Ta_3 interval can be further divided into two distinctive packages, where the uppermost package

comprises medium to high amplitude, discontinuous and slightly wavy inter-layering with parallel seismic facies. Underlying this package is a thicker package of low to dimmed amplitude reflectors with the occasional presence of localized, discontinuous high amplitude, and continuous and parallel seismic reflectors (Attachment 1).

In summary, the oldest known rocks drilled in the Tertiary sequence of the Malay Basin are Late Oligocene marginal marine sediments from the southern margin of the Tenggol Arch (first marine incursion). The presence of paleosols and pebbly basal strata overlying the basement complex in sub-basins along the Western Zone may also indicate older basal strata of possible Early Tertiary/Paleogene age. Most of the basal strata are barren of fossils. By contrast, markers related to Late Oligocene to Miocene/Pliocene sequences are well defined and consistent due to the presence of fossils in wells drilled all over the basin. The seismic facies characteristics of the Synrift package were used to assist interpretations of the older sequences. The seismic facies characters of the basal sequence appear to be fairly similar to the Upper coastal plain sediments of the proven Late Oligocene sequence. Late Oligocene/Early Miocene to Recent packages indicates a general transgressive sequence depositional system.

The seismic facies have also been calibrated against the litho facies log developed for the Malay Basin Integrated Regional Study (PETRONAS,

2006(b)). An interpretation of the Ta_3 interval suggests that the uppermost seismic facies is a sand-prone fluvial system characterized by channels and flooding surfaces, deposited mainly within a lower coastal plain environment. The underlying unit is a thicker package of fine grained sediments (shale to claystone), which is possibly associated with a transgressive system tract of a marginal marine depositional environment (Attachment 10 and Attachment 11). These interpretations are further supported by gamma-ray logs of the Late Miocene interval (Figure 2.4d).

Similar sequences to the Miocene-Pliocene strata of the Malay Basin are present in restricted Tertiary basins developed along the Western Domain of the Peninsular Malaysia (Mahendran et. al., 1981). Miocene strata here are associated with coal mining. Hence, the Malay Basin and surrounding basins (Penyu and West Natuna) are major sediment accommodation spaces during Middle Tertiary whilst much of Peninsular Malaysia was above sea level with deposition occurring in restricted localized Upper Coastal Plain lake environments.

2.2.2a Peninsular Malaysia: Paleozoic Continental Group

The basement rocks of the Tenggol Arch are likely to correlate with Paleozoic rocks exposed in the East domain of Peninsular Malaysia. Here, the rocks can

be divided into two major subgroups. The first subgroup is of Carboniferous age and comprises of argillaceous metasediments, most commonly carbonaceous slate, phyllite and psammite with minor occurrences of metaquartzite in lenses. The second subgroup is of Permian age and comprises of continental slope deposits – a basal conglomerate, sandstone and shale, with some occurrences of volcanics and limestone. The locations of important exposures along the East coastline are shown in Figure 2.3. The Permian continental unit is exposed north of Peninsular Malaysia at Bukit Keluang (Figure 2.5) (e.g Che Aziz et. al, 2000, 2001, Kamal Roslan et. al, 2000, Tjia, 2005). Geological studies by Shafeea et al. (1999, 2000) have identified plant fossils in an argillaceous succession, which confirms the Late Permian age of these strata (Appendix 9).

A metasedimentary unit comprising mainly psammites and pelites crops out within the Bukit Bucu Complex, exposed at Kuala Terengganu. Che Aziz & Kamal (2001) have identified Carboniferous fossil assemblages within this unit. Similar metasedimentary packages have been observed at other locations along

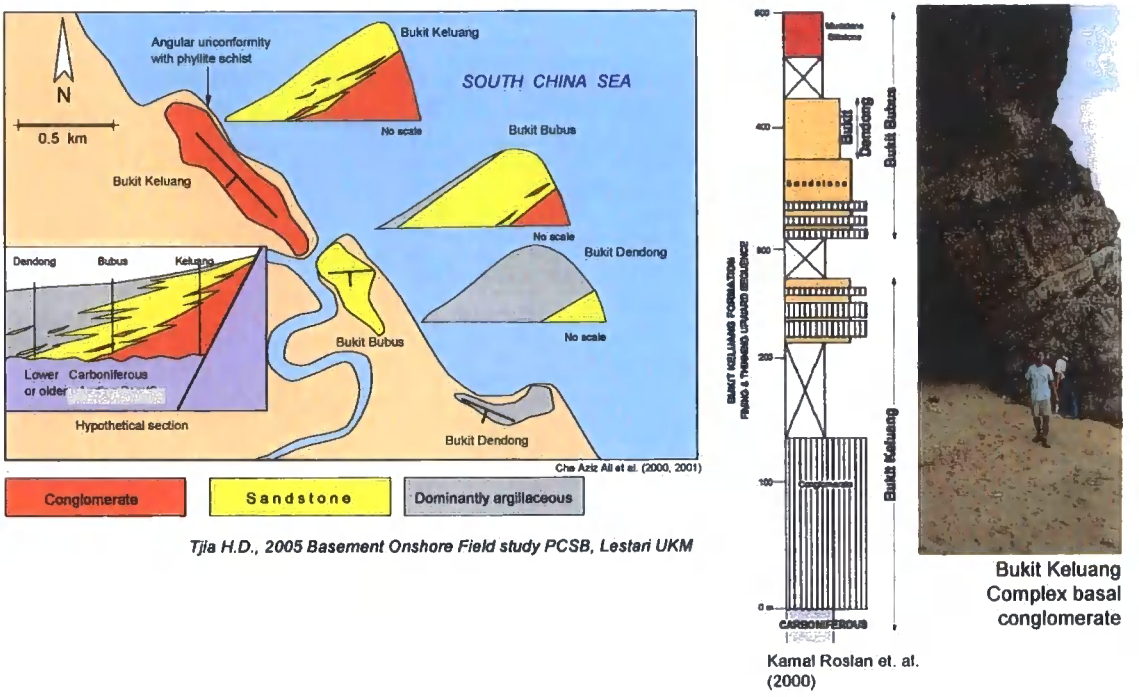

Figure 2.5 Field data from the Bukit Keluang (see Fig. 2.3 for location) locality showing (left) a simplified geological map with (inset) a schematic reconstruction illustrating the inferred stratigraphic relationships between the mapped lithological units. (Centre) Composite sedimentary log through the mapped outcrops and (right) a field photograph illustrating the thick basal conglomerate at the Bukit Keluang location.

the Johore coastline (Figure 2.3). These lithological observations demonstrate that the Carboniferous to Permian rocks exposed in the East domain are most likely to be equivalent to the basement complex of the Tenggol Arch offshore.

Radiometric age dating to determine of the timing of emplacement of igneous rock in Peninsular Malaysia, (e.g. Bignell and Snelling, 1977), provides ages ranging from 270 to 200 Ma. The age of igneous rocks onshore appears to be older than igneous rocks in the offshore area (in the Malay Basin, on Natuna-Anambas Island and in the Mekong Basin) which are mainly Cretaceous based on dating of well core materials and cuttings. This observation suggests that

intrusive igneous activity in the Malay Basin potentially occurred during the Cretaceous, whilst that in Peninsula Malaysia was predominantly Triassic and Permian (Table 4), with Post-Triassic dykes and sills in localized areas (Appendix 5). Igneous activity may have occurred initially in the western margin of Sundaland closest to the Sumatra trench and propagated eastwards. As subduction continued, the magma volume increased, causing massive igneous activity during the Mesozoic (see Figure 2.6 and Figure 1.3, and Table 4). Magmatic activity may have caused updoming of continental crust during the Cretaceous to Late Cretaceous, generating the swell, known as the Malay Dome (Tjia, 1989). The up-doming model was thought to have covered a region of approximately 500 km in radius, encompassing an area that includes the present-day Malay Basin, Penyu Basin, Natuna-Anambas and Mekong Basin (Figure 2.1).

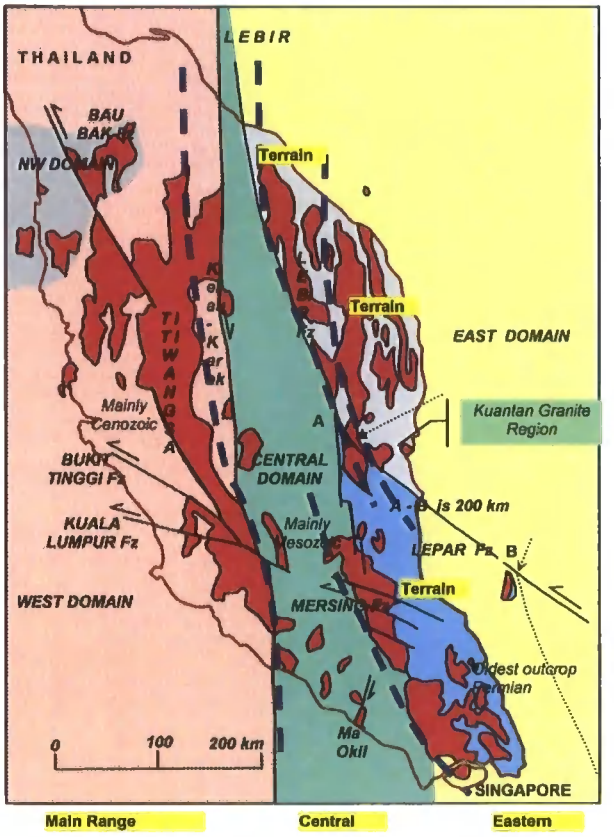

Map modified from Tjia, 1978, 1998, granite terrains based on Hutchinson (1996) and Yin and Shu (1973) simplified

Figure 2.6 Distribution of Mesozoic igneous rocks in Peninsular Malaysia (red) superimposed upon a map of Tjia's (1978; 1998) geological domains. Igneous rocks of the East domain have been classified into three different "igneous terrains" (A, B & C) by Yin & Shu (1973) and Hutchinson (1996). See text for explanation.

2.2.2b Peninsular Malaysia: Permian to Triassic Volcanic Activity

Wells drilled into the basement complex on the Tenggol Arch have confirmed the general lithological similarities with basement rocks exposed along the east coast of Peninsular Malaysia (i.e. within the East domain). Some wells have penetrated doleritic or andesitic igneous rocks, whilst others situated north of Tenggol Arch revealed limestone with occasional volcanic rocks and some occurrences of meta-tuffites and highly feldspathic volcanics (*Well Completion*

Reports, unpublished). Onshore equivalents of these volcanic rocks can be widely identified in the Mesozoic sequences that crop out in the Eastern and Central Belts, which include meta-tuffite, vitric rhyolitic to dacitic and andesitic meta volcanics, with age ranges from Permian (the Dohol Formation, Luit Tuff and Seri Jaya Beds; Rajah, 1989; Lee C.P., 1990) to Upper Middle Permian-Middle Triassic age (Sedili Volcanic; Rajah, 1986). The Sedili Volcanic comprises ignimbrite, tuff, agglomerate, lava and volcanic ash of various compositions and appears to have erupted synchronously with deposition of the continental clastics of the Linggui Formation. Plant fossils obtained from argillaceous members of this formation confirmed a Permian to Upper Permian depositional age.

The presence of foraminifera and bivalve fossils preserved within some of the onshore volcanic units has led to the interpretation of a shallow marine to inner neritic volcanic arc environment during Permian to Triassic times (e.g from Sedili Volcanics, Luit Tuff (Appendix 9)). Ignimbrites in the Sedili Volcanics, are associated with a shallow neritic volcanic arch and limestone coral build-ups like those found in the S-field on the Tenggol Arch. This supports an interpretation of a shallow marine inner neritic environment in this region during Permian to Triassic times.

2.2.2c Peninsular Malaysia: Post-Triassic dykes and sills

Post-Triassic dykes and sills are abundant in Kuantan Granite Region. Olivine tholeiite to quartz tholeiite dykes with K-Ar ages of 104± 10 Ma (Albian) cut the Kuantan Granites (Haile et al, 1983, Hutchinson, 1996). The igneous compositions are highly variable. Dolerite dykes at Bukit Laboh, Kijal (Figure 2.3) which also cross-cut late plutonic pegmatites and aplites (Ramlee, 1990) are possibly analogous to the dolerite dykes found on the Tenggol Arch (Appendix 5). Towards the east coast of the islands of Terengganu and Johore, dolerite and lamprophyre dykes and sills are found to cut Triassic granite (Hutchinson 1996). Exploration wells in the M field on the Tenggol Arch have drilled into dolerite dykes below a layer of volcanic rock (*Well Completion Report, unpublished*). Age dating of the volcanic rocks in the M field suggests that the igneous rocks are Cretaceous.

Studies of the Segamat Basalt have verified its alkaline origin (Grubb, 1965) with K-Ar dating providing a possible 62Ma or at least Upper Cretaceous age (Bignell & Snelling, 1977b). The presence of alkaline volcanics has led to the suggestion that their intrusion is related to a period of rifting during the Cretaceous or Upper Cretaceous period.

The common occurrence of Cretaceous felsic granite in Sundaland may be consistent with the opening of the Malay Basin having been influenced by the

presence of a mantle plume in the region (Tjia (b), 1998, Khalid et al, 1996). However it is also understood that presence of a mantle plume does not always result in rifting of the continental crust, though it commonly causes regional-scale dynamic uplifts of hundreds of kilometers in radius (White, 1992). The widespread distribution of Triassic to Cretaceous granitic rocks throughout Southeast Asia (Table 4) was the basis for interpreting a possible Cretaceous to Late Cretaceous mantle plume in Southeast Asia, possibly covering an area of circa 500km radius (Tjia, 1998(b)).

The development of the Malay Dome was followed by crustal cooling. According to Tjia (1995), doming led to the development of three major fault zones, which met at a 'triple-junction'. This 'triple-junction' is believed to be the origin of the Malay, Penyu and West Natuna basins (Figure 2.1). However, the top of the Malay Dome, interpreted as Late Cretaceous/Early Paleogene to possibly Early Oligocene, is not clearly observable or correlatable in seismic sections.

2.3 Summary

Carboniferous-Permian lithologies observed within the East domain of Peninsular Malaysia are similar to those found in wells that penetrate into the basement complex of the Tenggol Arch. Attachment 5 shows the stratigraphic groups that crop out within each onshore tectonic domain. The Central and East domains

are characterized by mainly Carboniferous to Permian or Early Triassic formations. Basement rocks on the Tenggol Arch consist mainly of low grade argillaceous metamorphic rock, and are likely equivalent to the Sungai Perlis Beds and Dohol Formation (Figure 2.3). The recrystallized packstone of the Tenggol Arch is most likely to be equivalent to the Panching Limestone formation (Figure 2.3). Both Sungai Perlis Beds and the Panching Limestone belong to the Kuantan Group which has been dated as Carboniferous, based upon the analysis of fossil assemblages (Appendix 9). Onshore, volcanic layers (e.g. the inter-fingering Linggui Formation and Seri Jaya Beds dated as Permian to Middle Triassic) are consistent with volcanic rocks found inter-fingering with carbonate rocks on Tenggol Arch.

Plutonic-volcanic igneous rocks on the Tenggol Arch and in surrounding areas within the Malay Basin are of Cretaceous age, and originated during Mesozoic magmatism in Southeast Asia (Tjia, 1995). Exploration wells on the Tenggol Arch have drilled into dolerite dykes or sills and granitic rocks in the M-field. Both igneous rocks were dated Cretaceous and similar granite has been drilled south of the Tenggol Arch and on the Eastern flank of Malay Basin (Figure 1.3). Granite in Peninsular Malaysia has been dated Triassic to Jurassic (Bignell and Snelling, 1977a; Liew, 1983; Liew and McCulloch, 1985) (Table 4). Observation of older (Triassic-Jurassic) igneous rocks onshore, and younger (Cretaceous) igneous rocks offshore in the Malay Basin, can be interpreted as being related to the Australia-India oceanic plate subduction beneath Sumatra, with subsequent

eastward propagation of magmatic activity. Tholeiite dykes dated as Albian (104 ± 10 Ma) (Haile et. al.,1983; Hutchinson, 1996) cutting across the Triassic Kuantan Granite Region (Figure 2.6), are possible onshore analogues to dyke and sill swarms observed in seismic and well data from the Tenggol Arch. In conclusion, geological observations from offshore and onshore regions show that the basement complex of Tenggol Arch is a continuation of the rocks exposed along the east coastline of Peninsular Malaysia.

2.4 Major structures in Peninsular Malaysia and their relation to the Tenggol Arch

Peninsular Malaysia: Geological domains

Peninsular Malaysia has been divided into five tectonic domains, namely the Northwest, West, Central, East and Southeast domains (Figure 2.3). These geological domains were defined on the basis of the dominant structural trends, as interpreted from lineament patterns and fold axes mapped in the field (Tjia, 1978). The lineament map has recently been updated based on interpretations of satellite images during the 2006 integrated Malay Basin regional study (Attachment 4). The Northwest domain is characterized by NW-SE and E-W trending structures. The oldest outcrop identified is the Macinchang formation (Attachment 5) in Northwest Langkawi, which comprises a conglomerate-

sandstone-shale succession with acid tuff beds and dated Cambrian fossil assemblages (Jones, 1961, 1981, Lee, 1983, Shafeea, 1997). Within the northwest of the peninsula, NW-SE trending fault zones are prevalent, for example the Bok-Bak fault, in Kedah (Burton, 1965, Raj, 1983; Table 3), across which sinistral displacements of Triassic rocks have been observed.

The West domain of Peninsular Malaysia is characterized by a cool-climate Cambrian-Ordovician fauna fossils and diamictite, which has been consistently correlated with equivalent rocks in Thailand and the North Australian aulacogen basins (Hutchinson, 1996, Metcalfe, 1987, Burret & Stait, 1984). By contrast, the Laurasian terrain of the East Domain was dominated by Paleozoic flora and fauna from a warm climatic environment (Hutchinson, 1987a, 1996; Tjia, 1989). The West Domain has therefore been interpreted as a Gondwana micro-continent, which drifted northward, possibly since the Carboniferous and finally docking along present-day Bentong-Raub Suture Zone during Middle or Late Triassic to Early Jurassic (Figures 1.5 and 2.7).

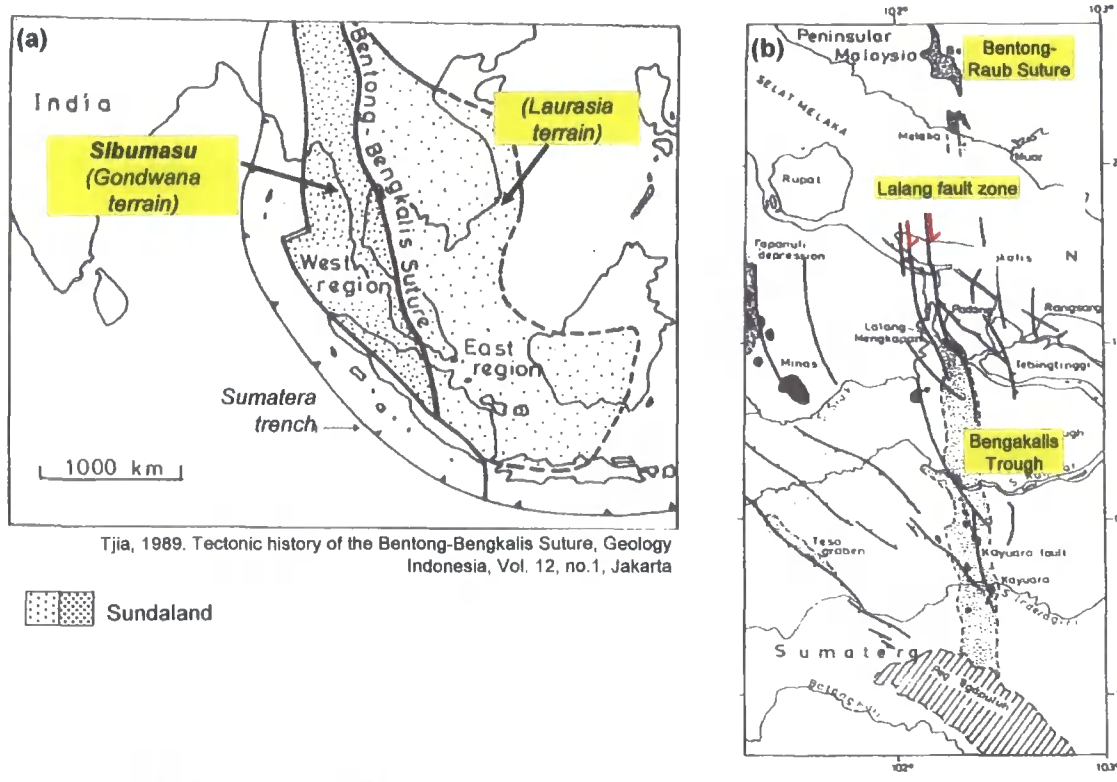

Tjia, 1989. Tectonic history of the Bentong-Bengkalis Suture, Geology Indonesia, Vol. 12, no.1, Jakarta

Figure 2.7 (a) Map showing that the Malaysian terrains originated from collision of Sibumasu and Laurasia terrain along the Bentong-Bengkalis Suture. The Suture is a key pre-Cenozoic tectonic element of Sundaland (Hutchinson, 1996). (b) The Bengkalis Trough in Sumatra is a continuation of the Bentong-Raub Suture in Peninsular Malaysia (Tjia, 1989).

2.4.1 Geological Setting of the West Domain

The West domain is characterized by a mostly northwest-southeast trending structural grain. The faults in the West Domain cut all Pre-Tertiary rocks and most granites in the peninsula. Major northwest-striking faults include the Bukit Tinggi Fault zone and Kuala Lumpur Fault zone, which also appear to extend towards Mersing Fault Zone in the Western Domain (Appendix 14). The Kuala Lumpur-Mersing Fault Zone appears to be left-laterally displacing the Bentong Raub Suture Zone in the south of Peninsular Malaysia (Figure 2.3). Strongly

gneissic granite identified along the Bukit Tinggi Fault zone, which extends across Peninsular Malaysia's Main Range granite, preserves evidence for left-lateral motion along this fault zone (Gobbett and Tjia, 1973). The interpretation of left-lateral displacement along Bukit Tinggi Fault zone-Mersing Fault zone is shown in Appendix 14.

Hutchinson (1992, 1996) has also suggested the possible importance of rotational deformation along northwest-striking faults associated with left-lateral motion in Peninsular Malaysia. However the magnitude and sense of the postulated rotation of fault blocks about vertical axes were uncertain and no further research (e.g. palaeomagnatic studies) have been pursued.

2.4.2 Geological Setting of Central Domain

The Central domain is characterized by the north-south trending Bentong-Raub Shear Zone which includes a wide range of different lithologies, including partially sheared metasandstone and metatuffite clasts set in a phyllitic matrix, olistostrome deposits of various different ages, and a Silurian to Permian schist unit. The olistolith consists mainly of limestone and chert. The youngest limestone olistolith dated from fossil assemblages so far is Early Triassic. Other non-olistostrome units such as metaclastic rocks, volcanics, chert and limestones have been dated as Ordovician to Lower Triassic (Tjia, 1989). A minor

occurrence of serpentinized mafic to ultramafic volcanic rocks in the assemblage was interpreted as having been derived from a submarine lava flow (Hutchinson, 1996).

2.4.2a Bentong-Raub Suture Zone

The north-south trending Bentong-Raub Suture zone has been identified as one of the significant features in the tectonic framework of Sundaland. This north-south trending line has been recognized part of a former plate boundary extending from Yunnan province (Huang et. al., 1984) towards Thailand and Peninsular Malaysia (Hutchinson, 1971a). Hutchinson (1987a, 1996) has inferred that the suture records the closing of the Paleo-Tethys Ocean during the major Indosinian orogeny; closure probably occurred no later than the Middle Triassic. The suture zone is up to 18 km wide and extends for approximately one hundred kilometers down the centre of the Malay Peninsula (Figure 2.6 and 2.7). It comprises interleaved units of schist or phyllite, with sheared quartz lenses, olistostromes, clastic (chert and carbonate) diamictite, tuffaceous phyllite and basalt (Tjia, 1998a). Mapping of the Karak Formation (also known as the Bentong Group) within the suture zone demonstrates the presence of sheared olistostromes with various lithologies that range from Lower Devonian to Carboniferous/Permian in age (Tjia, 1987). Outcrop studies of sheared porphyroclasts within the Karak Formation suggest there have been several

phases of movement along the Bentong-Raub suture zone, including down to the east, normal dip-slip and southeast-directed oblique extension with possible right-lateral motion along the Bentong Suture (Tjia, 1987).

The Bentong Suture appears to extend northward towards Thailand and also southward towards Melaka (Figure 2.7). Hamilton (1979) proposed that the Bengkalis Trough may represent the southward continuation of the Bentong Suture in Central Sumatra, i.e. across the Strait of Melaka, a proposal supported by subsequent field studies (Tjia, 1989).

2.4.2b Bentong-Raub Suture Zone correlation to Bengkalis Trough, Sumatera

Structural investigations carried out along the Bentong-Bengkalis suture have concluded that the Bengkalis trough has been subjected to regionally-significant tectonic extension during Late Cretaceous to Early Tertiary times, which resulted in the development of localized basins with north-south trending boundary faults (Tjia, 1998). These north-south trending faults are referred to as the "Meridian-Parallel" fault set, and are prevalent throughout Sundaland; it is believed to represent the oldest mapped fault set within the region (Tjia, 1998). A younger set of northwest-striking faults has been interpreted to have developed post-Triassic, following closure of the paleo-Tethys Ocean. The region was

suggested (Tjia, 1989a), to have subsequently experienced regional NE-SW compression during the Early to Late Cretaceous. Tjia (1989b) suggests that this compression event gave rise to tensile fractures and faults oriented parallel to the regional compression direction mainly observed in the Miocene/Pliocene sequence and may extend to shallow basement unit in the Malay Basin.

The youngest phase of deformation identified in Central Sumatera occurred during the Pliocene, which resulted in the development of NW-SE trending strike-slip faults that displaced the pre-existing north-south faults in a dextral sense. Evidence for dextral strike-slip motion can be observed along the Lalang Fault zone, located to the north of the Bengkalis Trough (Tjia & Zaiton, 1985; Tjia, 1989) (Figure 2.6 and 2.7).

Observations in onshore Peninsular Malaysia suggest that the development of northwest-striking, major fault-controlled localized basins (e.g. the small Tertiary coal basins) was associated with an Early Tertiary transtensional event; such evidence is prevalent within the West Domain (Mahendran et. al., 1991, IRS Malay Basin, 2005).

Right-lateral strike-slip motions observed along major faults in Peninsular Malaysia were interpreted by previous workers to reflect the N-NE orientation of the maximum compression direction during the Miocene/Pliocene. This has not been identified unequivocally in onshore areas, except along north-striking

Kelau-Karak strike slip fault located in the north of the zone (Figure 2.6), which displays 5 to 10km, post-Cretaceous right lateral displacement in the Central domain (Jaafar Ahmad, 1995; Khoo, 1968; Tjia, 1972, 1989; Shu, 1971). However, the right-lateral movement along Kelau-Karak fault has also been attributed to the effects of pluton emplacement during intrusion of the Main Range granite (Table 4). This issue can only be resolved once radiometric dating has been carried out along this fault to confirm its origin and timing relative to peninsula granite emplacement (*personal discussion with Tjia, H.D.)*. Other northwest striking strike-slip faults in the peninsula display evidence for left-lateral displacement, where the youngest dated slip motion occurred in the Late Eocene, based on radiometric age dating of mylonite from Bukit Tinggi Fault zone (Tjia & Zaitun, 1985).

In the Malay Basin, evidence for Miocene compression is widely observed in offshore areas. This evidence includes the development of east-west trending folds and thrust faults in the Eastern and Central Zones (Figure 1.7). Observations from the Malay Basin in general and the Tenggol Arch in particular suggest that the compressional deformation continued until Pliocene times. Clear examples of reactivation of the Miocene fault system can be seen to offset seismic marker horizons equivalent to Lower/Upper Pliocene age rocks (Figure 2.4a-d). The structural grain observed within Pliocene strata of the Malay Basin shows dominantly north-south trends in the central basin, with more northwest-southeast trends becoming pervasive towards the Western basin margin.

To summarize, Sumatera, the Straits of Melaka and the West Domain of the Peninsular Malaysia probably comprise a single, coherent tectonic unit that was assembled during the closure of the paleo-Tethys Ocean and later experienced regional Miocene compression, as did the Malay Basin (Tjia & Zaiton, 1985, Tjia, 1989). However, despite the evidence for compressional deformation in the Miocene/Pliocene sequence in the central basin, the West and South margins of Malay Basin (which includes the Tenggol Arch) display predominantly extensional regime with north-northwest striking normal faults are pervasive over the arch. Due to these complex structural styles, previous regional studies which suggested regional compressional event have not able to fully explain the present-day structural style. Therefore an alternative kinematic model will be pursued in this study. This study will try to test the possibility that a transtensional model can explain the complex present-day structural styles in the basin (Chapter 4).

Although Sundaland behaved as a single "tectonic block" during Miocene to Pliocene times, fault reactivation and basement inheritance are likely to have played a key role in controlling the structural geometry and kinematics of the region. In offshore areas, the mechanical properties of the thick Tertiary clastic sequences are also likely to have been an important influence on the structural evolution of the Malay Basin. For instance, the presence of thick, possibly mobile, shale sequences (Figure 2.4b and Figure 2.4d) could potentially act as a

decollement surface between the basement complex or Late Oligocene and Miocene successions. The presence of such a weak basal of a decollement /detachment surface was suggested as a contributing factor in transition of stress and shear (Bonini, 2007) which will give rise to distinctively different fault patterns in Early Tertiary and Miocene. Strata (see section 3.3.2). Hence, the variations in structural styles observed between the Malay Basin, Tenggol Arch and Peninsular Malaysia may be due to some combination of basement inheritance, fault reactivation and/or the mechanical properties of the basin fill. An interpretation and discussion on the effects of a possible detachment shale layer on the structural pattern of Tenggol Arch will be further discussed in Chapter 3.

2.4.3 Geological Setting of East and Southeast Domain

The East domain extends over an area from north Kelantan to south of Johore, and is characterized by north to northeasterly striking fault zones with north-south trending faults found mainly in the north at Kampung Buluh-Ping Teris, Terengganu (Appendix 6). The northwest-southeasterly trending Lepar and Lebir Fault zones displaced the Carboniferous to Cretaceous rocks in a left-lateral sense by 20 to 40 km In the southern part of the East domain, the Mersing Fault zone trends northwesterly-westerly and displays a sinistral offset in Permian to Cretaceous rocks of 20 km (Appendix 14).

2.4.4 Microcontinent rotation in Peninsular Malaysia

Paleomagnetic studies of Paleozoic rocks from Peninsular Malaysia and Thailand that lie within the Sibumasu block (part of the Gondwana terrain) (Figure 2.7) and the Indochina block (part of the Laurasia terrain), suggest that clockwise rotations of crustal blocks occurred as far south as Langkawi island located just to the north of the west coastline of Peninsular Malaysia (Attachment 4; Ritcher and Fuller 1996). There is evidence suggesting both clockwise and anti-clockwise rotations occurred in the area south of Langkawi Island, whilst anti-clockwise rotations are dominant in Borneo (Fuller et. al., 1991). These findings suggest that the southern part of Peninsular Malaysia marks a transitional zone between clockwise rotated blocks to the north and anti-clockwise rotated blocks to the southeast and towards eastern Borneo (Ritcher and Fuller, 1996). This interpretation also supported by Southeast Asian Cenozoic plate reconstructions, which suggest that Peninsular Malaysia did not act as a single rigid block during possibly the Cretaceous to Paleogene (Hall, 1998, 2002; Fuller et. al., 1991).

2.5 Geological Setting of Tenggol Arch

As described above, the Malay Basin is of continental origin, being floored by basement rocks equivalent to those that crop out in the East Domain of Peninsular Malaysia. Radiometric dating of rock samples from deep exploration wells suggests that the ages of basement rocks on the Tenggol Arch and in the Malay Basin range from Carboniferous to Permian or older. The rocks comprise mostly phyllite and metaquartzite rocks which are unconformably overlain by continental slope deposits (conglomerate, sandstone and argillaceous members). The slope deposits, which are of Permian age are inferred to have been deposited along the margins of basement lows in the Malay Basin and Tenggol Arch.

2.5.1 Pre-Tertiary deposition environment over Tenggol Arch

The depositional environments within the Malay basin and Tenggol Arch during the Carboniferous (or older) to Permian are interpreted to have been continental. Subsequently, the depositional setting of the basin gradually changed to a marginal marine or inner neritic environment during Permian to possibly Triassic or Jurassic times[6].

[6] Interpretation based on fossil assemblages of Peninsular Malaysia, Malay Basin and Peninsular Thailand (Rucha Ingawat-H, 1993).

Most areas of Sibumasu (i.e. regions of Gondwana affinity) were subjected to marine to shallow marine conditions during Late Permian to Triassic times. This interpretation of a marine environment was based on sedimentological studies of the Semanggol Formation in Peninsular Malaysia, which indicates deep a marine fan and sub-marine environment (Hutchinson, 1996).

Prior to docking along the Bentong-Raub Suture Zone, the region once again become more continental (Hutchinson, 1996) and continental deposits of Jurassic to Cretaceous age are prevalent in Peninsular Malaysia, including the Gagau Formation of the Tembeling Group (Appendix 9). Southeast Asia and the Malay Basin in general are believed to have experienced low humidity conditions from Cretaceous until Paleogene times (Morley, 1998), based on interpretation of humidity using patterns of Tertiary plant dispersal over the region.

The Malay Basin and Tenggol Arch areas remained continental throughout this period, with sediment deposition focused within localized basement lows of possible lacustrine environments (PRSS, 1997; IRS Malay Basin; PETRONAS, 2006(b))[7] (Appendix 2 and 3a). Cooling of the inferred mantle plume during the Early Tertiary caused gradual thermal subsidence, providing the continuous development of sediment accommodation space possibly until the Oligocene. The Tenggol Arch appears to have remained a basement high during this period, based on the apparent absence of Early Tertiary sediment on the Tenggol Arch

[7] Unpublished internal reports; Regional Study of Malay Basin (PCSB, 2006(b)) and Well Biostratigraphic Analysis Report (PRSS, 1997).

(Appendix 1). Deep exploration wells on the Tenggol Arch have confirmed that the Paleozoic to Cretaceous basement complex on Tenggol Arch is consistently overlain by Late Oligocene to Early Tertiary lacustrine to marginal marine clastic deposits (Figure 2.4b and Figure 2.4d).

2.5.2 Tertiary marine incursion in the region of the Tenggol Arch

A second marine incursion in this region occurred during the Late Oligocene, as shown by the presence of arenaceous foraminifera samples recovered from wells situated near the southern and southeastern margins of the Malay Basin (PRSS, 1997). Miocene sediment was continuously deposited throughout the basin, and conformably overlies the Tenggol Arch, as has been consistently proven in wells drilled in the area. Findings from basin analysis suggests that basin sag occurred prior to the Late Oligocene and continued until Late Miocene/Pliocene times, punctuated by a regional compression events during the Middle to Late Miocene (Khalid et. al., 1996). Regional mapping demonstrates that shortening was accommodated by the development of east-west trending folds within intra-Miocene strata along major north-south trending fault zones (Figure 2.1; IRS Malay Basin; PETRONAS, 2006 (b)).

The east-west trending folds created localized depressions at the flanks of the anticlines, within which syn-deformational sediments were deposited.

Interpretation of syn-deformational sedimentation has been supported by observations of channel facies along the flanks of anticlines, with finer grained facies deposited towards the centres of synclines as observed along RC93 regional 2D seismic lines (Appendix 2). Peak regional compression, as inferred from the youngest unconformity in the basin, occurred during the Late Middle Miocene. This unconformity can be mapped throughout basin and is known as the sb1900 marker (IRS Malay Basin; PETRONAS, 2006 (b)). Strong folding is predominant in the central and eastern areas of the basin, but gradually dies out towards the western margin of the basin with less influence along the Western Hinge Fault Zone. Following the Miocene compression, major faults were reactivated during Upper Early Pliocene to possibly Late Pliocene deformation and appear to have propagated upwards to offset the sb1200 marker[8].

2.5.3 Pre-Cenozoic: Early structure of Tenggol Arch

Hutchinson (1996) attributed the early structural development of the Tenggol Arch and Malay Basin to the Indosinian orogeny during the Paleozoic to Early Mesozoic (Middle to Late Triassic) which resulted from collision between the Sibumasu and Indochina blocks. Later study by Tjia (1998) has suggested the orogeny were subsequently rotated 20^0 to 33^0 clockwise[9] during the Cenozoic, thus giving rise to the present-day north-south trending "meridian-parallel" faults.

[8] Similar structure events an be map on the Tenggol Arch at equivalent stratigraphic marker, Ta_1

[9] A 20 to 30 degree clockwise rotation was documented in paleomagnetic study of Mesozoic rocks over Mayanmar-Thailand and in the northwest part of Peninsular Malaysia (Richter & Fuller, 1996).

These north-south trending faults should be no younger than Middle to Late Triassic, which was the age of final docking along the Bentong-Raub Suture (Tjia, 1989, 1998). Following the collision, a series of southeast-striking faults were generated and are prevalent across Peninsular Malaysia (Hutchinson, 1996) and the Tenggol Arch area. The northwest-striking faults cut Triassic to Cretaceous rocks in Peninsular Malaysia and mostly extended into the Main Range granite. This implies that the northwest-striking faults are post-Triassic/Cretaceous (Figure 2.6). Hence, it can be concluded that in general, north-south and northwest-striking faults are the earliest faults formed in the region of the Tenggol Arch and Malay Basin.

During the Jurassic to Cretaceous, there was increasing magmatic activity in the region, peaking in the Late Cretaceous based on the presence of Cretaceous granitoids in offshore areas (Figure 1.3). Magmatism during the Cretaceous was associated with regional uplifts and attenuation of continental crust prior to the collision of Sibumasu[10] with Indochina that initiated opening of the Malay Basin and neighboring basins (Tjia, 1998; Khalid et. al. 1996).

Following Cretaceous to Late Cretaceous rifting, the Malay Basin and Tenggol Arch are believed to have undergone wrench modification similar to movements observed along the Three Pagodas Fault Zone which indicates dextral motion during Early Tertiary/Paleocene times (Lacassin et. al., 1997; Rhodes et. al.,

[10] The Sibumasu block (Gondwana affinity) was described by Metcalfe (1984a, 1986) - it is also known as Sinoburmalaya (Gatinsky & Hutchinson, 1984). It is a continental block which includes Yunnan, Burma, Western Thailand and Peninsular Malaysia.

2004). The wrench possibly contributed to development of rhombic basement lows in both the basin and Tenggol Arch (Figure 2.2).

2.5.4 Cenozoic: Regional compression and wrench modification

Regional structural mapping of Early Miocene and Middle Miocene markers in offshore areas, including the Malay Basin and Tenggol Arch, suggest that the area is highly segmented by major north-south and northwest-southeast trending fault zones (IRS Malay Basin; PETRONAS, 2006 (b)). The presence of left stepping en-echelon faults trending northwest-southeast and approximately east-west trending anticlines in Miocene strata suggest that the basin has experienced dextral wrench motions along its major fault zones. The dextral deformation seems to be more persistent towards centre of basin and gradually lessens towards the western flank and the northwest-southeast trending Western Hinge Fault Zone.

It has previously been suggested (IRS Malay Basin; PETRONAS, 2006(b)) that lateral displacements during Middle Miocene times within the Malay Basin were driven by tectonic "extrusion" of Southeast Asia away from the Australia-India plate collision with Eurasia. This should cause fault blocks (in the Central and Eastern zones) to migrate south and southeastward (Figure 1.2). However, mapping over the Terengganu Platform and Tenggol Arch (IRS Malay Basin)

indicates extensional structure styles, which suggested that the arch and platform were potentially relatively rigid in comparison to central Malay Basin (Figure 1.2 and Figure 1.7). The IRS Malay Basin regional study also suggested that the Eastern zone experienced the greatest magnitude of southward migration along the Laris Fault zone (Figure 1.7). This interpretation was based on the pronounced development of east-west-trending folds and thrust faults in the Eastern zone. The folding becomes more subtle towards the West margin of the basin and is increasingly limited to fault-dependant folds with axes oriented parallel to major fault planes (Figure 1.7).

Isochore maps of the Malay Basin (IRS Malay Basin, 2005) have shown that the Eastern zone contains the thickest sediment accumulations, with high shale to sand ratios in the Miocene sequences. In contrast, the Western zone becomes increasingly sandy and sequences gradually thin, eventually wedging-out over the western flank of the basin (Appendix 7). Cross-sections across the basin illustrate that folding occurs mainly within areas characterized by high shale to sand ratios and greater sediment thicknesses. Hence most major anticlines are developed in the Eastern and Central zones of the basin. In areas where sediment thicknesses and shale to sand ratios are low, reverse fault movements are more typical, with normal faults becoming prevalent toward the basin flanks (Appendix 2 and Appendix 7).

Observation from seismic sections across the the basin, depicts distinctive folding in Tertiary sequence is consistent with presence of thick shale strata in the basin. However, there is no analogue model that demonstrates high shale content layer (ductile layer) contribution to formation of folds, although study by Bonini (2007) suggested that coupling of ductile and brittle layers prone may cause slip or fold formation between coupling layers. His study also indicates condition of decollement or detachment layer will distinctively resulting in complex structure styles.

Dextral motion along the Tenggol Fault Zone of the Tenggol Arch and Western Hinge Fault Zone has been suggested based on the development of a series of left stepping short-lived en-echelon faults in Miocene strata (Figure 1.7). The presence of ellipsoidal sub-basins at basement level in the region of the Tenggol Arch may also be related to wrench movements during the Early Tertiary (Figure 2.2). Possibly equivalent age events have been identified in Peninsular Malaysia (Table 2a). If the regions have experienced a similar history, then the Tenggol Arch should have experienced regional compression during the Cenozoic northward advance of the Australia-India as it collides with the Eurasia plate.

2.6 Summary and Conclusions

From the foregoing account, it appears that there are good reasons to believe that the basement complex of the Tenggol Arch region offshore is stratigraphically correlateable to equivalent rocks exposed in onshore Peninsular Malaysia. The Tenggol Arch basement comprises predominantly argillaceous low grade metasediment, mostly phyllite with minor metaquartzite lenses and limestones equivalent to similar formations found in the Kuantan Group and Dohol Formation onshore. As a result, the age of basement complex of the Tenggol Arch is most likely to be Carboniferous to Permian.

Emplacement and eruption of igneous rocks on the Tenggol Arch occurred during the Mesozoic, with peak magmatism during the Cretaceous being associated with basin opening in Malay Dome region (i.e., initiation of the Malay, Penyu and West Natuna basins). Evidence of plutonic and volcanic igneous activity can be observed onshore in Peninsular Malaysia and from wells drilled in the Tenggol Arch region (Figure 1.3). These igneous bodies can be distinctively identified in seismic sections from their characteristic seismic facies variation (Figure 2.4a; Chapter 3).

Igneous rocks in the East Domain of Peninsular Malaysia are dominantly Permian to Late Triassic (Figure 2.6 and Table 4), but Post Triassic intrusive igneous rocks include the Bukit Labohan dolerite dyke and sill swarms that are

most likely to be equivalent to Cretaceous dolerite and igneous bodies seen in the M-field offshore.

Figure 1.3 illustrates other basement cored wells in the basin, and the type of basement rock found. Though radiometric age dating has yielded mainly Cretaceous ages, meta-tuffite layers from the S-field are older and appear to be associated with Permian to Triassic volcanic activity recorded onshore in Peninsular Malaysia

In general, major faults and structural lineaments recognized in Peninsular Malaysia can be extended offshore onto the Tenggol Arch using bouguer gravity anomaly maps. Major structures include the Lepar and Lebir Fault Zones, the Mersing Fault Zone and the Ping Teris Fault Zone (Figure 1.3).

The next chapter focuses on the stratigraphic - structural interpretation and analysis of the Tenggol Arch and its relation to the Malay Basin. 3D seismic acquired in the study area in 2004 will be interpreted and an analysis of faults folds and fractures will be carried out based on interpretation of multi seismic attributes.

3.0 Study Area and Geophysical Methods

The Tenggol Arch is characterized by a Carboniferous-Permian or younger basement complex, which separates the Malay Basin from the Penyu Basin to the south (Figure 1.1). The structure of the arch is dominated by the NW-SE trending Tenggol Fault zone, which is characterized by the development of isolated pull-apart basins in its hanging wall (Figure 2.2). A total of 10 exploration wells have been drilled within the area, with Miocene sandstones as the primary targets. Wells drilled into the basement complex have typically penetrated low grade metamorphic (phyllite) and intrusive igneous rocks. A few wells drilled at the northern margin of the Tenggol Arch penetrated Mesozoic limestone.

Three oil fields are present within the study area, with the main producing hydrocarbon reservoirs mostly being located in Early to Middle Miocene strata. However some wells indicate the presence of oil shows in the basement complex. The field locations and data coverage are illustrated in Figure 3.1. The M-field has encountered an oil show in a fractured dolerite basement, whilst the A-field encountered oil in fractured phyllite.

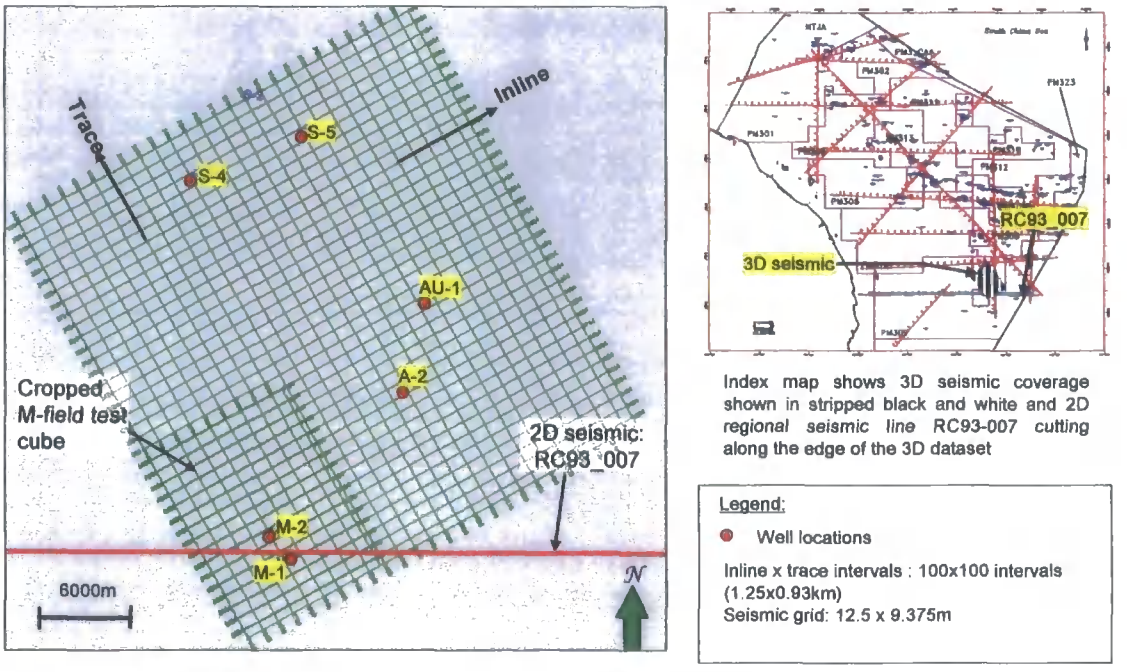

Figure 3.1 3D seismic basemap of the Tenggol Arch study area which covers an area of approximately 400km^2. The data includes 6 exploration wells from three fields, namely the M-, A- and S-fields. Inset map shows the location of the 3D seismic data and the RC93_007 line in relation to the regional seismic data for the entire Malay Basin.

3.1 Database

The detailed structural analysis presented here uses a 400 km^2 3D seismic dataset that covers an area straddling the eastern margin of the Tenggol Arch (Figure 3.1). The average water depth is 70m with a fairly flat and uniform seabed, apart from the occasional presence of recent seafloor channels. Some man-made obstructions (oil platforms and Floating Processing and Storage Operating (FPSO) units) have restricted seismic data acquisition within the northern and southern parts of the study area (see sections 3.1.1 & 3.1.2). Additional data included in this study are 2D regional seismic lines through the

M-field, together with cores, cutting samples and biostratigraphic data from well completion reports. The Bouguer anomaly map of Malay Basin and satellite images of Peninsular Malaysia from the 2005/2006 IRS of the Malay Basin have also been used, together with the results of previous field studies carried out in the East Domain of Peninsular Malaysia.

3.1.1 Seismic Data

The 3D pre-stack time migration (PSTM) seismic data utilized in this project was acquired in 2004, prior to the discovery of oil in fractured metasediment (phyllite) in the hanging wall of Tenggol Fault zone (TFz). The 3D marine seismic acquisition was designed to image major faults in this area, with the primary reservoir targets being basement at 1.6 to 2.5 s two-way travel time (TWT) and Miocene coastal plain plays at 1.0 to 1.5 s TWT. The acquisition and processing details are shown in Appendix 4.

High frequency data are preserved at shallow levels. Frequencies of 120Hz with 72db/oct slope are preserved between 0 and 1 s TWT below the seabed, and 100Hz with 72db/oct slope between 1 and 2 s below the seabed. Lower frequency ranges were preserved at deeper levels: 70Hz at 2.0 to 3.0 s, 50Hz at 3.0 to 4.0 s and 30Hz at 5.0 to 6.0 s (e.g. of seismic sections as in Figure 3.2a-c). The higher frequencies were intended to image Miocene channels and fluvial

systems on the Tenggol Arch. Although the Miocene channel sand beds are fairly thin, (ranging from 10 to 15 meters or occasionally 18 to 20 meters gross thickness), these data have allowed prospecting for stratigraphic plays within Miocene strata. The reservoir thickness range was proven and consistently observed along the Western Zone of Malay Basin by exploration wells drilled in the region.

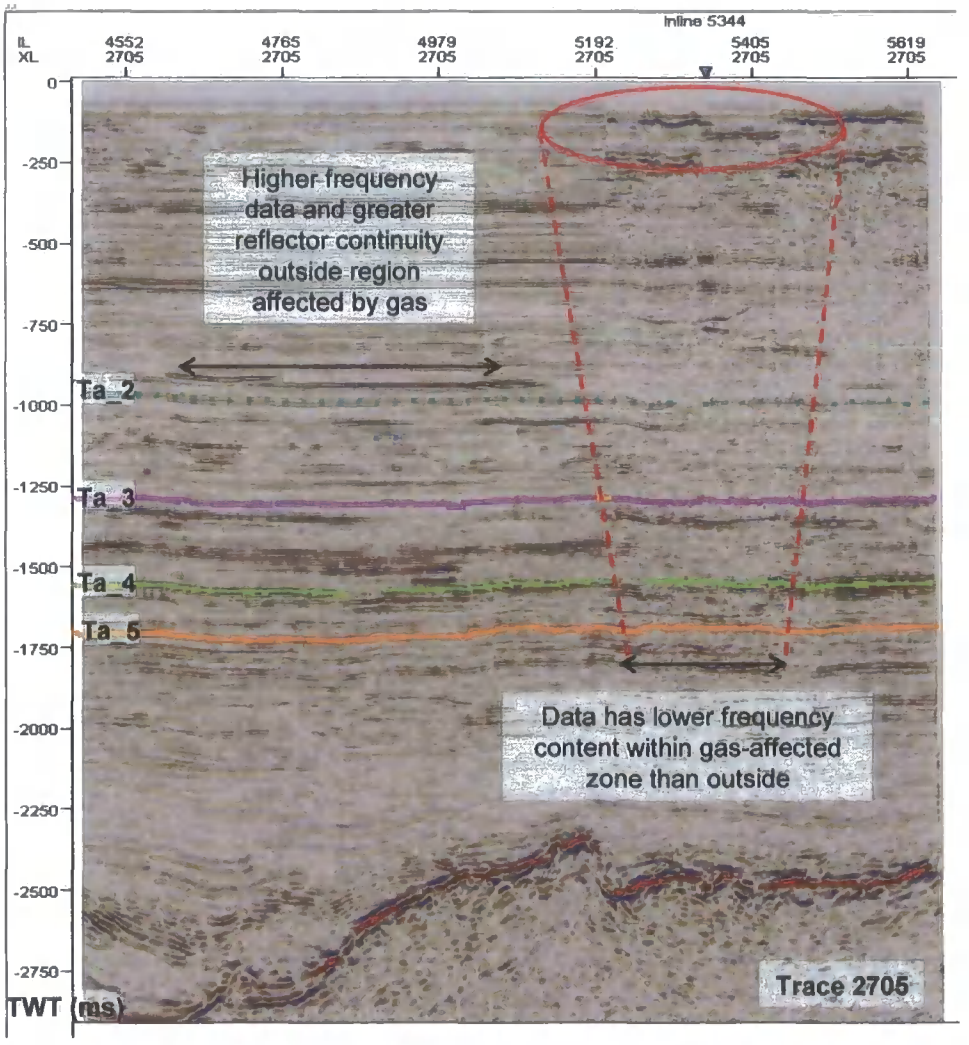

Figure 3.2a Seismic section along Trace 2705 highlighting the interpretational uncertainties due to the presence of gas and shallow channels in the area (circled in red). Gas chimney-effect within the dashed lines causing distorted and poorer fault and seismic markers imaging.

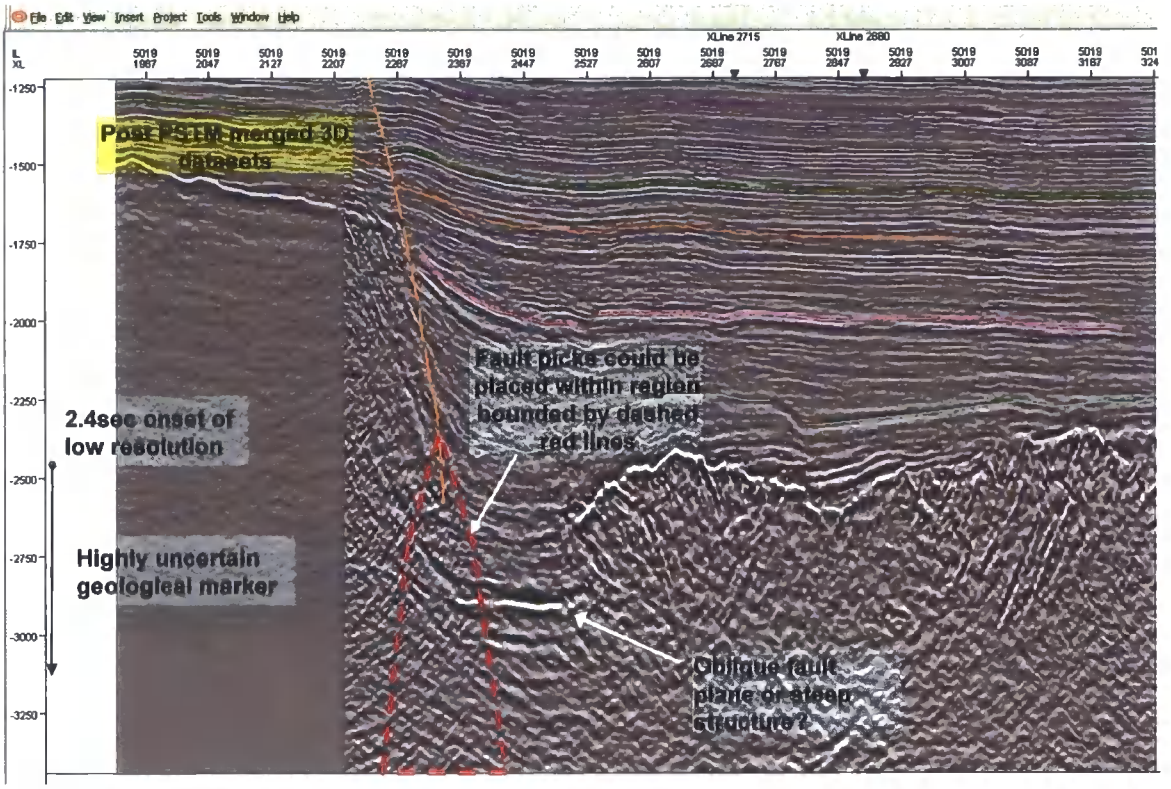

Figure 3.2b Seismic section along inline 5019 highlighting the increased uncertainty in fault interpretations with increasing depth.

The 2004 3D seismic was shot with a southwest-northeast sail line. This direction is at right angles to the Tenggol Fault zone, but is oblique to faults within the AU-1 and A-fields (Figure 3.3a). Fault imaging within these two fields is of moderate quality becoming poorer at deeper levels (Figure 3.2b). There are some occurrences of gas-bearing channels at shallow depths from the seabed to less than 100 milisecond. The gas-bearing channels give rise to prominent chimney effects in some parts of the data. However time- and space-variant inverse Q filtering was not applied in the processing, resulting in amplitude and phase inconsistencies within the gas chimney zone. Amplitude and attribute extraction

within gas chimney zones will therefore be distorted and poorly normalized. Thus, amplitude-based interpretations need to be done with caution as the images may indicate either true geological features or geophysical artifacts.

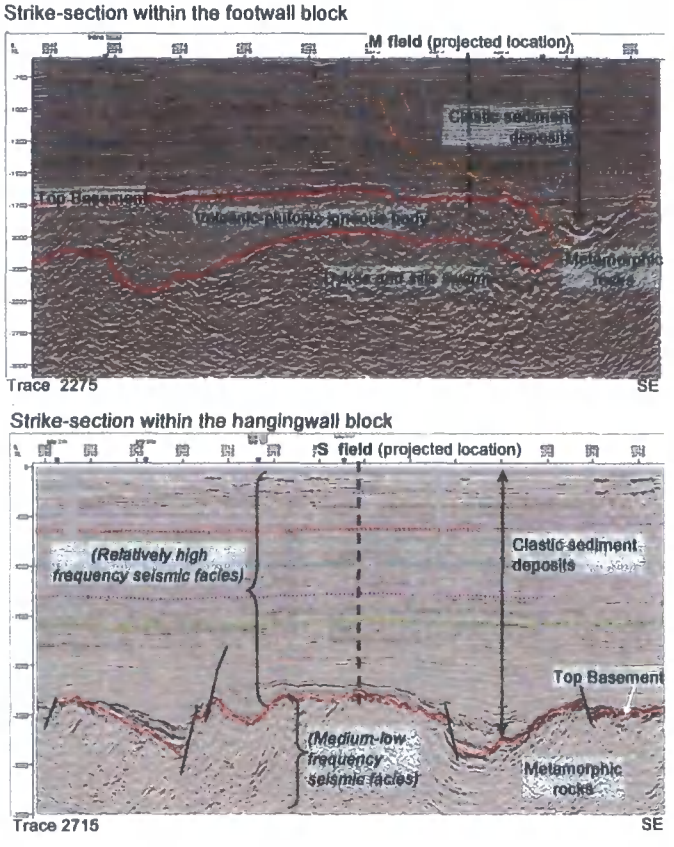

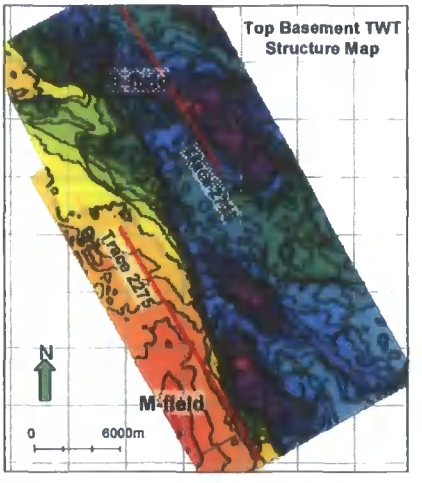

Figure 3.2c 3D seismic sections in the up-thrown (top left) and down-thrown (bottom left) blocks of the Tenggol Fault. Locations shown on the Top Basement time structure map (below). Sections are oriented approximately parallel to the strike of the Tenggol Fault. The Top Basement marker shows fairly low relief where it coincides with the top of the inferred volcanic-plutonic body along much of the footwall section. The relief increases where the Top Basement marker coincides with the top of the metasedimentary unit within the hangingwall section and at the SE end of the footwall section.

Shallow channels, which also cause ray path distortion and static problems occur within the data (Figure 3.2a). Interpretation of Miocene channels within the 1.0 to approximately 2.0 second window should be done with caution. However, the top basement marker will only be affected by gas chimney effects where it is shallower than 2.5 second.

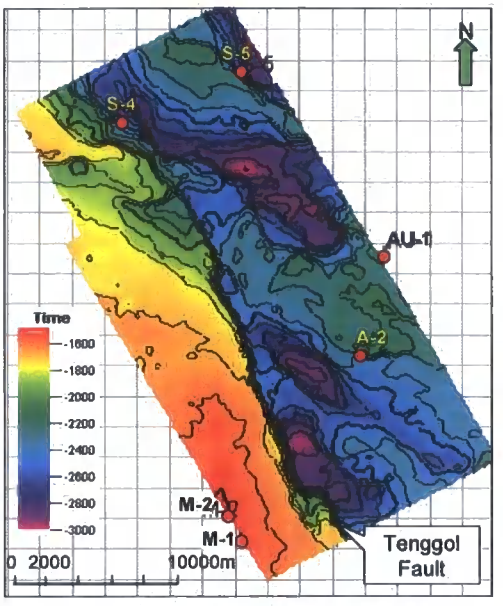

Top Basement TWT Structure Map of cropped study area.

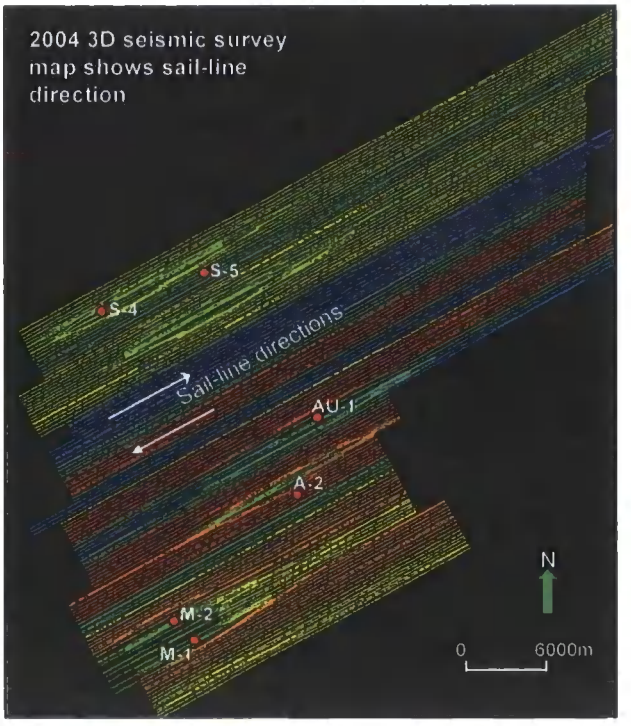

Figure 3.3a The map on the right shows the seismic acquisition sail lines, which are oriented at right angles to the NW-SE trending Tenggol Fault (seen in the time structure map of the Top Basement marker, left), but oblique to the WNW-ESE trending faults associated with the A- and S-fields situated in the hangingwall of the Tenggol Fault.

Two satellite platforms and an FPSO were the main obstructions during acquisition, where undershooting was done to minimize data loss. Minor occurrences of high swells of 3 meters or more and fishing activities resulted in some missing traces in the data. Missing data interpolation was carried out and surface static correction was done during pre-processing.

3.1.2 Seismic interpretation Uncertainties

The Pre-Stacked Time Migrated 2004 3D seismic dataset was merged with the earlier M-field 3D dataset acquired in 1990's (Figure 3.2a and 3.2b) in order to achieve a complete image of the study area. The merged data have been corrected for time shift, and amplitude balancing was applied. However, the earlier dataset primary targets were shallow Early to Middle Miocene reservoirs located at 1.0 to 1.5 seconds so that seismic acquisition and processing were focused on this zone. As a result, not much interpretation can be carried out below the top basement marker. This post-merged data covers approximately 40 percent of the M-field at basement level and deeper.

Data loss occurred towards the eastern edge of the S field due to the presence of oil platforms. Undershooting was done during acquisition to minimize data loss, but shallow sections from the seabed to 1.0 second are still unrecovered. Data-loss due to offshore obstructions affected only approximately 20 percent of S-field area.

4.8 km cable length was used for the 2004 3D seismic acquisition to achieve good data resolution down to 2.4 to 3.0 seconds, with acquisition bins at 6.25 by 18.7 meter grids designed to properly image variations in fault plane geometry and orientation. The seismic resolution gradually deteriorates below 3.0

seconds, which can be consistently observed in all seismic sections (Figure 3.2b). The data are therefore suitable for seismic interpretation of fractures on the up-thrown side of the Tenggol Fault, where the top basement marker ranges from 1.6 to 1.8 seconds TWT (Figure 3.2b and 3.2c). However, on the down-thrown side, where the top basement marker ranges from 2.3 s to deeper than 2.8 s TWT, poorer data resolution is to be expected at top basement levels and below due to natural signal attenuation. The interpretation of the bases of sub-basins along the Tenggol Fault was highly uncertain as this marker is likely to occur at around 3.0 second TWT or deeper (Figure 3.2b).

A 1km by 1 km grid was used to define the first level velocity model, which was used in the first pass NMO (normal move-out) migration of the dataset. A second level velocity model was generated from the first velocity cube using a 50 by 500 meter grid, which was later smoothed for second level NMO migration of the dataset. This information is crucial when interpreting fault segments and the base of sub-basins on the Tenggol Arch because seismic resolution and the dimensions of geological structures are closely inter-dependant. For instance, in the example given in Figure 3.2b, two closely spaced geological structures, represents closed geological intervals. If velocity sampling intervals over the closed intervals are larger, this will result in low resolution seismic imaging of the structures. Faults edges will be smoothed-out, meaning that the area within the closed interval is being under sampled in the sub-basins (Figure 3.2b); closely spaced parallel faults will also be below seismic resolution. Smearing or

scattered reflectors should be anticipated along basin edges where these types of structures are present. Thus, an understanding of the interpretational risks will later be one of driving factors in determining the best geological (static) model for the fractured basement in the present study.

In general, the uncertainties associated with the seismic interpretations carried out during the present study are as follows:

1) Fault segment, structure and seismic facies interpretation can be carried-out confidently in the shallow section above 2.4 second TWT. However in areas where gas reservoirs and gas chimneys are present, the quality of seismic data will be adversely affected by amplitude absorption below strongly reflective gas reservoirs. The presence of gas filled reservoir resulted in lateral variations in frequency within the strata. .

2) Signal attenuation at depths below 2.7 or 3.0 s TWT and deeper means that the interpretation of basement fractures on down-thrown fault blocks becomes less certain and more ambiguous.

3) Under-sampling of the velocity grid during seismic migration may occur in areas where geological structures are narrow or closely spaced.

Another important factor that must be considered in this study is the lithological variation of the basement complex. As pointed out in Chapter 2, it is clear that the Tenggol Arch basement complex is probably equivalent to rocks found exposed along the coast of the East Domain of Peninsular Malaysia. The

basement complex on the Tenggol Arch comprises of wide range of lithologies, but is dominated by argillaceous metasediments. Plutonic-volcanic igneous rocks are encountered in wells along the up-thrown block of the Tenggol Fault zone, with some carbonates along the northern margin of the Tenggol Arch. Therefore, in order to differentiate lithological variation, the seismic facies interpretation method was used to interpret the basement complex of the Tenggol Arch. The method and results of the seismic facies interpretation will be discussed further in the seismic interpretation chapter.

3.2 The Definition of Seismic Markers

The seismic markers used in this study were established by applying seismic sequence stratigraphic methods, where major sequence cycles were identified from the dominant seismic facies observed in each sequence. The correlation between the seismic markers and the regional sequence boundary (SB) markers is shown in Attachment 1 and Attachment 2. The age definition of these seismic markers was established by correlating the seismic markers with the Malay Basin regional markers (IRS Malay Basin, 2005) as shown in Attachment 3. The interpreted seismic facies and observed marker characteristics are shown in these attachments. The seismic stratigraphy, seismic facies and well log curve interpretations were based on the Exxon working model of Haq et al. (1987) and Prosser (1993).

3.2.1 Top Basement seismic marker (Attachment 2)

Definition: A major sequence boundary between Pre-Tertiary and Tertiary sequences, which is marked by an angular unconformity or possibly an indication of a hiatus.

The first horizon identified as a major sequence boundary was the top basement seismic marker, which appears as an angular unconformity separating the Tertiary strata and Pre-Tertiary strata. The seismic marker is characterized by a high amplitude and low frequency, and is highly continuous throughout the dataset. Strata below the Top Basement seismic marker are interpreted as belonging to the Pre-Tertiary basement complex. Top basement was confirmed in exploration wells of drilled within the M, A and S fields (*Well Completion Reports, unpublished*). Radiometric age dating of basement rock cutting samples and core suggests that the basement complex is of Cretaceous age or older.

The basement is characterized by highly variable seismic facies characteristics, which potentially reflect the heterogeneous lithology of the basement complex, a suggestion that is seemingly confirmed by exploration wells from the Tenggol Arch. The changes in seismic facies are clearly demonstrated in vertical sections (e.g. Figure 3.2c) and by near top basement time-slices (Figure 3.3a). Core

samples show that the M-1 and M-2 wells from the footwall of the Tenggol Fault penetrated a layer of volcanics and fractured dolerite dykes. The A-1 well in the hanging wall of the Tenggol Fault drilled into phyllite, which underlies Late Oligocene to Early Miocene sand-shale strata. The S-5 well drilled into possible Mesozoic carbonate, which also underlies Late Oligocene to Early Miocene sand-shale strata. All top basement markers appear as strong reflective surfaces characterized by a marked angular unconformity in seismic sections. The top basement seismic marker on the Tenggol Arch is likely to be equivalent to the top basement seismic marker of Malay Basin as a whole (IRS Malay Basin, 2005).

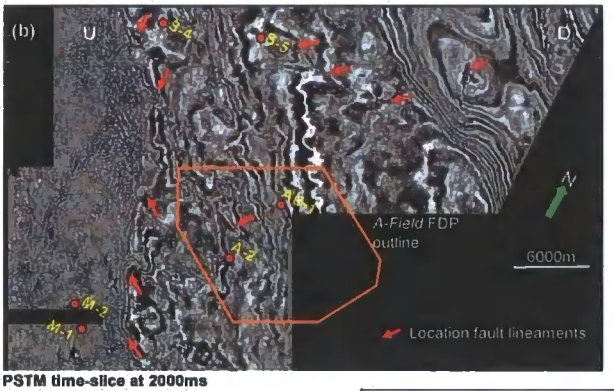

PSTM time-slice at 2000ms

Figure 3.3b The figure on the left showing data coverage of 2004 3D seismic. There is a large time different between upthrown (U) and downthrown (D) blocks, a timeslice within basement unit is selected to show general overview of the 3D seismic data quality, facies regime and fault lineaments. Red arrows indicate location of fault lineaments observed on the slice. The seismic facies of the upthrown block corresponds to igneous rocks which are penetrated by wells M-1, M-2. The downthrown corresponds to metamorphic rocks which are penetrated by wells AU-1, A-2, S4, S5. Brown polygon shows the location of Fig. 3.3c.

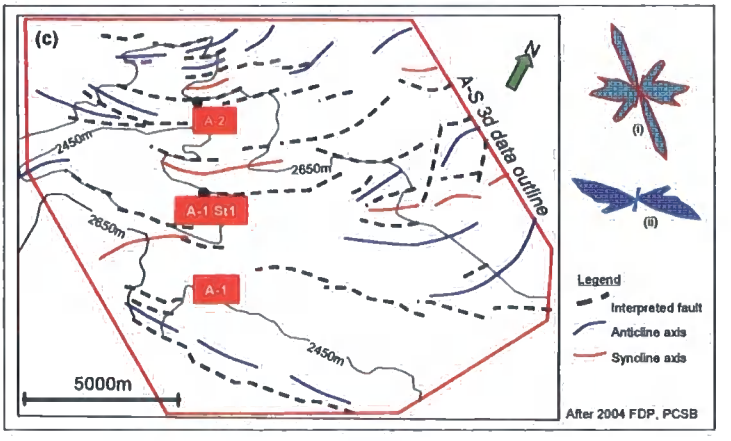

(c) Field development plan (FDP) map for the A-field showing the main structural elements (faults & folds) at Top Basement level in this area. (i) Rose diagram of fault orientations extracted from the 2330ms timeslice (2005 3D seismic survey). (ii) Rose diagram of fault orientations derived from the FDP map. WNW-ESE is the dominant fault trend in the A-field; the NNW-SSE trend is derived from the Tenggol fault, which lies to the west of A-field (not shown in the FDP map).

3.2.2 Top Synrift seismic marker (Attachment 2)

Definition: The top syn-rift seismic marker separates syn-rift from initial post-rift sequences and likely formed during a period of high sedimentation rate compared to subsidence rate (S. Prosser. 1993). The top syn-rift seismic marker on the Tenggol Arch is equivalent to SB100 (Late Oligocene) within the Malay Basin proper (see below; IRS Malay Basin, 2005). This marker appears to consistently abut along the edge of major fault zones and the sequence is characterized by dimmed reflectors with occasional high amplitude, low frequency discontinuous seismic reflectors within the sub-basins located on the Tenggol Arch.

3.2.2a Correlation of the Tenggol Arch Top Synrift marker with the Malay Basin

The deepest seismic marker interpreted in the Malay Basin is sb50 which has been mapped in the southern part of the basin and abuts against the eastern edge of the Tenggol Arch (Appendix 7). Although no well has penetrated the sb50 marker, stratigraphic considerations suggest that the marker should be of Paleogene age, and certainly no younger than Oligocene. The overlying sb100 marker is of Late Oligocene age, as defined from well data. Sb100 is consistent throughout the Malay Basin and can be mapped over the western margin of the

basin and onto the Tenggol Arch where the sequence appears as a transgressive systems tract in seismic sections. Therefore, sb100 strata are most likely to have been deposited in sub-basins along the western margin of the Malay Basin (Appendix 7). The transgressive systems tract is represented by a condensed section, which indicates a high shale content sequence that can be defined from seismic facies as continuous and dimmed seismic reflectors, as shown in Appendix 2 and 3a. The presence of a transgressive system tract is likely associated with an increase in sea level which would result in regressive coastline development from the Late Oligocene to Upper Early Miocene.

The `top-synrift' seismic marker on the Tenggol Arch is equivalent to sb100 when correlating with the Malay Basin proper. This seismic marker was also defined as the flooding surface of the syn-rift sequence or the immediate post-rift systems tract (Prosser, 1993). Age dating from pollen and palynomorph samples from sb100 cutting samples demonstrates that the strata are of Late Oligocene age. The flooding surface appears consistently throughout the basin and abuts along Tenggol Fault zone (Appendix 7). The syn-rift or sb100 strata mostly occur within the sub-basins observed along the hanging wall of the Tenggol Fault zone and within the Western Zone of the Malay Basin.

3.2.3 Oligocene Strata seismic marker (Attachment 2)

A Late Oligocene interval was defined by the Ta_6 seismic marker, which consistently appears in all deep exploration wells (total depth 2000m or deeper) and is equivalent to the sb200 marker in the Malay Basin (IRS Malay Basin, 2005). The sequence has a wedge-shaped geometry; the thickest sedimentary sequences occur mainly within the sub-basins in the hanging wall of the Western Hinge Line and Tenggol Fault zone (Figure 2.1). This seismic facies comprises medium to low amplitude, medium to low frequency and primarily parallel to sub parallel seismic reflectors and a wedge-shaped sediment package. Onlap markers can be clearly defined in some sections. The seismic characteristics (Appendix 2 and 3a) of this package suggest a coastal to shallow marine depositional environment. This is supported by the recognition of a Late Oligocene marine incursion recorded by the presence of foraminifera found in wells located on the southern and northern margins of the Tenggol Arch. (PRSS, Biostratigarphy Report, unpublished)

The Ta_6 seismic marker appears basin-wide, but is difficult to interpret towards the eastern margin of Tenggol Arch due to the poor resolution and low seismic amplitudes, possibly caused by high amplitude reflections located at shallower levels overlaying the Ta_6 strata (Attachment 2). In some areas around the M field, the strata appear to correlate across Tenggol Fault zone and to on-lap onto the M-field basement high. The presence of onlapping seismic reflectors onto

the top basement reflector is consistent throughout the seismic data and was interpreted with a high degree of confidence (Figure 2.4b and Figure 2.4d).

A biostratigraphic study of Oligocene sediments penetrated near the M field indicates a coastal to shallow marine depositional environment (Figure 1.3). The Ta_6 sequence was therefore interpreted as being transitional between continental lake deposits in the syn-rift, to marginal marine or shallow marine within the Late Oligocene and Early Miocene post-rift strata.

3.2.4 Intra-Miocene Strata seismic markers

Miocene intervals are represented by the Ta_5 to Ta_2 seismic markers, where Ta_5 is equivalent to the sb1000 marker (Late Lower Miocene), Ta_4 is equivalent to the sb1200 (Middle Miocene), Ta_3 is equivalent to the sb1900 marker (Late Middle Miocene) and Ta_2 is equivalent to the SB2000 (Upper Miocene).

The Ta_5 marker drapes over M field basement highs and is regionally extensive towards the northern margin of the Tenggol Arch. Throughout the area, seismic sections indicate fluvial environments with evidence of channel facies inter-layered with flood plain facies. The channel facies is characterized by medium to high seismic amplitudes, discontinuous basal reflectors, which probably

represent scours and are intermittently overlain by continuous medium to high amplitude parallel reflectors. The flood plain facies is characterized by medium to low amplitude, parallel continuous reflectors.

The flood plain facies appears to have a fairly uniform thickness throughout the dataset for every seismic sequence. In contrast, the fluvial facies shows variations in stratigraphic thickness for each sequence. Therefore for intra-Miocene strata, the seismic marker was picked at the top of the channel facies marked by a flooding surface. These seismic markers are better preserved and easier to populate throughout the data set compared to those developed at the base of channel facies. These markers also held less possibility of sediment loss due to erosion activities. All intra-Miocene seismic markers are continuous and consistent throughout the dataset, albeit with localized changes in amplitude.

3.2.5 Pliocene Strata (Attachment 1)

This sequence is defined by flooding surfaces above the last fluvial channel facies of the Late Miocene sequence. The marker was picked at the maximum flooding surface of Late Miocene to Early Pliocene flood plain strata. The Ta_1 marker coincides with PR15B palynological zonation, dated Early/Upper Pliocene (see section 1.3.2). The seismic marker shows consistently high amplitudes and is a continuous reflector throughout the dataset. Very minor folding can be

observed along major faults, with fold axes parallel to fault traces. Most faults have been interpreted to cut and offset the Ta_1 marker. The prevalence of normal faults at this level suggests a significant extensional event during the Pliocene.

3.3 Basis and Methodology of Seismic Interpretation

Seismic interpretation, mapping and geophysical analysis during this study were carried out using the PETREL™ geophysical package. Basic structural interpretation was carried out using a normalized amplitude SEGY cube and a variance cube. The variance cube, which was generated from the normalized amplitude SEGY, was mainly utillized in fault interpretation in conjunction with the SEGY cube.

A total of eight markers were interpreted using the normalized amplitude SEGY data; each surface was interpreted at an interval of every 32 inlines. Fault segment interpretation was carried out at an interval of every 5 inlines, using the SEGY data. Structural interpretation using the variance cube was done on time-slices at 50ms intervals.

These eight surfaces were used to perform the structural and geophysical attribute analyses and interpretations. The surfaces provided the basis for

calculating isochore and stratigraphic thickness maps and geophysical attributes such as amplitude, dominant and interval frequency and dip-azimuth surface maps. These surfaces were also used in *Antracking*™ attribute mapping. Prior to *Antracking*™ attribute mapping, an *Antracking* cube must be generated. *Antracking* parameters used in this study are shown in Appendix 8.

3.3.1 The basis of the time domain interpretation: The issue of velocity modeling

Velocity modeling was not carried out during this study due to insufficient well data. This lack of data, which results mainly from the limited number of well penetrations, is compounded by the incomplete suite of sonic logs and density logs in some wells. For example, some wells have only raw log suites that require a lot of petrophysical editing due to the poor bore-hole condition, as indicated by caliper readings, during open-hole logging. Only one well has a complete, corrected log suite. However if data from only one well are used for velocity modeling, the velocity model generated will be overly simplified, and is likely to result in erroneous depth values and hence large uncertainties in structural geometries. For example, an overly simplified velocity model may cause structures to disappear completely, or to be displayed with incorrect geometries.

A basic analysis of the available check-shot data was done to identify the velocity trend within the study area and any possible velocity anomalies which could be an indicator of abnormal formation pressures or strong lithological heterogeneities. A qualitative comparison was made between the well check-shots and the regional velocity function used in 3D seismic data processing to identify any inconsistencies.

A time-depth plot of well check-shots from the seabed to 3000m in four exploration wells, (A-2, M-1, M-2 and S-2), indicates a consistent velocity function in all wells (Figure 3.6a), although there is a slight velocity anomaly identified at 2122m in A-2, which corresponds to a change in lithofacies (Figure 3.6b).

The velocity curve from regional spherical divergence (TV^2) plots (Figure 3.7b), displays a similar trend as the well check-shot data, except at approximately 1665m to 2420m, where the estimated velocity was slightly faster than that of the well check-shots. However, from the cumulative plot it appears that the seismic velocity was estimated to fit the A-2 velocity curve. The time-depth plots show a gradual increase in velocity with depth and no velocity anomaly in observed in the plot.

In conclusion, it is better to conduct the structural analysis in the time domain rather than the depth domain, as this could introduce further ambiguities and inconsistencies.

3.3.2 Fault Interpretation and Structure Mapping

All mapping was done in two-way time using the PETREL™ mapping application. In general, two distinctive fault patterns can be observed on the Tenggol Arch. The first fault pattern comprises north-northwest- and northwest-striking faults, which predominate within the basement to top syn-rift interval. The second fault pattern consists of en-echelon sets of north-northeast-striking splay faults within the overall northwest-trending Tenggol Fault zone. These predominate in Miocene to Pliocene strata (Ta_2 to Ta_1). Changes in fault orientation can be observed from fault-line mapping, as shown in Figure 3.5.

The development of two distinctive fault patterns at different stratigraphic levels within the same Tertiary basin may indicate the presence of a detachment surface (or package of strata) that separates Pre-Tertiary-Late Oligocene strata from Miocene-Pliocene strata. Such a decollement requires a thick shale or salt sequence or a highly overpressured interval. The latter suggestion is inconsistent with the results of the velocity analysis described above. In a

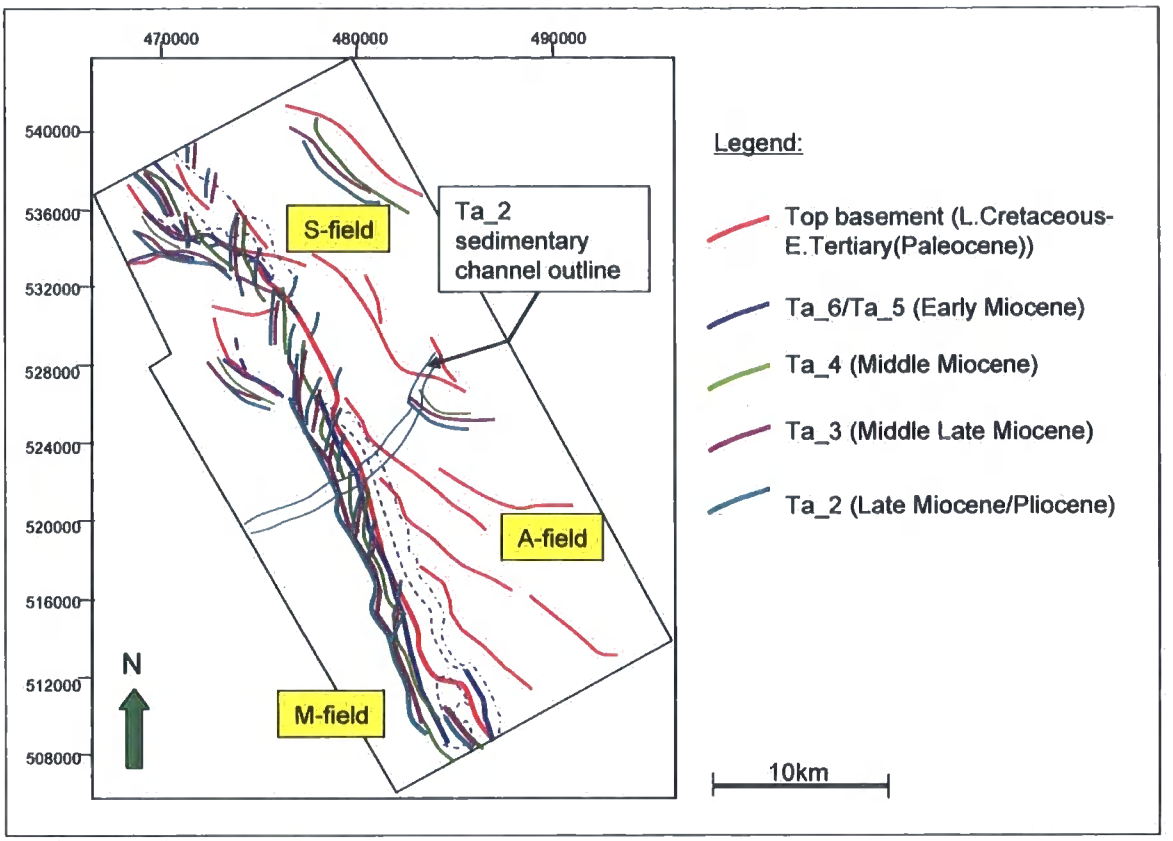

Figure 3.5 "Composite" fault-line map showing fault traces interpreted at Top Basement (Late Cretaceous) to Ta_2 (Lower Pliocene) levels. Note the differences in fault trends observed at Top Basement and Miocene levels.

marginal marine to lower coastal plain depositional environment, which was characteristic of the Malay Basin during the Early Miocene, shale beds are more likely to develop than salt horizons for which there is no evidence from the available well data.

A c. 100 m thick sequence of transgressive shales has been consistently drilled in the central part of the Malay Basin. The top of this shale sequence is known as the mfs300 regional marker which was extensively mapped throughout the basin centre and gradually thins towards the flanks and southern margins of the

basin (Appendix 2). Lateral extension of msf300, or it equivalent transgressive shale package, onto the Tenggol Arch could further support the existence of the proposed decollement surface developed within the thick shale sequence. Hence seismic facies interpretation of Early Miocene and older strata was implemented in this study. Discussion of the seismic facies interpretation and its implications will be covered in *section 4.1.*

Fault mapping in this study has mainly utilized time horizons and time structure maps. Derivations of azimuth and dip attributes were also based on time horizons input. In early section 3.1.2, the study has identified seismic data resolution deteriorating at deeper depth, hence mapping within fault intervals may be inferred from highly interpretive surface horizons. Hence, dip and azimuth maps of this study although indicates clear defined fault pattern and structure style, however shows only apparent value of regional dips. In addition, azimuth mapping along the fault intervals may also be artefact of gridding process due to high interpretation uncertainties within fault intervals. In conlusion the result of azimuth and dips mapping of the study area may only indicate relative variation in regional dips across strata and defining fault pattern.

Mapping of the top basement and top syn-rift markers (Attachment 18) shows that the predominantly northwest- to north-northwest-striking faults have northeast to easterly dips. At top basement level, the NNW-striking faults are mainly normal faults with an apparent dip of 60^0, with some areas locally showing

an apparent dip of 70^0. The north-northwest-striking fault set is collectively referred to as the Tenggol Fault zone. The Tenggol Arch isolated basement lows (Attachment 12) occur within the hanging-wall of this structure and appear to have subsided continuously until Ta_6/Ta_5 times (Attachment 9). These north-northwest-striking bounding faults gradually developed into sub-parallel normal splay faults (Attachment 13-15) (see Chapter 4).

In Middle Miocene (Ta_4/Ta_3) strata, north-south- to north-northeast-striking faults with easterly dip directions become increasing prevalent and appear dominant within Upper Miocene to Pliocene strata (Ta_2/Ta_1; Attachment 17 and 19). These structure styles and present-day relief are illustrated by dip and azimuth maps of each interpreted surfaces (Attachment 16, 17, 18 and 19).

The top basement structure map shows extensive evidence of having been deformed in an extensional regime. The area is dominated by north-northwest-striking normal faults, namely the Tenggol Fault. The Tenggol Fault appears to be a major normal fault that downthrows towards the northeast. Northwest-striking normal faults, which bound northwest-trending sub-basins, dominate the down-thrown fault block of the Tenggol Fault. The long axes of the sub-basins appear to be sub-parallel to the northwest-striking fault zone, which suggests that the northwest-striking faults are bounding normal faults for these sub-basins. Sediment provenance into these sub-basins during the Early Tertiary was most

likely from the western margin of the study area and also from localized basement highs.

The northwest- and some easterly-striking basement faults continue upwards into the top syn-rift and are commonly found on downthrown fault blocks. A distinctive feature observed on top synrift horizon is the presence rhomboidal-shaped geometries that may possibly indicate inverted basement-controlled structures because the structures are uniquely associated with the NW-striking en-echelon stepping faults that likely are related to strike-slip deformation (see section 4.4.1) (Figure 3.4). This rhomboidal geometry is best delineated in the azimuth map for the top Synrift and top Basement markers due to the subtle nature of these structures. Other possible interpretations of these rhomboidal structures such as basement-drape features are also possible. Sediment provenance during the deposition of the syn-rift to Ta_6 sequences was dominantly from localized basement highs. Sediment depocentres were mostly concentrated in localized sub-basins and continuing eastward. Dip and azimuth maps of the top basement and top syn-rift indicate that folds are prevalent on the down-thrown fault block, with fold trends parallel to the northwest- and easterly-striking faults.

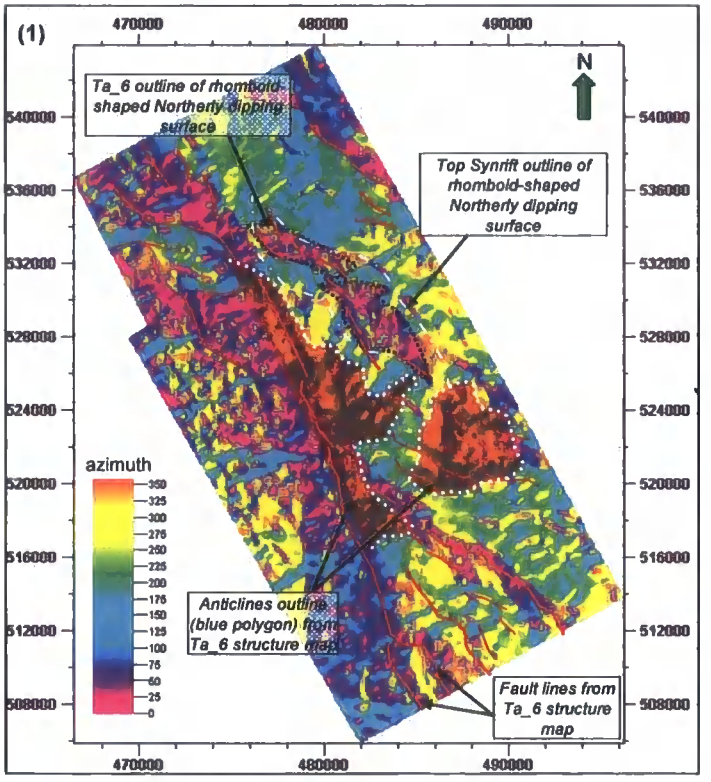

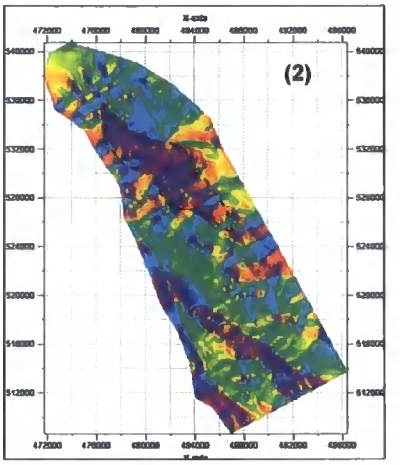

Index map shows Top Synrift azimuth map, the northerly dipping surface (magenta/pink) outlined in dashed line.

Ta_6 TWT structure map is shown in Attachment 3.4.

Figure 3.4 Ta_6 azimuth map (1) indicates distinctive two rhomboid-shaped patch of northerly dipping surface direction (black dashed polygon). The rhomboid-shaped patches distinctively combined and widen in surface area at deeper strata as shown in index map (2). The rhomboid-shape patches though clearly observed on Ta_6 and Top Synrift could possibly a repercussion of development of anticlines or fold structures within Top Synrift toTa_6 strata.

3.3.3 Geophysical Attribute Analysis

In general, the objective of geophysical attribute analysis is to identify and provide additional information on structural and stratigraphic features in the study area. Some attribute mapping was conducted on the top basement marker in order to further investigate the faults, fractures and lineament patterns. Similar attribute extraction and mapping was done in the Miocene strata to delineate channel features. The channel features may show lateral displacement in Middle to Late Middle Miocene due to strike-slip fault movements if such movements

occurred in this region, and therefore provide a useful test of previously proposed hypotheses (Chapters 1 and 2). Geophysical attribute variation was also used to verify and identify stratigraphic features and facies variations.

The data used for geophysical attribute mapping was the 2004 3D seismic normalized amplitude SEGY data. Attribute extraction and mapping was carried out using the PETREL™ geophysical application. A single geophysical attribute is not sufficient for geological interpretation as each geophysical attribute is non-uniquely related to one or more combinations of rock and fluid properties. For instance, seismic amplitude shows the general distribution of high and low amplitude values, which may correspond to geological variables such as facies variations, porosity, deformation intensity, the presence of a gas-filled reservoir or the tuning effect of thin beds. In addition, these geophysical attributes may also be affected by geophysical artifacts associated with seismic acquisition and processing. Hence, the results of attribute analysis studies depend on the quality of seismic data. Other seismic attributes such as seismic phase and wavelet polarity are not included in this discussion due to geophysical tool limitation and poor results.

Mathematically-derived geophysical attributes such as variance, chaos and *Antracking* (PETREL) were generated to further support the geological interpretation of instantaneous geophysical attributes. These attributes are mainly designed to highlight breaks or trends in seismic phase, polarity, peak

(wavelet) and maximum amplitude, thus helping to define lineament patterns on interpreted surfaces. The lineaments may either indicate true geological events or geophysical artifacts; hence interpretation of these lineaments again requires a combination of more than one single geophysical attribute.

Attribute extractions were performed on the top basement marker to delineate faults or channel features in the study area. The edge of the footwall of the Tenggol Fault zone was clearly delineated using the Variance cube; however, fault lines on top basement were not clearly defined. The extraction of the variance attribute along the Ta_5 and Ta_3 markers was able to clearly delineate fault trends on these surfaces. Based on this observation, the variance cube was used to assist fault interpretation mainly within Miocene strata. Note that fault segments were always picked using SEGY sections in the dip-line direction.

An RMS amplitude map with a window of 50ms from the top basement marker indicates that there are patches of especially high amplitude, which could possibly correspond to particular basement lithofacies. High amplitude patches are concentrated within the topographically low area on the hanging-wall close to the edge of Tenggol Fault zone. Some high amplitude zones are also found in the footwall of the fault zone. However, no clear depositional pattern can be identified here. High amplitude patches observed near to the edges of the fault zone on the hanging-wall side are interpreted as slope deposition or perhaps alluvial fan deposits. High amplitude anomalies in the footwall are most likely to

be associated with a poorly cemented sedimentary package (e.g. highly porous clastic rocks) or possibly a layer of weathered igneous material.

The dominant frequency of the 50ms window from the top basement marker shows a high frequency range in the footwall, and a lower frequency range in the hanging-wall of Tenggol Fault zone. Frequency variations on basement again probably correspond to lithological variations. It is also possible for seismic frequency to naturally attenuate at deeper levels across a fault. However, it is clearly observed in seismic sections (Figure 3.2c) that relatively low frequency seismic facies generally represent the metasedimentary rocks (Trace 2715) and the relatively high frequency seismic facies are associated with igneous bodies (Trace 2275) (Figure 3.2c). Wells drilled into the basement unit in the hanging wall of the Tenggol Fault zone have proved mainly to be argillaceous, low grade metasediments. Wells drilled into basement in the footwall have recovered predominantly igneous rocks. Therefore, in the study area the high frequency range may correspond to igneous rocks and low frequency range may correspond to low grade metasedimentary rocks. Instantaneous frequency mapping was carried out on the top basement marker using the same extraction window as the dominant frequency (i.e. 50ms window from top basement marker) in order to further delineate possible sedimentary geometries at top basement level. The attribute map shows high frequency ranges from 27Hz to 38Hz in the footwall and low frequency range of 10Hz to 27Hz in the hanging-wall. Similar frequency attribute extraction is done for Miocene strata to

delineate channel edges or other sedimentary geometries that may show lateral displacement along major faults in the Miocene strata.

A variance cube was generated from PSTM (Pre-Stack Time Migrated) 3D seismic data to facilitate fault mapping at deeper levels within the Tertiary sequence (Ta_5 to Top Basement). Horizon slices were generated using the variance cube, and variance maps of the Ta_5 and Ta_3 surfaces show clear definition of the fault lines in map view. These horizon slices provide a regional overview of the study area and were also used to verify fault picks made on vertical seismic profiles. Although variance maps of the Ta_3 and Ta_5 horizon slices show clear fault definition, the attribute quickly deteriorates with depth approaching the top basement surface. At top basement level, faults are generally not sharply defined. However, the edge of the Tenggol Fault (i.e. the edge of the footwall block) is clearly defined in the south of the study area and becomes gradually less well defined to the north of the Tenggol Arch (Figure 3.9). Therefore, the variance maps generated using the surface slices were used mainly to verify fault line picks in Miocene strata. Fault segment interpretation in deeper strata (Later Oligocene and top basement) was done using only vertical seismic sections.

Two *Antracking* volumes were generated for this study. The first cube was generated for shallow Tertiary sedimentary strata and the second volume was focused on basement. *Antracking* requires two input volumes, which are a

structurally smoothed volume and Variance cube, both of which are extracted from the PSTM 3D seismic volume. The smoothed volume was generated from normalized amplitude PSTM 3D seismic data. The smoothed cube was used in-order to enhance the expression on stratigraphic surfaces of any lineaments of structural origin. The variance cube was generated from normalized amplitude PSTM 3D data; the variance cube was used to further enhance faults or fractures related lineaments in the cube.

The *Antracking* volume generated to investigate the shallow Tertiary sedimentary strata has vertical range of 500ms to 1550ms. The *Antracking* volume used to further investigate the basement complex has a vertical range of 1550ms to 3000ms. Details of the *Antracking* parameters used in this study are shown in Appendix 8. Results from this analysis show that the deeper *Antracking* volume was able to clearly delineate faults and fractures within the basement complex especially in the footwall of the Tenggol Fault (Figure 3.7). The shallow *Antracking* volume gives a clear definition of stratigraphic surfaces, but poorer definition of faults and fractures. Based on this observation, the *Antracking* volume was used mainly to aid interpretation of the basement faults and fractures, while fault interpretation of shallow level was mainly conducted using the PSTM normalized amplitude cube and Variance cube (Figure 3.7).

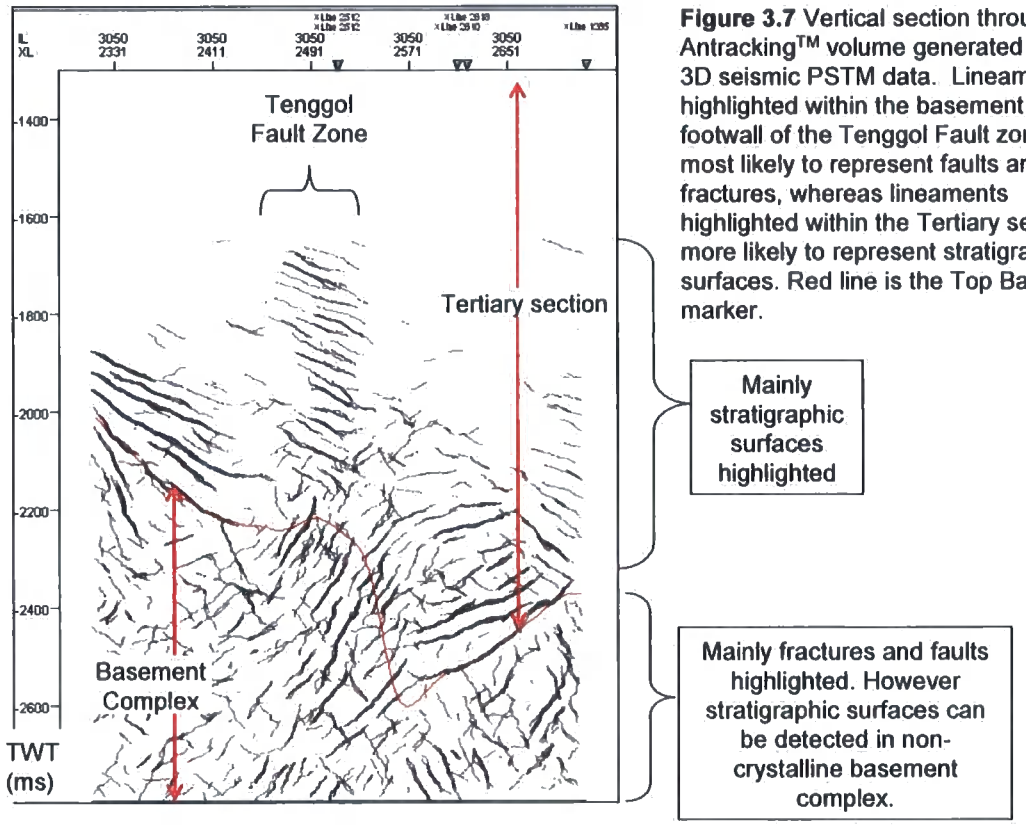

Figure 3.7 Vertical section through the Antracking™ volume generated from the 3D seismic PSTM data. Lineaments highlighted within the basement in the footwall of the Tenggol Fault zone are most likely to represent faults and/or fractures, whereas lineaments highlighted within the Tertiary section are more likely to represent stratigraphic surfaces. Red line is the Top Basement marker.

Discussion of the interpretation of the *Antracking* volume concerning faults and fractures in the basement complex will be carried out in Chapter 5.

3.4 Seismic facies interpretation

3.4.1 Objective

Seismic facies interpretation was performed on a few selected vertical sections from the PSTM (Pre-Stack Time Migration) 3D seismic volume. The objectives of this interpretation were, firstly, to verify the lithological variation within the

basement complex on the Tenggol Arch in order to ascertain any possible correlations that might exist between the fault or fracture patterns and the host rock lithology (see section 2.2). A second objective was to identify and verify the lateral extent of the thick shale strata within the Early Miocene sequence and to identify the possible presence of similar thick shale facies in the older sequence. The thick shale facies may act as a decollement surface that could potentially explain the distinctively different fault patterns observed in Pre-Tertiary-Late Oligocene strata and Miocene-Pliocene strata (see section 3.3.1).

Seismic facies interpretation was done by identifying the character of seismic reflectors within the mapped sequence surfaces. The basis for seismic reflector characterization was adapted from seismic sequence stratigraphic methods, as described by Prosser (1993). A similar approach was applied in the 2005 Malay Basin regional study and the seismic facies identified were calibrated to wells and translated to lithological facies. Seismic facies and seismic reflector descriptions used in the Malay Basin regional study are shown in Appendix 3a.

3.4.2 Seismic characteristics and major facies

The seismic facies that can be identified in Malay Basin comprise:

1) medium to high amplitude, discontinuous slightly wavy reflectors;

2) medium to high amplitude, divergent and sigmoidal reflectors,;

3) high amplitude discontinuous reflectors,;

4) medium to low amplitude, parallel and discontinuous reflectors; and

5) medium to low amplitude, parallel and continuous reflectors, occasionally dimmed and featureless.

A well calibration was done for each seismic facies to identify the lithofacies and depositional environment using gamma-ray logs and well cutting samples or core data. Wells used in the calibration are mainly wells that were drilled along or close to the selected seismic lines (Figures 2.4b and 2.4d). The above listed seismic facies were identified as the five major seismic facies in basement lows over the Tenggol Arch. Additional seismic facies identified over the Malay Basin that are associated with specific stratigraphic intervals are shown in Appendix 3a.

The seismic facies method was also applied to distinguish various lithologies in the basement complex (Figure 2.4a). I have decided to apply the seismic facies method in the basement complex to explain some the geophysical features identified in the dataset (see above).

3.4.3 Findings from seismic facies interpretation

Two seismic sections were selected for this interpretation: a dip-line through the M-field and a dip-line through the S-field (Figure 2.4b and 2.4d). Dip-lines were used because they are likely to be sub-parallel to sediment transport directions. Sediment transport directions on the Tenggol Arch were determined based on the shapes of the Tertiary sediment packages, which wedge towards the western

edge of the study area (Appendix 2). Isochore maps of the Tertiary sedimentary units (Attachment 1), suggest that, in general, the sediment transport direction was most likely to have been eastward, i.e. along dip-lines through the Tenggol Fault. Therefore depositional features should be more easily observable along dip-lines (i.e. seismic Inlines) in comparison to seismic lines parallel to basin margin (i.e. seismic traces).

Lithofacies interpretation away from well locations was done by means of extrapolation. In this study, the identified seismic facies packages were calibrated to well logs from the M- and S-fields. The colour scheme employed during the present study is such that "hot" hues (red to yellow) indicate sand prone zones, "cool" hues (blues and greens) indicate shale prone zones (Figure 2.4b and Appendix 2 and 3a).

Lithofacies interpretation using calibration against the M-2 well (which was drilled onto a basement high into the top section of the Ta_5 sequence; Figure 2.4d) was based on basic gamma-ray curve patterns within this siliciclastic sequence. The basic gamma-ray curve patterns were adapted from the lithofacies interpretation of sequence stratigraphic and seismic sequence stratigraphic working models (cf. Haq, 1992; Exxon sea level curve, Haq et. al., 1987). These models suggest that: 1) a 'bell-shaped' curve represents a fining upward succession; 2) a 'blocky-shaped' curve with a sharp-based contact represents a channel or incised valley fill; 3) a 'funnel-shaped' curve represents a coarsening

upward succession (usually stacking-up), interpreted as a coastal to marginal marine depositional environment in a deltaic facies association; and 4) a `crescent-shaped' curve is interpreted as a slope deposit, usually associated with an alluvial setting. The gamma-ray curve patterns and their facies interpretations are illustrated in Attachment 21.

The gamma-ray curve patterns interpreted from wells on the Tenggol Arch are based on sequence stratigraphic methods that were developed to explain the response to eustatic sea-level variations of siliciclastic depositional systems (Carter et. al., 1993). The transgressive systems tract (TST) is represented by a condensed section and maximum flooding surface, which are associated with increasing mean sea level. Highstand systems tract (HST) deposits develop during sea level regressions, whilst lowstand systems tract (LST) sediments are deposited during minimum mean sea level. The sequence stratigraphic concepts applied in this study are shown in Attachment 21. The lowstand system tract (LST) is correlated with `blocky-shaped' and `bell-shaped' gamma-ray curve patterns, which are thought to be associated with basal fluvial facies. The highstand system tract (HST) is correlated with `funnel-shaped' gamma-ray curves which is thought to be associated with splay or deltaic fan deposits. The transgressive system tract (TST) is primarily represented by fining upward successions followed by a maximum flooding surface that is thought to correspond to a condensed section in the sequence.

3.4.3 a Interpretation of azimuth mapping

Azimuth maps of interpreted surfaces over the Tenggol Arch were generated using the PETREL azimuth mapping application which depict general azimuth (bearing) as shown in Attachment 16 and 17. The pre-Miocene sequence is shown in Attachment 16 shown by Top Basement (d) and Top Synrift (c) and Early Miocene strata comprises Ta_6 (b), Ta_5(a). Azimuth maps of Middle to Late Miocene strata shown in Attachment 17, where Middle Miocene strata comprises Ta_4 (d) while Upper Miocene comprises Ta_3 (c), while Miocene/Pliocene strata shown by Ta_2(b) and Ta_1 (a).

Interpretation of seismic facies across the Tenggol Arch (section 3.4) reveals the presence of a condensed section within Early Miocene strata, which is represented by the Ta_6 /Ta_5 sequence. This sequence is 'sandwiched' by brittle layers; crystalline basement underlies and sandstone rich clastic sediment overlies the Ta_6/T_5 sequence. According to Bonini (2007), the presence of a weak basal horizon or detachment layer will affect stress propagation which will result in complex structures styles across layers. Hence, based on this theory, a case representative of this analogue model should be able to be demonstrated through azimuth maps across brittle-ductile layers on Tenggol Arch.

Azimuth map of pre-Miocene strata (Top Basement and Top Synrift) indicate dominant southeast (green-yellow) orientation surface azimuth with localized indication of north-south (blue-magenta) orientation surface azimuth (Attachment 16 (c) and (d). As emerging Early Miocene (Ta_5 and Ta_6), the predominant azimuth shown as near combination of southeast and northerly orientation and gradually became predominantly northerly direction along the Ta_5 surface (Attachment 16 (a). As shallowing-up to Middle Miocene/Pliocene strata, the azimuth maps indicate predominantly north-south surface azimuth from Ta_4 to Ta_1 (Attachment 17).

The observations above suggest that surfaces azimuth of strata below ductile/ detachment layer have different azimuth orientation (i.e southeast orientation) as surface overlying the ductile layer (northerly orientation). Thus, in general the ductile, shale strata of Ta_6/Ta_5 strata affecting stress propagation across the layers, hence generally contributes in development if complex structure styles of the Malay basin and Tenggol Arch present-day structure styles. In conclusion, azimuth mapping of surfaces markers indicate regional dips differences above and below a detachment however the presence of detachment would be best demonstrated using a vertical seismic section (Appendix 16).

3.4.4 Basement Complex Seismic Facies

3.4.4.1 Volcanic-plutonic igneous facies

The interpretation of seismic facies within the basement complex was carried out along Trace 2275 which runs parallel to the M-field (Figure 3.2c). A trace over the footwall block along the M-field was selected for this analysis because very little deformation took place in the footwall compared to the hanging wall. Therefore, the seismic facies can be clearly defined, with less uncertainty due to geophysical or processing artifacts (Figure 2.4a). The line runs along the footwall of the Tenggol Fault zone with a northwest trend, parallel to the fault plane (Figure 2.4a). Three major basement complex seismic facies can be identified from the section. The first facies consists of dimmed, structureless reflectors, which appear to be consistently bounded by a high amplitude reflector. Generally, the topography of top basement appears to be a flat plateau with a low-angle stepping feature (Figure 2.4a). A well (M-2) drilled into this facies indicates the presence of volcanic-plutonic igneous rocks (Well Completion Reports). The geometry of this facies suggests magmatic bodies or layers, which may have been emplaced into Mesozoic sandstones and shales.

3.4.4.2 Low grade metamorphic facies

The second facies, consists of high amplitude seismic reflectors, mostly continuous and conformable. Stratigraphic surfaces are clearly observed near the top of this unit (Figure 2.4a). This facies appears to be dominant in the basement complex, and wells from the Tenggol Arch suggest that it comprises predominantly phyllite, psammite with subordinate metaquartzite.

The third facies identified consists of high amplitude discontinuous reflectors with variable orientations. No well has penetrated into this facies, but it may correspond to dykes and sills that have been consistently mapped along the eastern coastline of Peninsular Malaysia.

3.4.4.3 Carbonate facies

A few wells on the north margin of the Tenggol Arch penetrated into carbonates. The S-1 well penetrated into a recrystallized packstone in the basement. This lithofacies gives rise to high to medium amplitude reflectors with a chaotic character (Figure 2.4b).

3.4.5 Syn-rift, Late Oligocene and Early Miocene strata

3.4.5.1 Inline 5369 (M-2 well)

Inline 5369 is located in the south of the study area, and includes the M-2 well. Seismic facies interpretation of syn-rift to Late Oligocene and Early Miocene strata along Inline 5369 indicates mostly shale-prone strata in Sequence Ta_5 (Figure 2.4d). The Ta_5 strata show a fairly uniform thickness basinward (East) and gradually thin towards the western margin. The Ta_6 and Syn-rift sequence show greater sand to shale ratio compared with the younger strata. The Syn-rift sequence in the seismic section (Figure 2.4d) appears to be characterized by sandy packages deposited along slope of the basement low, and is represented by medium to high amplitude divergent, sigmoidal and slightly wavy reflectors (Figure 2.4b and Figure 2.4d). The depositional environment of the Syn-rift sequence along Inline 5369 was interpreted to be an upper coastal plain or lacustrine environment with some marine influence at shallow levels. The M-2 well did not penetrate into the Syn-rift sequence, which was therefore interpreted mainly based on seismic facies characteristics.

The M-2 well did, however, penetrate into the Ta_5 sequence, which overlies basement highs in the footwall of the Tenggol Fault Zone (Figure 2.4d). The Ta_5 sequence in the region of the M-2 well displays medium to high amplitude, discontinuous and slightly wavy seismic reflectors. The gamma-ray curve pattern of the Ta_6 sequence indicates that a stacked 'bell-shaped' or fining-upward

succession overlies a `funnel-shaped' or coarsening upward succession (Figure 2.4d). The fining-upward succession indicates a transgressive systems tract (TST) with an overlying maximum flooding surface (MFS) (Attachment 21), is followed by a coarsening-upward succession which indicates a high-stand system tract (HST). A low-stand systems tract (LST) is represented by a `block-shaped' gamma-ray curve pattern. The Ta_5 sequence was interpreted as coastal to fluvial system with predominantly near marine, channel and flood-plain deposits (Attachment 7).

Overlying the Ta_5 sequence is the Ta_4 sequence which comprises lower coastal plain to marginal marine, channel and deltaic facies (Figure 2.4d).

3.4.5.2 Inline 2629 (S-1 well)

Inline 2629 is located near the northern margin of the study area and runs close to the S-1 well and along the dip-line of the S-field basement low (Figure 2.4b). Seismic facies analysis of the Early Miocene and Syn-rift sequences suggests that the Syn-rift and Ta_6 sequences are shale facies. Sandy facies are limited to the slope of basement lows and are not extensive. The shale strata of the Ta_5 sequence overlie basement highs around the S-1 well. The environment of deposition at the S-1 well was interpreted as being marginal marine with distal lobe facies in the Ta_6 sequence. The syn-rift sequence and the package facies

are interpreted as possibly being associated with the distal facies of an open lake environment, with marine influences in shallower strata. Interpretation of Syn-rift strata was mainly based on seismic facies characteristics.

3.4.5.3 Inline 2400 (S-5 well)

Inline 2400 is located in the north of the study area close to the S-5 well. The seismic line runs along the dip-line of the S-field basement low. Seismic facies of the Syn-rift sequence along this line are interpreted as a lacustrine to open lake depositional setting with a sandy package deposited within the inter-deltaic area (Attachment 8). The interpretation of a lacustrine depositional environment was based on the increasing presence of *bosedinia sp.* (freshwater algae) in borehole core and cutting samples from wells drilled in the section immediately overlying the Syn-rift package (Figure 1.7b). The centre of the basement low is dominated by fine grained facies based on the presence of continuous and dimmed seismic reflectors (Figure 2.4b, 2.4d).

The Ta_6 sequence is characterized by dimmed seismic facies and structure-less reflector patterns (Figure 2.4e). This sequence was penetrated by the S-5 well on the eastern margin of the basement low (Figure 2.4e). The well penetrated into calcareous shale and claystone facies with subordinate sandstone from circa 1032m to 1080m (approximately 1750 to 1950ms),

equivalent to the Ta_4 to Ta_5 sequences, dated basal Middle Miocene. Glauconite was found in abundance in the well section, consistent with a marine depositional environment. Calcareous nannofossils, arenaceous foraminifera and various rotaliids were also identified, which further supports a marginal marine or possibly deltaic environment. The deeper section, from 1260 to 3028m (equivalent to the Ta_5 and Ta_6 sequences), appears to show marginal marine to open marine characteristics. However the age of the basal section in well S-5 was not determined due to the absence of age-diagnostic foraminifera in the section[1].

The syn-rift sequence identified along this section was also interpreted as representing a lacustrine to open lake depositional setting similar to Inline 2629. Fine grained sediment was expected to be deposited in the central basement low and more sandy packages deposited along slope within the inter-deltaic area and as slope deposits (Attachment 22).

3.5 Discussion and Conclusions

The data resolution and structural imaging within the 3D seismic dataset used in this study is good to fair within the Tertiary sedimentary basin. Mapping of eight seismic markers across the data set can be done with a fairly high degree of

[1] Well data extracted from Well Completion Report and Paleontology Report of S-5 well. Lab services for the well were done by Petronas Research and Scientific Services.

confidence. No velocity model was generated in this study for time to depth conversion due to insufficient well data. Therefore, all evaluation was done in the time domain. However, a quick-look interpretation of time-depth curves from available check-shot data has been done to evaluate the velocities within the study area. In general, the average velocities as seen on plots of the check-shot data (Figure 3.6a and Figure 3.6b) indicate a gradual increase of average velocity with depth. This observation is consistent with normal compaction without any distinctive abnormal velocity anomaly. Therefore, down to the top basement marker, no drastic velocity effects on faults or other structures should be expected in the study area.

Seismic markers in this study were developed based on seismic stratigraphic methods and were tied back to regional markers in the Malay Basin. Eight major seismic markers were selected for mapping; these eight markers represent important geological events in the development of the Tenggol Arch, based on the 2005 regional study. These markers include: 1) the rift surface of possible Late Cretaceous period (see section 2.2); 2) the Late Oligocene initial post-rift / top syn-rift surface; 3) an Early Miocene, early post-rift surface, 4) a reflector that may have been deposited during Middle Miocene regional compression (see section 2.6.2); 5) a reflector deposited during the Middle Late Miocene peak regional compression (see section 2.6.2); 6) the major Miocene/Pliocene unconformity and 8) a reflector deposited during the youngest (Lower/Upper Pliocene) tectonic event to affect the area. Structural and thickness mapping of

these markers was carried out to further evaluate and delineate important tectonic or geological events in the Tenggol Arch region. Generally, from these eight markers, four markers have been identified that have a significant effect on the structural evolution of the Tenggol Arch. These are: 1) Upper Cretaceous (Top Basement), 2) Early Miocene (Ta_6/Ta_5), 3) Middle-Late Miocene (Ta_3) and 4) Pliocene. Evaluation of the structural patterns and fault geometries in the Tenggol Arch region will be covered in Chapter 4.

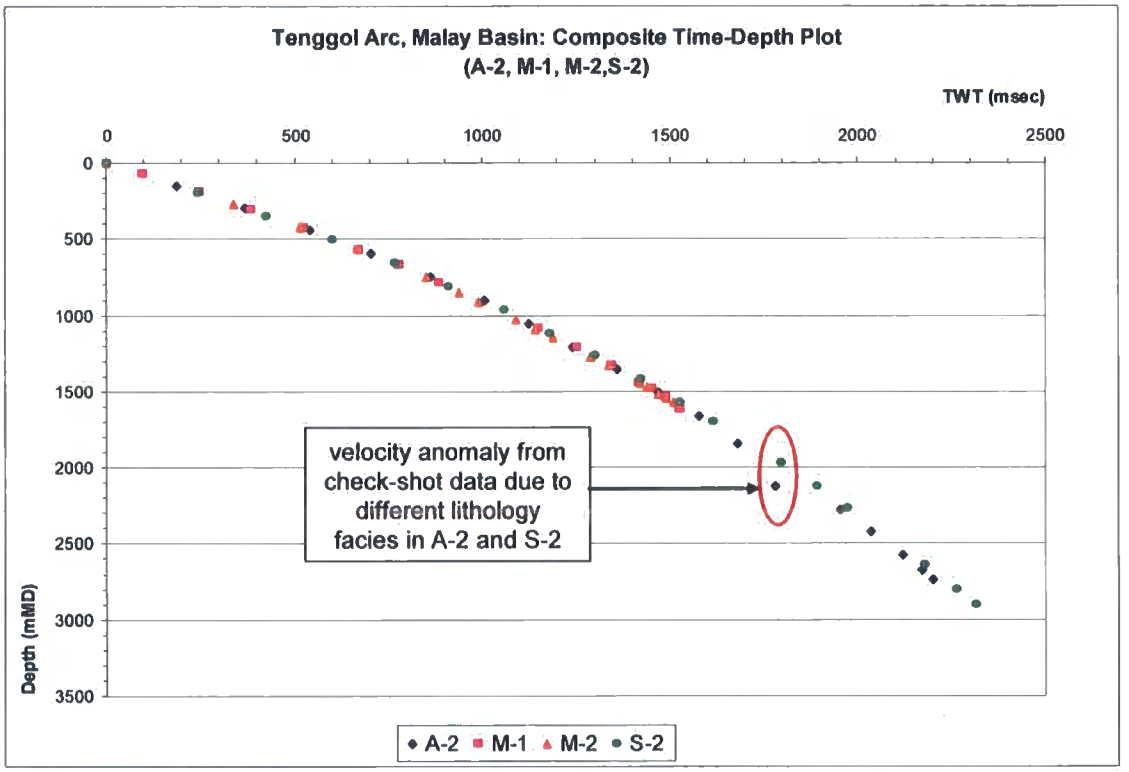

Figure 3.6a Compilation of time-depth (check-shot) data from the A-2, M-1, M-2 and S-2 wells. The M-1 and M-2 wells are located on the upthrown side of the Tenggol Fault; A-2 and S-2 are located in the hangingwall. Both M-1 and M-2 penetrated igneous rocks (dolerite and granite); the A-2 and S-2 wells penetrated predominantly metasedimentary rocks (phyllite and quartzite), however with minor presence of volcanic and carbonate in S-2.

In general, the various lithologies of the basement complex are distinguishable by identifying their seismic reflector characteristics. From the interpretation it can be concluded that the basement complex of the Tenggol Arch comprises mainly

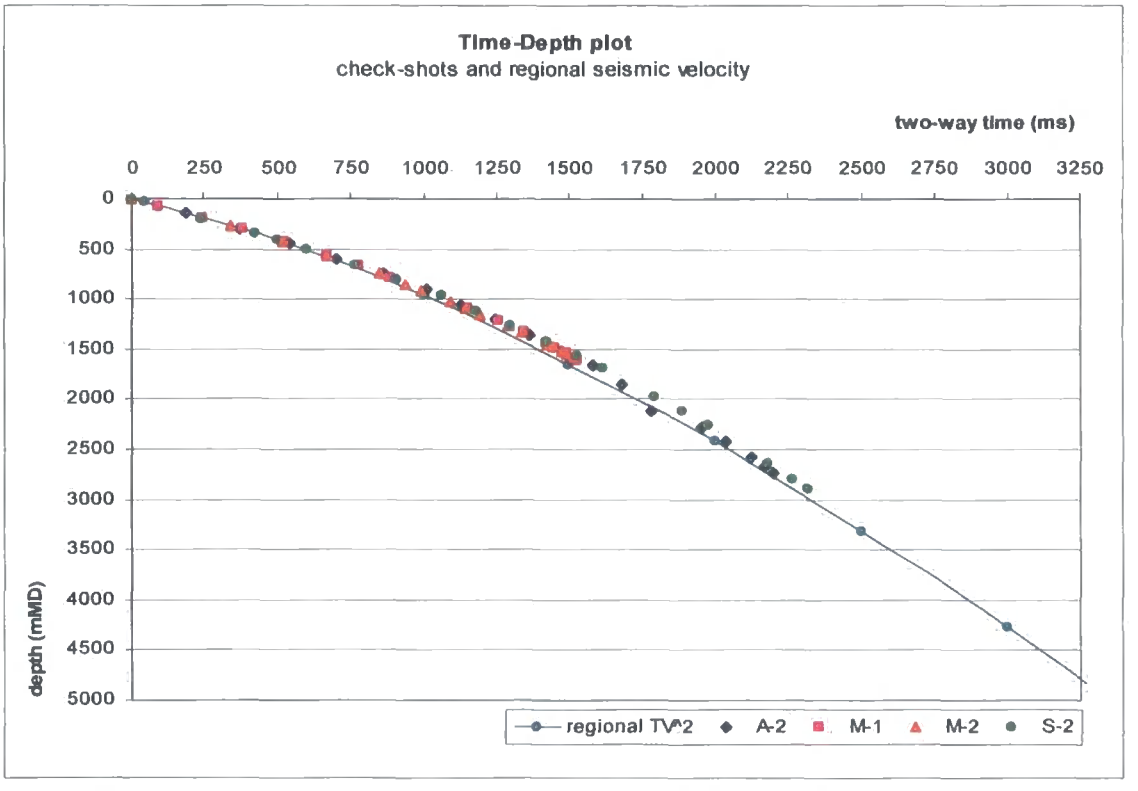

Figure 3.6b Graph showing the check-shot data plotted with the regional velocity function (solid curve) used to process the seismic data. In both cases, the velocity is shown to increase with depth. There is a reasonably good fit between the seismic velocity curve and the check-shot data; however, between c. 1500 and 2400m MD the predicted velocities are slightly higher than those obtained from the check-shots.

of low grade metamorphic rock of argillaceous origin (predominantly phyllite with minor bands of metasandstone) of possible Late Paleozoic to Mesozoic age (Figure 2.4a). The phyllite and metasandstone beds are shown in seismic sections as high amplitude seismic reflectors with clear stratigraphic bedding. Dykes and sills were later intruded into the metasediment and are represented by variably oriented, discontinuous high amplitude seismic reflectors (Figure 2.4a).

This hypothesis concerning the nature and distribution of basement lithologies can be tested by future deep drilling.

Seismic facies interpretation of Pre-Miocene sequences indicates the presence of shale strata underlying the post-rift sequence, which are likely of marginal marine to inner neritic facies that can be consistently found over the Tenggol Arch in both the south to north of the study area. The shale strata are thickest in the central basement low, in the footwall of the Tenggol Fault Zone, and gradually thin towards the western margin of the study area. From seismic sections, most syn-rift-associated faults appear to terminate upwards at or beneath the Ta_6 shale sequence. This observation may suggest that the shale strata act as a decollement between Late Oligocene/Early Miocene strata and younger rocks. Hence, the decollement surface will potentially explain the distinctively different fault patterns observed in the Pre-Miocene and Post-Miocene sequences.

In the next chapter, I discuss the structural evolution of the Tenggol Arch and perform an analysis of faults at the levels of the selected major surfaces described above, which appear to record evidence for the major tectonic events in the study area.

4.0 Geometry and kinematics of the Tenggol Fault, Tenggol Arch and Malay Basin

The main objective of this chapter is to define the tectonic and structural evolution of the Tenggol Arch in particular and of the Malay Basin in general. Further refinement of the tectono-dynamic model of the Malay Basin is required to address some of the outstanding issues associated with the regional framework, which have been highlighted in Chapters 1 and 2. Of particular importance is a better understanding the nature and significance of the Middle Miocene to Late Miocene/Pliocene regional compression event that has been recognized within the central Malay basin (PETRONAS, 2006(b)).

The first part of Chapter 4 describes the structural styles (faults, folds and basins) observed on the Tenggol Arch at Top Basement level and within the Ta_5/Ta_6 and Ta_2/Ta_3 intervals. This analysis also encompasses the early (pre-Oligocene) history of the Tenggol Arch. Next, the relationship between the faults and Miocene sedimentary channel bodies is discussed in order to constrain the kinematics of the Tenggol Fault zone during the Neogene. Isochore maps are also utilized to interpret the timing and distribution of Miocene to Pliocene faulting on the Tenggol Arch.

The second part of Chapter 4 integrates these results with the regional studies summarized in Chapter 2 to propose a new kinematic model for the Malay Basin

and Tenggol Arch during the Middle to Late Miocene/Pliocene (i.e. post-rift) period.

4.1 Structural styles and fault patterns

The principal structure on the Tenggol Arch is the segmented Tenggol Fault zone. It strikes in a northwesterly direction and dips towards the east. The fault zone consists of a series of normal faults that appear to be linked at Top Basement level (Figure 4.1), and which bifurcate upwards in the shallow (post-rift) sequence (Figure 4.2). Within the post-rift sequence, the Tenggol Fault zone comprises an en-echelon array of synthetic (i.e. E-dipping) faults which typically strike between 005^0 and 015^0. These faults die out upwards within Upper Pliocene strata.

At Top Basement level, the Tenggol Fault comprises several parallel normal faults, which interact across transfer (or relay) zones (e.g. Peacock & Sanderson 1991). The Tenggol Fault has an average throw of 600 ms in the southern part of the study area (Figure 4.3). The fault throw gradually decreases northward, with an average throw of 200 ms in the northern part of the study area (Figure 4.3). Thus, it could be argued that the Tenggol Fault initiated in the south and

propagated northward across the Tenggol Arch, although further analysis of the associated growth strata is required to test this hypothesis (cf. Childs et al. 2003).

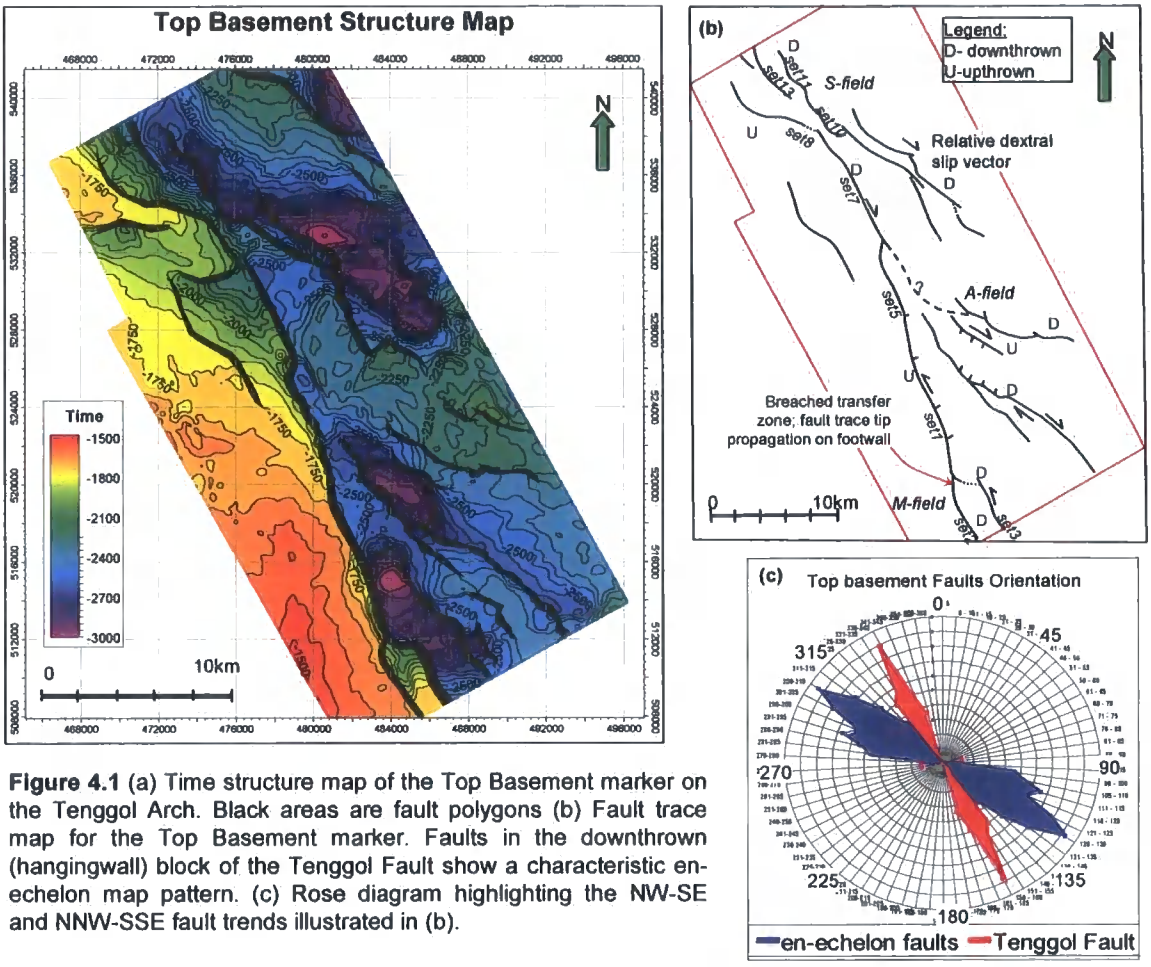

Figure 4.1 (a) Time structure map of the Top Basement marker on the Tenggol Arch. Black areas are fault polygons (b) Fault trace map for the Top Basement marker. Faults in the downthrown (hangingwall) block of the Tenggol Fault show a characteristic en-echelon map pattern. (c) Rose diagram highlighting the NW-SE and NNW-SSE fault trends illustrated in (b).

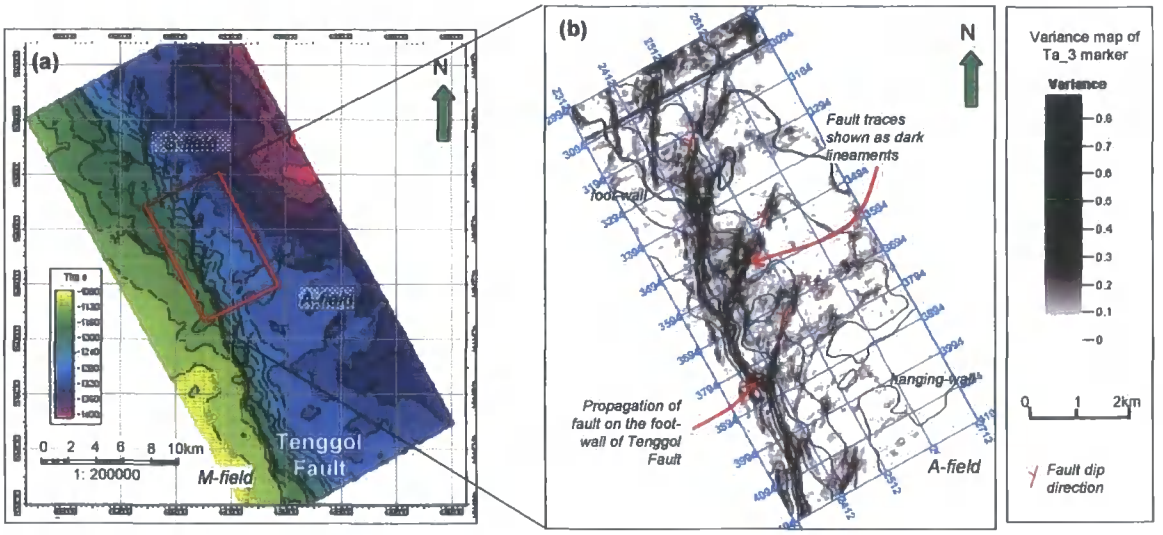

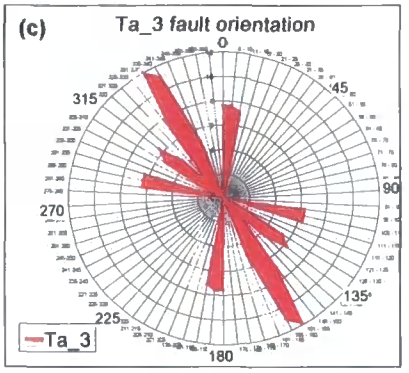

Figure 4.2 (a) Time structure map of the Ta_3 seismic marker. Note the segmented nature of the Tenggol Fault at this level. (b) Variance map of the Ta_3 horizon. The dark lineaments are fault traces. Note that some, but not all of the segments appear to be hard-linked by faults. (c) Rose-diagram showing the trends of faults on the Ta_3 marker. The overall trend of the Tenggol Fault zone is NW-SE; minor fault segments strike between 005^0 and 015^0 (c).

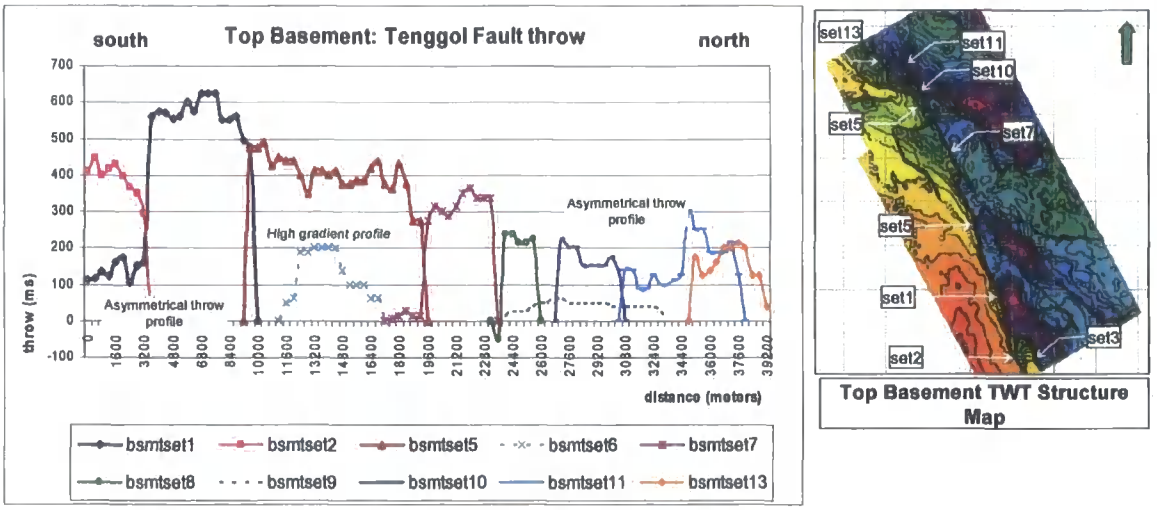

Figure 4.3 Top Basement throw profile for the Tenggol Fault. The throw decreases progressively from south to north along the fault. Colours indicate the different fault sets that have been identified (see text for explanation). The largest maximum throw (c. 600ms) is associated with fault set 1. Fault set 8 shows a small apparent reverse offset (see Figure 4.3b.

The Top Basement marker on the downthrown block of the Tenggol Fault is dominated by en-echelon faults that strike between 111^0-115^0 and 126^0-130^0, and by small rhomboidal basins (basement lows) with typical dimensions of c. 6km x 2km. These small basement lows appear to be elongated in a NW-SE direction and are characterized by increased thicknesses of the overlying sedimentary strata, as exemplified by the Ta_6/Top Basement isochore map (Figure 4.4). The possible kinematic significance of these basins in the early (pre-Oligocene) history of the Tenggol Arch is discussed below (section 4.4).

Miocene to Pliocene strata are characterized by N- to NNE-striking synthetic faults that display an en-echelon arrangement in map view. Fault transfer zones are distinctively observed on the Ta_3 marker and are further emphasized at Ta_2 marker (Attachment 14 (b), Attachment 15 (a)). On the Ta_1 marker, the synthetic faults appear to be widely spaced in the region adjacent to the S-field (North), with very low throws averaging 13ms (Figure 4.5). Figure 4.2(b) shows a variance map of the Ta_3 marker (Middle Late Miocene), which highlights the fault traces as dark lineaments. The Miocene sequence on the Tenggol Arch is also dominated by NNE-striking faults arranged in a stepping, en-echelon pattern. The NNE faults have normal offsets and are synthetic to the NW-striking trace of the Tenggol Fault observed at Top Basement level. These faults dip at fairly low angles towards the E or NE (Attachment 19). The NE-striking fault set can be traced from the Upper Early Miocene/Middle Miocene to the Pliocene equivalent surfaces.

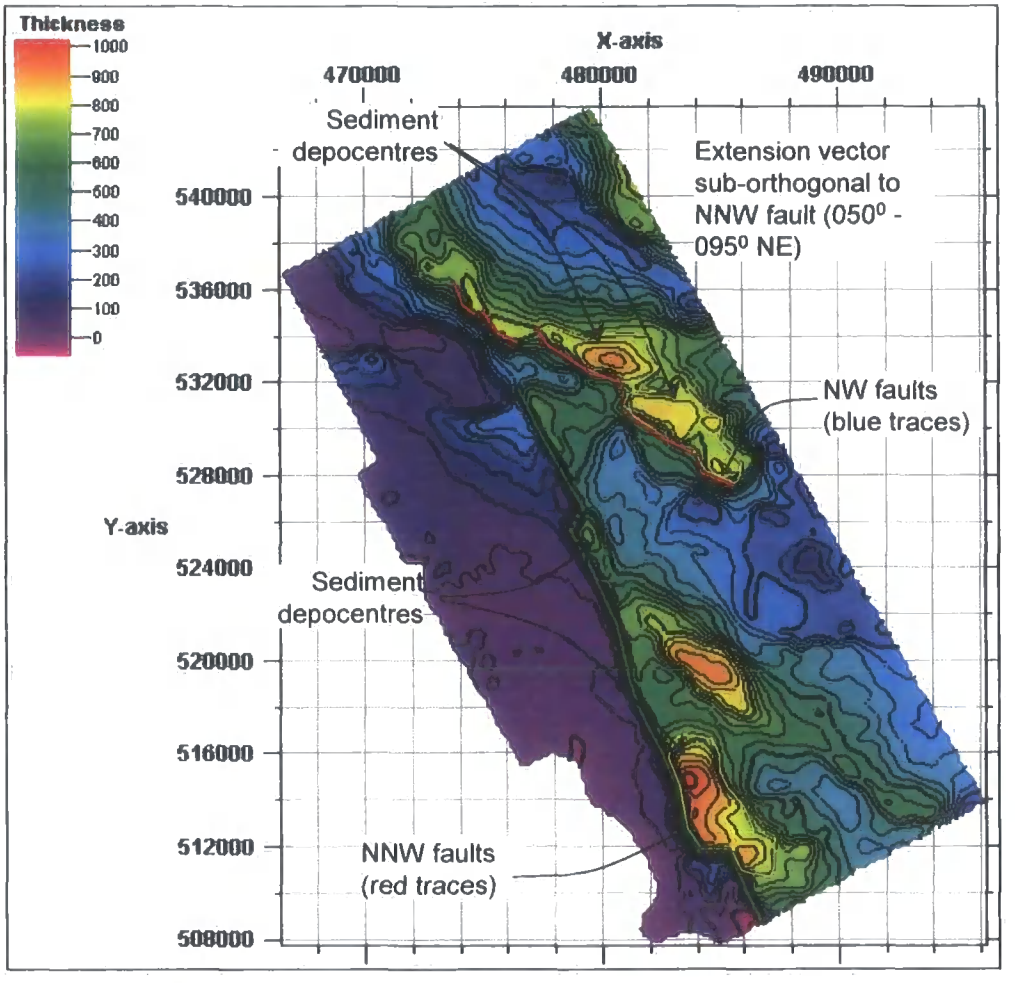

Figure 4.4 Late Oligocene isochore map (Ta_6/Basement) shows thick sediment depocenters (yellow) filling in isolated rhomboid-shaped basement lows.

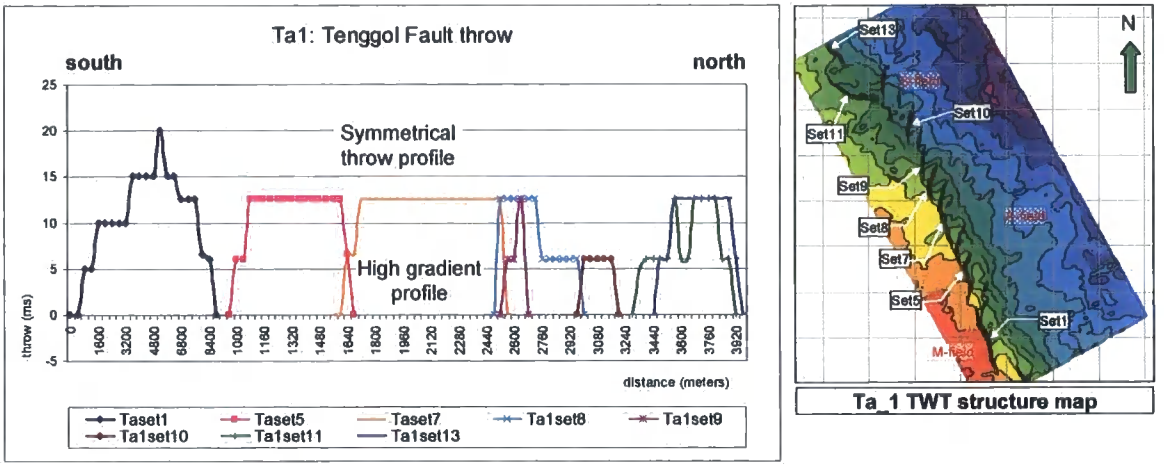

Figure 4.5 Ta_1 throw profile along the Tenggol Fault. Throws are typically around 13ms. Throw profiles for fault sets 8, 9 and 11 are asymmetrical suggesting a degree of interaction with neighboring structures. The remaining fault sets appear to have fairly symmetrical throw profiles.

Dip maps of Early Miocene-equivalent surfaces (Ta_5 and Ta_6), show that at this stratigraphic level, the Tenggol Fault zone is characterized by a broad zone within which bedding reflector dips are significantly higher than the regional dips observed within the adjacent footwall and hanging wall blocks (Attachment 18). For example, a dip map constructed for the Ta_5 marker (Attachment 18) shows that horizon dips range from 5^0 to $>14^0$ within transfer zones, compared with a regional dip of 1^0 to 2^0 (dips estimated assuming a reasonable velocity; see Chapter 3). The dip map for the Ta_6 marker shows a similar trend, where horizon dips within transfer zones range from 10^0 to $>32^0$, whereas the regional surface is fairly gentle with dips of $<2^0$ to 5^0 (Attachment 18). This observation suggests that bed rotation within transfer zones took place due to accumulation of displacement along the upward bifurcating, basement-rooted faults (cf. Childs et. al., 1995). Bed rotations within transfer zones have been observed above upward bifurcating normal faults elsewhere (e.g. Kristensen et al., 2008). In addition, the Tenggol Fault zone is characterized by `smeared' seismic

amplitudes where it cuts and offsets the Ta_5 and Ta_6 sequence. These strata correspond to the shale-prone facies of the Ta_5 and Ta_6 sequences (section 3.3.2).

Narrower zones of anomalously dipping reflectors are observed on dip maps produced from the Top Basement and Ta_4 to Ta_1 markers. As observed on the Top Basement marker, the younger surfaces are characterized by dips ranging from $>40^0$ to $>70^0$ along and near Tenggol Fault, which compare with regional dips of 5^0 to 10^0. The Ta_4 to Ta_1 interval is also characterized by clearly defined reflector terminations (cut-offs) along the Tenggol Fault zone (Attachment 19). The better-constrained cut-offs could be indicative of fault-related deformation in brittle or sand-prone rocks. This interpretation is consistent with both the presence of a proven sand-prone section in the Ta_4 to Ta_1 interval.

4.2 Fault throw profiles

Throw profiles were generated along the Tenggol Fault based on the cut-offs of three selected surfaces: Top Basement, Ta_6 and Ta_3. These surfaces preserve evidence for the main tectonic events identified from regional studies (see section 3.2). The Top Basement marker is representative of the Late

Cretaceous or Early Tertiary rifting event. The Ta_6 surface represents the initial Early Miocene post-rift deposition across the Tenggol Arch and Malay Basin, whilst the Ta_3 surface (of Middle Late Miocene age, equivalent to the sb1900 regional marker) preserves evidence for regional transtension across the Malay Basin. On the throw profile plot along the Tenggol Fault trace, each fault segment is labeled using a numerical system and each is color-coded. Measurements were made for normal faults located on the up-thrown block of the Tenggol Fault zone (example Figure 4.5). The objective of this throw profile analysis is to quantify the movement history along the Tenggol Fault zone. The interpretation of the throw profiles is supported by dip maps of these markers and by interpretation of a variance map of the Middle Late Miocene (Ta_3 marker).

4.2.1 Top Basement fault throw profile

Figure 4.3 shows throw profiles measured along the trace of the Tenggol Fault at Top Basement level. The magnitude of the throw along the Tenggol Fault at this level gradually decreases towards the north of the study area. Generally, the fault sets can be divided into two groups, the first group (south group) consists of fault set 1, set 5, set 7 and set 8. The second group (north group) consists of fault set 10, set 11 and set 13. The two fault sets are clearly separated at the 26000m point (Figure 4.3 and 4.6).

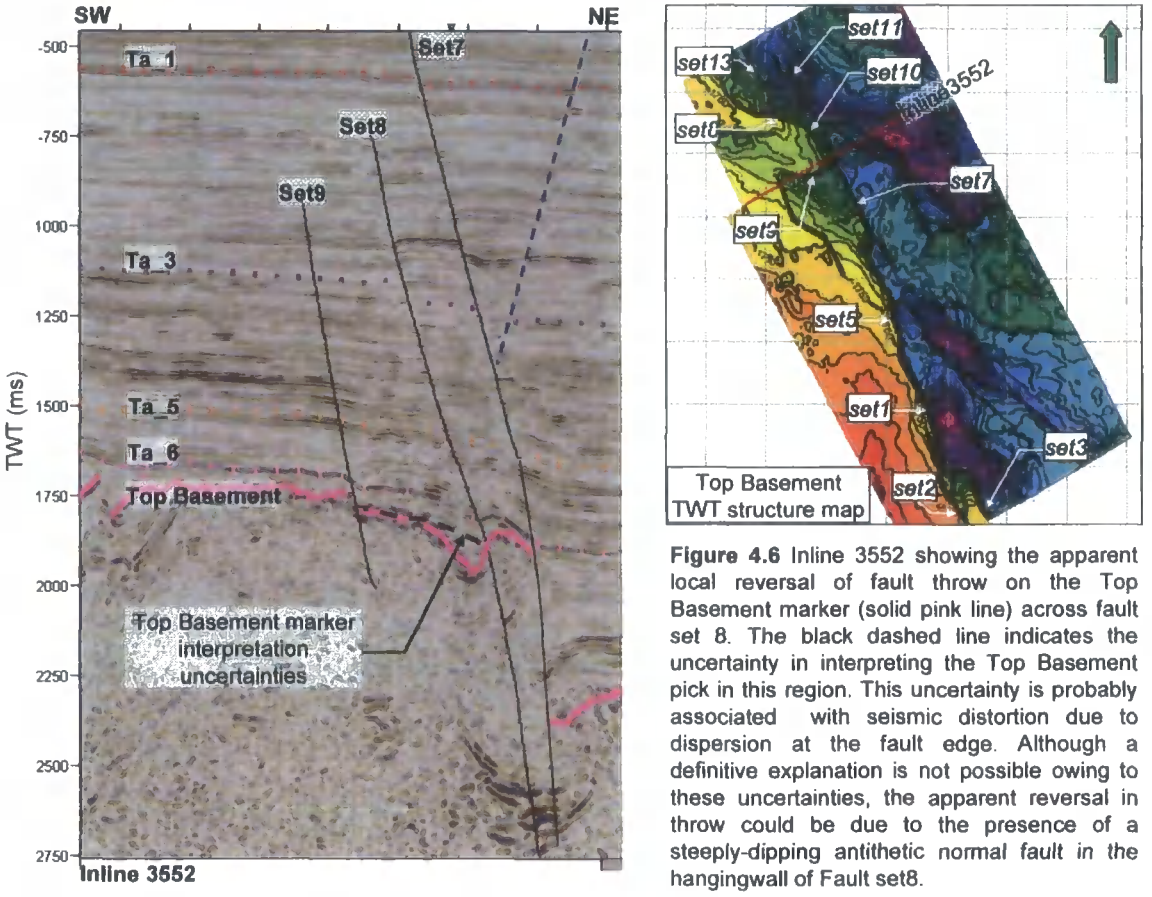

Figure 4.6 Inline 3552 showing the apparent local reversal of fault throw on the Top Basement marker (solid pink line) across fault set 8. The black dashed line indicates the uncertainty in interpreting the Top Basement pick in this region. This uncertainty is probably associated with seismic distortion due to dispersion at the fault edge. Although a definitive explanation is not possible owing to these uncertainties, the apparent reversal in throw could be due to the presence of a steeply-dipping antithetic normal fault in the hangingwall of Fault set8.

Fault set1 has an asymmetrical throw profile with a horizontal throw gradient of 0.2ms/m in the south and a relatively high gradient of 1.2ms/m in the northern part of the profile. Asymmetrical throw profiles can be interpreted as an indication of interaction (displacement transfer) or linkage between adjacent fault segments (e.g. Childs et. al., 1995). Figure 4.3 shows that fault sets 1 and 2 are linked. The northern fault set 1 overlaps with the southern end of fault set 5. Fault set 5 is characterized by horizontal throw gradients of 1.2ms/m and 0.7ms/m at the southern and northern ends, respectively. The high throw gradients observed in the overlap zone between Fault sets 1 and 5 are characteristic of displacement transfer across a relay fault zone (e.g. Peacock &

Sanderson 1991; Huggins et. al. 1995). To the north, fault set 5 overlaps with fault set 7. Fault set 7 also has an asymmetrical throw profile, with a geometry similar to fault set 1, but with smaller throw magnitudes. Once again, the asymmetrical throw profiles suggest a kinematic linkage between the fault segments for fault sets 5 and 7.

The southern end of Fault set 7 has a horizontal throw gradient of 0.2ms/m, whilst the northern flank is measured at 0.8ms/m where it overlaps with fault set 8. Fault set 8 has the smallest throw magnitude with a maximum throw of 238ms. The throw gradients are 0.3ms/m and 0.6ms/m at the southern and northern ends, respectively. The overlapping zone between fault set 7 and fault set 8 also displays a relatively high gradient value of 0.8ms/m. A reversal in the throw value near the southern tip of fault set 8 (Figure 4.3) suggests there may have been localized structural inversion along the relay (transfer) zone between fault set 7 and fault set 8. Childs et al., (1995) have suggested that upward realignment along fault segments can occur in the presence of oblique pre-existing faults. Observations along vertical seismic sections for fault set 7 and 8 indicate reversals in throw directions or slip vectors (Figure 4.6). Alternatively, these apparent reversals in throw could be due to the presence of poorly-imaged (hence unmapped) antithetic faults in the immediate hangingwall of the Tenggol Fault (e.g. Figure 4.6).

The northern group of faults comprises three fault sets, namely fault set 10, fault set 11 and fault set 13. The throw profile for fault set 10 is slightly asymmetric with a horizontal throw gradient of 0.6ms/m at its southern end, and 0.2ms/m in the north where it overlaps with fault set 11. Fault set 11 has an asymmetric throw profile with a gradient of 0.4ms/m in the south and 0.3ms/m in the north. Fault set 11 also overlaps with fault set 13 in the north of the study area (Figure 4.3). The throw profile of fault set 13 is essentially symmetrical with the horizontal throw gradient measuring 0.1ms/m in the south and 0.2ms/m at the opposite end of the fault. Throw profile gradients of for fault sets 11 and 13 within the over-lapping zone are 0.3ms/m and 0.2ms/m, respectively.

In general, throw gradients associated with the northern group have relatively low values - the highest gradient measured was 0.6ms/m. This contrasts with the southern group which has a maximum gradient value measured at 1.2ms/m. The higher gradients associated with the southern group of faults are indicative of displacement transfer zone development between overlapping faults within this fault group. In general, the geometry of fault throw profiles at Top Basement level shows that throws are greatest in the southern part of the study area – i.e. along the M-field – gradually decreasing to the north, i.e. towards the S-field (Figure 4.3). This observation suggests that the Tenggol Fault may have originally initiated in the south near the M-field, and gradually propagated towards the northern margin of the Tenggol arch.

4.2.2 Ta_6 fault throw profile

The throw profile of the Tenggol Fault on the Ta_6 surface has a similar geometry to the throw profile at Top Basement level. Fault throws in the southern part of the study area have high magnitudes and gradually decrease towards the north. 10 fault sets have been mapped, with one fault set located on the up-thrown block (shown as a dashed line in Figure 4.7). These fault sets are mainly the upward continuations of faults observed at Top Basement level, apart from fault set 9 which is a minor fault located in the footwall of the Tenggol Fault.

The fault throw profile of fault set 1 overlaps with fault set 5. The horizontal throw gradients within the overlap zone are 0.1ms/m and 0.1ms/m for fault set 1 and fault set 5, respectively (Figure 4.7). Fault set 5 has an asymmetric fault throw profile with a gradient of 0.03ms/m in the north and a maximum fault throw of 152ms, which is the largest throw magnitude recorded on the Ta_6 surface.

Fault set 7 has an asymmetric throw profile and overlaps with fault set 9 to the north with very low gradient (0.03ms/m). The throw magnitude decreases abruptly from a maximum throw of 152ms at fault set 5 to a maximum fault throw of 50ms at fault set 7 (Figure 4.7). Fault sets 9, 11 and 13 to the north show generally symmetrical throw profiles and lower throw magnitudes, with average fault throws of circa 30ms. A small overlap zone is observed between fault set 7 and fault set 8, with throw gradients of 0.03ms/m and 0.01ms/m respectively.

Throw profiles gradients of fault set 11 and fault set 13 ranges from 0.03ms/m to 0.06ms/m.

In general, the throw profile gradients for the Tenggol Fault on Ta_6 are lower compared to the Top Basement level. The similarities in fault throw profile geometry on Ta_6 and Top Basement suggest that the faults on Ta_6 are upward continuations of the basement faults.

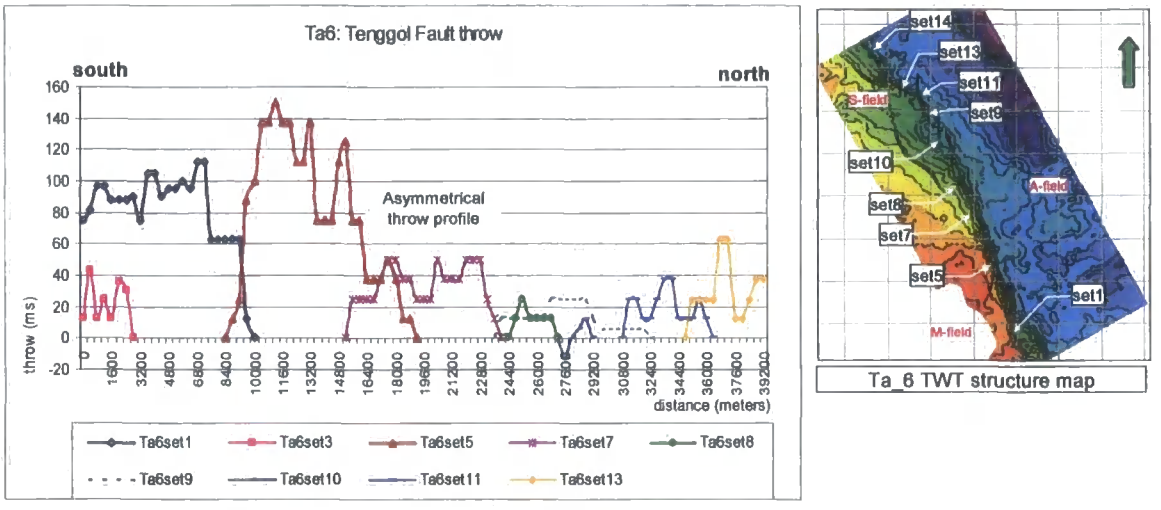

Figure 4.7 Ta_6 throw profile along the Tenggol Fault. This profile shows a broadly similar pattern to the Top Basement throw profile. Note, however, that the maximum throw is significantly lower (c. 140ms) at the level of the Ta_6 marker. Fault set 10 is shows an apparent minor reversal in fault throw (see Figure 4.4b). Note that Fault set 9 is located on the up-thrown block of Tenggol Fault.

4.2.3 Ta_3 and Ta_1 fault throw profiles

In general, throw profiles for the Tenggol Fault on the Ta_1 and Ta_3 horizons are fairly symmetric (Figure 4.5 and 4.8). Some fault sets, including fault sets 1,

5, 6, 7, 8, 11 and 13, represent the upward continuations of basement faults (Figure 4.8). Fault throws are fairly subtle at this level along the Tenggol Fault, with throw values averaging 50ms and 13ms at Ta_3 and Ta_1 levels, respectively. The northern and southern fault groups described in the previous sections can be identified on structural maps of the Ta_3 and Ta_1 surfaces (Attachment 14 and 15).

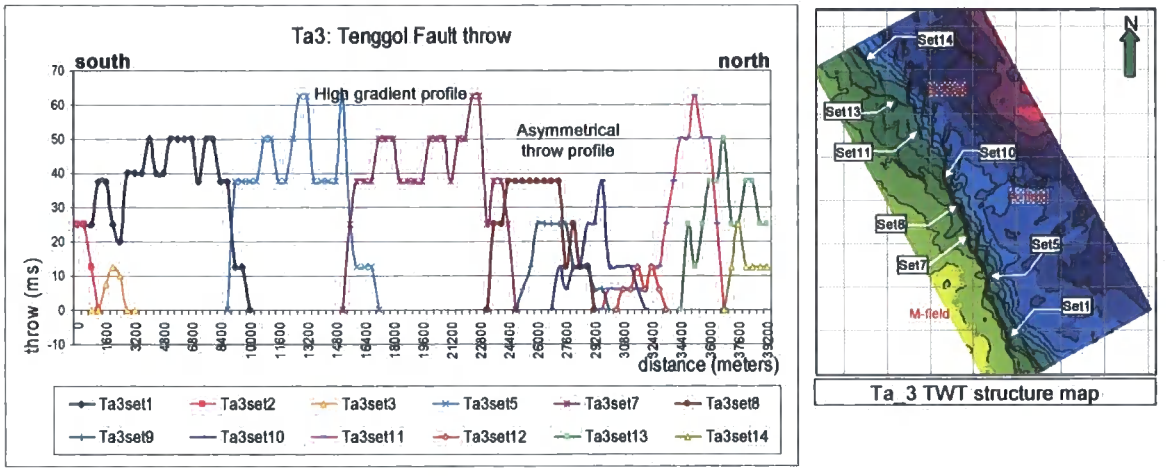

Figure 4.8 Ta_3 throw profile along the Tenggol Fault. Maximum throws typically range from 40ms to 60ms, although smaller maximum throws are associated with fault sets 9, 12 and 14. All fault sets consistently show normal offsets at the Ta_3 level.

4.2.4 Summary: fault geometry and throw profiles

In map view, the Tenggol Fault zone comprises a series of en-echelon fault segments. The throw profiles for the Tenggol Fault at Top Basement level display high throw gradients within fault overlap zones, consistent with displacement transfer across relay zones (Childs et. al., 1995). Asymmetrical

throw profiles provide evidence for linkage between parallel-trending fault traces, pointing to the existence of fault relay zones prior to breaching and linkage (Childs et. al., 1995, Huggins et. al., 1995). Vertical seismic sections across the Tenggol Fault zone are characterized by sub-parallel splay faults with significant normal offsets that are suggestive of predominantly extensional movements (Figure 4.5, 4.9). However, the presence of en-echelon fault segments as observed in map view may also be an indication of strike-slip deformation, a possible interpretation that is discussed further in section 4.5

In conclusion, the Tenggol Fault at the level of the Top Basement appears to have been active as a normal fault, which subsequently propagated upwards into the shallow post-rift sequence. It dies out within Late Pliocene strata and represents the primary tectonic boundary fault on the Tenggol Arch. Small reverse displacements are locally observed along the fault plane and may have developed in response to localized tectonic movements or due to the presence of poorly imaged (hence unmapped) antithetic faults in the immediate hangingwall of the Tenggol Fault.

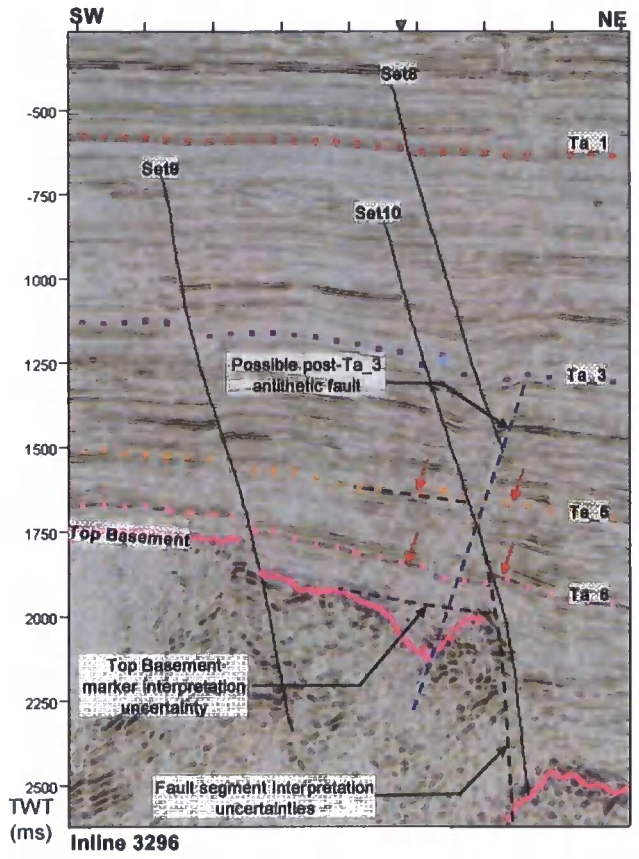

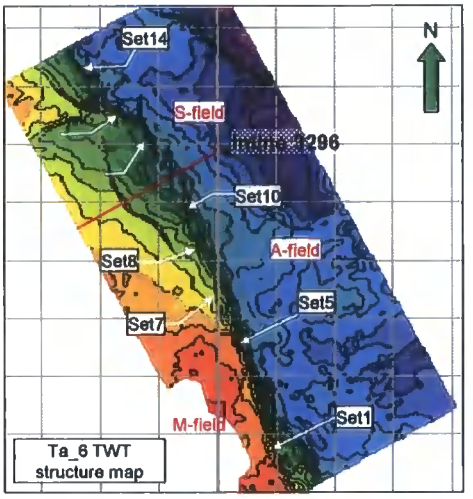

Figure 4.9 Inline 3296 showing a local, apparent reversal in fault throw across fault set10 on the Ta_6 and Ta_5 markers (red arrows). Black dashed lines indicate interpretational uncertainties associated with the fault and horizon picks. The uncertainties are likely to be associated with seismic distortion due to dispersion at fault edges. Although a definitive explanation is not possible owing the these uncertainties, the apparent reversal in throw could be due to the presence of one or more antithetic normal faults in the hangingwall of Fault set10.

Throw profiles along the Tenggol Fault show that the largest displacements and longest-lived period of growth faulting and sedimentation occurred in the southern part of the study area. The fault displacements lessen to the north. Here, there is no apparent increase in sediment thickness from the footwall to the hangingwall, suggesting that the fault may not have been active around the northern margin of the Tenggol Arch during the Late Oligocene to Early Miocene (Figure 4.10a). However, the Late Miocene/Pliocene strata display a marked increase in sediment thickness from the footwall onto the hanging-wall of the fault in this area, which suggests that growth faulting occurred later near the northern margin of the study area compared to the area further south. This observation is

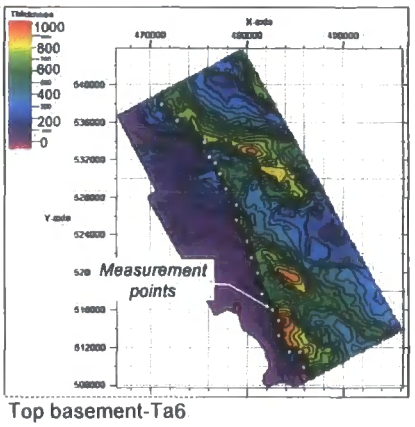

Top basement-Ta6

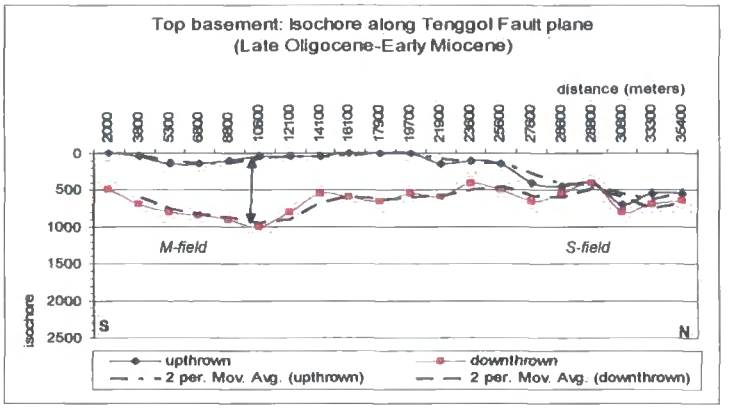

Figure 4.10a Late Oligocene/Early Miocene sequence thickness profiles along Tenggol fault along M-field (south) shows thin strata on the up-thrown block compared to downthrown block, suggests growth faulting along south of Tenggol Fault. As the fault dies-out to the north, thickness profiles indicates fairly similar thickness across fault. Throw profile of Late Oligocene/Early Miocene (Ta_6 seismic surface) indicates normal faulting with large throw profiles in the south and gradually decreases in the north, along S-field.

consistent with analyses of the Malay Basin, which show that regional sediment depocentres moved northward with time, resulting in a shallower margin and thinner Late Miocene/Pliocene sediments on the Tenggol Arch compared with elsewhere in the basin (Appendix 13a and 13b). Table 3.1 summarizes the movement history of the Tenggol fault zone (see also Attachment 20).

4.3 Isochore maps and Miocene basin evolution

Isochore maps have been used to illustrate the thicknesses of sedimentary sequences during different depositional intervals. The maps highlight sediment depocentres (i.e. where the isochore values are the highest) and basin margins or flanks (i.e. where the isochore values are lower). Therefore, any changes in basin geometry during the basin evolution will be reflected in the isochore maps.

Changes in basin geometry may be controlled by differential subsidence along or across major fault systems, such as the Tenggol Fault zone. The previous regional study of the Malay Basin (PETRONAS, 2006(b)) has highlighted the general changes in basin geometry throughout the Miocene to Pliocene interval. During the present study, isochore maps of the Tenggol Arch were generated for the Late Oligocene/Early Miocene, Middle Miocene and Late Miocene/Pliocene sequences (Attachment 9).

Regional isochore maps of the Middle Miocene (sb1200) to Late Miocene/Pliocene (sb1200) strata produced during the previous regional mapping study (PETRONAS, 2006(b)) show an abrupt change between the sb1200 (Middle Miocene) sequence to the sb1900 (Middle Late Miocene) sequence. The sb1200 sequence was deposited during a period of tectonic quiescence, but the sb1900 records the development of the tight, east-west trending folds that dominate the central and northern zones of the Malay basin.

These east-west trending folds are associated with major N- and NNW-striking fault zones (Appendix 13). The east-west trending folds appear to be less prominent at the sb2100 (Pliocene) level, where prominent N-striking normal faults cut the folds in the centre of the basin orthogonal to their axial traces. These later north-south trending faults are potentially associated with the present-day 005^0 maximum horizontal compression direction that has been derived from borehole breakout data in the Malay Basin (Appendix 10).

Isochore maps generated over the Tenggol Arch in this study show sediment depocentres switching from the southern margin during Early Miocene times, to the northern margin during Middle Late Miocene times. The isochore maps also indicate that the Tenggol Arch has undergone a period of tectonic quiescence during the Early Miocene period (Ta_5 to Ta_4 marker). (Attachment 9 (b) and (c)).

During Early Miocene times (Ta_6 and Ta_5 sequences), the isochore maps of the Tenggol Arch display greater thicknesses on the hanging wall of the Tenggol Fault compared with equivalent footwall sequences (Attachment 9 (a) and (b)). This observation is consistent with Late Oligocene/Early Miocene isochore maps for the Malay Basin, which show that the sediment depocentres were located mainly along the southern margin of the basin (Appendix 14 (a)). On the Tenggol Arch, the isochore map of Ta_4 (Middle Miocene) sequence shows a fairly uniform thickness along the southern margin, gradually thickening towards the northern margin of Tenggol Arch (Attachment 9 (c)).

The isochore map of Ta_3 (Middle Late Miocene) also shows fairly uniform thicknesses (similar to Ta_4 sequence) with sequence thicknesses ranging from 250 to less than 350 ms (Attachment 9 (d)). The thickness gradually increases towards the northern margin of the Tenggol Arch. The time-equivalent isochore for the Malay Basin shows that, at this time, the active depocentres were located

close to the present-day centre of the basin (Appendix 13 (b)). However, the Ta_2 sequence (Late Miocene/Pliocene) isochore map indicates a slight increase in stratal thicknesses in the hanging wall of the Tenggol Fault (compared with the footwall), which gradually increases towards the North and Northeast margin of the Tenggol Arch (Attachment 9 (d)). This observation is consistent with Middle Miocene isochore maps from the Malay Basin (sb1200) which show distinctive sediment depocentres close to the northern margin of the basin (Appendix 13 (c)). These observations suggest that the basin was possibly tilted northward and that the southern margin of the basin, which includes the Tenggol Arch, was an area of relatively high topography during the Middle Miocene. The regional sediment depocentres have remained in the central parts of the Malay basin since the Late Miocene/Pliocene until the present day.

Thickness profiles along the Tenggol Fault for the Late Oligocene to Early Miocene, Middle Late Miocene and Late Miocene/Pliocene intervals (Figures 4.10a, 4.10b and 4.10c) show consistently higher thicknesses on the downthrown block of the southern part of the Tenggol Fault. The thickness profile for the Late Oligocene/Early Miocene sequence, which is near-equivalent to the Ta_5 sequence and the Middle Late Miocene, which is near-equivalent to theTa_3 sequence, shows large across-fault differences in sediment thickness in the south, with sediment thicknesses gradually becoming more uniform in the north (Figure 4.10b).

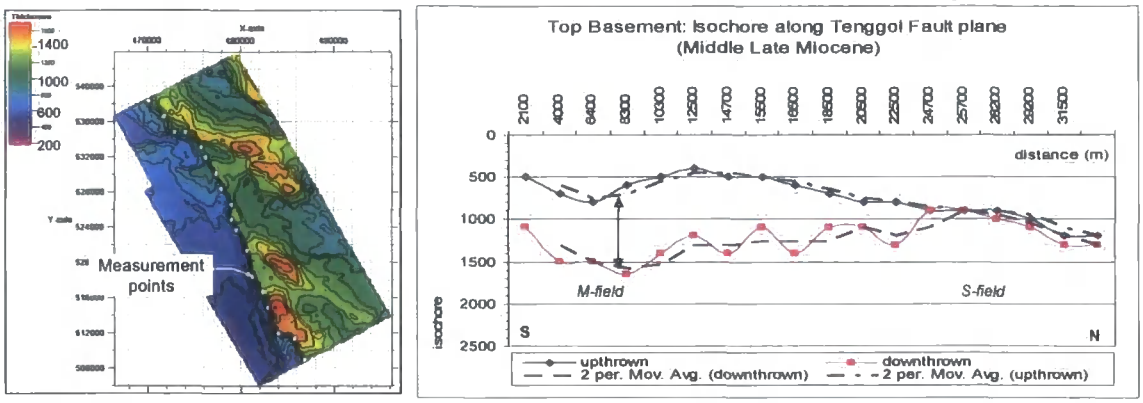

Figure 4.10b Similar thickness profiles patterns are observed along Tenggol Fault from Middle Late Miocene sequence. Large thickness differences, where thin strata on the up-thrown compared to the downthrown block are prevalent in south demarks growth faulting. Fault throw profiles of Middle Late Miocene denotes reverse in throw as indicated in figure on the right (black arrows). Reversed in fault throw interpreted as local inversion along Tenggol Fault.

The observed changes in sediment thickness suggest that growth (i.e. active deformation) along the southern part of the Tenggol Fault occurred throughout the deposition of the Miocene/Pliocene sequence. A thickness profile of the Late Miocene/Pliocene sequence, which is equivalent to Ta_3 (Figure 4.10c) also indicates growth faulting near the southern margin of the area. However sudden increases in sediment thickness on the downthrown block near the northern margin suggest that growth faulting occurred during Late Miocene/Pliocene times adjacent to the S-field (Figure 4.10c). The presence of reverse fault throw profiles along Tenggol Fault during the Middle Late Miocene may also indicate local inversion events occurring along Tenggol Fault (but note the alternative interpretation described in section 4.2) (Figure 4.10b). Such growth faulting and possible local structural inversions along fault planes are most likely associated

with transtensional tectonics in the Malay Basin during Miocene-Pliocene times (see section 4.6).

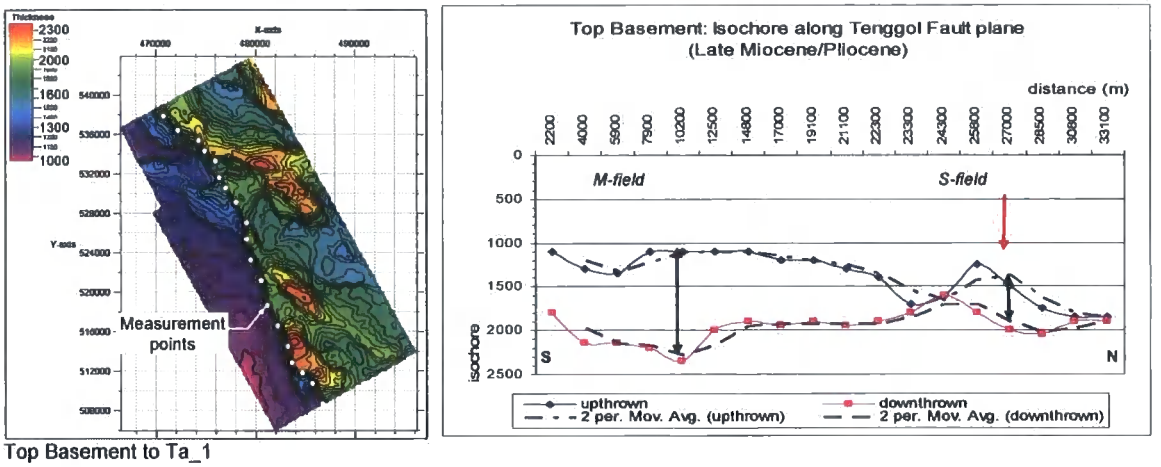

Figure 4.10c thickness profile along Tenggol Fault at shows large differences in thickness across fault along M-field suggests growth faulting in the south of Tenggol Fault. Strata thickness gradually becomes fairly uniform as emerging S-field in the north. However sudden increased in thickness differences along S-field suggested the fault has experienced growth faulting along S-field

4.4 Structure and tectonic evolution of the Tenggol Arch and Malay Basin

4.4.1 Top Basement structure and pre-Oligocene structural evolution of the Tenggol Arch

The pattern of faulting observed on the Top Basement structural map is characteristically curved and anastomosing in appearance and can be sub-divided into 3 main geometric types: 1) `S-shaped NNW-striking faults; 2) paired S-shaped and Z-shaped fault bends; and 3) stepping faults with en-echelon

arrangements (Figure 4.11). Such patterns are prevalent only at Top Basement levels and appear to be associated with the formation of small pre-Oligocene sub-basins. These are in turn likely to be associated with pre-existing basement faults that are of post Late Cretaceous to no younger than Oligocene age. These sub-basins are younger than the Malay Basin proper, which is interpreted to have initiated during the Late Cretaceous (see Chapter 2). Thus the earliest sediment packages deposited in the Malay Basin are not equivalent in age to the earliest packages deposited in the sub-basins over the Tenggol Arch. This interpretation is shown clearly on a regional 2D seismic section (Appendix 7) which shows the correlation of the Top syn-rift seismic marker across the Tenggol Fault zone from the basin centre.

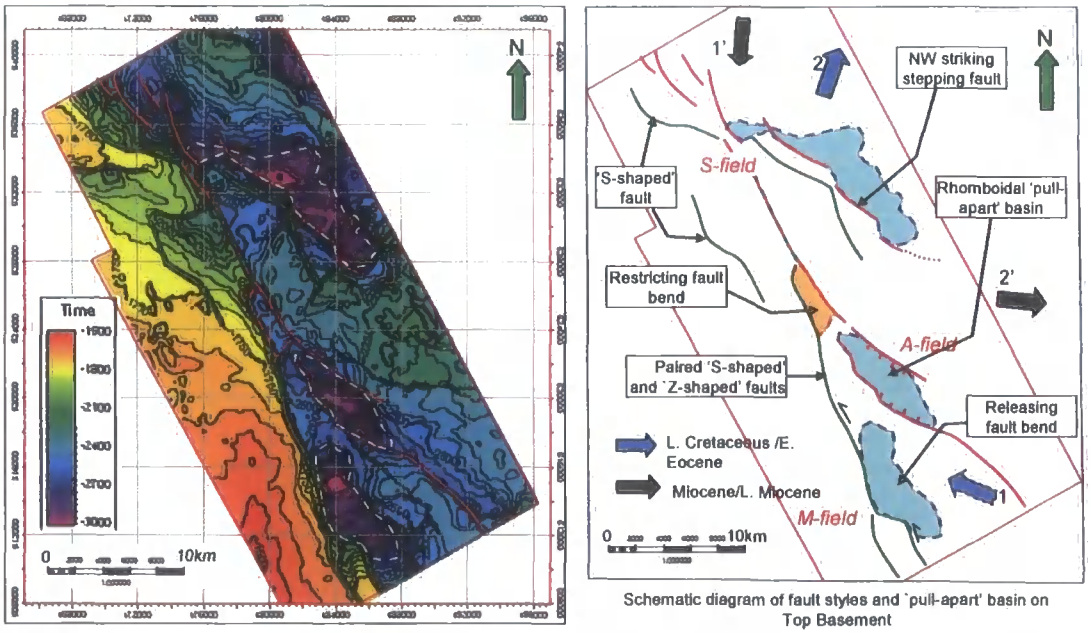

Figure 4.11a Top Basement time structure map (left) and schematic fault / depocentre map (right) showing the development of rhomboidal 'pull-apart' basins during an "early" phase of sinistral strike-slip along the green fault traces. This deformation probably took place sometime after rifting during the post-Late Cretaceous to Late Eocene interval. NW-striking faults (shown as red traces) appear to be younger. The most pragmatic explanation for these younger faults and associated depocentres is that they developed during a phase of NE-SW extension. See text for explanation. The blue arrows labeled (1) and (2) indicate the *inferred orientation of the minimum* horizontal stress during sinistral strike-slip and extension, respectively. Note the slight clockwise rotation of the inferred stress field between these deformation events.

The depocentres associated with 'S-shaped' and 'Z-shaped' fault trace geometries in the hanging wall of the Tenggol Fault could be interpreted as being pull-apart basins that developed at releasing bends or stepovers during sinistral strike-slip deformation along the N- to NNW-striking faults (Figures 4.11a & b). There is little direct evidence for strike-slip deformation from the offshore dataset. Nevertheless, pre-Oligocene strike-slip faults with sinistral displacements have been identified onshore in Peninsula Malaysia and in Central Sumatra (Bengkalis Trough) (see section 2.4.2b). As discussed previously, these faults may be reasonable analogues for some of the basement structures preserved on the Tenggol Arch. Furthermore, research done by other workers on major strike slip faults throughout Southeast Asia suggests that sinistral deformation occurred along major Southeast Asian strike-slip zones such as the Three Pagodas, Mae Ping and Red River Fault zones. This regionally important sinistral deformation event is most likely to have taken place during Early Tertiary to Paleogene times (Lacassin et. al., 1997, Harrison, 1992, Morley et al, 2007). Table 2.2 summarizes the major events recorded along the major strike slip zones of Southeast Asia in comparison to Peninsular Malaysia and offshore areas, including the Malay Basin and Tenggol Arch.

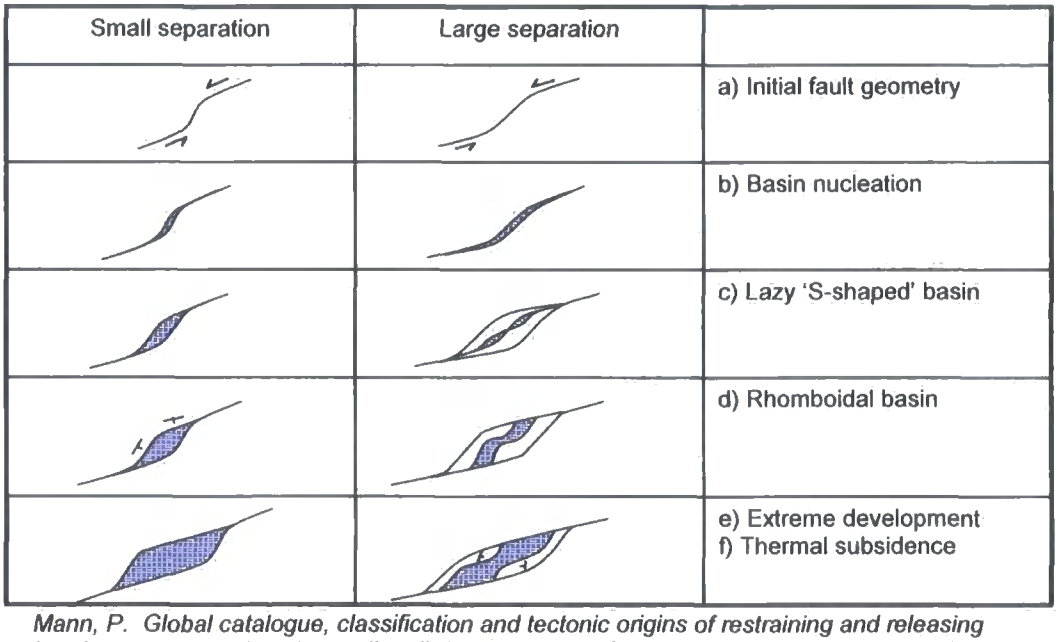

Mann, P. Global catalogue, classification and tectonic origins of restraining and releasing bends on active and ancient strike-slip fault systems. Geological Society, Special Publication

Figure 4.11b Schematic diagram illustrating the development of 'rhomboidal' pull-apart basins during sinisitral strike slip (after McClay & Bonora 2001; Mann 2007).

Despite the strong evidence onshore for early Tertiary sinistral strike-slip, this kinematic model cannot explain the development of all structural lows observed at Top Basement level on the Tenggol Arch. For example, the "rhomboidal pull-apart basins" in Figure 4.11a appear to be associated with right-stepping faults that would in fact have acted as restraining bends during sinistral strike-slip. The most pragmatic explanation is that these structural lows are depocentres in the hanging walls of segmented normal faults that probably developed following cessation of sinistral strike-slip, but prior to the onset of Late Miocene transtension in this region (see sections 4.5 & 4.6). If correct, this inference

suggests there was a clockwise rotation of the regional extension direction during the Paleogene.

4.4.2 Folding

Folds on the Tenggol Arch are gentle with fold axes generally running parallel to fault traces. Folding is prevalent in Late Miocene to Pliocene strata, which are equivalent to the Ta_3 to Ta_1 surfaces. A seismic section across the Tenggol Fault zone illustrates the subtle folds with average amplitudes of 20ms (Figure 2.4d). Fault-dependant anticlines plunge gently towards the NNE, parallel to the north-south and north-northeast striking en-echelon faults that cut the Late Miocene to Pliocene (Ta_3 to Ta_1) strata (Figure 4.12a, Attachment 13). Fault–parallel folds are first identified on Ta_4 strata and gradually become more widespread in Middle Late Miocene strata (Ta_3). The folds are less obvious in Pliocene strata (Ta_2/Ta_1). Changes in fault surface topography along the Tenggol Fault zone can be observed in azimuth maps for each of the Ta_3 to T_2/Ta_1 surfaces (Attachment 17).

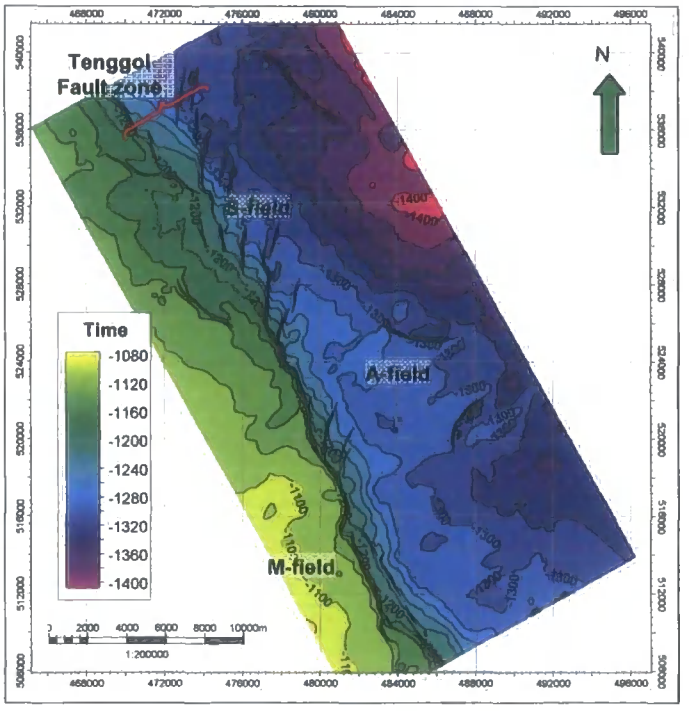

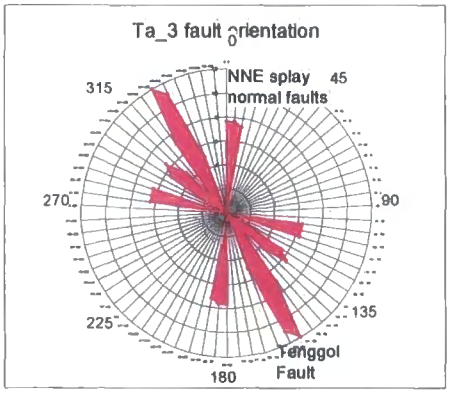

Figure 4.12a Ta_3 time structure map (left) showing the en-echelon N- to NNE-striking fault segments within the Tenggol Fault zone. *Subtle fault dependant folds are prevalent in* the Middle/Late Miocene with fold axes plunging N-NNE parallel to fault planes. The rose diagram (above) highlights the dominant NW-SE trend of the Tenggol Fault and the NNE-striking splay faults.

Figure 4.12c shows a seismic vertical section that represents a dip-line to the Tenggol Fault. The section clearly demonstrates folding of strata between the Ta_6 and Ta_3 seismic markers. The fold amplitude decreases upwards into younger strata (Ta_2 to Ta_1). On time structure maps, the fold appears to be a subtle feature, with the fold axis running parallel to the major boundary fault planes (Attachment 15). A strike-line within the hanging wall of the Tenggol Fault does not illustrate strong folding features and the thicknesses of strata within the Ta_1 to Ta_3 interval appear to be fairly uniform (Figure 4.12d). This observation is consistent with folding features observed on maps and along the seismic dip-line (Figure 4.12c). Internal seismic reflectors within the Ta_3 to Ta_6 sequence appear to be parallel with no clear presence of on-lapping seismic reflectors onto the fold crest. Nevertheless, the fold amplitude decrease

upwards above the Ta_3 marker, suggesting that the fold developed after the deposition of the Ta_6 to Ta_3 sequence.

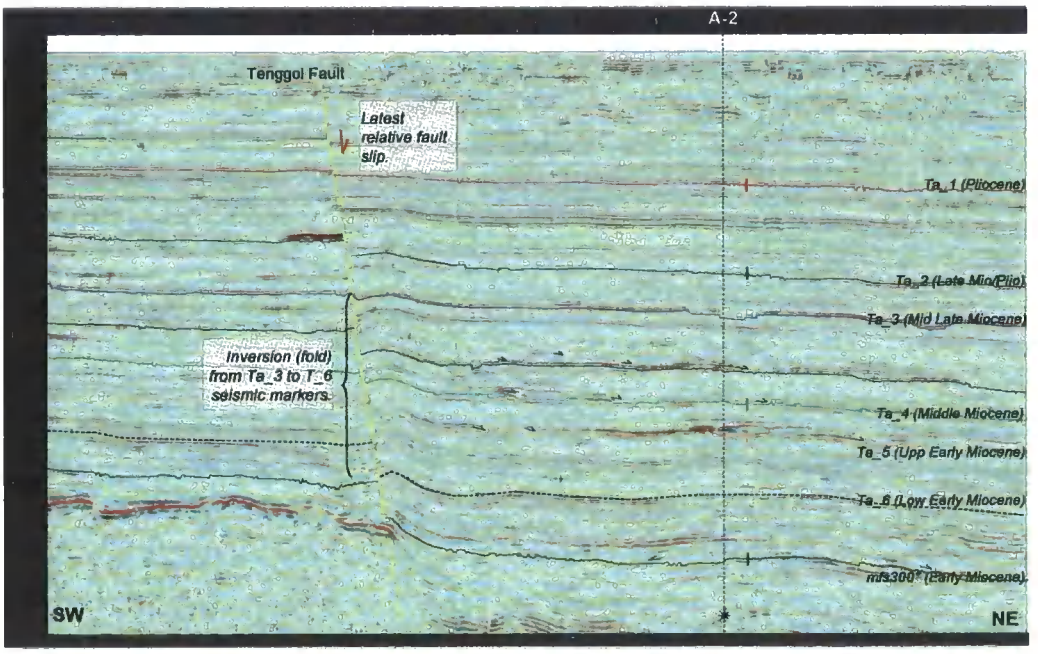

Figure 4.12c A dip-line (2D seismic) across Tenggol Fault shows clear folding from Ta_3 and dies out to Ta_6. The fold is interpreted as inversion structure which occurred during Middle Late Miocene (Ta_3). Non-present of on-lapping seismic reflectors on fold crest made it uncertain to determine origin of fold. The red arrow indicates youngest fault slip direction.

The fold geometries are reminiscent of the inversion folds described by Turner & Williams (2004). There is no reversal in fault throw across the Tenggol Fault, which suggests that any inversion that occurred in this area was mild. An important question is to establish whether the folds are related kinematically to the East-West trending folds in the centre and East margin of Malay Basin. These folds within the Malay Basin are believed to have developed synchronous with the deposition of the SB1900 marker (Appendix 13a), i.e. during the Middle Late Miocene (SB1900). In contrast, the folds adjacent to the Tenggol Arch

appear to have developed slightly later, *after* deposition of Ta_3 (equivalent to SB1900). Thus, the Tenggol Fault may have experienced a period of mild inversion immediately following transtensional deformation across the Tenggol Arch and elsewhere in the Malay Basin (section 4.5).

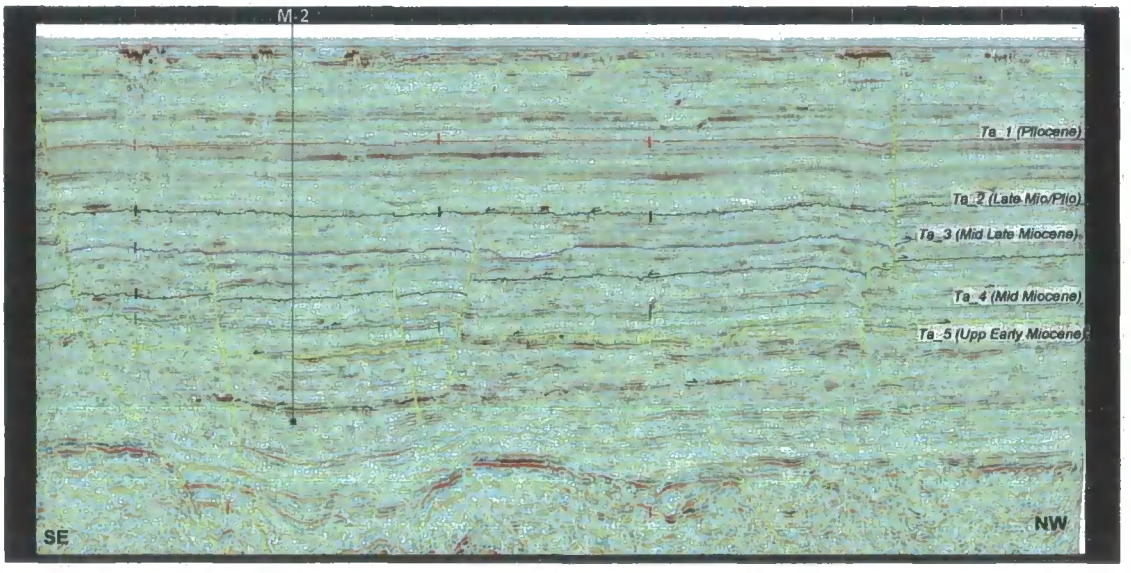

Figure 4.12d Strike-line along the hanging wall of the Tenggol Fault shows uniform thickness of strata Ta_1 to Ta_2 with no clear folding feature. Gentle folds observe along fault from Ta_3 to T_6 similarly as in dip-line.

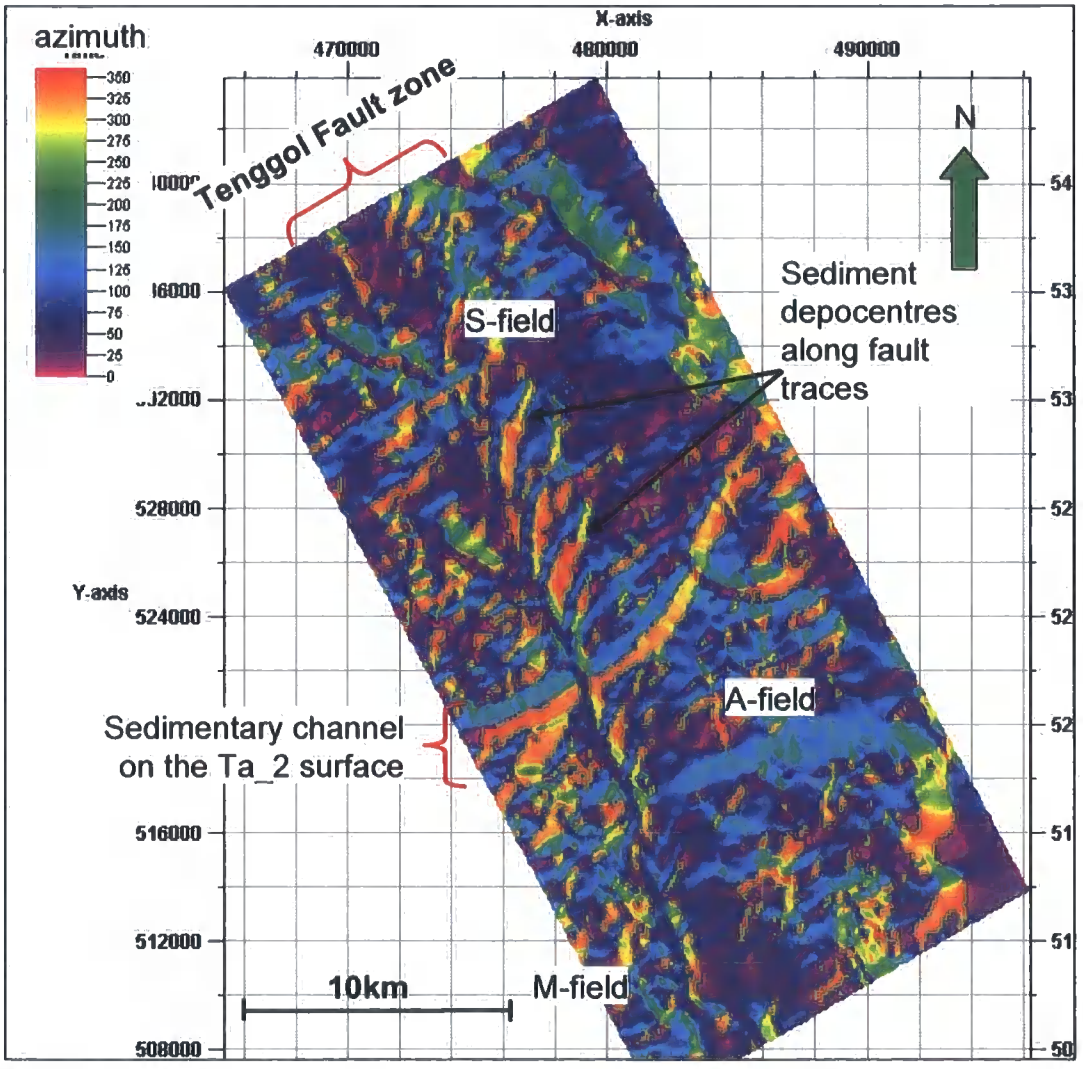

Figure 4.12b Ta_2 azimuth map (above) highlights the distinctive crescent-shaped geometries northerly oriented surface on the downthrown side of the NNE-striking fault segments suggest syn-sedimentary system along the fault zone during Upper Miocene/Early Pliocene. Presence of base of channel scouring through the Ta_2 surface shows no visible lateral displacement. This observation also suggests syn-depositional during Late Miocene.

4.4.3 Fault-related channel attributes

Geophysical attribute extractions within the Middle to Late Miocene strata were carried-out to delineate channel features within these intervals. Channels that are cut and offset by faults provide piercing points, which allow the local fault slip vectors to be constrained. Geophysical attributes extracted during the present study include dominant frequency, seismic amplitude, relative acoustic impedance, seismic polarity and attenuation. The last two attributes give poor results. This poor imaging is due to noise and geological attributes that are below the resolution of the seismic data. In this section, I will therefore only discuss results from the first three attributes mentioned above. Attribute analysis was done mainly on Channel 1, which flowed between the M- and A-fields (Figure 4.13a and Figure 4.13b). Mapping was limited to the base of Channel 1 where it crosses the Tenggol Fault. The second channel (Channel 2) mapped for this analysis is within the Ta_2 surface and flows across the Tenggol Fault adjacent to the A-field and towards the northeast margin of the study area (Figure 4.13b). All attribute parameter testing was carried out on Channel 1 whilst only selected attributes which showed the best results were applied to Channel 2.

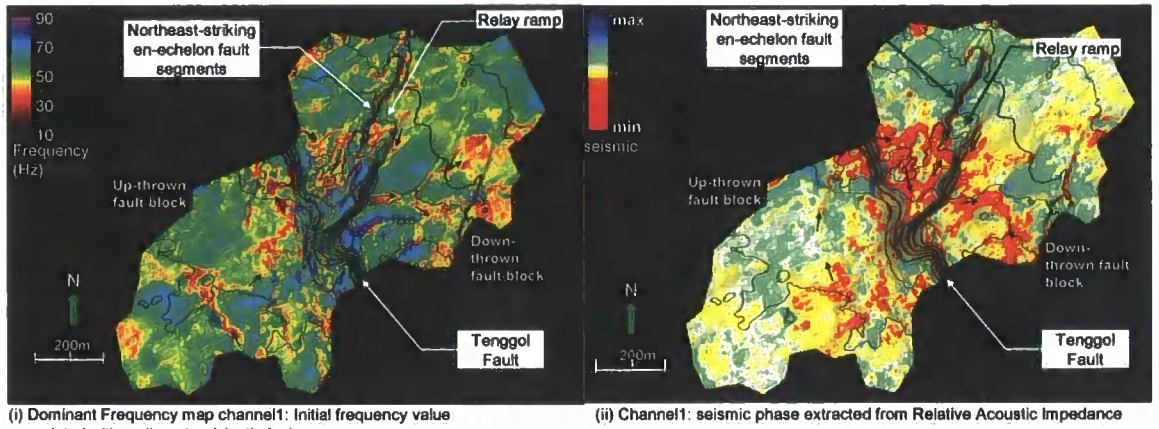

(i) Dominant Frequency map channel1: Initial frequency value associated with sedimentary/clastic facies

(ii) Channel1: seismic phase extracted from Relative Acoustic Impedance

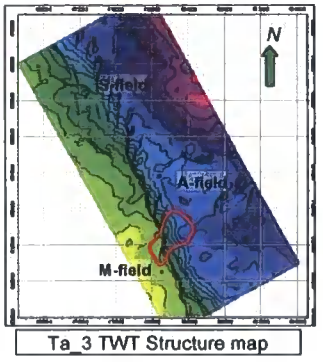

Figure 4.13a Maps showing (i) dominant frequency and (ii) relative acoustic impedance attributes for the Channel1 sedimentary channel in the region where it cuts the Tenggol Fault zone at Middle Miocene (Ta_4/Ta_3) levels. The index map (right) shows the location of Channel1 within the overall study area. In (i), the channel-fill is indicated by low frequencies (red-yellow), whilst high frequencies (blue-magenta) are more likely to be channel levee and flood plain deposits. The channel flowed from the up-thrown fault block (arrow) across the Tenggol Fault, along the NE-striking fault (as shown by arrow) and down the relay ramp. Deposition probably occurred within the structural low situated in the hangingwall of the NE-striking fault. Offset of piercing points (i.e. where the channel intersects the footwall and hangingwall of the Tenggol Fault) demonstrates a normal dip-slip displacement across the Tenggol Fault.

The dominant frequency attribute at Channel 1 (Figure 4.13a) shows a fairly good result in delineating the channel edge across the Tenggol Fault. An instantaneous frequency map shows Channel 1 tuning at 20Hz to 60Hz and the channel-fill corresponds to low frequency values (red-yellow attributes) whilst flood-plain deposits correspond to high frequency values (blue-magenta attributes). Similar responses can be observed in the dominant frequency map (Figure 4.13a (i)). The channel deposit, which is highlighted by arrows, appears to cross the main Tenggol Fault from the up-thrown block towards the down-thrown fault block without any clear evidence of lateral offset. Vertical displacement is therefore dominant along the Tenggol Fault and its en-echelon splay faults. The attributes show that Channel 1 continued to flow down-dip

along the northeast striking en-echelon faults and down along the relay ramp in-between two of these faults (Figure 4.9a(i)) These observations of the dominant frequency map are further supported by RMS amplitude data extracted from the Acoustic Impedence volume (Figure 4.13a (ii)). Here, the channel geometry is highlighted by high amplitude values (red-yellow hue) and shows that the channel flowed along the fault ramp and that sediment was deposited in minor lows along the fault planes (Figure 4.13a(ii)).

Channel 2 is located adjacent to the A-field and flows across the Tenggol Fault towards the northeastern margin of the study area. The Instantaneous Frequency of Channel 2 (Figure 4.13b) illustrates that the channel-fill tuning frequency ranges from 45Hz to 80Hz. No lateral displacement of Channel 2 is observed across the Tenggol Fault whilst large vertical displacements observed in seismic sections suggest normal dip-slip movements during Late Miocene times. This observation is consistent with the attribute mapping of Channel 1. Hence, the Tenggol Fault shows dominantly extensional movement, with a large down-throw towards the east. Evidence of syn-depositional activity, where sediment thickens across faults from the footwall into the hanging wall, can be observed along the North-Northeast striking en-echelon faults on the down-thrown block of the Tenggol Fault (Figure 4.13a). To summarize, findings from channel attribute mapping in the Late Miocene-Pliocene strata suggest that the en-echelon faults prevalent on the downthrown fault block of the Tenggol Arch are not associated with lateral offsets across the Tenggol Fault. There is good

evidence for significant dip-slip offsets consistent with the development of extension-related en-echelon fault patterns during Late Miocene-Pliocene times.

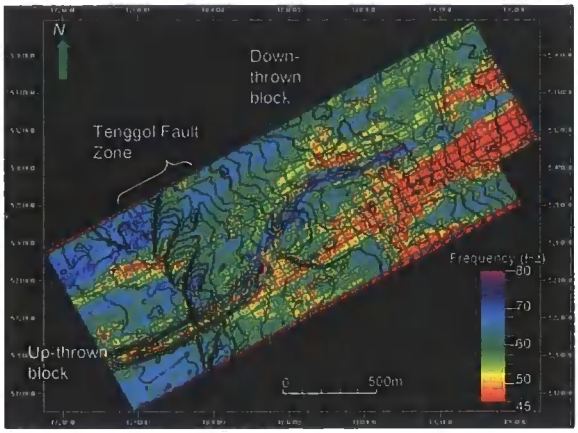

(i) Ta_2: Instantaneous frequency

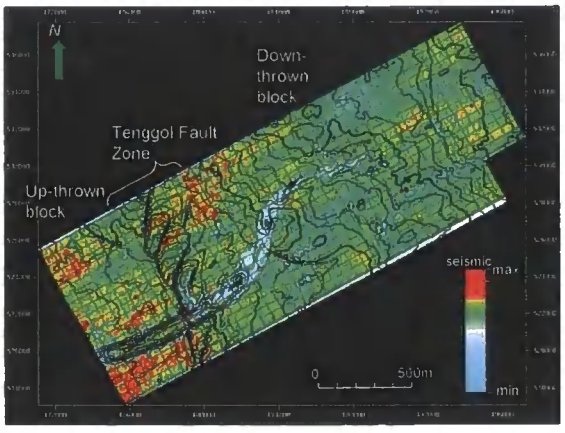

(ii) Ta_2: RMS Amplitude

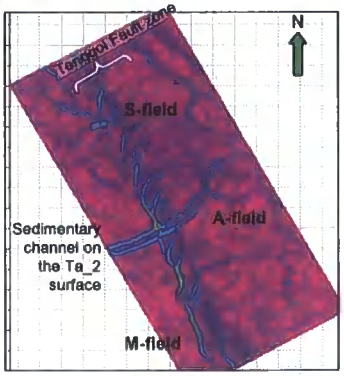

Ta_2 Dip-map: Map showing location of Ta_2 channel

Figure 4.13b Maps showing (i) instantaneous frequency and (ii) RMS amplitude on the Ta_2 surface where an ESE-WNW to NE-SW trending sedimentary channel intersects the Tenggol Fault zone. Note that there is no evidence for lateral offset of the channel cross the Tenggol Fault. High values of instantaneous frequency (in the range 73-85Hz) correspond to channel-fill on the down-thrown block (dark blue-magenta colours). Low values of instantaneous frequency (in the range 45-58Hz) correspond to channel-fill on the up-thrown block and areas of flood-plain deposits elsewhere (yellow-red colours). The RMS amplitude map shows that low amplitudes generally correspond to channel-fill (white-pale blue colour), whilst higher amplitude values (yellow-red colours) are mainly prevalent on the up-thrown block and within the flood-plain.

4.5 A Reassessment of the Miocene-Pliocene kinematics of the Malay Basin

4.5.1 Integrated Regional Study of the Malay Basin (2006)

The Integrated Regional Study of the Malay Basin (PETRONAS, 2006(b)) suggested that the structural styles observed in the Malay Basin were a consequence of extrusion-related tectonics during the Middle to Late Tertiary (see section 1.3.3). More specifically, this study identified evidence for pervasive Middle Late Miocene dextral strike-slip deformation along major N-S trending faults within the Malay basin (Figure 1.7).

Interpretations of the fault patterns seen at Top Basement level derived from 2D seismic and gravity maps highlight the presence of pervasive north-south trending lineaments in the northern and central parts of the Malay Basin. However, northwest-southeast trending lineaments are more prevalent towards the western margin whilst east-west trends dominate towards the eastern margin of the basin (Figure 1.7). The presence of tight, east-west trending folds in the central and eastern zones of the basin was interpreted as evidence for the southward migration of fault-bounded crustal blocks due to extrusion of the Southeast Asian crust along major strike-slip zones, leading to north-south regional compression during the Miocene/Pliocene period.

The 2005/06 study does not explain the spatial relationship between the north-south trending faults and the tight east-west trending folds which are found pervasively within the Late Miocene-Pliocene strata. Nevertheless, it concluded that pre-existing basement fabrics may have influenced the present day structural styles observed in the Malay Basin.

4.5.2 Basis and hypothesis to be tested

The structure map for the Middle Late Miocene sequence shows that east-west trending fold axes and north-south trending faults are predominant in the Central and Eastern Zones of the Malay Basin (Figure 1.7). The northwest striking Western Hinge Fault Zone fault runs parallel to the western margin of the Malay Basin stretching northwards towards the Gulf of Thailand and southward towards the Penyu Basin (Figures 1.7). Preliminary inspection of a structure map of the Middle Late Miocene sequence shows that different parts of the basin appear to have experienced contemporaneous compressional, extensional and strike-slip deformation during the Late Miocene-Pliocene. It is proposed that these observations are consistent with a single phase of dextral oblique extension (i.e. transtension) during this period (e.g. Figure 4.14a; De Paola et. al., 2005(a)).

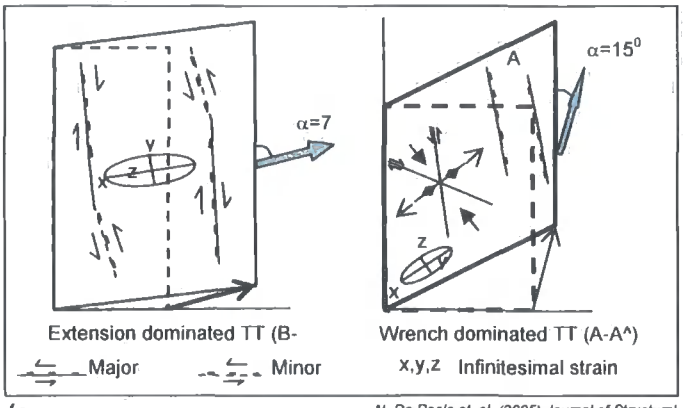

(a

N. De Paola et. al. (2005) Journal of Structural Geology 27, pp 607-625

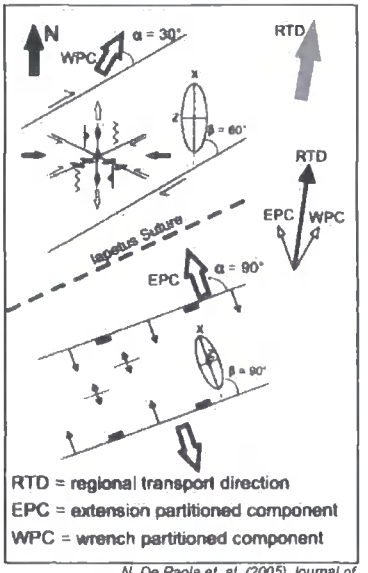

(b

N. De Paola et. al. (2005) Journal of Structural Geology 27, pp 607-625

Figure 4.14 **(a)** Schematic plan-view diagrams showing the structural styles predicted to develop during extension dominated (EDTT; left) and wrench dominated (WDTT; right) transtension (WDTT). α is the angle between the regional extension direction and the boundaries of the deforming zone. In this example, $\alpha = 75^0$ for EDTT and 15^0 for WDTT. **(b)** Example of strain partitioning in the Northumberland Basin, where the regional extension direction (RTD) is significantly oblique to the major basement structure in this area (Iapetus Suture). The oblique deformation has been partitioned between domains of EDTT (dominated by normal faulting) and WDTT (dominated by strike-slip faults and folds). β is the angle between the infinitesimal extension direction (equivalent to the minimum horizontal stress) and the boundaries of the deforming zone.

As noted previously, the Tenggol Fault zone is characterized by an upward bifurcating geometry in which the basement fault is linked to synthetic splay faults with a clear en-echelon arrangement within the Miocene/Pliocene sequence (Figure 4.2). These structures appear to be analogous to the structural styles seen within the basement-influenced Pattani basin in the Central Thailand province (Morley, 2004). Comparison with the Pattani basin therefore implies a potential basement influence on the structure styles observed within the Miocene sequence of the Malay basin. Furthermore, the possibility that oblique tectonics were important during the kinematic evolution of Peninsular Malaysia has been highlighted by early researchers (Hutchinson, 1996; Tjia, 1987) (see sections 2.4.1 and 2.4.2). The increased exploration activity – and hence the better

availability of geological and geophysical data – offshore Peninsular Malaysia since the mid-1980's now provides a basis on which to test these early ideas of oblique extension.

This section aims to test the hypothesis that regional extension oblique to the northwest-trending WHFZ gave rise to a dextral wrench-dominated transtension (WDTT) in the Central and Northern Malay Basin. In particular, a WDTT model could explain the evidence for contemporaneous E-W extension and N-S compression within the Malay Basin during the Middle Late Miocene. Strain analysis has therefore been performed with reference to structures observed on the sb1900 (Middle Late Miocene) marker. In addition, the 2006 regional study postulated that the Laris Fault Zone could represent an important tectonic boundary fault that controlled the structural styles observed in the Eastern Zone of the Malay Basin (cf. Figures 4.14b). This structural analysis will evaluate the possible roles of both the WHFZ and Laris Fault zone as the principal tectonic boundaries to the Malay Basin. Following this analysis of the Central and Northern parts of the Malay basin, section 4.6 then addresses the kinematic evolution of the Tenggol Arch study area.

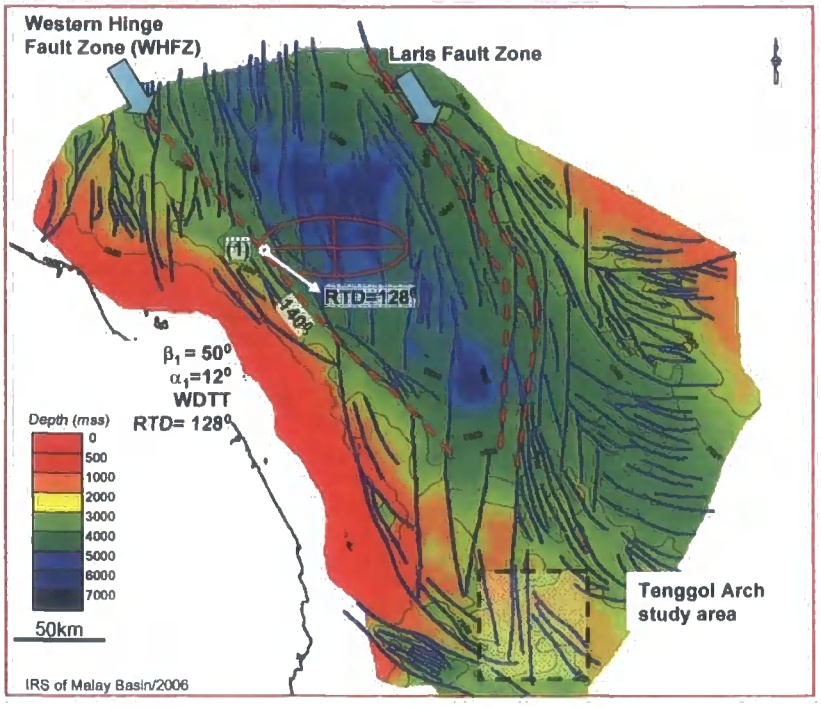

Figure 4.14b Time structure map of the Top Basement marker within the Malay Basin based on 2D seismic mapping and regional Bouguer anomaly gravity map. Dashed red lines highlight the regional trends of the Western Hinge Fault Zone (WHFZ) and Laris Fault Zone. The azimuth of the WHFZ is c. 140° The long axis of the red ellipse represents the orientation of the Miocene infinitesimal extension direction in the northern and central Malay Basin, which is inferred to be parallel to the E-W trending folds – see text for explanation. RTD = regional transport direction. The meanings of other symbols are explained in Figure 4.10a and in the text. The approximate location of the study area is highlighted by the dashed black line.

4.5.3a Kinematic modeling: assumptions and methodology

The following interpretation of the structural and kinematic evolution of the Malay Basin is based upon the models of oblique extension proposed by Morley (2004), Withjack & Jamison (1986) and De Paola et al. (2005(a)). The analysis makes the following assumptions. First, that sandstone and shale beds comprise the predominant basin-fill whilst the basement complex comprises mostly crystalline igneous or carbonate-rich rocks. Second, that the culmination of the major tectonic 'inversion' event in the region (i.e., 'peak structuration') coincided with

the deposition of the youngest folded surface, which has been dated as Middle Late Miocene in age (see section 2.0). Third, that the Middle Late Miocene infinitesimal extension axis was oriented parallel to the axes of the folds (i.e. 095^0; cf. Ramani & Tikoff, 2002). Fourth, that the finite strains associated with folding are low and that crustal shortening was homogeneous throughout the area of folding. Fifth, that the basement expressions of the northwest-trending Western Hinge Fault Zone and Tenggol Fault zone were the principal tectonic boundaries to the Malay basin and Tenggol Arch (section 4.6), respectively. The assumptions about the dominant lithologies and deformation zone boundaries are discussed in more detail below.

According to De Paola et. al., (2005(b)), the Poisson's ratio (ν) of the dominant basin fill is an important control on the kinematics and structural styles observed during oblique extension. Poisson's ratio (ν) provides a measure of the compressibility of the basin fill, and is a key control on whether a basin experiences wrench- or extension-dominated transtension (e.g. De Paola et al. 2005(b)). Thus, both the pre-existing basement fabric (i.e. structural anisotropy) and Poisson's ratio will control the structural pattern observed within the basin. Due to the limited amount of information regarding the petrophysical and mechanical properties of the rocks within the Malay Basin, the Poisson's ratio (ν) value used in this assessment is taken to be approximately 0.3, a general value of ν applicable to many types of rocks in nature (e.g. De Paola et. al., 2005(a)

and (b)). A Poisson's ratio of 0.3 gives a critical transport direction (α_c; see following paragraph and Figure 4.14c) of 31^0.

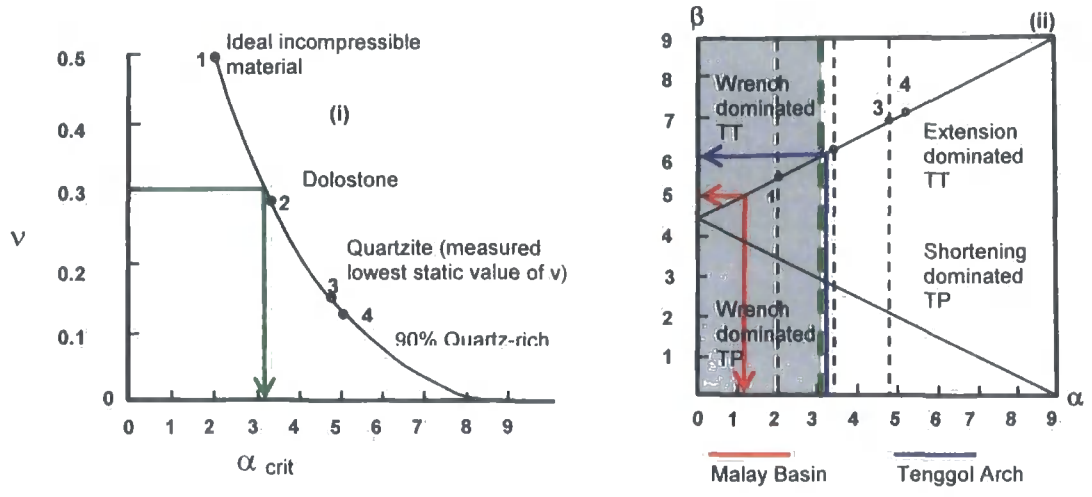

Figure 4.14c (i) Plot showing the variation in critical transport direction (α_c) with the Poisson's ratio (ν) of the host rock, after De Paola et al. (2005a,b). The green lines show that the critical transport direction for a "typical" rock with a Poisson's ratio of 0.3 is 31°. See text for explanation. (ii) A β vs α plot showing the predicted relationship between the β and α angles (see text) for transtension and transpression. The red lines have been used to predict the regional extension direction within the northern and central parts of the Malay Basin, assuming an angle (β) of 50° between the Western Hinge Line and the inferred orientation of the Miocene infinitesimal extension direction in this region. This part of the basin is predicted to undergo wrench-dominated transtension (shaded part of graph). The blue lines have been used to predict the angle (β) between the Tenggol Fault and the Miocene infinitesimal extension direction on the Tenggol Arch, assuming the same regional extension direction as that inferred for the northern and central parts of the Malay Basin. The Tenggol Arch is predicted to undergo extension-dominated transtension (unshaded part of graph); however, small variations in the orientation of the Tenggol Fault and/or regional extension direction could give rise to localised areas wrench-dominated transtension.

During oblique extension, the deformation is predicted to be wrench-dominated transtension if the angle (α) between the regional extension direction and the tectonic boundary of the deforming basin (in this case, assumed to be the WHFZ or Tenggol Fault zone) is less than the critical transport direction angle (α_c). Conversely, if $\alpha > \alpha_c$, the deformation is predicted to be an extension-dominated transtension (c.f. N. De Paola et al. 2005(a); Figure 4.14c). Note that α angles of

0^0 and 90^0 are the conditions required for strike-slip simple shear and orthogonal pure shear extensional deformation, respectively.

The structural styles that have been mapped within Miocene/Pliocene strata clearly suggest that the northwest-trending Western Hinge Fault Zone (WHFZ) is the primary tectonic boundary of the Malay Basin (Figure 4.15a). The Western Hinge Fault Zone (WHFZ) is a major normal fault system that runs parallel to the east coast of Peninsular Malaysia and defines the western margin of the Malay basin. The WHFZ continues towards the southern margin of Malay Basin where, at basement depths, it appears to merge with the N-S trending Laris Fault zone (Figure 4.14b). Both the WHFZ and Tenggol Fault zone are likely to have deep-seated structural expressions, having (probably) originated during the final assemblage of the SE Asian continental crust (see Chapter 2). In vertical seismic sections, these structures are also seen to juxtapose well-consolidated sediments and/or crystalline rocks in their footwalls against rift-related sediments in their hanging walls. The mechanical anisotropy associated with these basement structures is therefore likely to have been a critical control on Miocene-Pliocene deformation within the Malay basin and on the Tenggol Arch.

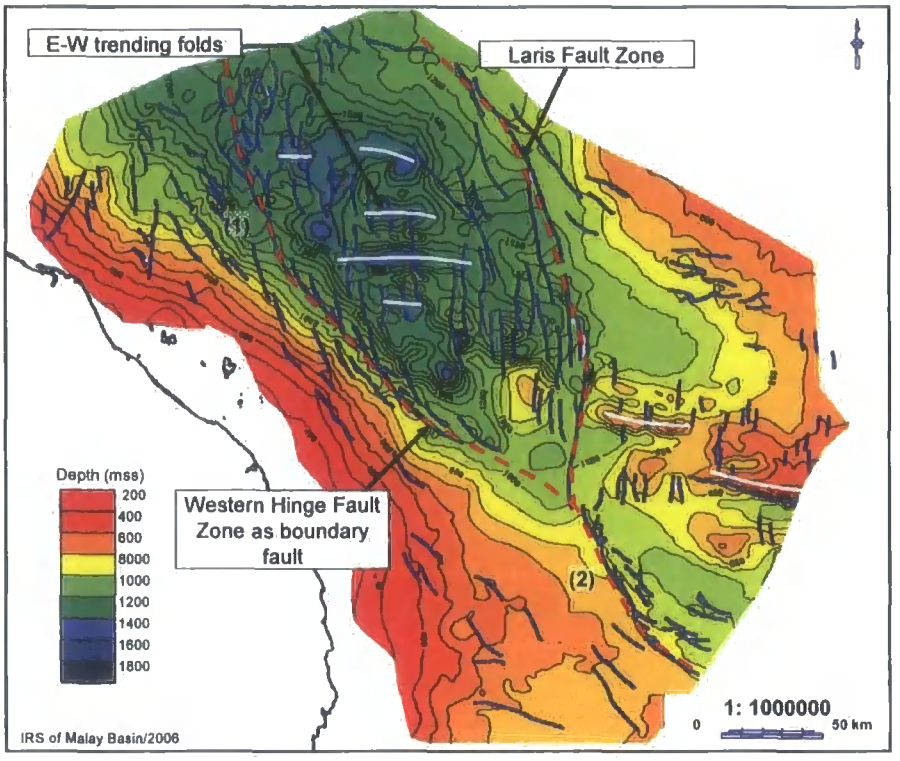

Figure 4.15a show structure styles on Malay Basin in Late Miocene to Pliocene (on the left) structure maps-structure trends. Right-hand side shows Middle Late/Pliocene structure style over Tenggol Arch, indicates infinitesimal strain axis misfits relationship to regional block motion vector. The misfits relationships suggests transtension condition. (1) Shows structure styles of northern and central Malay Basin region and (2) shows structure style in the south margin including Tenggol Arch region.

4.5.3b Results and discussion

The first step in the kinematic analysis was to measure the acute angle (β) between the tectonic boundary fault (i.e. the NW-SE basement expression of the WHFZ) and the inferred infinitesimal extension direction (i.e. the direction parallel to the Miocene fold axes). This angle (β) was used to calculate the angle (α) between the regional extension direction and the tectonic boundary, and hence to discriminate between domains of extension- and wrench-dominated transtension within the Malay basin (cf. De Paola et al. 2005(a) & (b); 4.14c).

The geometry and orientation of the WHFZ were determined from the Top Basement structure map produced during the Integrated Regional Study (2005; Figure 4.14b). This map has been derived by integrating regional mapping done using 2D seismic lines of various vintages with the Bouguer gravity anomaly map. Thus, there is a high degree of uncertainty associated with the detailed fault trace interpretations. Nevertheless, the general *trends* of major fault traces have been ground-truthed in regions where 3D seismic data are available (e.g. on the Tenggol Arch), and appear to be robust. This provides confidence in the results of the kinematic analysis described below. The first part of this section addresses the role of the Western Hinge Fault Zone in controlling transtensional deformation in the central and northern zones of the Malay basin. The second part considers the possible kinematic importance of the Laris Fault zone in eastern part of the basin.

The infinitesimal extensional axes, oriented parallel to the fold axes in the Middle Late Miocene sequence (Figure 4.15a), generally trend between 090^0 and 095^0, i.e. approximately E-W. The trace of the Western Hinge Fault Zone at location (1) - situated along the western boundary of the central Malay basin – has a strike of 140^0 giving a β angle (the angle between the infinitesimal extension direction and the boundary fault) of approximately 50^0 (Figure 4.14b). Reference to the β vs. α plot (De Paola et al. 2005(a) & b; Figure 4.14c) implies that such an infinitesimal extension direction results from a regional extension direction oriented at 12^0 to the WHFZ, i.e. with an azimuth of 128^0. Based on the previous

discussion about the likely Poisson's ratio of the basement rocks and basin fill (section 4.5.3a), these kinematic boundary conditions are likely to be consistent with a dextral wrench-dominated transtension (WDTT). The results of this semi-quantitative analysis appear to support the hypothesis that the contemporaneous extensional and compressional structures in the central and northern zones of the Malay basin developed during Middle Late Miocene wrench-dominated transtension.

A further test would be to quantify the amount of shortening accommodated by folding and to compare this with theoretical models of transtensional deformation (e.g. Teyssier & Tikoff 1999). A study made previously by PETRONAS (PETRONAS, 2006(b)) has carried out a general assessment of the crustal shortening associated with the development of major anticlines within Miocene/Pliocene sequences in the Malay Basin. However, these estimates were made using geo-seismic sections derived from regional 2D seismic lines that run sub-parallel to the anticlinal fold axes. The values derived from this measurement therefore do not represent the true percentage shortening within the Miocene/Pliocene sequences across the basin. The locations of the geo-seismic sections and results from the above analyses are shown in Appendix 15. It is therefore recommended that proper measurement of crustal shortening across Malay Basin should be included in a future assessment in-order to validate the present interpretation of Miocene/Pliocene kinematics in the basin.

The IRS regional study has concluded peak compression occurred during Late Middle Miocene-Middle Late Miocene (sb1800-sb1900) followed by extension in the Late Miocene-Pliocene (sb2000) (Appendix1). The interpretation was supported by pervasive E-W trending folds in the centre and East margin of the basin at sb1900 which was clearly identified on isochore and structure maps (Appendix 13a and 15). However in this study it is noted that on Tenggol Arch, during Ta_3 (sb1900 equivalent), shows a geologically quiescence period (Attachment 9). As suggested previously in section 4.4.2, folding and possibly structure growth along Tenggol Fault is likely to occur after deposition of Ta_3 which was also hypothetically suggested as non-kinematically related to folding in the centre of Malay Basin during Middle Late Miocene.

The western margin of the Eastern Zone of the Malay Basin is defined by the Laris Fault. This structure has a N-S to NNW-SSE trend at Top Basement and Middle Late Miocene (Ta_3) levels (Figure 4.14b and Figure 4.15b). If the maximum infinitesimal extension direction during Late Tertiary deformation is again taken to be oriented parallel to the E-W trending folds axes, then the angle (β) between this direction and the hypothesized tectonic boundary (i.e., the Laris Fault zone) would around 80^0. This value of β corresponds to an α angle of approximately 70^0, which is consistent with a dextral extension-dominated transtension. However, the structural styles (contemporaneous folding and extensional faulting; Figure 4.15a and 4.15b) observed within the Eastern Zone of the Malay basin are not consistent with those observed in domains of

extension-dominated transtension elsewhere (e.g. normal faults within parts of the Northumberland Basin, Figure 4.14a; De Paola et al. 2005(b)). The most likely explanation for this apparent discrepancy is that the Laris Fault, although a regionally-important structure, did not act as a boundary to the deforming zone. Put another way, if this fault were an important deformational boundary, a change in the orientation of the associated fold axial traces would be expected.

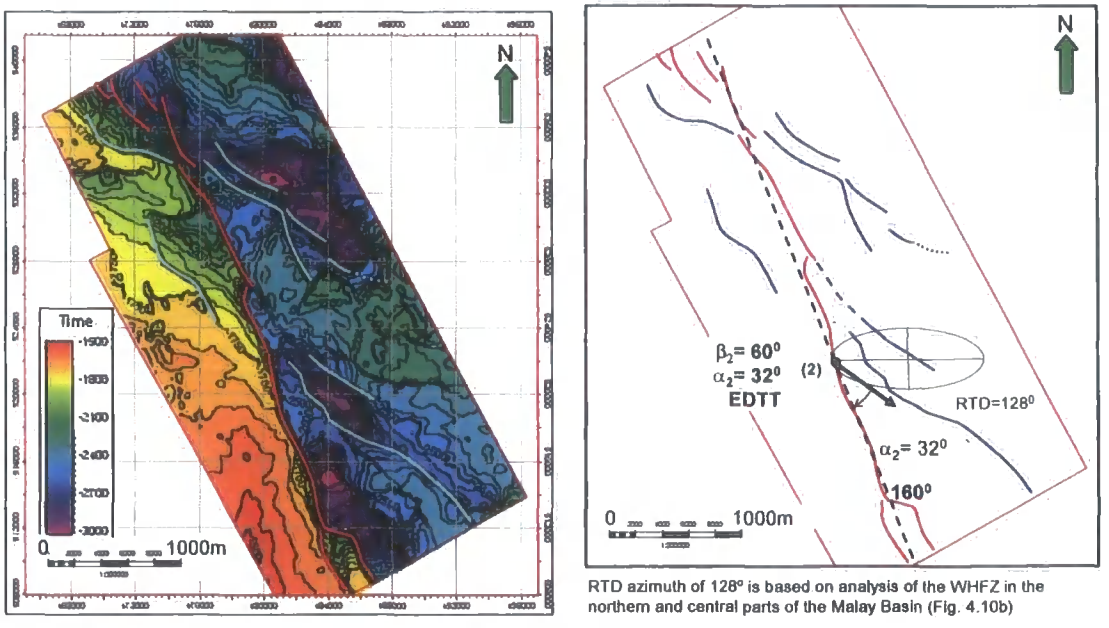

RTD azimuth of 128° is based on analysis of the WHFZ in the northern and central parts of the Malay Basin (Fig. 4.10b)

Figure 4.15b (Left) Time structure map of the Top Basement marker within the Tenggol Arch study area based on 3D seismic mapping. (Right) Schematic Top Basement fault trace map. Red traces represent the main strand of the Tenggol Fault Zone (TFZ). The overall azimuth of the TFZ is c. 160°, i.e. clockwise of the WHFZ. Blue traces are subsidiary faults in the footwall and hangingwall of the TFZ. The long axis of the grey ellipse represents the orientation of the Miocene infinitesimal extension direction on the Tenggol Arch, which is inferred to be perpendicular to the trends of Miocene fault segments – see text for explanation. Other abbreviations are explained in Figs 4.10a & b

4.6 Miocene-Pliocene kinematics of the Tenggol Arch

The Tenggol Arch differs from the Malay basin proper because there is no evidence for folding or crustal shortening – only extensional faulting. Thus, the structures observed on the Tenggol Arch appear to have developed during Miocene/Pliocene extension or extension-dominated transtension (EDTT) rather than during wrench-dominated transtension. In order to test this hypothesis, the regional extension direction calculated for the central and northern zones of the Malay basin, which has an azimuth of 128^0, has been used to estimate the angle between the infinitesimal extension axes and the Tenggol Fault zone at Location (2) within the 3D seismic study area (Figure 4.15b).

At this location on the Tenggol Arch, the Tenggol Fault zone (i.e. the tectonic boundary fault) has a strike of 160°, which yields an α angle of 32^0 (Figure 4.15b). Reference to the α vs. β plot gives the β value of 60^0, implying a dextral extension-dominated transtension deformation (Figure 4.14c). Importantly, this analysis shows that the application of a transtensional model to the central and northern zones of the Malay basin and to the Tenggol Arch yields an internally-consistent result. The interpretation of extension-dominated transtension on the Tenggol Arch is also supported by observations of sedimentary channels that show significant normal – but negligible lateral – displacements across the Tenggol Fault (section 4.4.2).

4.7 Discussion: Structural Evolution of Tenggol Arch (Chronology)

To summarize, the Top Basement structure on the Tenggol Arch is characterized by Northwest-Southeast trending basement lows (sub-basins) on the arch as repercussion of regional extension operating within north-northeast direction (Figure 4.11a) possibly occurred no younger than Early Miocene (Early Tertiary?/Oligocene).

The Malay Basin and Tenggol Arch were subsequently subjected to a dextral transtensional deformation during the Late Miocene/Pliocene. In the Malay Basin, the Late Miocene/Pliocene surface is deformed by tight East-West trending folds that are associated with contemporaneous North-South striking extensional faults. Semi-quantitative analysis of the inferred infinitesimal extension direction and tectonic boundary fault (the Western Hinge Fault Zone) suggests that folding and extensional faulting developed during dextral wrench-dominated transtension associated with a regional extension direction of 128°. Application of this extension direction to the Tenggol Arch leads to an internally-consistent interpretation of a dextral extension-dominated transtension on the Tenggol Arch during Late Miocene/Pliocene times.

In conclusion, the Malay Basin has undergone dextral transtensional deformation during Miocene/Pliocene period which was WDTT in the centre and North margin

and EDTT in the South margin which includes Tenggol Arch. This kinematic model builds upon the idea that pre-existing basement fabrics and oblique tectonics were important in the development of the Malay basin, as suggested in 2005 Integrated Regional Study. However, the dextral transtension model contradicts previous interpretations, in which the basin was believed to have experienced regional compression during the Middle-Late Miocene/Pliocene period following Early-Middle Miocene thermal sagging (EPIC, 1994). The results of the present study show that the Malay Basin and Tenggol Arch have not been subjected to a tectonic inversion event; rather, that the basin has experienced intermittent extension throughout the Tertiary. The presence of pre-existing basement fabrics, coupled possibly to the rotation of Sundaland (causing a change in the boundary fault orientations), would potentially have given rise to strain partitioning which resulted in both compressional and extensional structure styles in the Middle and Late Tertiary sequence as observed at present.

The structural chronology of the Tenggol Arch is summarized in Attachment 20. In general this structure chronology also represents structure evolution for the Malay Basin in general.

5.0 Antracking Volume: Fracture interpretation

"Antracking" is a proprietary algorithm within Schlumberger's Petrel reservoir interpretation and modeling software that highlights linear and planar discontinuities within a 3D seismic volume. These discontinuities can arise due to the presence of faults, fractures, stratigraphic truncations or geophysical artifacts. The Antracking algorithm is designed to highlight discontinuities that have significant spatial extent and/or orientations that fall within a specific, pre-determined range and are thus more likely to represent faults or fractures rather than, say, noise or other artifacts. Antracking has been used to aid the recognition and definition of fracture patterns within the basement complex of the Tenggol Arch. Given the limited number of wells that have penetrated the basement, calibration of the Antracking results is problematic using offshore data alone. The approach adopted in this study has therefore been to compare the discontinuities within the seismic data highlighted by the Antracking tool on and below the Top Basement marker adjacent to the A-field with the fracture patterns observed onshore within basement rocks of the Ulu Paka region, Malay peninsula. The first part of this chapter describes the fracture patterns observed at Ulu Paka. The second part then describes the results of the Antracking study and compares these with the onshore analogue and with the fractures interpreted from an FMI log of the AU-1 well on the Tenggol Arch.

5.1 Onshore analogue: Structural styles at Ulu Paka, Terengganu

A structural interpretation of the fractures exposed at Ulu Paka, Terengganu was carried-out using the geological map of Fateh Chand (1978; Figure 5.1). The basement at Ulu Paka comprises igneous and argillaceous metamorphic rocks. The igneous rocks, which have alkaline granitic-granodoritic and adamalitic-dioritic compositions, have been dated as Lower Permian to Upper Carboniferous age. The metamorphic rocks are mostly phyllites and metasandstones with depositional ages dated as Lower Carboniferous (cf. Tjia, 2005: Fateh Chand, 1978). The mapped structural lineaments at Ulu Paka are dominantly N-S to NNE-SSW and NW-SE trending (Figure 5.1). Fault-related lineaments are most commonly observed within the igneous rocks, whilst the axial traces of isoclinal folds are mostly restricted to within the metamorphic rocks. There appear to be two sets of folds within the metamorphic rocks. The axial traces of the first set run parallel to the NNE-striking faults, whilst the second set of axial traces trend NW-SE, approximately 15^0 counter-clockwise to the NW-striking fault lineaments.

Fateh (1978) (cf. Tjia, 1986) proposed that the isoclinal folds may have originated during emplacement of granitoid bodies during the Late Paleozoic. The presence of faults that cut the Late Paleozoic intrusive rocks suggests post-intrusion faulting – or reactivation – during later, post Late Paleozoic tectonic movements. These mainly en-echelon, NNE-striking faults have similar

orientations to fractures on the upthrown (footwall) block of the Tenggol Arch, which are discussed below.

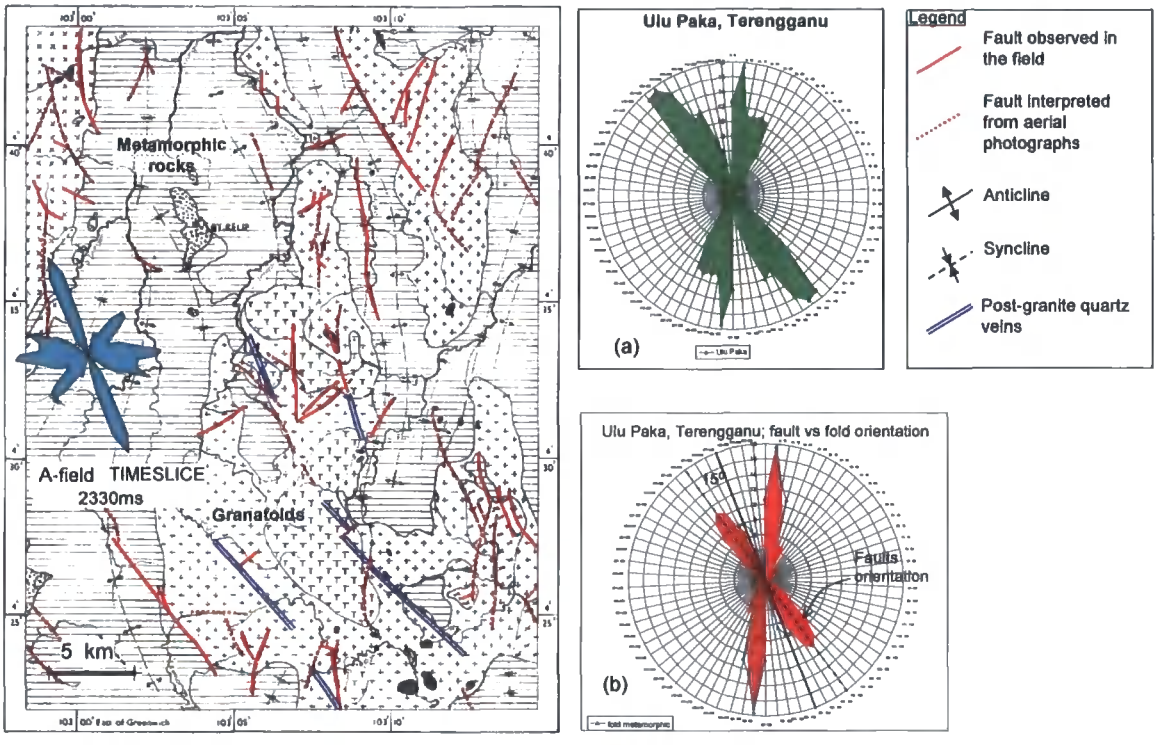

Figure 5.1 Structure orientations at Ulu Paka, Terengganu shown in rose-diagram (green) show predominantly Northwest and North-Northeast striking faults. Isoclinal fold orientation shown rose-diagram (red) denotes fault parallel folds (NNE) and folds that are slightly oblique at 15^0 CCW to NW striking faults.

The structure at other comparable onshore localities - for example at Kuala Abang, Terengganu, which is situated on the east coast of the Peninsular Malaysia (Figure 2.3) – is characterized by overturned to recumbent folds with westerly vengeance (Abdullah, 2001; Appendix 11). Here, the host rock lithology is dominated by low grade phyllite and thin lenses of metasandstone. These are equivalent to the basement lithologies that have been proven to exist within the downthrown block of the Tenggol Fault (see section 2.1).

5.2 Fault and fracture patterns of A-field, Tenggol Arch

The A-field is located on the downthrown block of the Tenggol Fault and is a proven oil play in fractured basement. Two wells, AU-1 and AB-1, were drilled to test this play. A side track of the AU-1 well encountered hydrocarbons within the fractured basement complex. The second well (AB-1) was drilled immediately to the north of AU-1, but was characterized by poor or minor indications of hydrocarbons within the basement target (Attachment 23). AU-1 penetrated low grade metasediments (phyllite and lenses of metasandstone; see Appendix 11), whilst AB-1 encountered granitoids of andesitic composition (Appendix 12). The basement rocks offshore therefore comprise similar lithologies to those found at Ulu Paka and elsewhere along the eastern coastline of the Malay peninsula. The Top Basement structure map for the A-field is characterized by predominantly E-W (105^0 to 120^0) trending faults and fault-parallel folds (Figure 5.2). However, it is important to note that the A-field is only representative of structural styles encountered in the *downthrown* block of the Tenggol Fault.

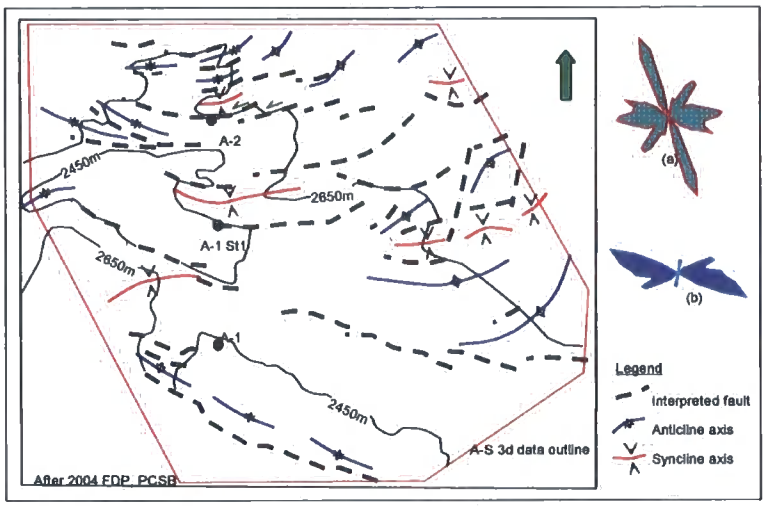

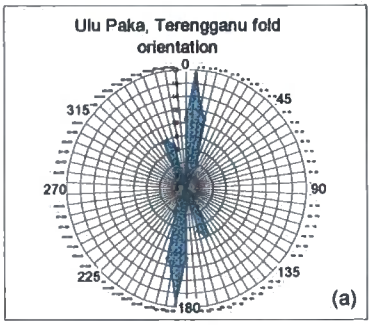

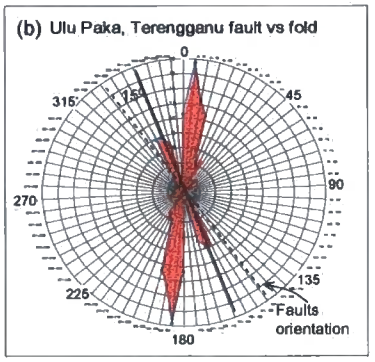

Figure 5.2 Fault orientation stereo net plot of top basement at A-field, (a) plot from 2005 3d time-slice at 2330msec (b) plot extracted from FDP map. WNW-ESE is dominant fault trend in A-field, NNW-SSE trends represents major Tenggol fault to the west of A-field (not shown in Field Development Plan map). Rose diagram (blue) show folds orientations and (red) fold vs fault orientations from Ulu Paka east coastline of Peninsular Malaysia

5.2.1 Well data: AU-1 basement complex

The time-depth curve for the AU-1 well was derived from Vertical Seismic Profile (VSP) acquisition in the borehole. The curve shows a strong positive "kick" in interval velocity at around 1.75 to 2.2 s, which is equivalent to *c.* 2600 mtvdss (meters total vertical depth sub-sea; Figure 5.3). Below this depth, the velocity increases to between 4700 m/s and 5500 m/s, which is typical of the metasediments and andesitic igneous rocks of the basement complex within the A-field (Figure 5.3).

Time/Depth Curve
Well: AU-1 ST1 (sidetrack-1)
Location: Offshore Malaysia
Survey: Zero Offset VSP

SRD (seismic reference datum): MSL (mean sea level)
KB (kelly bushing): 31.8m above MSL
GL (gun level): 74.3m below MSL

Gun/Hydrophone Offset: 50m
Gun/Hydrophone Azimuth: 125deg

Gun depth: 5m below MSL
Hydrophone arrays depth: 8m below MSL

Legend:

(Va)-average velocity
(Vrms)-RMS velocity
(Vint)-interval velocity
(VSP)-shot data
(DT)-sonic

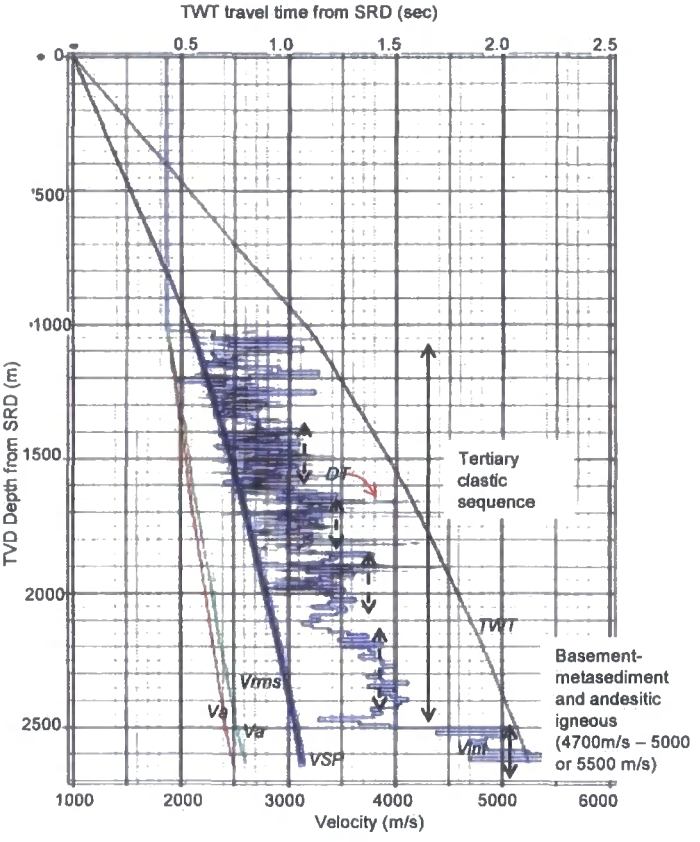

Figure 5.3 AU-1 Time-Depth Curve from VSP (Vertical Seismic Profile) from AU-1 well VSP Report (Schlumberger). Onset of Top Basement marker identified at circa 2480-2500m.

A Formation Micro Imager (FMI) log was acquired by Schlumberger in the basement section of the open borehole of the AU-1 well. The FMI data are used to image bedding, foliation and fracture plane orientations. The data shows that natural fractures in the basement complex have predominantly ENE-WSW trends and dip steeply (between 70^0 and 90^0) towards the south (Figure 5.4). Foliation or bedding planes within the basement unit trend NW-SE and dip between 10^0 and 30^0 towards the southwest. Thus the FMI data show that the fracture planes in the downthrown block of the Tenggol Arch are steeply dipping, whilst other planar fabrics dip more shallowly. .These findings are consistent with the orientations of the E-W to NW-SE trending faults that can be mapped on the Top

(a) Manually picked foliations orientation

(b) Manually picked natural fracture orientation

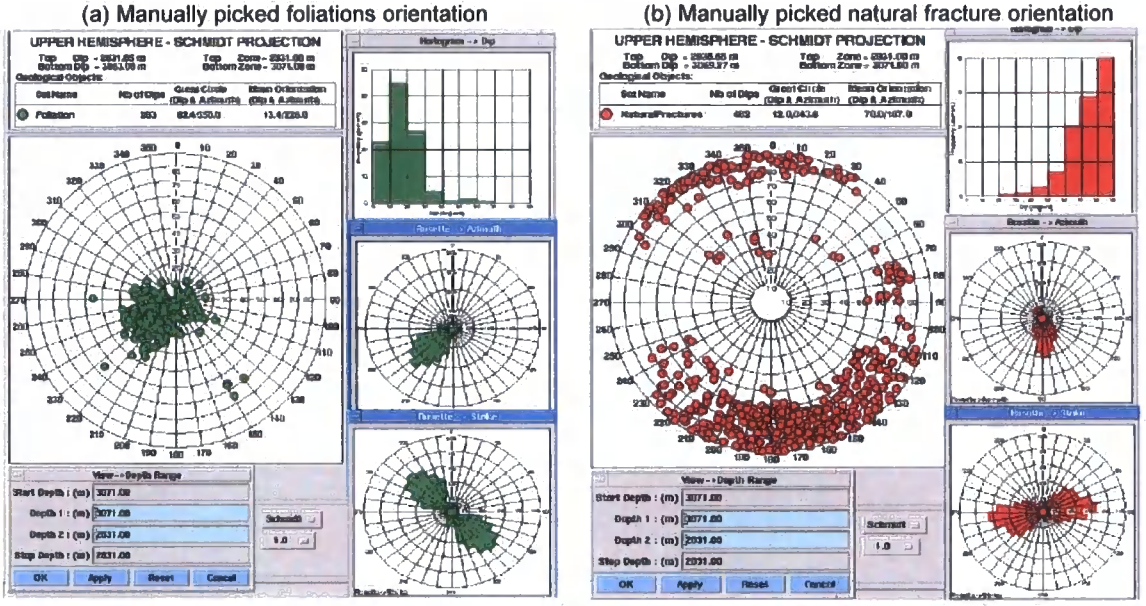

Figure 5.4 Foliation and fracture orientations are manually picked from FMI logs. Manually picked foliations (green), dip-magnitude histogram and azimuth plot indicate foliations are represented by Northwest-Southeast trending lineaments with dip magnitude of 10^0 to 30^0 Southwesterly. Manually picked fractures (red) are striking Easterly with dip-magnitude of 70^0 to 90^0 dipping Southerly.

Basement seismic marker in this region (Figure 5.2). The interpretations of the FMI data from the AU-1 well therefore give confidence to structural interpretations of the seismic data, and can also be used to calibrate the Antracking volume.

5.3 Interpretation of the Antracking Volume

5.3.1 Methodology: Comparison of fracture pattern from AU-1 FMI data to Antracking along the Tenggol Fault.

The basement unit in the AU field comprises low grade metasediment, mainly phyllite and lenses on thin layered metaquartzite. Recent field studies along the east coast of Peninsular Malaysia have suggested the basement unit to be of equivalent age and lithofacies of Lower Carboniferous/Late Permian phyllite-metaquartzite, where outcrop along Kuala Abang and Mersing show highly foliated formation with some presence of calcite-filled fractures (Appendix 11 and 14). The FMI data from the basement unit encountered in the AU-1 well was able to delineate both foliations and fractures in the basement. In general, the orientation of foliation in basement at AU-1 location shows dominant 130^0 to 140^0 directions with surface dip-magnitude of 10^0 to 30^0 southwesterly (Figure 5.4 (a)). The fractures in basement are shown as dominantly striking easterly with dip-magnitude of 70^0 to 90^0 southerly (Figure 5.4 (b)). The FMI results well AU-1 provide a reference when interpreting lineaments in the Antracking volume, as lineaments extracted using this application may also indicate geophysical artifacts. In addition, the results of the Antracking greatly depend upon the seismic data quality (acquisition and processing artifacts) and resolution (high resolution in deeper basement (deeper than 2000ms)).

Therefore when interpreting lineaments from the Antracking volume, I have used the known strike orientations and dip values as guide-lines during parameter testing to try to discriminate potential fractures or geological events from geophysical artifacts. The final interpretation therefore picks out lineaments (i.e. potential fractures) with orientations similar to those seen in the AU-1 well, but also lineaments with other orientations that have been highlighted in regions where the quality of the Antracking cube is good. Antracking cube calibrations done in this study are mainly qualitative, based upon cross-comparison methods of several test cubes with various ranges of test parameters. In the future, when more basement wells are available on the arch or along the West margin, a more structured quantification can be apply when dealing with Antracking analysis,

The final parameters used for this study is shown in Appendix 8. These parameters may only true for Tenggol Arch specifically; their application to elsewhere along the Western margin of Malay Basin will have a higher degree of uncertainty.

The Antracking volume was generated by convolving two seismic volumes: the PSTM (pre-Stack Time Migration) volume and a variance volume derived from the smoothed PSTM cube. Variance is an attribute derived from the PSTM data that calculates the dissimilarity between adjacent seismic traces. A cross-comparison method was applied to determine the best Antracking parameters for defining the basement fractures in this dataset. A small volume was selected

and series of different parameters was applied to produce several test cubes. The tests were conducted within the 500-3000 ms window and the final parameters used for Antracking volume generation are shown in Appendix 8. A qualitative cross-comparison was then carried out between these cubes to determine the best result, based on the clearest delineation of likely fault trends, the lowest noise levels, the least attenuation and balanced amplitudes. A comparison was also made between vertical sections derived from the Antracking cubes and the original SEGY data (Figure 5.5a). The purpose of this comparison was to identify possible geophysical or mathematical artifacts within the original dataset that might be highlighted within the Antracking volume.

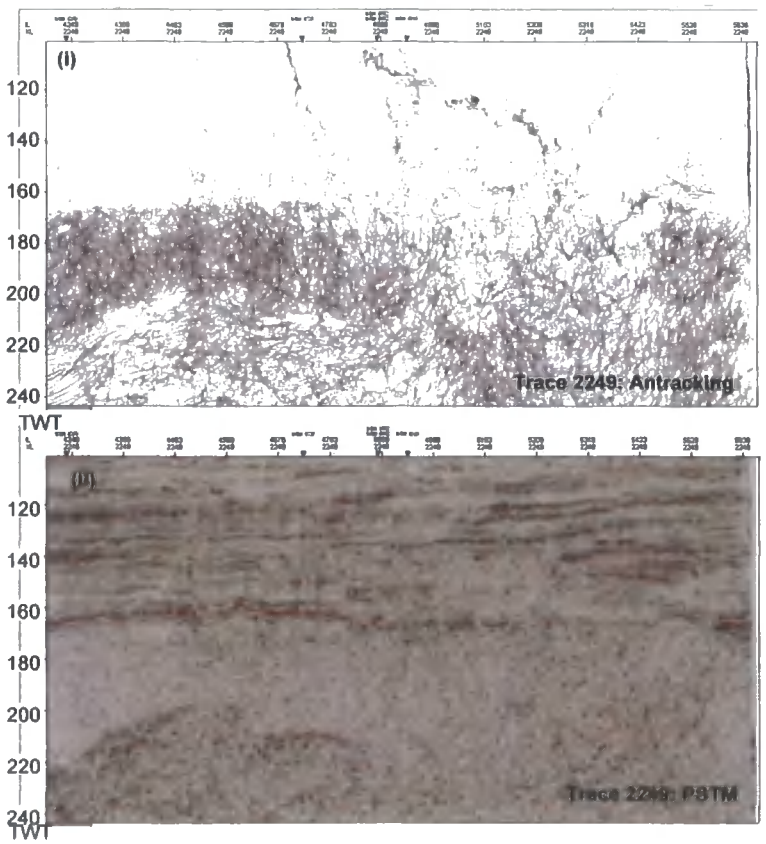

Figure 5.5a (i) shows a vertical section along Trace 2249 from the Antracking volume; (ii) shows a vertical section along the same trace from the PSTM volume. The Antracking section (ii) illustrates better the delineation of faults and consistent incoherency in the basement complex. The incoherence in basement complex represents both structure and stratigraphic related lineaments and attenuates by low signal to noise ratio near base

5.3.2 Results from Antracking

The Antracking volume provides better definition of structural lineaments or fracture patters within the basement complex (1500ms to 3000ms) than at shallower levels (500ms to 1500ms). At shallow levels, the Antracking volume highlights lineaments associated with stratigraphic boundaries, which are the dominant features within the Tertiary sequence on the Tenggol Arch (e.g. Figure 3.7). Horizon slices from the Antracking volume generated using the "test" cube show that structural lineaments within the basement are most clearly defined in the footwall of Tenggol Fault (Figure 5.5b). The following analysis therefore focuses on an Antracking volume that encompasses basement rocks located on the upthrown side of the Tenggol fault.

The Top Basement seismic marker was used as a reference to create horizon slices within the basement complex. Horizon slices were sampled through the Antracking volume at 50 ms intervals, within a 300 ms window beneath the Top Basement marker. A limit of 300 ms below this marker was selected due to the marked deterioration in resolution at greater depths. The horizon slices show that the southern and western parts of the study area are characterized by ubiquitous N-S striking fractures, which are mostly concentrated at the edge of basement high (Figure 5.5b). The fracture patterns observed near the northern

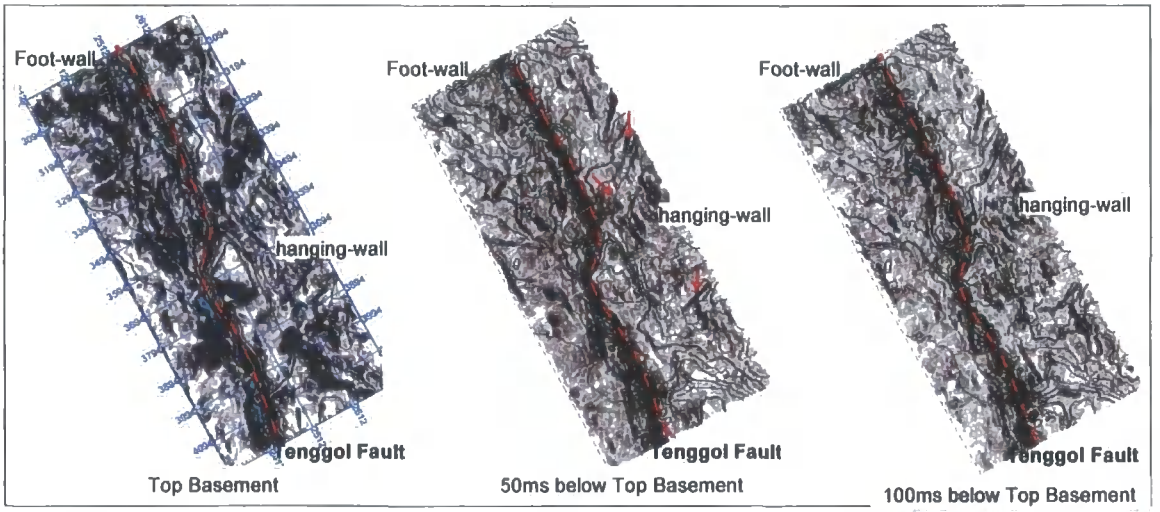

Figure 5.5b Maps above show horizon slices from the Antracking volume of basement complex **near A-field** (centre Tenggol Fault). In general, Antracking volume denoted fractures traces and Tenggol Fault as dark attributes. The downthrown block shows some possible NW striking and NE striking fracture traces (red arrow). However, fracture traces on the hanging-wall gradually diminishing at deeper depth.

Index map on the right showing location (red box) of Antracking test cube done along the Tenggol Fault

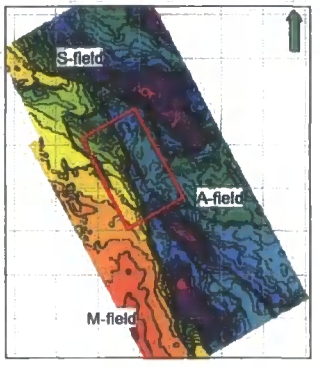

margin of the study area (in the vicinity of the S-field) appear to be more complex, and are discussed in more detail below (Figures 5.6a and 5.6b).

Comparison between the fracture patterns observed on horizon slices through the Antracking volume and the faults mapped at Top Basement level suggests that some fractures are developed preferentially within the hangingwalls of faults whose map-view traces are concave towards the downthrown block (Figures 5.7, 5.8, 5.9 and 5.10). "Fracture swarms" have also been identified, which are not directly associated with specific faults (cf. Aguilera, 1995: Nelson, 1985 ;

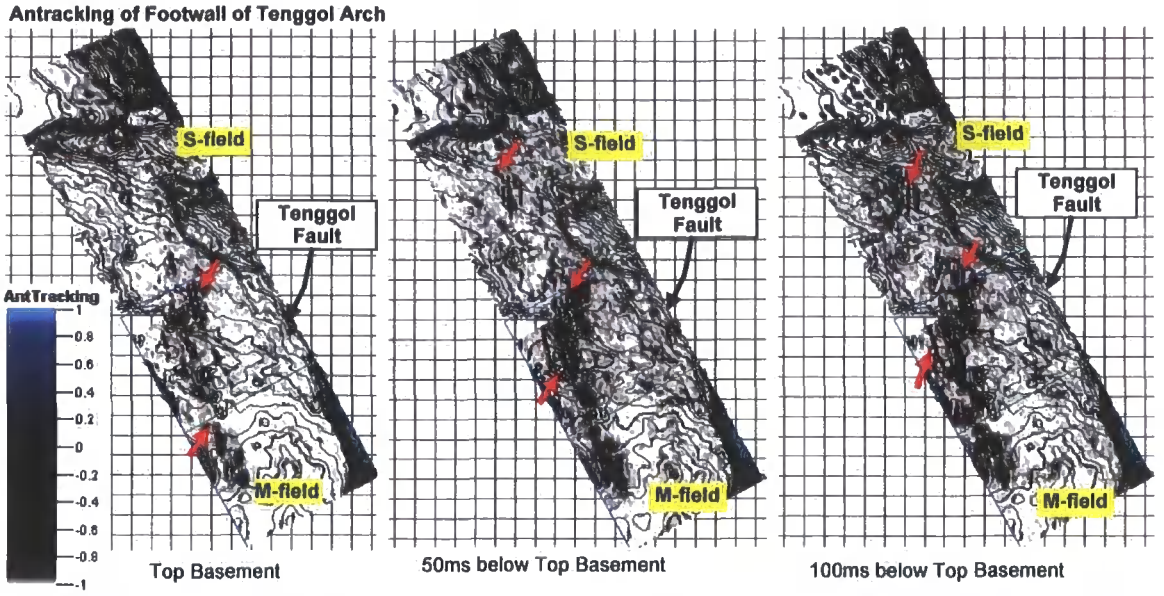

Figure 5.6a Horizon slices of the Antracking volume in the footwall of the Tenggol Fault. Fracture traces and fractured zones marked as dark attribute. Gray-light gray zones are possibly associated with background fractures. Generally North-South trending lineaments dominates the southern of Tenggol Arch and west margin of M-field (red arrow). The color-scale represents relative amplitude value of the Antracking volume displays in fractions within the range of 1 to -1. The value associated with dissimilarities in seismic (phase), where -1 showing relatively highest dissimilarities and 1 as lowest dissimilarities. The gap is interpreted as changed in seismic phase along the surface which associated with fault traces and fractures.

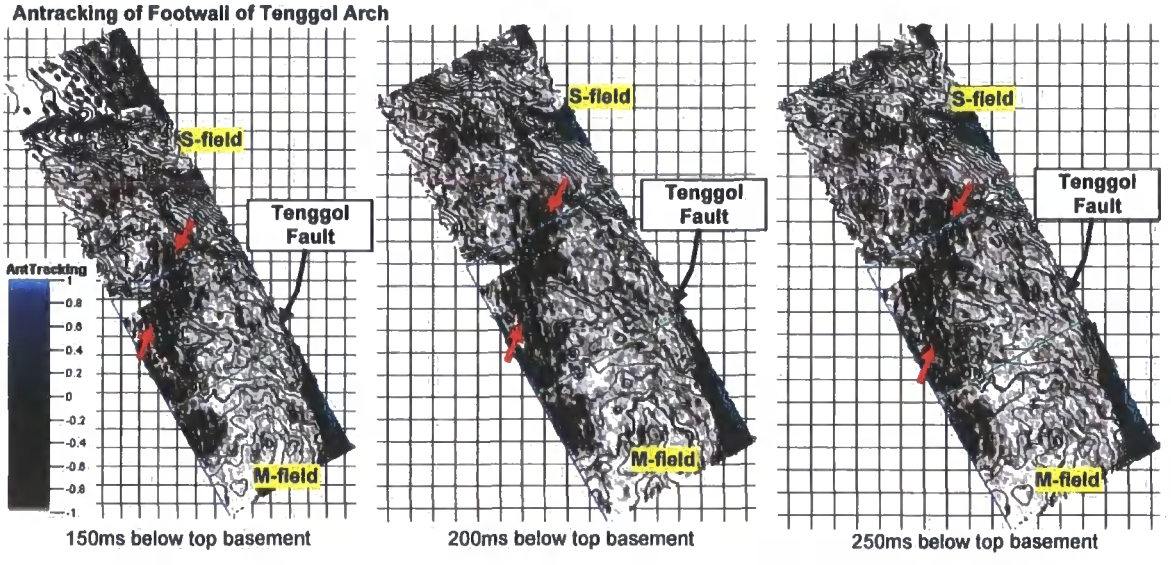

Figure 5.6b Antracking Top Basement horizon slices of in the foot-wall of the Tenggol Fault volumes (continuation of deeper horizon slices). Similar North-South trending lineaments dominates the southern area and west margin of M-field. The color-scale represents relative amplitude value of the Antracking volume displays in fractions within the range of 1 to -1. The value associated with dissimilarities in seismic (phase), where -1 showing relatively highest dissimilarities and 1 as lowest dissimilarities. The dissimilarities is interpreted as break along the surface which associated with fault traces and fractures.

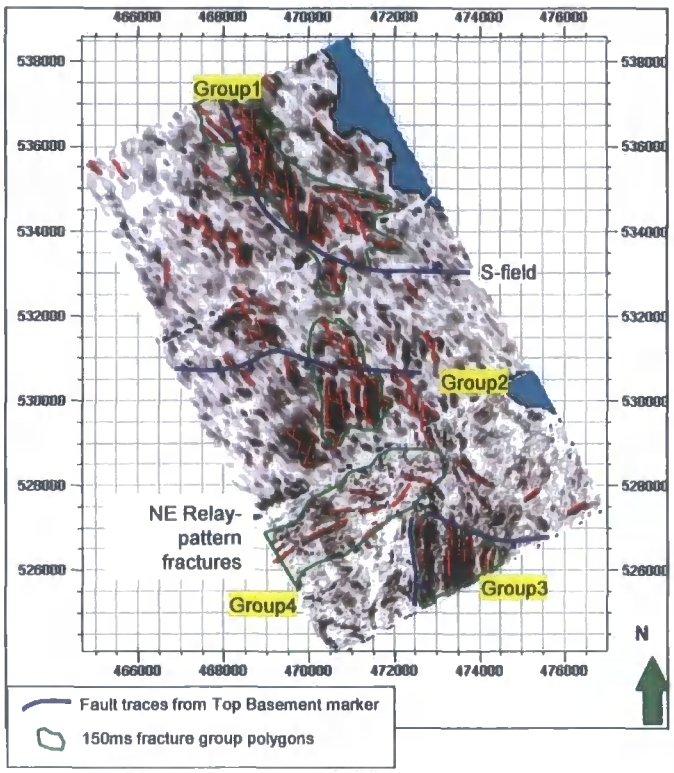

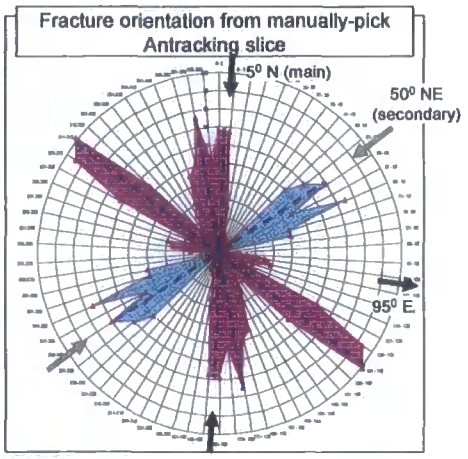

Figure 5.7 Horizon slice at **150ms below** Top basement marker of *Nbsmt* volume near S-field. Fracture traces interpretation shown as red traces. Fracture groups polygons from previous slices are included to illustrate fracture distribution at every slices. Figure on the right shows fracture orientations consistent to interpreted maximum horizontal compression direction from bore-hole data (Appendix 10).

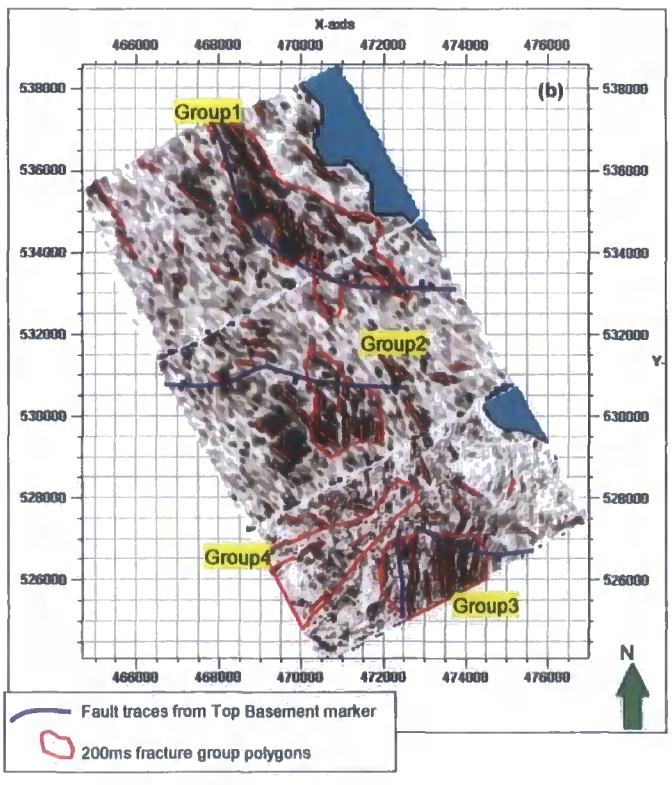

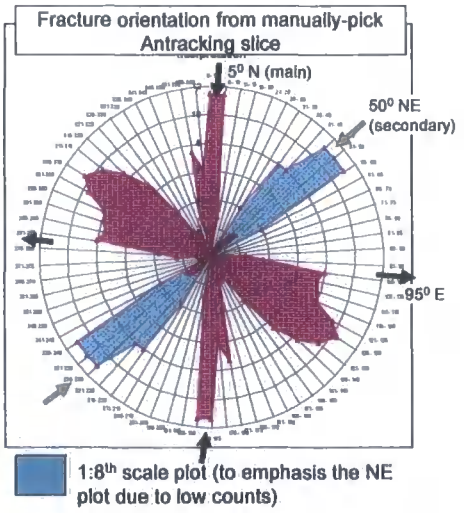

Figure 5.8 Horizon slice at **200ms below** Top basement marker of *Nbsmt* volume near S-field. Fracture traces interpretation shown as red traces. Fracture groups *polygons from* previous slices are included to illustrate fracture distribution at every slices. Figure on the right shows fracture orientations consistent to interpreted maximum horizontal compression direction from bore-hole data (Appendix 10).

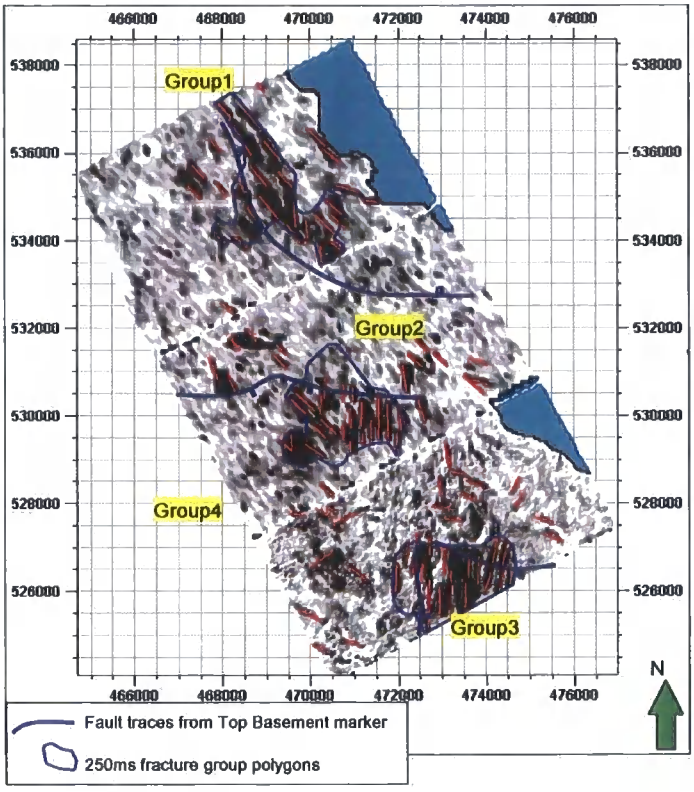

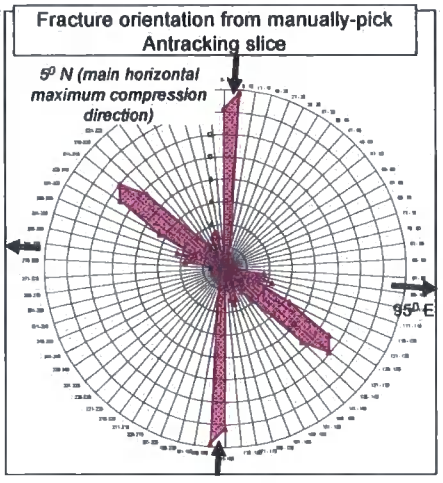

Figure 5.9 Horizon slice at **250ms below Top basement** marker of *Nbsmt* volume near S-field. Fracture traces interpretation shown as red traces. Fracture groups polygons from previous slices are included to illustrate fracture distribution at every slices. Figure on the right shows fracture orientations only consistent with interpreted maximum horizontal main compression direction from bore-hole data (Appendix 10).

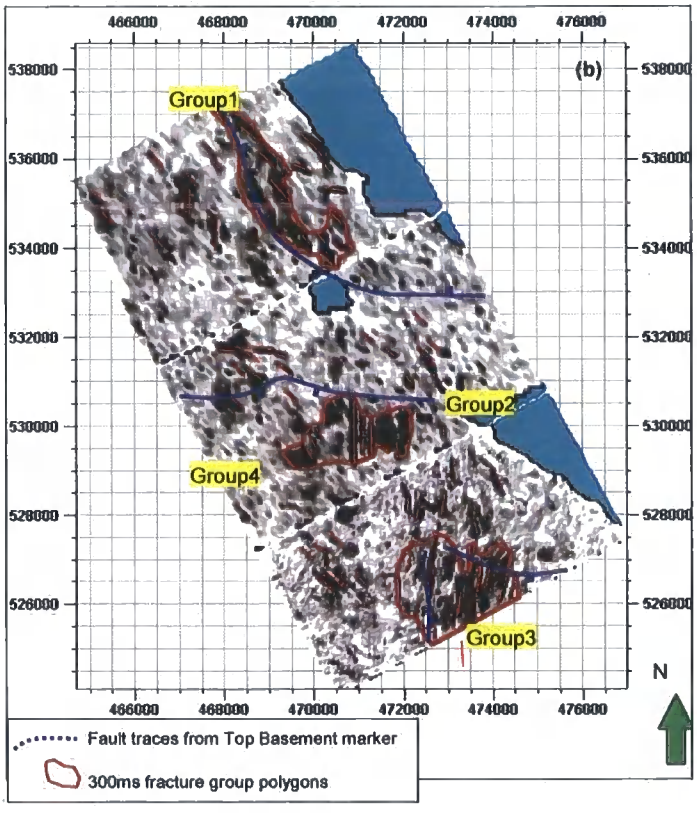

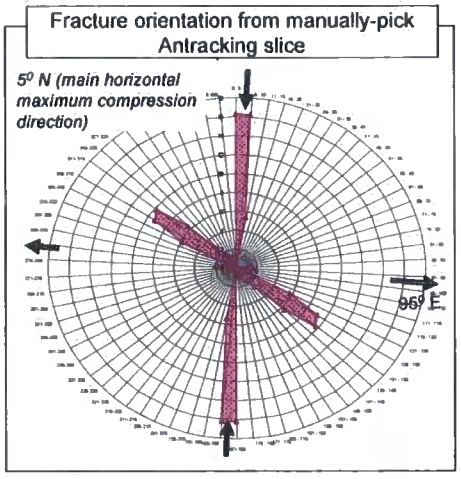

Figure 5.10 Horizon slice at **300ms below** Top basement marker of *Nbsmt* volume near S-field. Fracture traces interpretation shown as red traces. Fracture groups polygons from previous slices are included to illustrate fracture distribution at every slices. Fracture Group4 (relay-pattern NE striking fractures) is not present at 300ms horizon slice.
Figure on the right shows fracture orientations still consistent with interpreted maximum horizontal main compression direction (5⁰N) from borehole data (Appendix 10).

Figure 5.11). The density of fractures associated with these "swarms" appears to be lower than that of the fault-related fracture sets. The principal fracture orientations in the basement complex are N-S and NW-SE. E-W trending fractures are locally present on every horizon slice except at 250ms below Top Basement, where NE-SW trending fractures are present (Figure 5.7, 5.7a, 5.8 and 5.8a). The fracture traces appear to form clusters, namely: Group 1, Group 2, Group 3 and Group 4 (Figure 5.11). The locations of these clusters remain consistent on every horizon slice and can be mapped to 300 ms below the Top Basement marker. Most groups are characterized by predominantly N-S and NW-SE fracture orientations, except for Group 4, which is characterized by a low density of E-W trending, en echelon fractures. Groups 1 and 3 are situated in the hangingwall of mapped faults. In contrast, Groups 2 and 4 comprise fracture swarms.

Both Groups 1 and 2 consist of "lattice" (or rhomboidal) fractures. Group 3 predominantly comprises N-S striking fractures (Figure 5.11). The NW-SE and N-S trending fractures appear to be prevalent at deeper levels based on the maximum mapped depth at 300ms below Top Basement marker. Horizon slices below 300ms beneath Top Basement are characterized by high amplitude anomalies in these orientations, an observation that suggests these fracture sets are deeply-rooted. The E-W trending fractures (e.g. Group 4) are present only at shallow levels (50-200 ms) beneath the Top Basement marker.

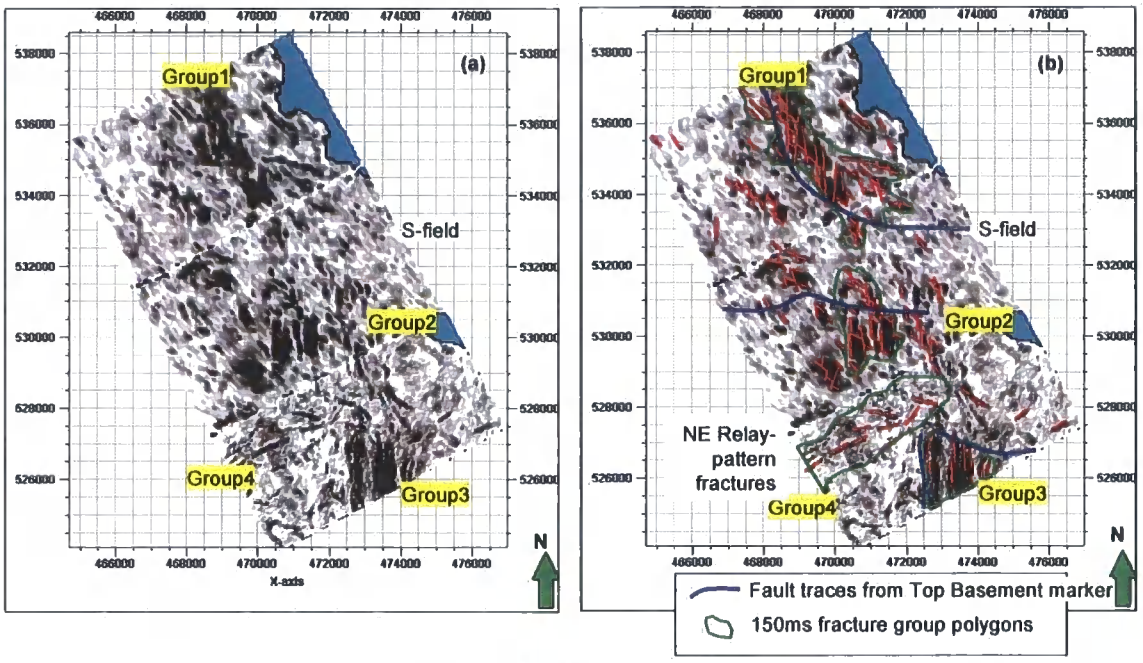

Figure 5.7a shows (a) Antracking horizon slice at **150ms** below Top Basement marker without fault and fracture traces interpretation. (b) Shows the same map with fault and fractures traces interpretation indicates predominantly N-S and NW striking fractures

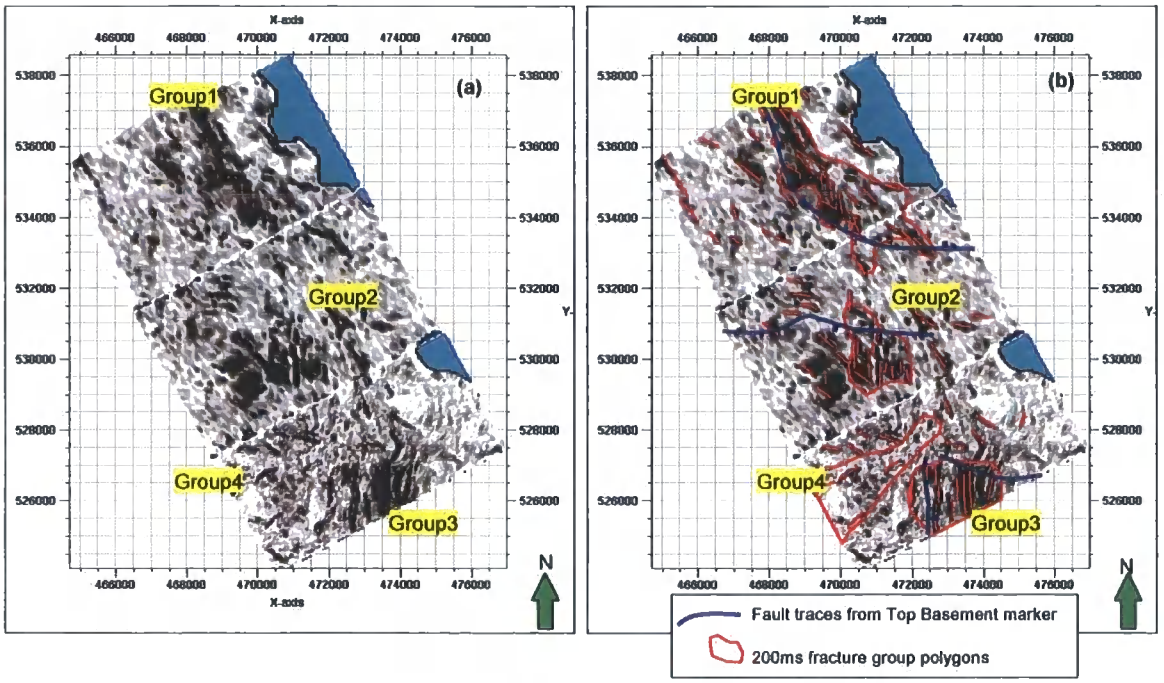

Figure 5.8a shows (a) Antracking horizon slice at **200ms** below Top Basement marker without fault and fracture traces interpretation. (b) Shows the same map with fault and fractures traces interpretation indicates predominantly N-S and NW striking fractures

To summarize, interpretation of the Antracking volume has identified two major fracture styles within the basement rocks in the footwall of the Tenggol Fault. The first (namely Group 1 and Group 3) comprise of predominantly N- and NW-striking fractures situated in the hangingwalls of seismically-mapped normal faults. The second, namely Groups 2 and 4 consists of fracture swarms with N- and E-striking fractures, respectively.

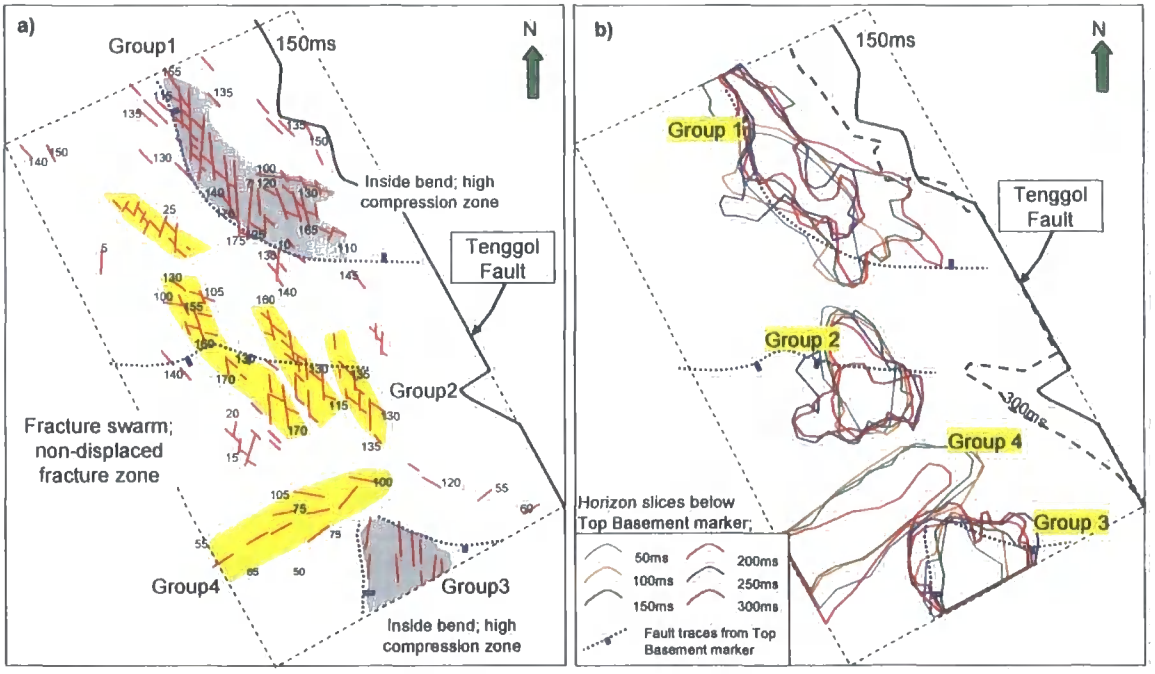

Figure 5.11 Figure (a) shows fault related fractures in basement complex. Fault traces are projected from Top Basement. Grey polygons indicate fault related fractures and yellow polygons highlighted fracture swarms. (b) Figure shows all group polygons appear at similar locations at every horizon slices illustrates vertical continuation of each fracture group. Group 4 is absent at horizon slice 300ms below Top Basement marker, this fracture group gradually diminished at 250ms horizon slice.

5.4 Discussion and conclusions

5.4.1 Comparison of Antracking results with the regional kinematic history and stress orientations

Analysis of the horizon slices shows that the NW-striking fractures within the basement complex are generally cut by N-S trending fractures, as shown in Figure 5.11. Similar fracture trends and 'lattice-patterns' are observed at Ulu Paka, which further support the interpretation of the Antracking volume presented above. Figure 5.1 shows that N-S (and subsidiary NNE-striking) faults cut the NW-striking faults and other structural lineaments, including NW-SE trending post-granite dykes and sills and fold axial traces. Interpretations of lineament patterns using satellite images of Peninsular Malaysia also highlight similar structure styles, in which N-S trending faults cut NW- and NE-striking faults or structural lineaments (Attachment 4).

The younger, N-S trending fractures may have developed during Late Miocene/Pliocene deformation are associated with a broadly E-W extension direction. This is parallel to the inferred infinitesimal extension direction during Late Miocene/Pliocene extension-dominated transtension (see section 4.5.2). This interpretation is consistent with evidence of the N-striking faults and fractures cutting other trends as observed in fracture maps of the Tenggol Arch in

this study. Similar cross-cutting relationships can be observed in lineament map of Peninsular Malaysia which indicates predominantly NW-striking lineaments cut by a N-striking set (Attachment 4). As discussed previously, outcrop evidence from Peninsula Malaysia suggests that the NW-SE fault accommodated post-Jurassic/Cretaceous left lateral movements (Appendix 14), consistent with the idea that these are amongst the oldest structures preserved on the Tenggol Arch.

To summarize, based on the results of the Antracking analysis, the NW-striking fractures are likely to be the oldest imaged fracture set within the basement complex in the footwall of the Tenggol Fault. These fractures are cut by N-S trending fractures that probably developed during Late Miocene/Pliocene tectonic movements. The N-S trending fractures are therefore most likely to have better lateral continuity and are less likely to have been reactivated than the earlier fracture sets. The postulated continuity of these fractures makes them potential targets for future drilling. However, well calibration is required to further support this conceptual model. Further study should also be made of the reservoir-scale seismic response of the fractured basement layer – in particular, how its seismic character varies according to the nature of the fluids (e.g., brine, fresh-water, gas and oil) held within the fracture porosity.

5.4.2 Conclusions and implications for hydrocarbon exploration

The key points derived from interpretation of the Antracking volume are as follows:

1) Lineaments derived from attribute mapping of the Antracking volume do not always represent structural – or even geological – lineaments. The lineaments may represent stratigraphic surfaces or truncations, foliation planes or geophysical artifacts. Knowledge of the regional structural trends and kinematic history of the Tenggol Arch is of critical importance in identifying real structural lineaments and eliminating possible geophysical artifacts.

2) The N-S trending fractures appear to be the youngest fractures observed on the Tenggol Arch. These fractures are oriented perpendicular to the present-day minimum horizontal stress direction (095-275^0) in the Malay Basin, which has been interpreted from borehole breakout data (Appendix 10). They are also perpendicular to the inferred infinitesimal extension direction during Late Miocene/Pliocene extension-dominated transtension. The fractures are thus potentially `open' (Yaacov, 1989). However this open-fracture concept is yet to proven by well calibrations on the Tenggol Arch.

3) The northern end of Tenggol Fault zone (i.e., in the vicinity of the S-field) is likely to have the greatest potential to facilitate across-fault hydrocarbon migration (hence filling potential reservoirs within the footwall block). This interpretation is based on throw profiles along the Tenggol Fault, which show that the northern area is characterized by relatively small throws in comparison with the southern area. The presence of similar or equal thicknesses of Late Miocene to Pliocene strata across the northern part of the fault may promote sand-sand juxtapositions across the fault plane in this area. In addition, the segmented nature of the fault (Chapter 4) suggests that intact, low-displacement relay zones may provide conduits for across-fault hydrocarbon migration.

4) Fault-related fractures within the basement complex on the Tenggol Arch are mostly concentrated within the hangingwalls of seismically-mapped normal faults. The curved map-view traces of these faults are typically concave towards the hangingwall. These fractures display "lattice" (or rhomboidal) patterns and, may have relatively high lateral connectivity based on the consistent, high amplitude anomalies observed on horizon slices. Good vertical connectivity may also attributed this fracture sets, because the fractures occur consistently, and are well defined on each horizon slice down to 300ms below the Top Basement marker.

5) Fracture swarms in the study area comprise N- and NW-striking fractures within NW-SE trending swarms (Group 2) and sparse, E-striking en echelon sets within NE-SW trending fracture swarms (Group 4). The Group 4 fracture swarm is present only at shallow levels within the basement; this group of fractures can be mapped confidently down to 200ms beneath the Top Basement marker, but appears to be absent on and below the 250 ms horizon slice. The E-W trending fractures resemble those interpreted using the FMI data from the AU-1 well (Figure 5.4). This observation may suggest that the AU-1 well has penetrated an NE-SW trending fracture swarm. AU-1 has proven that oil is present within the fractured basement. However, the presence of a dry well within a similar play to the north of AU-1 may suggest that the fracture zone tested has fairly low fracture connectivity. In addition to lateral and vertical less extensive, Group 4 fracture set also shows generally radial-like distribution and only present at shallow depth within M-Field basement complex. This observation may also suggest that the Group 4 set may have originated from cooling of igneous rock (Kulander et al., 1990). This 'thermal gradient' fracture set is also consistent with the igneous basement rocks inferred around the M-field. If this is correct, the Group 4 fracture set is the least attractive for hydrocarbon play potential due to its origin which resulted in poor connectivity and least extensive.

6) The N-S and NW-SE trending fractures that together define a lattice or rhomboidal pattern could potentially be characterized by high connectivity that may have allowed hydrocarbon migration from the source kitchen along the NE margin of Tenggol Arch. Hydrocarbons may have entered the fractured footwall basement in the vicinity of the S-field, and subsequently migrated up-dip towards the structurally-higher M-field adjacent to the southern margin of the study area. However, at present no well data are available to prove oil staining or a residual oil column within the basement complex of the S-field. This lack of data is because the current exploration and development targets associated with the S-field are mainly within Miocene strata. Thus, basement complex in the S-field and over the Tenggol Arch in general, is under-explored.

In conclusion, the Antracking volume interpretation was able to distinguish different styles of basement fracturing on the Tenggol Arch. The 'lattice' pattern fractures with N-S and NW-SE trends may have good reservoir potential due to their high lateral and vertical connectivity. The presence of N-striking fractures, which are pervasive on the footwall of the Tenggol Fault suggests that a similar fracture pattern may be present elsewhere within the Western Zone based on evidence from fault and fracture mapping from seismic data and the kinematic model proposed in Chapter 4. However, systematic mapping of fractures and faults in basement within the zone of inferred wrench-dominated transtension along the Western Hinge Line is required in order to characterize the local

fracture pattern and potential leads for drilling candidates in this region. The findings presented here suggest there is new exploration potential of fractured basement on the Tenggol Arch and the Western Zone generally. However, other geological uncertainties such as cap rock effectiveness and reservoir effectiveness still require proper geological and geophysical assessment in order to further develop into drilling candidates. These remaining assessments should be carried out as part of a reservoir or prospect scale evaluation of the fractured basement play. There is a possibility that the youngest North-South fracture set is characterized by open fractures. Nevertheless, factors such as mineral precipitation within the fractures – which may affect the fractured reservoir permeability – cannot be ruled out and should be investigated further. Hence, this fractured play concept needs further support from reservoir-scale geophysical attribute analysis using higher resolution seismic data at basement level and a greater density of well data for geological calibration.

Antracking is useful to define the fracture distribution and geometry, but cannot be used to identify potential fluid types or reservoir properties. To do this, we need to integrate various different types of geophysical attributes. In this section, I combine true amplitude, variance and frequency attributes to draw preliminary conclusions about the petroleum leads on the Tenggol Arch. True Amplitude from seismic data generally reflects rock or reservoir properties which includes porosity, rock density and formation fluid. High amplitude values can also be an indicator of a gas-filled reservoir or tuning effects due to thin beds or geological

bodies below seismic resolution (i.e. thickness below $\lambda/4$, where λ is the dominant seismic wavelength).

The frequency attribute generally highlights hydrocarbon filled reservoirs as regions of low frequency, whilst a "clean", water-filled reservoir is characterized by higher frequency values. This attribute is always referring to relatively high or low frequencies. However, the frequency content will also decrease with depth hence to fully understand the frequency (and also amplitude) attributes of a reservoir requires well calibration.

Variance works similarly by identifying dissimilarities or inconsistencies in seismic data. The dissimilarities indicate breaks in data that may be associated with faults, fractures or channel edges. However, the result (confidence level) of a variance cube depends strongly on the quality of the seismic data (i.e. seismic data with various acquisition and processing artifacts will degrade the result of the variance cube).

A qualitative cross-comparison analysis was done between these three attributes on two test areas (Figure 5.12 and 5.13). The first area is located in the centre of the study area due north from the M-field and south of S-field (Figure 5.12). The second area is located in the northern part of the Tenggol Arch, within the vicinity of S-field (Figure 5.13). Results from this analysis show that area 1 (Figure 5.12 (c)) is characterized by high amplitudes and low frequencies within the fractured

zones on the hanging wall of the Tenggol Fault. Attribute mapping in area 2 shows high amplitudes mainly within the footwall of the Tenggol Fault, with low frequencies mainly found on the hanging wall of the fault zone (Figure 5.12 (c)). All these observations require some calibration to well data to fully understand each attribute. However, in general these findings can be use as preliminary guidance in identifying potential leads for fractured basement in study area.

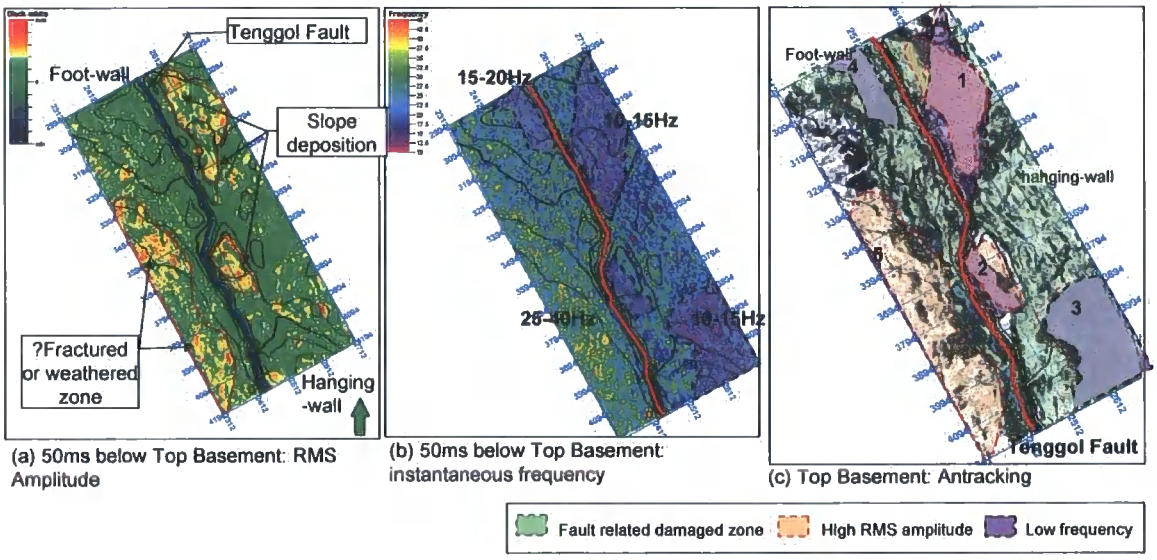

(a) 50ms below Top Basement: RMS Amplitude

(b) 50ms below Top Basement: instantaneous frequency

(c) Top Basement: Antracking

Figure 5.12 (a) RMS amplitude map of Top Basement marker at centre of Tenggol Arch shows high amplitude values (yellow-red) are represents by red polygons. While low amplitude are predominant as background amplitude (green). The high amplitude was interpreted as possible associated with geological events with clear variation combination of rock properties (density, porosity or formation fluid). Low frequency value from instantaneous frequency derived from 50ms window below Top Basement marker (b) similarly indicates combination of variation in basement rock properties indirectly corresponds to attenuation factor in basement layer. Low frequency values are most likely represents low density reservoir layer, relatively higher porosity which mostly corresponds to hydrocarbon-filled reservoir. Antracking volume (c) shows fault-related damaged zones along the Tenggol Fault (green polygons). Polygons (1) and (2)indicates presents of both high RMS amplitude and low frequency while both located within Tenggol Fault damaged zones.

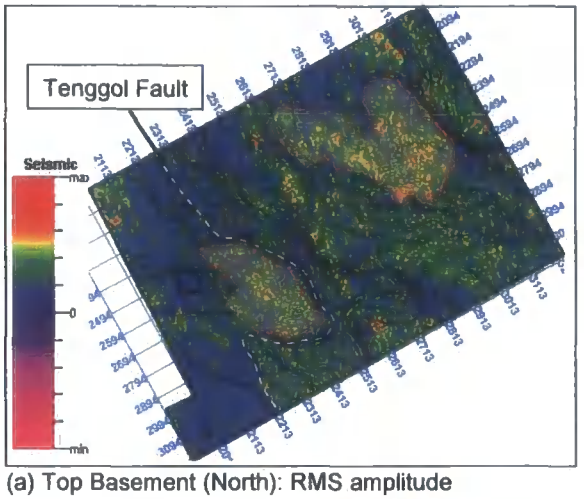

(a) Top Basement (North): RMS amplitude

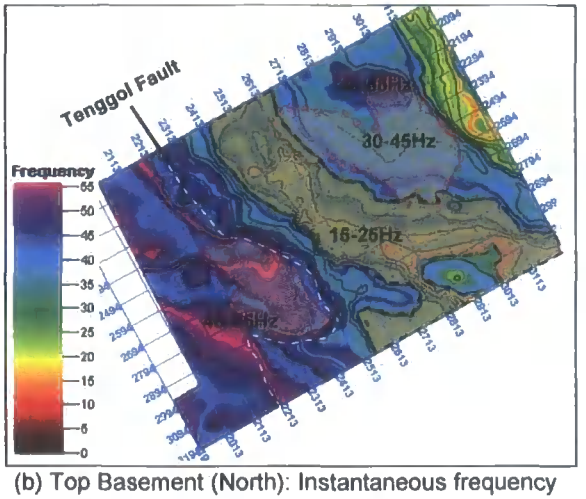

(b) Top Basement (North): Instantaneous frequency

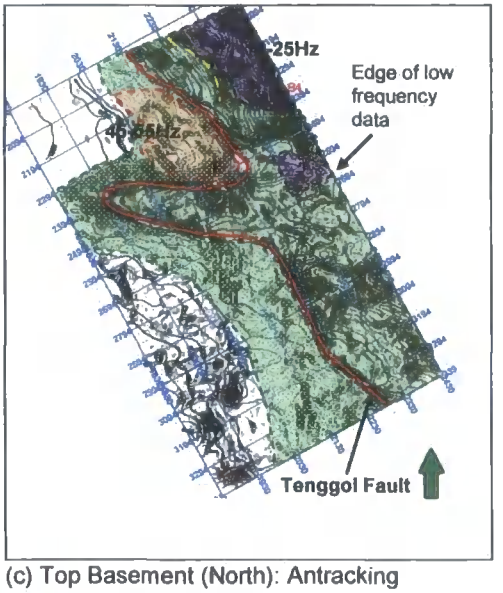

(c) Top Basement (North): Antracking

Fault related damaged zone

High RMS amplitude

Low frequency

Figure 5.13 Antracking map of north area of Tenggol Arch shows possible fault-related damaged zone (*green polygon*). Low frequency zone (purple) shown predominant on downthrown block corresponds to damaged zone on downthrown block. However high amplitude zones (a) corresponds to damaged zone (1) on the footwall (c) with high frequency value (45-55Hz).

Further analysis of the seal (cap rock) properties is also required in order to constraint the possible impact of the sand-rich sequence that overlies the fractured basement. The presence of sand-prone strata will promote leakage or breaching of traps within fractured basement play. Potential hydrocarbon column heights will be overestimated unless an analysis of the seal capability is carried out.

A geochemical study of to correlate kerogen types between oils from the S- and M-fields may provide data on which to develop a more robust model for hydrocarbon migration through basement-hosted fractures from the S-field up-dip towards the M-field. If a hydrocarbon migration pathway can be proven within the footwall of the Tenggol Fault, an analysis of seal capability is the next step required to upgrade this conceptual model to potential drilling candidates. The occurrence of both successful and dry wells along the Tenggol Fault suggests that the fault has both seal and leak points along its length. The presence of leak points may permit hydrocarbon migration along and across the fault, thus filling footwall reservoirs. Therefore critical factors yet to be quantified for this play are the cap-rock sealing capabilities and reservoir effectiveness such as permeability and porosity.

6.0 Discussion, Conclusion and Recommendation

6.1 Petroleum conceptual model: Fractured Basement

This chapter presents a conceptual petroleum systems model (i.e. an integrated analysis of reservoir, trap, source rock and timing of hydrocarbon migration) for the fractured basement play on the Tenggol Arch. The model has been derived by synthesizing the onshore and offshore structural histories developed during the present study with previous basin modeling results based upon offshore seismic and well data. Chapters 4 and 5 have shown that well-developed fracture sets are likely to exist within the basement complex and that the youngest (and perhaps best connected) N-S trending fractures could have developed during Late Miocene/Pliocene regional transtension. The principal geological risks associated with the fractured basement play are therefore not whether the fractures exist, but trap and reservoir effectiveness. A particular issue to consider is that the basement faults and fractures may behave either as conduits or seals, and that their behavior is likely to depend upon the movement histories of the major basin-bounding faults (i.e., the Western Hinge Line and Tenggol Fault). For example, late-stage (Pliocene) deformation along the WHL and Tenggol Fault could have compromised seal integrity due to dilation and shearing along fault planes. This possibility is consistent with the low success rate of oil discoveries along the Western margin of the Malay Basin (Attachment 23). A well-defined structural history is therefore a critical factor to understanding

the geological risks of the fractured basement play and for identifying future drilling candidates.

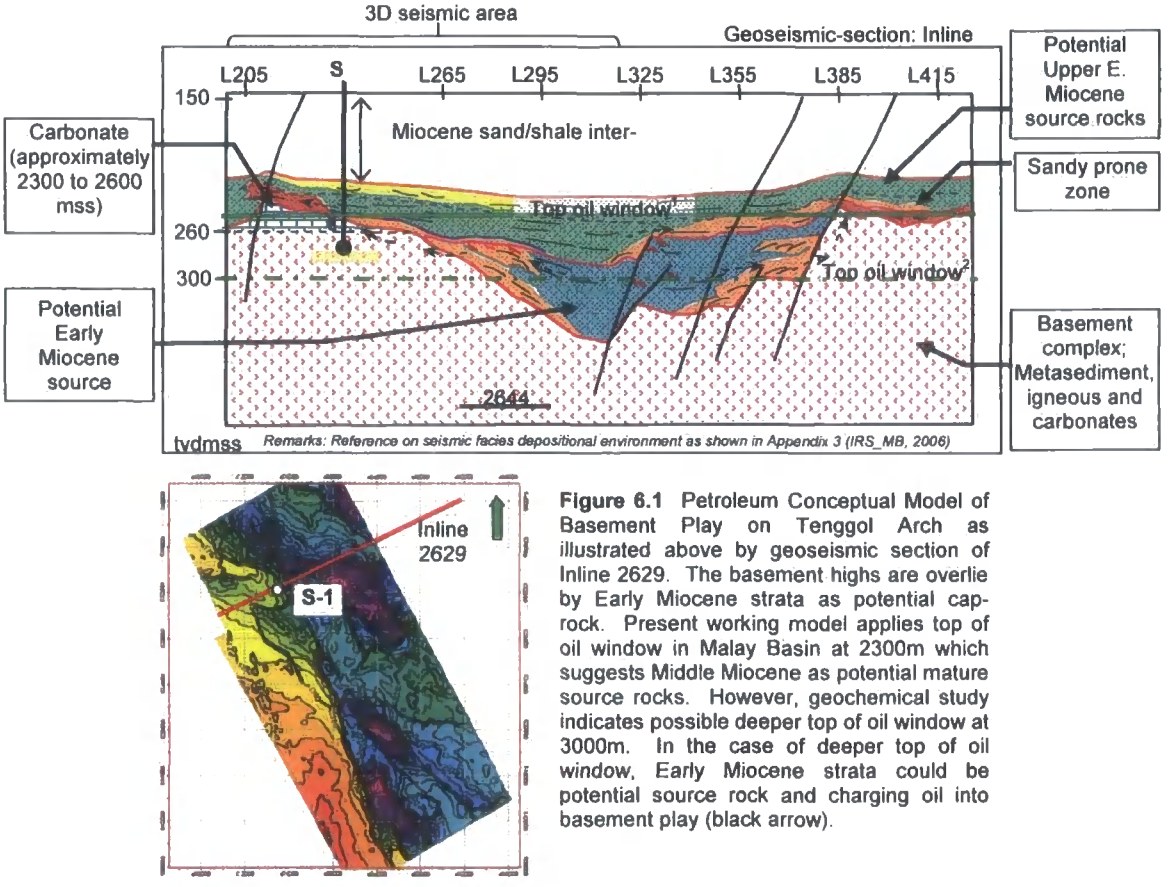

Figure 6.1 Petroleum Conceptual Model of Basement Play on Tenggol Arch as illustrated above by geoseismic section of Inline 2629. The basement highs are overlie by Early Miocene strata as potential cap-rock. Present working model applies top of oil window in Malay Basin at 2300m which suggests Middle Miocene as potential mature source rocks. However, geochemical study indicates possible deeper top of oil window at 3000m. In the case of deeper top of oil window, Early Miocene strata could be potential source rock and charging oil into basement play (black arrow).

6.1.1 Reservoir

The long-lived, basement-rooted Tenggol Fault is an important element in controlling the petroleum potential of the fractured basement play on the Tenggol Arch. Movements along the Tenggol Fault have caused extensive fracturing of basement rocks on both the up- and down-thrown sides of the fault zone (see

Chapter 5). It is these fractures that are likely to be the primary controls on the reservoir potential of the basement complex.

The results of the Antracking™ study conducted on basement rocks within the footwall of the Tenggol Fault (Chapter 5) shows that structural lineaments – features that are likely to represent important fault or fracture trends – can be consistently mapped down to 300ms below the Top Basement marker. However, higher resolution seismic reflection or other geophysical data are necessary to improve imaging of fractures at greater depths. The occurrence of mappable lineaments suggests that the fracture density is locally high; nevertheless, the paucity of wells means there is a large uncertainty in quantifying the density and spatial distribution of these fractures. In addition to the geometric / spatial uncertainty, the lack of well data means that there is also a high degree of uncertainty surrounding the connectivity and permeability of basement faults and fractures – for example, whether the fractures are open or infilled by mineral inclusions. The type of mineral infill will impact greatly on fracture apertures, which in turn control the porosity and permeability of the fracture network. In order to quantify these effects, future studies should investigate the possible impact on reservoir quality of hydrothermal activity, compaction, diagenetic effects of meteoritic or formation waters and the impact of subaerial weathering.

The strong vertical persistence of NW-SE and N-S trending fractures sets within the Antracking™ volume suggests that these structures may have a tectonic origin. Two fracture sets in particular – Groups 1 and 3 (see Chapter 5) – show a close spatial association with seismically-imaged faults (e.g. Figure 5.7). Both sets occur mainly within fault hangingwalls, which is again consistent with a tectonic origin. By contrast, the Easterly trending fracture set ("Group 4" in Chapter 5) are less commonly observed and occur only at shallow depths – 50 to 200ms – below the Top Basement marker. These fractures may be non-tectonic in origin. In particular, the more dispersed, generally radial-like distribution of the lineaments belonging to Group 4 could indicate that these structures originated as cooling joints within igneous host rocks (Nelson, 1985; Kulander et. al., 1990). Kulander et al. (1990) have shown that cooling-related fractures do not contribute greatly to the reservoir potential of fractured basement plays (see section 5.4.2(5)). Structures belonging to the Group 4 fracture set are therefore likely to have a relatively high risk for reservoir effectiveness compared with the NW-SE and N-S trending fracture sets. Igneous rocks constitute the principal basement lithology on the footwall (M-field), while metasediment prominent on the hanging-wall of the Tenggol Fault (Figure 1.3). The distribution of Group 4 fractures within the footwall of the Tenggol Fault therefore supports the idea of Group 4 fracture set as potentially non-tectonic origin.

The geological risk is compounded by the uncertainty over whether the better connected tectonic fractures have high permeability – and could therefore act as

fluid conduits – but low porosities and thus have poor potential to store economically-viable hydrocarbon volumes. In this case, the basement fractures could provide important secondary hydrocarbon migration pathways, with very little accumulated oil remaining in place. The importance or otherwise of secondary migration will depend very much on the type of lithology (e.g. its sealing potential) that overlies, or is in contact with the fractured basement.

6.1.2 Trap

The top seal or cap rock in this system is provided by the Tertiary strata that overlie – or are juxtaposed against – the Top Basement marker (Figure 6.1). The fracture leads on the Tenggol Arch are mostly found within the upthrown block of the Tenggol Fault (Figure 5.11). This region also defines the western flank of the Malay basin and was an important sediment source during the Tertiary. As a result, the western flank of the basin contains a high proportion of sand-prone strata (Figure 6.1). The effectiveness of the top seal for this lead could therefore be moderate or low in comparison to its reservoir effectiveness.

At present, only the M-1 and M-2 wells have penetrated into the basement complex on the upthrown block of the Tenggol Fault. These wells encountered clastic sediments with generally high sand to shale ratios overlying the basement rocks. The high sand content could potentially weaken the seal capability of

these strata and provide high permeability pathways for oil to migrate up into shallower (Tertiary) reservoirs. The petrophysical properties of these clastic sediments (e.g. their capillary pressure characteristics) will also control the present-day hydrocarbon column preserved in the basement (Jahn F. et al., 1989).

In conclusion, cap rock effectiveness remains uncertain within the fractured basement play, and should be taken in to account during lead evaluation to determine drilling candidates.

6.1.3 Source rock and hydrocarbon migration

Source rock

Source rocks in Malay Basin most commonly occur within Miocene strata, with addition source rock potential within the Late Oligocene/Early Miocene interval. Source rocks in the basin belong mainly to Groups E, I, J, K and L[1] and comprise shale or coaly shale. The Group E source rock (Late Miocene), which is the near-equivalent to the Ta_3 seismic marker on the Tenggol Arch occurs only within the Central Zone of the basin. The Group I source rock dated as Upper Early to Middle Miocene is fairly widely distributed throughout the basin and is the near-equivalent to the Ta_5 seismic marker. This source rock consists of coaly shale and is widely accepted as a major contributor to the gas and waxy oil

[1] Stratigraphic nomenclature used widely in the basin developed during EPIC 1994 study.

discoveries along the southern margin of the Malay Basin. Group J, Group K (Middle Early Miocene) and Top Group L (Lower Early Miocene) source rocks are equivalent to the Ta_6 seismic marker, while Top Group M is near-equivalent to the Top Synrift seismic marker on the Tenggol Arch, which is dated Late Oligocene (Attachment 3).

Based on geochemical analysis of source rocks in the Malay Basin (PRSS, 1994[2], PETRONAS, 2005(a)) it can be concluded that the important source rocks along the southern margin of the basin (including the Tenggol Arch) belong to Groups J, K and potentially L and M. These source rocks are widespread throughout the study area and are the most likely sources of oil and gas found on the Tenggol Arch. The PRSS (2005) also concluded that in general, Group J and K source rocks comprise mostly of shale, with some coaly shale in Group J. The TOC (total organic content) averages 0.5%. Group L and M source rocks are primarily observed within regions affected by the major upright anticlines of the Eastern Zone. The L and M Group source rocks are thought to be equivalent to the Oligo-Miocene Talang Akar Formation in the Sumatra basins, which are kerogen Type I/II oil-prone source rocks (Thompson et. al., 1994).

The top of the oil window in the northern part of the Malay Basin is situated at 2300m in the Joint-Development Area (JDA) based on a Bitumen Index (BI) plot of samples from this area. However the BI plots derived from regional studies

[2] PRSS, 1994 (unpublished) Geochemistry analysis of source rocks in the Malay Basin was carried out as part of regional study of the basin in EPIC project (1994).

(PETRONAS, 2006(a)) of two main source rock samples (Group I and Group K) from the central, eastern and southern Malay Basin show present of multiple top of oil window. The Group I BI plot indicates possible top of oil window at 1600m and 3000m. Group K source rocks BI plot indicates possible top oil window at 3000m and 3300m. The 1994 and 2006(a) in-house studies concluded that there is a possibility that the top of oil window in the Malay Basin should be deeper than perceived in present working model. A deeper oil window suggests that deep-seated plays (i.e basement and synrift plays) have a better chance to be filled by hydrocarbon. However there are many others geological variables/parameters need to be considered in order to fully evaluate this idea. The geological parameters include, over pressure factor, sealing effectiveness of the cap-rocks, hydrocarbon fairway and migration shadow.

Migration

Oil deposits in fractured basement reservoirs on the upthrown block of the Tenggol Fault have been encountered in the M-2 well. These observations suggest possible hydrocarbon migration pathways between the source rocks in the basin and the basement reservoirs in the footwall, i.e. across the Tenggol Fault. As discussed in the introduction to this chapter, leak points along the Western Hinge Line and Tenggol Fault could have enabled further oil migration out of the basement trap, allowing gas to displace oil in the fields. Analysis of throws and isochore profiles along Tenggol Fault (Chapter 5) suggest that the fault was reactivated during Late Miocene/Pliocene to Pliocene times, which

post-dates oil expulsion in the Malay Basin c. 7-7.5Ma. This possibility is supported by evidence the presence of oil legs in gas fields and by residual oil observed in cutting samples associated with bypass oil in fields situated along the Tenggol Fault.

Hydrocarbon territory

Oil expulsion and hydrocarbon habitat are critically dependent on the fluid pressure distribution in a basin. Overpressure is widely accepted as a driving mechanism to initiate oil expulsion from the source rocks. Overpressure also affects the overall behavior of the expulsion (i.e the magnitude and consistency of first oil migration from source rock beds into conduit beds or reservoirs) and general distribution of oil in the basin (England and Fleet, 1991).

Overpressure in the Malay Basin is generally encountered at depths between 3000m and 5000m; the section from 0m (seabed) to less than 3000m depth is under a normally pressured regime. The normal hydrostatic pressure regime is mostly associated with normal compaction. Interpretation of overpressure in the basin was based on analysis of seismic data calibrated against pressure data from wells. In terms of source rock potential, Group K shales are mainly distributed within normally pressured regime (above 2500m in depth). On the other hand, the Group L and M shale are generally distributed within overpressured regime, at depths greater than 2500m to 3000m.

As suggested by England and Fleet (1991), overpressure is an important factor in driving primary hydrocarbon migration, implying there is high potential for oil expulsion having occurred from the Group L and M source rocks. Discoveries of oil rims in producing gas fields in the centre of the Malay basin support the idea that the L and M shales behave as effective oil source rocks in deeper parts of the basin. The presence of deeper oil source rocks is likely to increase the potential for fractured basement and other deep plays to be charged by hydrocarbons (Figure 6.1). Nevertheless, it is important to consider the risk of carbon dioxide (CO_2) filling in deep basement reservoirs. CO_2 could be entering the system by vertical migration through faults from deep buried strata, over matured kerogen or cracking of liquid hydrocarbon of oil reservoirs (Waples and Ramly, 1996).

6.1.4 Summary

In summary, the important factors contributing to the success (or otherwise) of the fractured basement play on the Tenggol Arch are as follows:

1- Fracture sets that are deep-seated and have a tectonic origin are likely to have higher fracture density and connectivity (compared with fractures of non-tectonic origin), hence will contribute to the permeability of the reservoir.

2- Late Pliocene reactivation along the Tenggol Fault may have caused traps to leak leading to oil flushing and gas emplacement.

3- The deep top oil window (at 3000m) suggests there is a reasonably high possibility that the fractured basement and other deep reservoirs have a hydrocarbon charge. However, there could be a high risk of CO_2 domination.

6.2 Conclusions

1) The structural evolution of the Tenggol Arch and Malay Basin is an important control on the hydrocarbon potential of the fractured basement play. Understanding the structural history (fault and fold growth) allows a more objective evaluation of the geological risks associated with this play. The structural chronology deduced during the present study can be summarized as follows:

i) Indosinian orogeny and initiation of basement fabrics:

The dominant basement fabric of the Malay Basin and Tenggol Arch results from amalgamation of Gondwana fragments during closure of paleo-Tethys prior to the Middle Triassic (Hutchinson, 1996, Tjia, 1998a). The collision of the Sibumasu block with Indochina gave rise to Indosinian Orogeny and generated N-S trending sutures across Sundaland (Tjia, 1998a). NW-striking faults were

initiated following the final docking of the N-S trending Bentong Suture no later than the Middle Triassic (Tjia, 1998a). N- and NW-striking fault sets are prominent at Top Basement level on the Tenggol Arch. The Bouguer anomaly map of the Malay Basin suggests there is a pervasive, deep-seated N-S trending fabric throughout the centre of the basin.

ii) Extension (Late Cretaceous/Early Tertiary):

A rifting event initiated the opening of the Malay, Penyu and West Natuna Basins, and was centered upon a "Triple Junction" possibly associated with thermal uplift of the Malay Dome. Evidence for Late Mesozoic magmatic activity is widespread throughout the region and was interpreted to have been caused by a mantle plume (Tjia, 1998b). However the fact that active magmatism or mantle plume condition may not necessarily caused breaking up (rifting) of continental crust (White, 1992) was highlighted in this study. Although the role played by thermal uplift and the mantle plume in the opening of the Malay Basin origin remains uncertain, the development of a triple rift system seems to require the radial stress system associated with a continental swell (Tjia, 1998b). The clearest geological evidence for the development of the Malay Dome is the occurrence of shallow basement along the western margin of the Malay Basin and a Late Cretaceous-Late Oligocene angular unconformity towards the southern margin of the Malay Basin (Appendix 1, Figure 2.1; PETRONAS, 2006(b)).

iii) Post-rift extension (Early Tertiary?/ Oligocene):

The mainly NW-striking, en-echelon faults that cut the Top Basement marker on the Tenggol Arch are inferred to have accommodated post-rift extension. The interpretation of development of associated sub-basins on the Tenggol Arch are resultant of this North-northeast oriented regional extension possibly during ?Early Tertiary to Oligocene.

iv) Thermal sag (Early Miocene-Middle Miocene):

The Tenggol Arch is interpreted to have experienced a period of tectonic quiescence, giving rise to the relatively uniform thicknesses associated with Early Miocene to Middle Late Miocene (Ta_4 to Ta_3) strata.

v) Oblique extension (Middle Late Miocene):

Extension on the Tenggol Arch and in the Malay Basin during the Middle Late Miocene may have been related to regionally-important, Middle to Late Tertiary extrusion tectonics in Southeast Asia (Table 2a and 2b). The regional extension direction is interpreted to have been oblique to the major basin-bounding faults – the Western Hinge Line and Tenggol Fault. The obliquity between the inferred regional extension direction and the local strike of the basin-bounding faults is a key control on the observed structural styles. The central Malay Basin was characterized by dextral wrench-dominated transtension (WDTT), giving rise to contemporaneous folding (shortening) and faulting (extension). The southern margin of the Malay Basin (including the Tenggol Arch) was characterized by

dextral EDTT (extension dominated transtension), giving rise to normal faults (see section 4.5 and 4.6) (Figure 4.14b and 4.15 (b) and 4.14(c) respectively). The inferred orientation of the regional extension direction is consistent with the present-day orientation of the minimum horizontal stress derived from borehole breakout data in the Malay Basin (090^0 to 095^0; Appendix 10) and suggests continued clockwise rotation of the regional extension direction throughout the Paleogene-Neogene.

vi) Local extension (Early/Late Pliocene)

Early/Late Pliocene dip-slip reactivation of the Western Hinge Line and Tenggol Fault was associated with low magnitudes of vertical offset (throw) across these structures (see section 4.2.3). Despite the small displacements, this Late Tertiary movement may have impacted greatly upon hydrocarbon accumulation and leakage from traps along the Western Hinge Line and Tenggol Fault.

2) Three distinctive fracture sets occur at Top Basement level and below. These are N-S, NW-SE and NE-SW trending fracture sets. The fractures are heterogeneously distributed throughout the footwall of the Tenggol Fault. The north-south fractures are parallel to regional maximum horizontal stress direction interpreted from well bore breakout data, and could potentially be open fractures (Yaacov, 1989). The NE-striking fractures are most likely to be cooling joints, i.e. to have developed due to thermal gradients within the igneous host rock. Fractures with a tectonic origin are more likely to contribute to the reservoir

potential than the cooling joints. Each fracture group represents a potential lead for drilling candidates; however a proper geological risk analysis is required to further develop each lead into a drilling candidate. Geological risk assessment /analysis mentioned above includes seal effectiveness (cap-rock potential), risk on hydrocarbon migration and detailed reservoir mapping to properly evaluate the presence of lineaments identified here as geological events.

3) Geophysical attributes analysis was carried out on two small test volumes focusing on the Top Basement level. Standard geophysical attribute tests were carried out, such as true amplitude, phase, frequency and some mathematically-derived attributes such as variance and structural smoothing. However only three geophysical attributes gave interpretable results; others resulted in poorly defined images. The three attributes mentioned above include True Amplitude, Frequency and Variance, the results of which were summarized in Chapter 5.

4) The top of the oil window along the southern margin of the Malay basin occurs at around 3000m depth, and could contribute to a large hydrocarbon column within deep (basement) reservoirs (Figure 6.1).

6.3.1 Recommendations for future studies

1) Further well-calibration is vital to allow ground-truthing of the conceptual petroleum system model proposed by the present study. Future studies should plan for enhanced sampling and analysis of fractures in basement wells.

2) Pre-Stack Depth Migration (PSDM) reprocessing of the existing 3D seismic data would provide a significantly better velocity model and more accurate depth conversion of structural models for the deep basement play.

3) Cap rock and seal integrity remain major uncertainties in the fractured basement play. Evaluation of seal integrity should include: (1) a cap rock capillary pressure analysis; and (2) an analysis of the role played by "thief-sands" in draining of oil from fractured basement reservoirs.

4) Improving imaging of basement fractures through advanced geophysical pos-processing analysis method using available 3D seismic and well data. In particular, an advanced attribute analysis that can be easily performed using the available dataset and applications (software) includes seismic or velocity anisotropy and shear wave polarization (Marrett et. al., 2007, Barton, 2007). This analysis is based on the idea that the shear wave velocity will be greatest in orientations parallel to the fractures and lower in orientations perpendicular to the fractures. The velocity anisotropy could also be quantified using vertical seismic

profiles (VSP) acquired in wells that penetrate fractured basement. Integration of velocity anisotropy from well VSP and the PSTM seismic data set should be able to better refine anomalies extracted from 3D seismic. However the quality of image produced will still depend on overall quality of the dataset used as input. Although mapping of strike orientations of fractures in space (vertical and lateral dimensions) is important, identifying mineral inclusion and cementing growth pattern in fractures is equally important as cement properties (i.e. mineral type, growth patter, advance inclusion) will affect fluid-flows through the fracture network during production. However, the later study of mineral and cement growth are probably more applicable for reservoir characterization and requires well data (density, sonic, VSP, gamma-ray, resistivity, FMI, formation pressure etc) within the zone of interest. The integration works of seismic and well data should help improve imaging and understanding fractured reservoir properties on Tenggol Arch or Malay Basin.

5) Further study of fractures of onshore analogues (outcrop studies), in addition to new basement drilling results will allow detailed reservoir characterization. We are currently lacking in modern structure or fracture characterization studies of outcrop in Malaysia. New insights of local outcrops may provide vital information to further enhance the fractured basement play.

6) The risk of CO_2 contamination in deep (basement) reservoirs should not be over-ruled and properly accounted for prospecting purposes. A high percentage of CO_2 will down-grade the prospect or play (see below).

7) Evaluating the potential of oil accumulation below overpressure regime; it is possible that the top of the oil window in the Malay Basin is deeper (3000-3300mss) than anticipated in the current working model (PRSS, 1994, 2005). A deeper top of the oil window may indicate a higher potential for deep-seated plays to be filled-up with oil as opposed to shallow top oil window (2300m) which promotes hydrocarbon charging into the Early Miocene and younger strata. In addition, a deep top oil window lies within or below the overpressured regime in the Malay Basin. The top of the overpressured zone in the Malay Basin is generally shallow in the basin center (at ca.1500m)[3] and gradually deepens (to ca. 2300-3000m)[4] at the Western margin; similar distribution of overpressure should be anticipated in the Eastern flank. The presence of an overpressure regime overlying the top of the oil window provides a seal over deep-seated reservoir (basement and synrift plays), thus enhancing the oil column preservation in deep plays (basement and synrift) from Late Oligocene/earlier source rocks. However, there are still many uncertainties with this idea, such as deep source rocks and oil could have undergone further oil cracking resulting in a higher gas zone as opposed to oil preservation. Moving deeper towards

[3] Depth estimation is from (PCSB) wells in basin centre which encountered abnormal formation pressure below Upper/Middle Miocene strata.
[4] Depth estimation is from (PCSB) wells along WHFZ which encountered abnormal formation pressure within Early Miocene strata.

basement, CO_2 will be more prominent and will dominate the total gas content in the reservoirs, which will degrade the hydrocarbon potential of these plays. "Piercing" of the overpressured zone by active faulting may result in equilibration of reservoir pressures, thus driving secondary migration of oil towards shallower strata. Hence, the risks of having bypassed oil and residual oil shows in deep plays are also at large. Although hydrocarbon potential below the overpressured regime is possible, the concept is more likely to be applicable for Early/Middle Miocene clastic reservoirs in the central of Malay Basin due to all the above mentioned risks (i.e. gas prone zone, high CO_2 content and bypass oil).

REFERENCES

AGUILERA, R. (1995) Naturally Fractured Reservoir. 2nd Edition: PennWell Publishing Co. Copyright 1995, pp.1-77.

AIDAN M. Joy. (1993) Comments on the pattern of post-rift subsidence in the central and northern North Sea Basin. Edited by Williams G. D. and Dobb, A. (1993) Tectonic and Seismic Sequence Straigraphy: Geological Society Special Publication (71), p. 123-140.

ATLE ROTEVATN, Haakon F., Hammer J.H. et al. (2007) Are relay ramps conduits for fluid flow? Structural analysis of a relay ramp in Arches National Park, Utah. Edited by Lonergan, L., Jolly, R. J.H., Rawnsley, K. & Sanderson, D. J. (2007) Fractured Reservoirs: Geological Society London Special Publications (270), p. 55 – 71.

BANKWITZ, P., Bankwitz, E., Thomas R., et al. (2004) Age and depth evidence of pre-exhumation joints in granite plutons: fracturing during the early cooling stage of felsic rock. Edited by Cosgrove, J.W. and Engelder, T. The initaition, propagation and arrest of joints and other fractures: Geological Society London Special Publication (23), p. 25-47.

BARTHOLOMEW Nagy, (1967) Fundamental Aspects of Petroleum: Origin and Evolution of Petroleum (8), p. 331-369.

BARTON, Nick (2007) Anisotropy and 4D caused by two fracture sets, four compliances and sheared apertures: The Leading Edge, September, 2007, vol. 26, No. 9, p. 1112- 1117.

BASTIDA, F., Aller, J., Toimil N.C., et al. (2007) Some considerations on the kinematics of chevron folds. Journal of Structural Geology (29), p. 1185-1200.

BONINI, Marco (2007) Deformation patterns and structural vergence in brittle-ductile thrust wedges: An additional analogue modeling perspective: Journal of Structural Geology (29), p. 141-158.

BRIAN J. Skinner, Stephen C. Porter (1995) Metamorphism and Metamorphic Rocks: Kinds of Metamorphism: The Dynamic Earth: An Introduction to Physical Geology (3rd edition), p. 154-157.

CHILDS, C., Watterson and J.J. Walsh (1995) Fault overlap zones within developing normal fault system: Journal of Geological Society London (152), p. 535-549.

CHILDS, C., Andrew N., J.J. Walsh et. al. (2003) The growth and propagation of synsedimentary faults: Journal of Structural Geology (25), p. 633-648.

CHRISTOPHER G. St C. Kendall, Gregory L. Whittle (1995) Geometric responses in Neogene sediments of offshore New Zealand simulated as products of changes in depositional base level driven by eustacy and/or tectonic. Edited by Bilal U. Haq. Sequence Stratigraphy and depositional response to eustatic, tectonic and climatic forcing, p. 113-127.

ENGLAND, William A. and Fleet, Andrew J. (1991) Edited by W.A. England and A.J. Fleet Petroleum Migration: Geological Society Special Publication (59), p.1-6.

FRANK Jahn, Mark Cook and Mark Graham (1989) Hydrocarbon exploration and production. Developments in Petroleum Science: Capillary pressure and saturation-height relationships (46), p. 120-124.

FULLER, M. et al. (1991) Tertiary paleomagnatism of regions around South China Sea: Journal of Southeast Asia Earth Science (6-314), p. 161-184.

GETECH (unpublished) (2005) Malay Basin depth to basement study: Malay Basin GIS project Interim for PETRONAS by GETECH (Geophysical Exploration Technology Ltd.)

GUIDO Schreurs and Bernard Colletta (1998) Analogue modeling of faulting in zones of continental transpression and transtension: Continental Transpression and Transtension. Geological Society Special Publications (135), p. 59-79.

HAAKON Fossen and Basil Tikoff (1998) Extended models of transpression and transtension and application to tectonic setting: Continental Transtension and Transpression. Geological Society Special Publications (135), p. 15-33.

HALL, Robert (2002) Plate Tectonic Evolution of SE Asia & SW Pacific: computer based reconstructions model and animations. Journal of Asia Earth Science, p. 126-131.

HALL, Robert (1998) The plate tectonics of Cenozoic Southeast Asia and the distribution of land and sea. Edited by R. Hall and J.D. Hollaway, Biogeography and geological evolution of SE Asia, p. 99-124.

HARRISON, T.M. et al. (1992) An Early Miocene transition in deformation regime within the Red River Fault zone, Yunan and its significance for Indo-Asian tectonics: Journal of Geophysical Research (97- B5), p. 7159-7182.

HAQ, Bilal U. (1992) Book reviews of Phanerozoic sea level changes by Anthony Hallam: Perspectives in Paleobiology and Earth History, Series 3. Columbia University Press New York, N.Y., p. 316-318.

HUGGINS, P, Watterson, J.J., Walsh and C. Childs (1995) Relay zone geometry and displacement transfer between normal faults recorded in coal-mine plans: Journal of Structural Geology (17-12), p.1741-1755.

HUS, R., Acocella, V., Funiciello, R. And M. De Batist (2005) Sandbox model of relay ramp structure and evolution: Journal of Structural Geology (27), p. 459-473.

HUTCHINSON, C.S. (1996) Geological Evolution of Southeast Asia: 2nd edition publication of Geological Society of Malaysia, p.368.

HOLDSWORTH, R. E., C. A. Butler and A. M. Roberts (1997) The recognition of reactivation during continental deformation: Journal of the Geological Society, London (154), p. 73-78.

IMBER, J., R.E. Holdsworth, K.J.W McCaffrey et al. (2005) Early Tertiary sinistral transpression and fault reactivation in the west Voring Basin, Norwegian Sea:

Implications for hydrocarbon exploration and pre-breakup deformation in ocean margin basins: AAPG Bulletin, vol.89 (8), p. 1043-1069.

KHALID Ngah, Mazlan Madon & Tjia H.D. (1996) Role of Pre-Tertiary fractures in formation and development of the Malay Basin and Penyu Basin. Edited by Hall, R and Blundell, D., Tectonic Evolution of Southeast Asia: Geological Society Special Publication (106), p. 281-289.

KRISTENSEN, M.B. et al. (2008) The 3D geometry of small-scale relay zones between normal faults in soft sediment: Journal of Structural Geology (30), p. 257-272.

KULANDER, B.R., S.L. Dean and B.J. Ward Jr. (1990) Fractured Core Analysis: Interpretation, logging, use of natural and induced fractures in core: AAPG Methods in Exploration (8), p. 88.

LACASSIN, R., Maluski, Leloup and Tapponnier (1997) Tertairy diachronic extrusion and deformation of western Indochina: Structural and 40Ar/39Ar evidence from NW Thailand: Journal of Geophysical Research (102-B5), p.10013-10037.

LAWRENCE, David A., Grant R. G. and Erling, I.H.S. (1998) Sequence Stratigraphic and Reservoir Architecture of Middle to Late Miocene tidal and

fluvially influenced lower delta plain to marginal marine clastic in Block A-18, Malaysia-Thailand Joint Development Area (MTJDA): AAPG Annual Convention Abstract, Salt Lake City, Utah. May 17-28, 2008, p. 1-6.

LEE, C.P., Shafeea, L., Kamaludin, H., Bahari, N. and Rashidah, K. (2004) Stratigraphic lexicon of Malaysia: Geological Society of Malaysia, p. 87-118.

LEE, Hee-Kwon and Kim, Hyeong Soo (2005) Comparison of structural features of the fault zone developed at different protoliths: crystalline rocks and mudrocks. Journal of Structural Geology (27), p. 2009-2112.

LELOUP P.H., R. Lacassin, Tappoinner P. and Harrison (2001) Comment on "onset timing of left-lateral movement along the Ailao Shan-Red River shear zone: 40AR/39AR dating constraint from the Nam Dinh area, Northeastern Vietnam" by Wang et al. (2000): Journal of Asian Earth Sciences 18, 281-292. Journal of Asian Earth Sciences (20), p. 95-99.

LELOUP, P.H., Arnand, N. and Lacassin, R. et al (2001) New constraints on the structure, thermochronolgy and timing of the Ailao Shan-Red River shear zone, Southeast Asia: Journal of Geophysical Research (106), p. 6657-6671.

LEPVRIER C., Maluski H., Tich V.V., et al. (2004) The early Triassic Indosinian orogeny in Vietnam (Truong Son Belt and Kontum Massif); implications for the geodynamic evolution of Indochina: Tectonophysics (393), p.87-188.

LIRONG Dou, Liang Chang (2003) Fault linkage patterns and their control on the formation of the petroleum systems of the Erlian Basin, Eastern China: Marine and Petroleum Geology (20), p. 1213-1224.

LISA, D.G., Leloup and Harrison et al. (2003) Direct dating of left-lateral deformation along Red River shear zone, China and Vietnam: Journal of Geophysical Research (108-B2), p. 2127.

LUMADYO, E., McCabe, R., Harder, S. and Leet, T. (1993) Borneo: A stable portion of Eurasia margin since Late Eocene: Journal of Southeast Asian Earth Sciences (8, no.1-4), p. 225-231.

MADON, M., Khalid Ngah et al. (1999) The Petroleum Geology and Resources of Malaysia. PETRONAS. Kuala Lumpur (1999): 553-2809595 PET

MAHANDREN, G., Mustaffa K. S. & Raj, J.K. (1991) The stratigraphy of Batu Arang area: Geological Society of Malaysia, Annual Geological Conference 4 & 5 May 1991. Warta Geologi 17(3), p. 166.

MAILLOT, B., Cowie, P. and Lagne D. (1998) Simulating polyphase faulting with tensional 3D model of fault growth: Edited by Jones, G., Fisher, G.J., Knipe, R.J Faulting, fault sealing and fluid flow in hydrocarbon reservoirs. Geological Society London Special Publication (147), p. 209-216.

MANDEFRO Belayneh, Stephan Matthai, J.W. Cosgrove (2007) The implications of fracture swarms in the Chalk of SE England on the tectonic history of the basin and their impact on fluid flow in high-porosity, low permeability rocks: Edited by Reis, A.C., Butler, R.W.H. & Graham, R.H. Deformation of the Continental Crust: The Legacy of Mike Coward. Geological Society London Special Publications (272), p. 499-517.

MANN, P. (2007) Global catalogue, classification and tectonic origins of restraining and releasing bends on active and ancient strike-slip fault systems: Edited by Cunningham, W.D. and P. Mann, Tectonics of Strike-Slip Restraining and Releasing Bends. Geological Society Special Publications (290), p. 13-142.

MANN, P., Demets, C., Wiggins-Grandison, M. (2007) Toward a better understanding of the Late Neogene strike-slip restraining bend in Jamaica: geodetic, Geological and Seismic constraints: Edited by Cunningham, W.D. & P. Mann, Tectonics of Strike-Slip Restraining and Releasing Bends. Geological Society Special Publication (290), p. 239-253.

MARRETT, R., Laubach, S. E. and Olson, J. E. (2007) Anisotropy and beyond: Geologic perspectives on geophysical prospecting for natural fractures: The Leading Edge, September 2007, Vol. 26, No.9, p. 1106-1111.

McALLISTER, N., Fairchild L., et al. (1994) Basin History, Morphology and Evolution. Unpublished internal EPIC Study and Portfolios of Malay Basin. PETRONAS.

MENZIES, M.A., Barker,J., Bosence,D., et al. (1992) The timing of magmatism, uplift and crustal extension: preliminary observations from Yemen. Geological Society Special Publication (68): Edited by B.C. Storey, T. Alabaster and R.J. Pankhurst, Magmatism and the causes of continental break-up, pp.293-304.

MEYER B., Tapponnier P., et al. (1998) Crustal thickening in Gangsu-Qinhai, lithosperic mantle subduction and oblique, strike-slip controlled growth of the Tibet plateau : Geophysics Journal Int. (135), p. 1-47.

MORLEY, C.K., Gabdi, S., Seusutthiya, K. (a) (2007) Fault superimposition and linkage resulting from stress changes during rifting: Examples from 3D seismic data, Phitsanulok Basin, Thailand : Journal of Structural Geology (29), p. 646-663.

MORLEY, C.K. et al. (b) (2007) Evolution of deformation styles at a major restraining bend, constraints from cooling histories, Mae Ping fault zone, western Thailand: Edited by Cunningham, W.D. & Man, P Tectonics of strike-slip restraining and releasing Bends, p. 325-349.

MORLEY, C.K. et al. (2004) Activation of rift oblique and rift parallel pre-existing fabrics during extension and their effect on deformation style: examples from the rift of Thailand: Journal of Structural Geology, p. 1803-1829.

MORLEY, C.K. (2002) A tectonic model for the Tertiary evolution of strike slip faults and rift basins in SE Asia : Tectonophysics (347) Elsevier Science, p. 189-215.

MORLEY, C.K., N. Woganan, N. Sankumarn, et al. (2001) Late Oligocene-Recent stress evolution in rift basins of northern and central Thailand: implications for escape tectonics. Tectonophysics (334), p. 115-150.

MORLEY, C.K. (1999) How successful are analogue models in addressing in the influence of pre-existing fabrics on rift structure? : Journal of Structural Geology (21), p. 1267-1274.

MORLEY, Robert J. (1998) Palynological evidence for Tertiary plant dispersals in the Southeast Asian region in relation plate tectonics and climate: Biography and

Geological evolution of Southeast Asia: Edited by Robert Hall and Jeremy D. Halloway. Backbuys Publication, The Netherland, p. 211-234.

N. De PAOLA, R.E. Holdsworth, McCaffery, K.J.W., Barchi (a) (2005) Partitioned transtension: an alternative to basin inversion models. Journal of Structural Geology 27 (2005), p. 607-625.

N. De PAOLA, R.E Holdsworth, J.W McCaffrey (b) (2005) The Influence of lithology and pre-existing structures on reservoir-scale faulting patterns in transtensional rift zones. Journal of the Geological Society London (162), p. 471-480.

NEMCOK M., Moore J.N., Allis R. and McCulloch, J. (2004). Fracture development within a stratovolcano Edit by Cosgrove, J.W. and Engelder, T. The initiation, propagation and arrest of joints and other fractures: Geological Society London Special Publication (231), p.223-242.

PEACOCK, D. C. P. (2002) Propagation, interaction and linkage in normal fault systems: Earth Science Review (58) p.121-142.

PEACOCK, D. C. P., Knipe, R. J., Sanders (2002) Glossary of normal faults: Journal of Structural Geology, No. 22, p.291-305.

PEACOCK, D.C.P. and Sanderson, D. J. (1996) Effects of propagation rate on displacement variations along faults: Journal of Structural Geology (18), no. 2/3, p. 311-320.

PEACOCK, D.C.P and Sanderson, D.J. (1991) Displacements, segment linkage and relay ramps in normal fault zones: Journal of Structural Geology (13), no. 6, p. 721-733.

PETRONAS (unpublished) (2006(a)) Integrated regional study of Malay Basin: Source rock and hydrocarbon migration. PETRONAS Management Unit.

PETRONAS (unpublished) (2006(b)) Integrated regional study of Malay Basin: Structure Framework of Malay Basin. PETRONAS Carigali Sdn. Bhd. Exploration Division.

PETRONAS Carigali (unpublished) (1994) Regional Study of Malay Basin and Penyu Basin, Vol 1, PCSB March 1994. Petronas Carigali Sdn. Bhd. Exploration Division.

PETRONAS Exploration & Production Business Unit and Legal & Corporate Affairs Division (1999) The Petroleum Geology and Resources of Malaysia, ISBN: 983-9783-10-0, p. 665

PROSSER, Sarah (1993) Rift-related linked depositional system and their seismic expression. Edit by Williams, G.D. and A. Dobb, Tectonics and Seismic Sequence Stratigraphy: Geological Special Publication (71), p. 35-66.

REMUS, D., Webster M. and Kanjana Keawkan (1993) Rift architecture and sedimentology of the Phetchabun Intermontane Basin, central Thailand: Journal of Southeast Asian Earth Sciences (8) No. 1-4, p. 421-432.

REPLUMAZ, A., Lacassin, Tapponnier and Leloup, P.H. (2001) Large river offsets and Plio-Quaternary dextral slip rate on the Red River Fault (Yunan, China): Journal of Geophysical Research (106) No. B, p. 819-836.

RHODES, Brady P., et al. (2004) Three stage history of the 3 Pagodas Fault, Western Thailand. Denver Annual Meeting Nov, 7th 2004 (paper 2008-7): Recent advances in Himalayan Geology. Geological Society of America Abstracts with Programs (36) No. 5, p. 484.

RITCHER, B. and Fuller, M. (1996) Paleomagnetism of the Sibumasu and Indochina blocks: Implication of the extrusion tectonic model. Edit by Hall, R. and Blundell, D. Tectonics Evolution of SE Asia: Geological Society Special Publications (106), p.203-224.

ROBERTS, C. et al. (2002) Distributed quantitative and qualitative fault diagnosis, railway junction case study: Control Engineering Practice (10), p. 419 -429.

ROQUES, D., Matthews, S. J. and C. Rangin (1997) Constraints on strike-slip motion from seismic and gravity data along the Vietnam margin offshore Da Nang: Implications for hydrocarbon prospectivity and opening of the East Vietnam Sea. Edit by Fraser, A.J., Matthews, S.J. and Murphy, R.W., Petroleum Geology of Southeast Asia: Geological Society Special Publication (126), p. 341-353.

RAMANI, V.T., Tikoff, B. (2002) Physical models of transtensional folding: Geology (30), p. 523-526

RUCHA Ingavat-Helmcke (1993) Contribution to the Permian fusulinacean faunas of Peninsular Thailand: Journal of Southeast Asia Earth Sciences (8) No. 1-4, p. 67-75.

SCHLISCHE R. W. and Anders M.N. (1996) Stratigraphic effects and tectonic implications of the growth of normal faults and extensional basins: Geological Society of America Special Paper (303), p. 183-203. (crossed-ref from Morley et. al., 2007 (a)).

SHU, Y.K. (1971) The geology of new series map sheet 95, Jelebu district, Negeri Sembilan, Malaysia: Geological Survey Malaysia Annual Report for 1969, p. 72-81.

SHU, Y. K. (1969) Some northwest trending fault zones in Kuala Lumpur and other area: Geological Society Malaysia, Newsletter (17), p.1-5.

SHUN Z, Zhou D. et al. (2003) Experimental evidence for the dynamics of the formation of the Yinggehai basin, NW South China Sea: Tectonophysics (362), p. 41-58.

SMITH, M., Chantrapraset, S., Morley, C. K., et al. (2007) Structural geometry and timing of deformation in the Chainat duplex, Thailand. Edited by Cunnigham, W.D., and Mann P., Tectonics of Strike-Slip Restraining and Releasing Bends, p. 305-323.

TAPPONNIER P., Peltzer, G. and Armijo, R. (1996) On mechanics of the collision between India and Asia in collision tectonics. Edited by Loward, M. P. and A. C. Reis: Geological Society Publication (19), p. 115-157.

TAPPONNIER, P. et al. (1982) Propagating extrusion tectonics in Asia; new insights from simple experiments with plasticine: Geology Special Publications (10), p. 611-616.

TATE, Robert B. (2001) The Geology of Borneo Island compiled by Robert B. Tate. Geological Society of Malaysia Special Publication (CD-Rom).

TEYSSIER, C. and Tikoff, B. (1999) Fabric stability in oblique convergence and divergence: Journal Structural Geology (21), p. 969-974.

TEYSSIER, C. and Basil Tikoff (1998) Strike slip partitioned transpression of the San Andreas Fault System, lithospheric-scale approach: Continental Transpression and Transtension. Geological Society Special Publications (135), p. 143-158.

TEYSSIER, C., Tikoff, B. and Markley, M. (1995) Oblique plate motion and continental tectonics: Geology (23), p. 447-450.

THOMPSON S., Cooper B. S., Bernard P.C. (1994) Sample examples and possible explanations for oil generation from coal and coaly sequences. Edit by Scott A.C and Fleet , A.J. Coal and coal bearing strata as oil prone source rock?: Geological Society Special Publication (77), p.119-137.

TJIA, H.D. (2005) Basement onshore analogues, Eastern Domain of Peninsular Malaysia Field Study booklet November 2005: LESTARI, Institute for conservation and development, University Kebangsaan Malaysia.

TJIA, H.D. (2001) Wrench tectonics in Sundaland- Subsurface and offshore evidence: Geological Society of Malaysia Annual Geological Conference, June 2-3, 2001, p. 74-77.

TJIA, H.D. (a), (1998) Meridian parallel faults and Tertiary Basins of Sundaland: Geological Society Malaysia, Bulletin (42), December 1998, p. 101-118.

TJIA. H.D. (b) (1998) Origin and tectonic development of Malay-Penyu-West Natuna Basins: Geological Society Malaysia, Bulletin (42) December 1998, p. 147-160.

TJIA, H. D. (1997) The Kuala Lumpur fault zone revisited: Warta Geologi (23), No. 4, July-Aug 1997, p. 225-230.

TJIA, H.D. & K.K. Liew (1996) Changes in tectonic stress field in northern Sunda Shelf basins. Edit by R. Hall and D. Blundell, Geological Society Publications (106): Tectonic Evolution of Southeast Asia, p. 291-306.

TJIA, H. D. (1989) Tectonic History of the Bentong-Bengkalis Suture. Geology Indonesia (12), No.1. Jakarta, Indonesia, p. 89-111.

TJIA, H.D. (1987) Olistostrome in the Bentong area, Pahang, Malaysia: Warta Geology (13), No. 3, May-June 1987, p.105-111.

TJIA, H.D. and Idrus (1987) Tectonic implications of well-bore breakouts in Malaysian basins: Geological Society Malaysia, Bulletin (36), Dec 1994, p. 175-186.

TJIA, H.D. (1986) Geological transport directions in Peninsular Malaysia: GEOSEA V Proceedings Vol. II, Geological Society Malaysia, Bulletin 20, August 1986: p. 149-177.

TJIA, H.D. and Zaiton Harun (1985) Regioanal structures of Peninsular Malaysia: Sains Malaysiana. (14), No. 1, Earth Sciences, p.95 -107.

TJIA, H.D. (1978) Structural Geology of Peninsular Malaysia: 3rd Regional Conference on Geology and Mineral Resources of Southeast Asia, Thailand, p. 673-681.

TOWNSEND C., Firth I.R., Westerman R., et al. (1998) Small seismic-scale fault identification and mapping. Edit by Jones, G., Fisher, Q. J., R. J. Knipe, Faulting. Fault sealing and Fluid Flow in Hydrocarbon Reservoirs: Geological Society London Special Publication (147), p. 1-25.

TURNER P. Jonathan, Williams A. Gareth (2004) Sedimentary basin inversion and intra-plate shortening. Earth Sciences Reviews 65 (2004), pp 277-304.

WAKABAYASHI, J. (2007) Stepovers that migrate with respect to affected deposits: field characteristic and speculation on some details of their evolution. Edited by Cunningham, W.D. and Mann, P. Tectonics of Strike-Slip restraining and releasing bends, p. 169-188.

WALSH, J.J., Watterson, J., Bailey, W.R and Childs, C. (1999) Fault relays, bends and branch-lines: Journal of Structural Geology (21), p. 1019-1026.

WAPLES, D. and M. Ramly (1996) Geochemistry of gasses in Malay Basin: Geological Society of Malaysia. Buletin (39), p. 241-258.

WHITE, Ian R. and Juliet G. Cider (2006) Extensional fault propagation folds; Mechanical models and observations from the Moddoe Plateau, NE California: Journal of Structural Geology (28), p. 1352-1370.

WHITE, R.S. (1992) Magmatism during and after continental break-up. Edit by Storey, B.C., Alabaster, J., R.J. Pankurst, Geological Society (68), p. 1-16.

WILLIAMS G.D. and J. W. Cosgrove (1982) Introduction to small-scale geological structure: Department of Geology Imperial College of Science and Technology, Publication 1982, p. 24-26.

WITHJACK, M.O and Jamison, W.R. (1986) Deformation produced by oblique rifting: Tectonophysics (126), p. 99-124.

YAACOV Arkin (1989) Large scale tensional fractures along the Dead Sea-Jirdan, Rift Valley: Tectonopysics (165), p. 143-154.

YASSIR, N.A. (1990) The un-drained shear behavior of fine grained sediments Edit by Knipe, R.J. and Rutter, E.H. Deformation, mechanisms, rheology and tectonics: Geological Society Special Publication (54), p. 339-404.

Table 1 Present-day heatflow reading recorded throughout Malay Basin and neighbouring region

Location	Present-day heatflow	Remarks
Malay Basin	35 to 55°C/km Average: 1.95 HFU Range: 1.6 to 2.4 HFU	2.4 HFU at southeast margin of Malay Basin.
Penyu Basin	Average: 38°C/km	**Tenggol Arc** average heatflow: **45.3°C/km**.
West Natuna Basin	36.3 to 51.8°C/km Average: 34.2°C/km	
Sokong sub-basin (East Natuna)	45.8 to 64°C/km	29.2°C/km north margin of sub-basin.
Gulf of Thailand Basin	40 to 50°C/km	73°C/km highest value recorded from deeper wells at approx. 2600m.
Tonkin Basin (Gulf of Bacbo)	Average: 40°C/km Sediment fill: 2 to 10km Oldest known rock: Eocene	Interpreted to be associated with Quaternary alkaline basalt. NE extension of Tonkin Basin, sediment fill: 4 to 6km (Li, 1984).
Pearl River & South Taiwan Basin (South China Shelf)	42 to 38°C/km Sediment fill: 3 to 8km Oldest strata known: Lower Jurassic	
East China Sea Basin	Average: 33°C/km Oldest strata known: Paleocene	Basin-fill sediment thickness: 5 to 8km (Li, 1984)

After Madon (1999), Hutchinson (1996), Wan Ismai (1984)

Table 2a Cenozoic tectonic stages related to onshore and offshore Peninsular Malaysia

Cenozoic Tectonic Stages	**Three Pagodas Fault Zone** *(Lacassin et al, 1997; Rhodes et al, 2004)*	**Peninsular Malaysia (PM)** *(Tjia & Zaitun, 1985; Chakrabhorty, 1980; Tjia, 1978)*	**Malay Basin (MB)** *(PCSB ,2005)*
Early Tertiary / Paleogene	**Sinistral** motion along 3PFZ (?Eocene- Oligocene)	**Sinistral** motion along KL-BT FZ. Radioactive age dating of Mylonite indicates Eocene – Late Eocene.	Tenggol Arc **?rhomboid sub basins**. Possible indicator of strike slip modification on normal grabens/ half grabens.
Middle to Late Tertiary	**Dextral** motion associated with transtension.tectonic along the fault zone.	Dextral motion along Kelau-Karak Fault Zone (?Tertiary). Dextral motion along Ma' Okil Fault (?Tertiary).	**Dextral** motion along major fault zones of MB at (Late Lower Miocene) sb1000 to sb1200 stratigraphic levels. Dextral motion continues to sb1900 stratigraphic level (Late Middle Miocene).
Late Tertiary	**Dextral** motion associated with transpression tectonic along the fault zone. Age dating (Biotite-gniess) shows possible youngest motion during Holocene.	**Kuantan basalt** (K-Ar 1.7Ma) comprises of alkaline olivine basalt which related to faulting of cratonized continental crust. No dextral motion identified at outcrop of major PM major fault zones.	Youngest **structuration** mapped at sb2100 stratigraphic level (Lower – Upper Pliocene)

Table 2b Cenozoic tectonic stages related to onshore and Tenggol Arc

Cenozoic Tectonic Stages	**Three Pagodas Fault Zone** *(Lacassin et al, 1997; Rhodes et al, 2004)*	**Peninsular Malaysia (PM)** *(Tjia & Zaitun, 1985; Chakrabhorty, 1980; Tjia, 1978)*	**Tenggol Arc (MB)** *(2008)*
Early Tertiary / Paleogene	**Sinistral** motion along 3PFZ (?Eocene- Oligocene)	**Sinistral** motion along KL-BT FZ. Radioactive age dating of Mylonite indicates Eocene – Late Eocene.	**Pre-Oligocene/Early Miocene:** **Extensional**, normal faults with relay fault patterns on Top Basement marker.
Middle to Late Tertiary	**Dextral** motion associated with transtension.tectonic along the fault zone.	Dextral motion along Kelau-Karak Fault Zone (?Tertiary). Dextral motion along Ma' Okil Fault (?Tertiary).	**Early Miocene/Middle Miocene:** **Oblique extension**, rotated bed in transition zones at Ta_6 and Ta_5 markers. Changed in stress orientation, crustal block CW rotation repercussion of extrusion tectonic. (Figure 4.5.3b)
Late Tertiary	**Dextral** motion associated with transpression tectonic along the fault zone. Age dating (Biotite-gniess) shows possible youngest motion during Holocene.	**Kuantan basalt** (K-Ar 1.7Ma) comprises of alkaline olivine basalt which related to faulting of cratonized continental crust. No dextral motion identified at outcrop of major PM major fault zones.	**Middle Late Miocene**: **Oblique extension (WDTT & EDTT);** strain partitioned in Malay Basin, the centre & north are WDTT and south margin (Tenggol Arch) is EDTT. (section 4.6)

Table 3 Summary of Pre-Cenozoic deposits of Central and East Domain of Peninsular Malaysia

Period	Central Domain	East Domain	Reference
Mesozoic	**Tebak Formation** (Upper Jurassic- Lower Cretaceous) Lithology: Mainly arenaceous, minor siltstone and mudstone. Fossil assemblages: Plant; *Cornites spinulosus* *Carpolithes sp.* Environment of deposition: Continental	**Gagau Group** -Badong Conglomerate (?Jurassic) -Lotong Sadstone (U. Jurassic – L. Cretaceous) Lithology: Conglomerate, sandstone, subordinate volcanics, thin lenses of coal. Fossil assemblages: Bivalve; *Trigonoides konairai* Plant; *Cornites spinulosus* Environment of deposition: Continental	Rajah (1968) Rishworth (1974) Khoo (1983) Kobayashi & Suzuki Kon'no
Paleozoic	**Raub Group** -Kepis Beds (Lower Permian) -Aring Formation (U.Carboniferous-L. Triassic) Lithology: Metalimestone (dolomite marble), volcanic (tuff), extrusive igneous (rhyolite), intrusive igneous (andesite). Red brownish-purplish carbonaceous shale, rare red sandstone with minor conglomerate, lenses of carbonaceous limestone. Fossil assemblages: Foraminifera; *Fusulina sp.* Brachiopod; *Schizophoria sp.* Bivalve; *Claria griesbachi concentrica* (Yabe) Environment of deposition: Marginal, shallow marine with volcanic activities.	**Kuantan Group** -Dohol Formation (Mid Permian) -Sg Perlis Beds (Lower Carboniferous) -Panching Limestone (Mid Carboniferous) Lithology: Limestone. Argillaceous metasediment; carbonaceous slate, minor quartzite. Fossil assemblages: Bryozoa; *Fanestella sp.* Environment of deposition: Inner neritic to shallow marine with volcanic activities.	Khoo (1973) Chand (1978) Rajah (1986) Aw (1990) Metcalfe, Idris&Tan (1980) Loganathan (1993)

Table 4 Distribution of igneous rock emplacement onshore and offshore Peninsular Malaysia

Location	Igneous type	Age	References
Peninsular Malaysia	**1) Main Range** *Volcano-plutonic arc*	200 to 220Ma	Liew, 1983 Liew and McCulloch, 1985
	2) Terrain A *Granatoid plutons* *Mixed I and S-type* *Location: Kelantan to Kuantan*	255 to 270Ma (Rb-Sr isochrons, U-Pb zircon radioactive dating)	Liew, 1983
	3) Terrain B *Sub-volcanic I-type granite* *Location: SE Johor to Singapore*	220 to 240Ma	McElhinny et. al. (1974b) Bignell & Snelling, 1977a Liew, 1983
	4) Terrain C *Mixed I and S-type granite*	220 to 240Ma	Liew, 1983
Malay Basin	Belumut granite Malong volcanic Sotong (volcanic inter-beds)	Cretaceous Cretaceous ?Mesozoic	*Well Geological evaluation internal reports PCSB, EPMI.*
Mekong Basin & adjacent shelf	Granite - granidiorite	110 $\pm$ 10 Ma 97 – 178 Ma (shelf area)	Areshev et al, 1992
Natuna – Anambas Islands	Felsic granite	70 -90 Ma	Katili, 1973
Pearl River & South Taiwan Basins	Granites	Mesozoic	Li, 1984

Attachment 1 Tenggol Arc (Ta) seismic markers definition of Miocene-Pliocene strata along Inline 2294

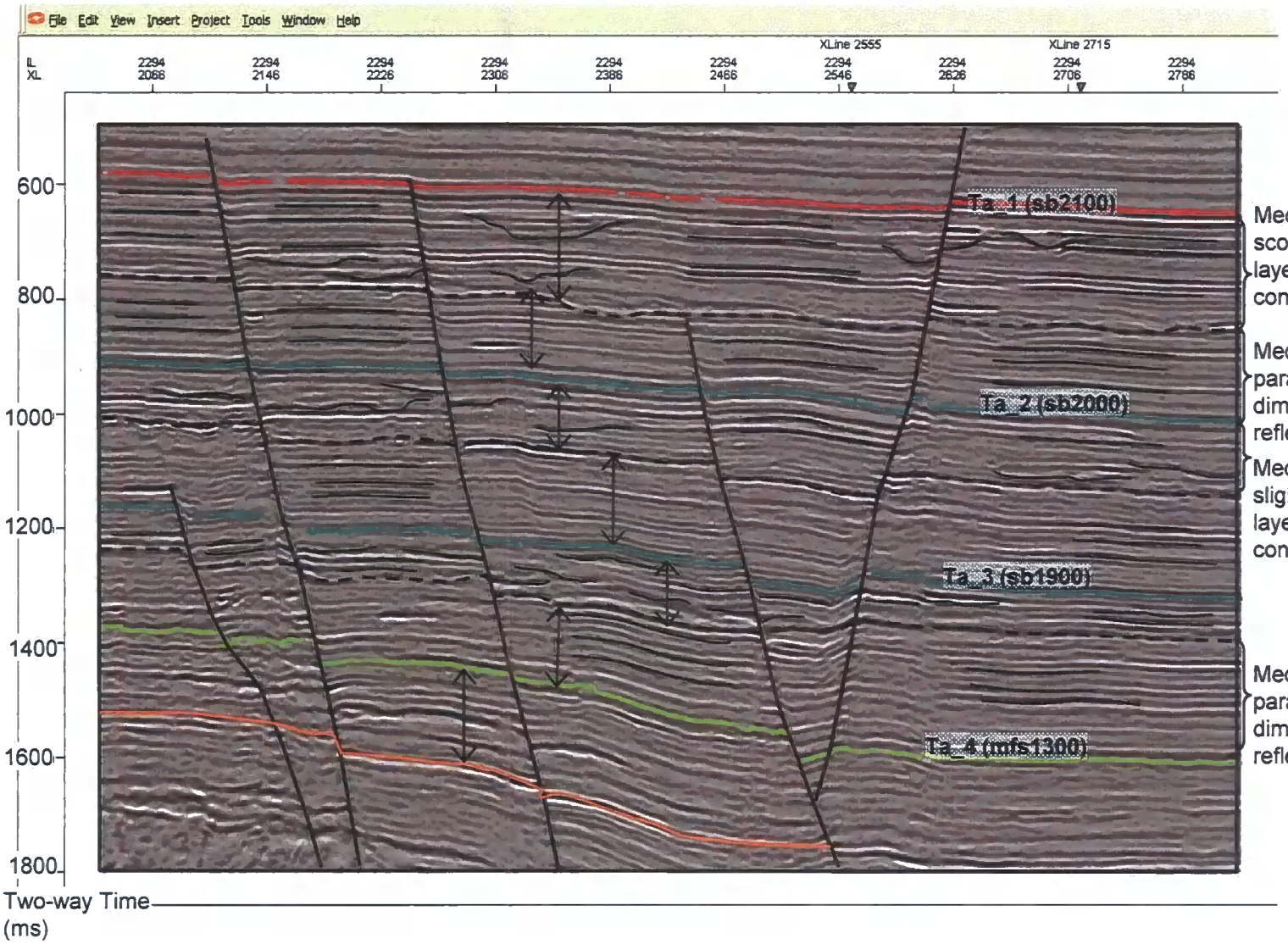

Attachment 2 Tenggol Arc (Ta) seismic markers definition of Oligocene-Basement strata along Inline 2294

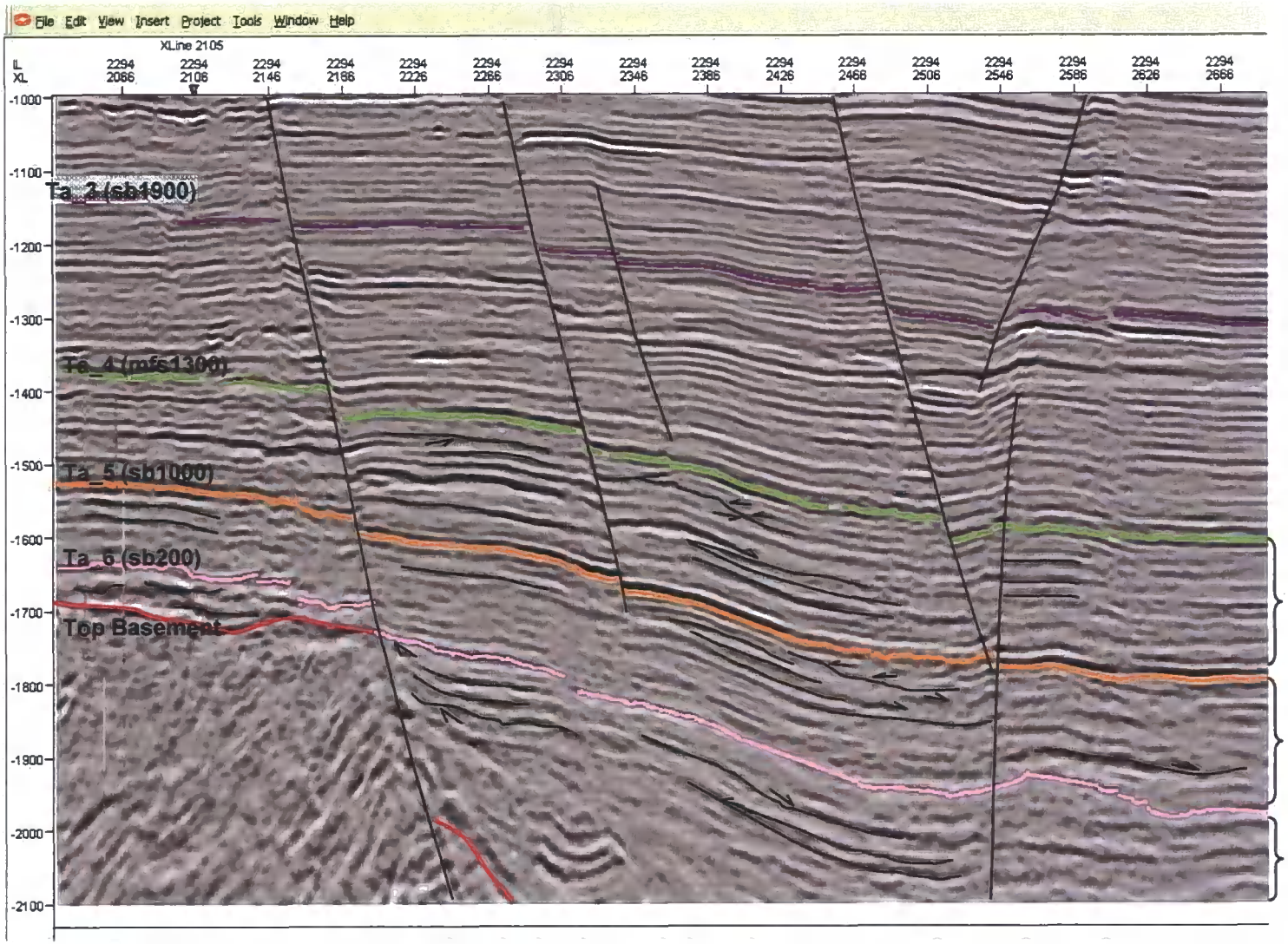

Parallel to sub parallel, truncation features, medium to high amplitude reflectors.

Parallel to sub-parallel, dim, continues to slightly wavy reflectors.

Parallel to sub-parallel, dim, truncation and on-lap features, continues to slightly wavy reflectors.

Attachment 3 Description of seismic markers of Tenggol Arc and their relation to Malay Basin Stratigraphic Scheme

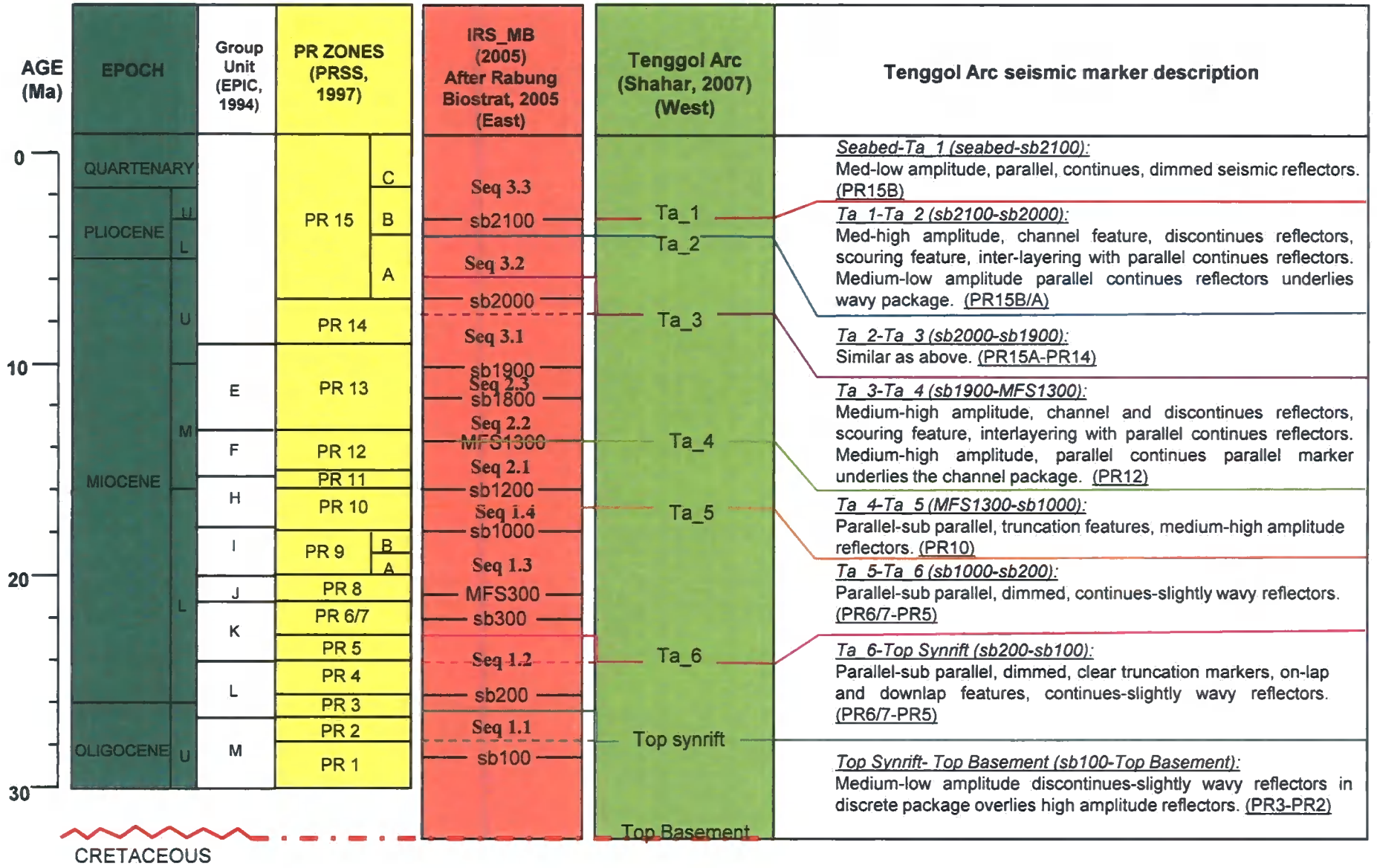

With additions modified after Integrated Regional Study of Malay Basin, PCSB 2006 ater PRSS, 1997, Rabung Biostratigarphy Study, PRSS 2005.

C:\pmirs_2005_06\xd\pcsb\suhaile

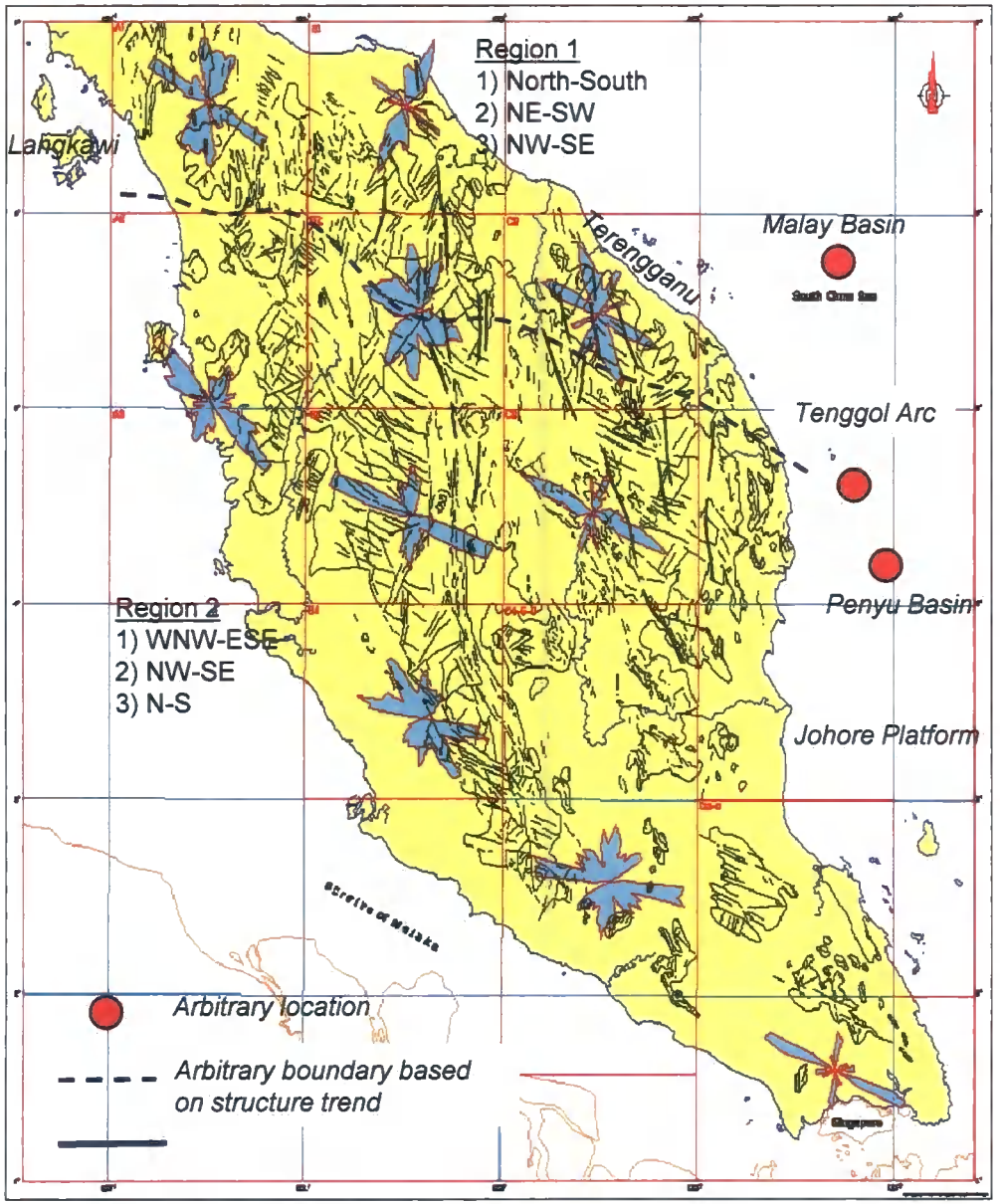

Radarsat image lineaments interpretation from PCSB, Integrated Regional Study of Malay Basin, 2005.

Attachment 4 Lineaments interpretation of Radarsat, Peninsular Malaysia

- North peninsula (Region 1) appears to be most similar to Tenggol Arc ?Middle-Late Miocene fault pattern.

- South peninsula (Region 2) most similar to Tenggol Arc basement and Late Oligocene/Early Miocene fault pattern.

- Regions correspond to paleomagnetic value which concluded from south of Thai's peninsula to north Malaysia peninsula (south of Langkawi) CW rotation. (*Chapter1*)

- South of peninsula, which is from south of Langkawi shows mixed range of CW-CCW rotation which became distinctively CCW as emerging towards Sumatera and west of Borneo. (*Chapter1*)

- N-S striking faults in Northeast of peninsula cutting the NW and NE striking faults. Interpretation of NW and NE striking faults are of earlier structuration

Attachment 5 Simplified Paleozoic stratigraphic scheme of Peninsular Malaysia

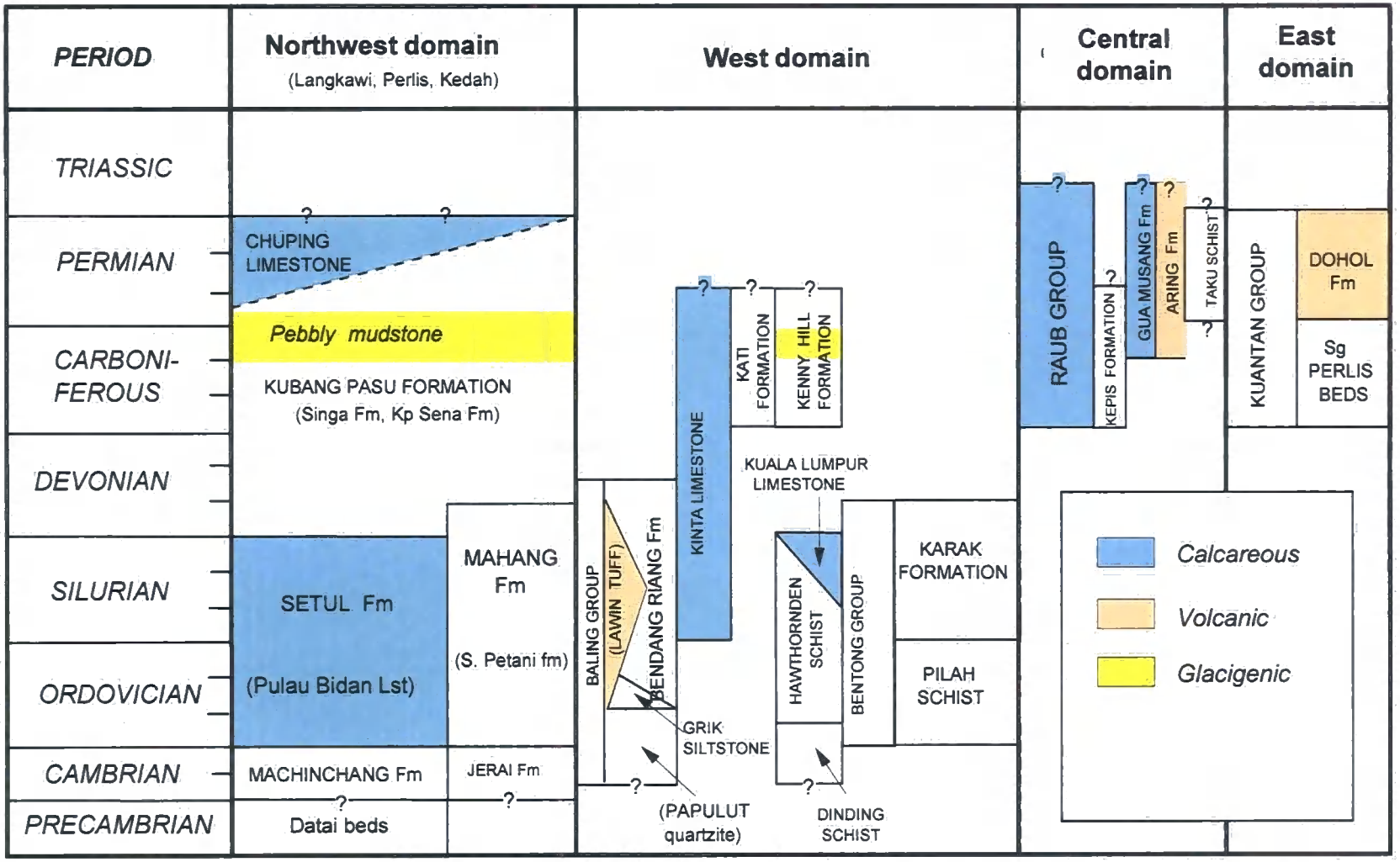

PALAEOZOIC STRATIGRAPHY OF PENINSULAR MALAYSIA

After K.Y. Foo (1983) with additions

Tjia H.D., 2005 Basement Onshore Field study PCSB

Attachment 6 Correlation of Jurassic-Cretaceous sections of East Domain to TB-1 well offshore Peninsular Malaysia.

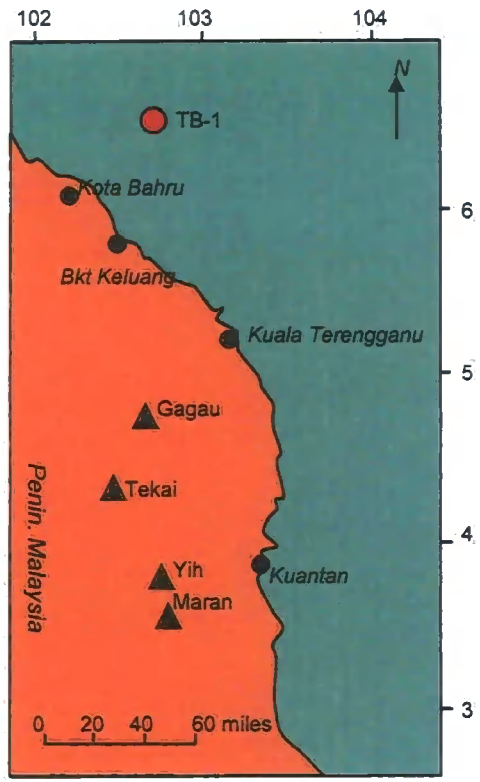

Map of northeast coastline of Peninsular Malaysia shows location of onshore outcrop locations and TB-1 (offshore) north Malay Basin.

Maran-Tembeling Area stratigraphic section

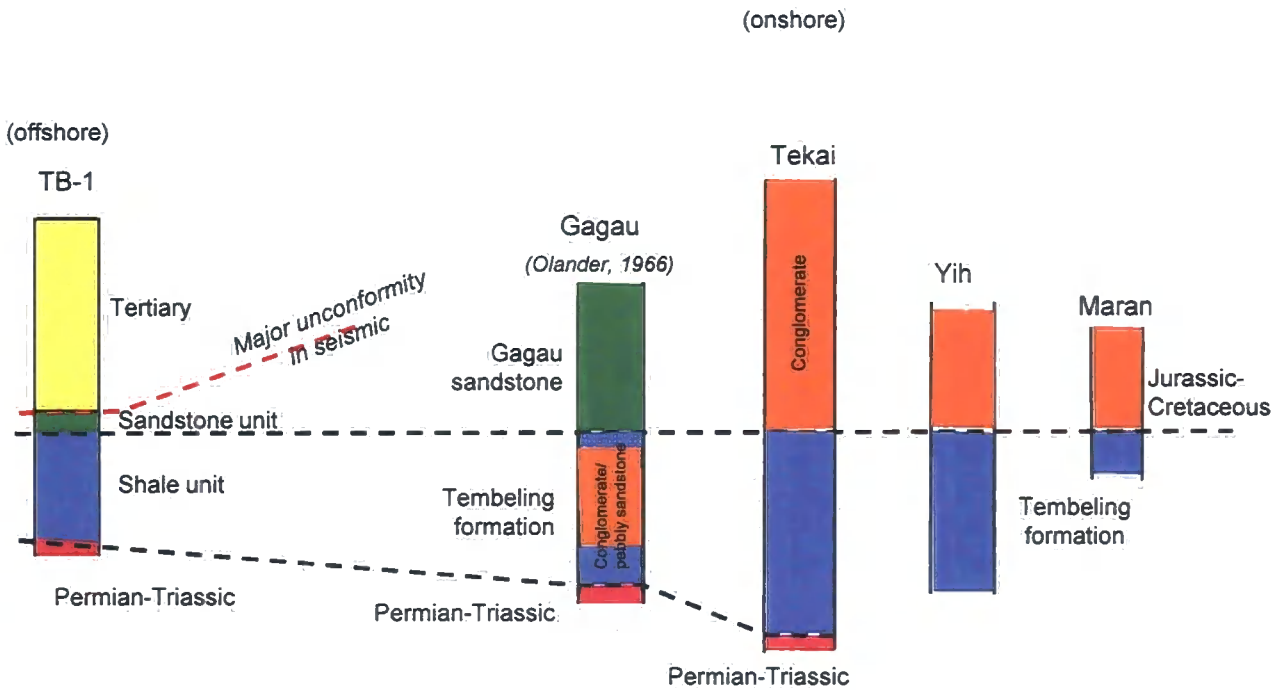

TB-1 Geological Well Completion (unpublished), after Smiley, 1970, H.H. Khoo & Fox, 1971

Attachment 7 Model of Depositional Environment adapted in Malay Basin (Lower coastal plain-coastal environment)

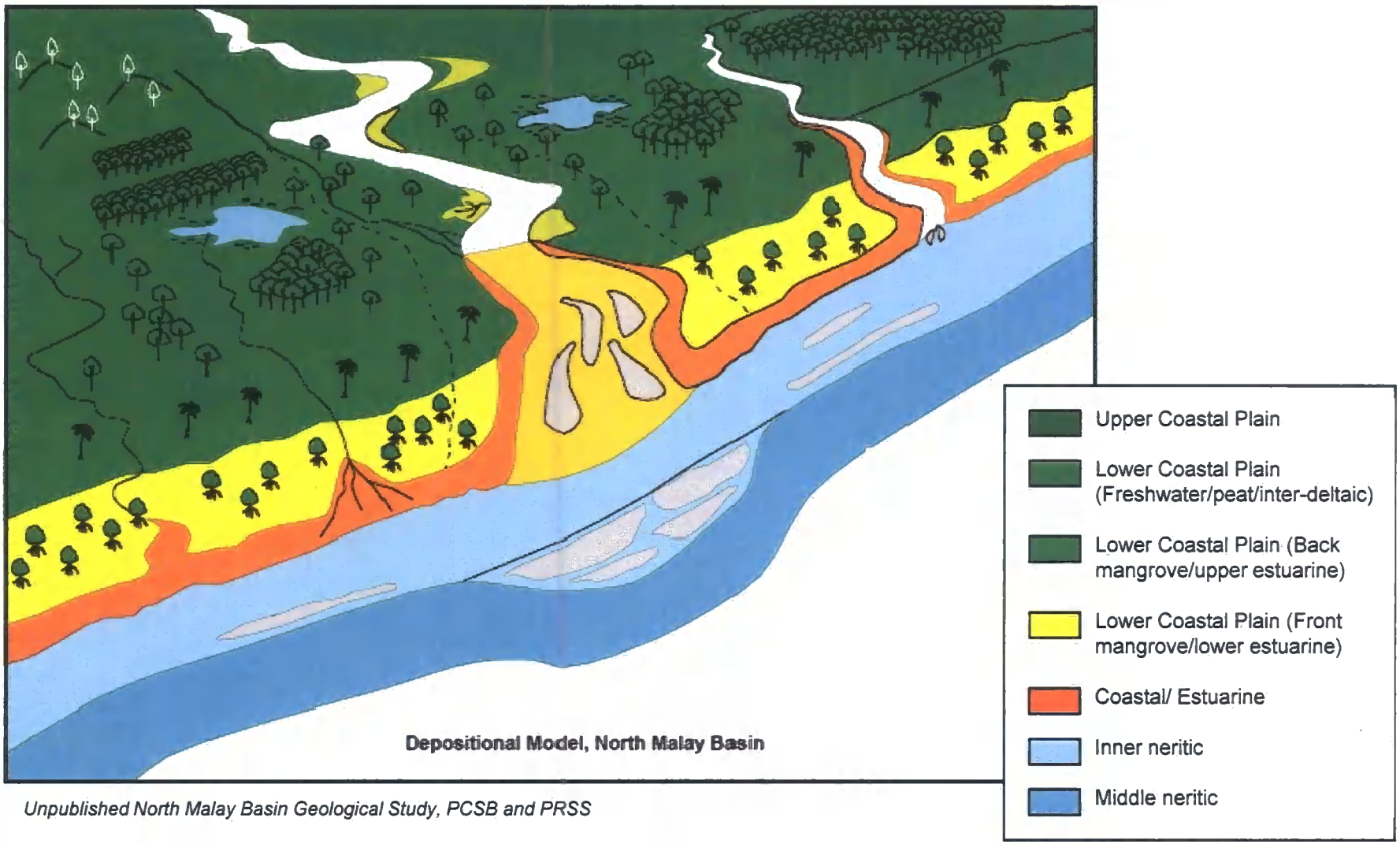

Unpublished North Malay Basin Geological Study, PCSB and PRSS

Attachment 8 Block diagram of Depositional Environment adapted in Malay Basin (Upper coastal plain, lacustrine setting)

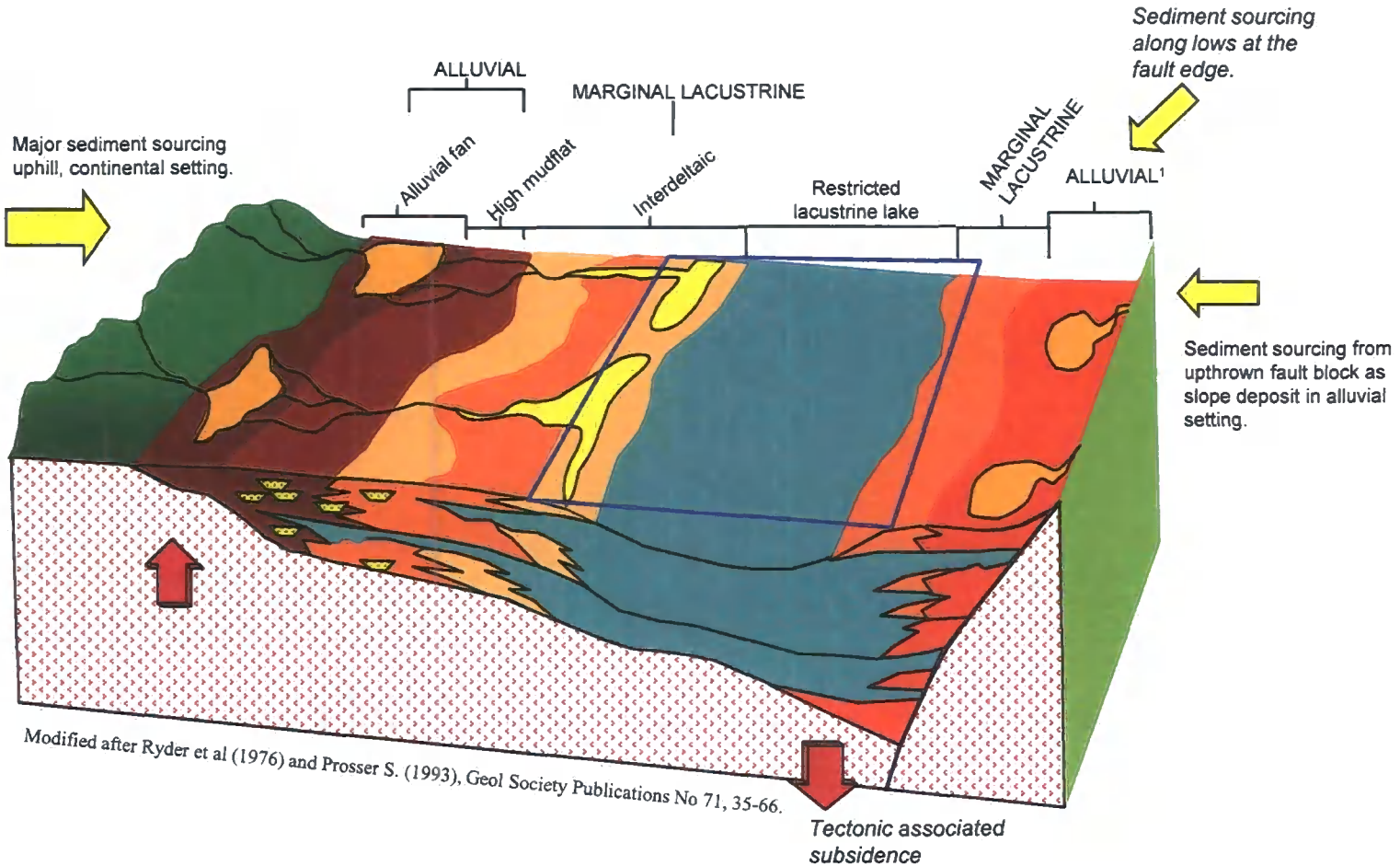

Attachment 9 Isochore maps of Miocene intervals over Tenggol Arch

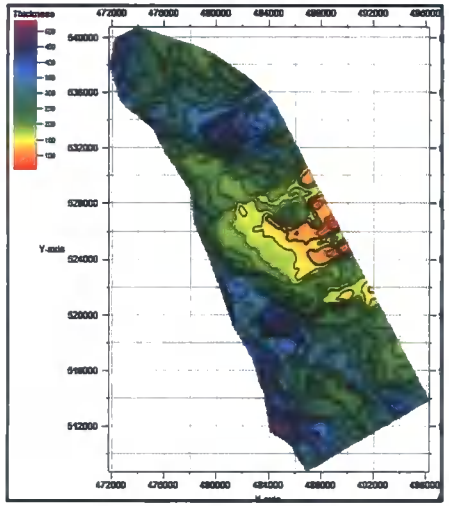

a) Sequence Ta_6 (Lower Early Miocene)

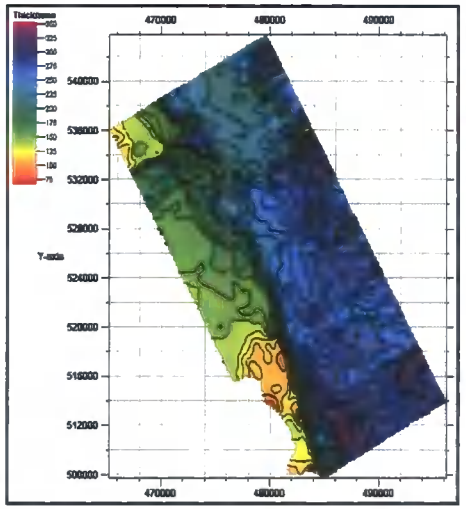

b) Sequence Ta_5 (Upper Early Miocene)

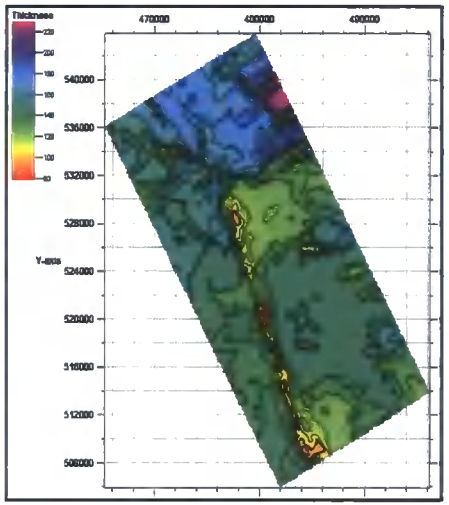

c) Sequence Ta_4 (Middle Miocene)

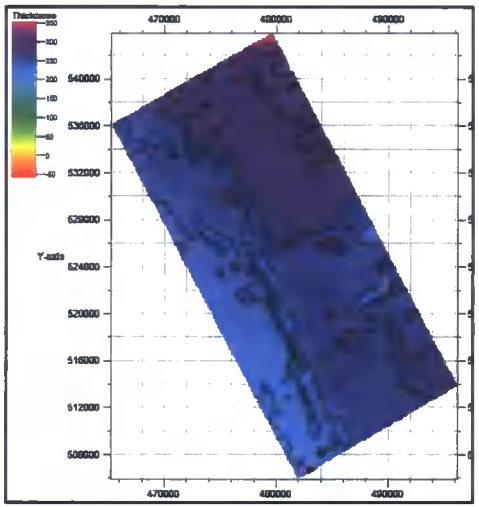

d) Sequence Ta_3 (Middle Late Miocene)

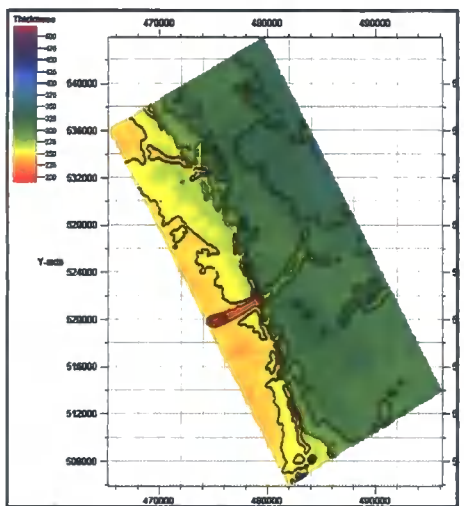

e) Sequence Ta_2 (Late Miocene-Pliocene)

Isochore maps from Lower Early Miocene to Late Miocene/Pliocene shows how sediment thickness varies on Tenggol Arch over Miocene interval. This variation in sediment thickness are related to paleo topography of Tenggol Arch during Miocene interval.

Lower Early Miocene (Ta_6) shows sediment deposited in localized sub-basins primarily subsequent to Late Cretaceous/Early Tertiary rifting on Tenggol Arch.

Since Upper E. Miocene (Ta_5), sediment depocentres have gradually changed easterly where fairly uniformed thick sediment deposited on the hanging-wall of Tenggol Fault zone. Sediment depocenters has gradually changed to north-northeasterly as shown in Ta_4 and Ta_3 levels.

This variations also indicate changes in surface topography of Tenggol Arch during Miocene intervals. Interpretation of these observation was, early deposition of Early Miocene sediment was controlled by early basement structure. Basin flooding, which was related to marine incursion (Early Miocene) caused sediment depocentres concentrating eastwardly on hanging-wall of Tenggol Fault zone. Since Middle Miocene, south of Tenggol Arch has been uplifted, generally the basin was tilted to the north forcing sediment deposited northerly.

Seismic Facies interpretation of Ta_6 sequence along Inline 5369

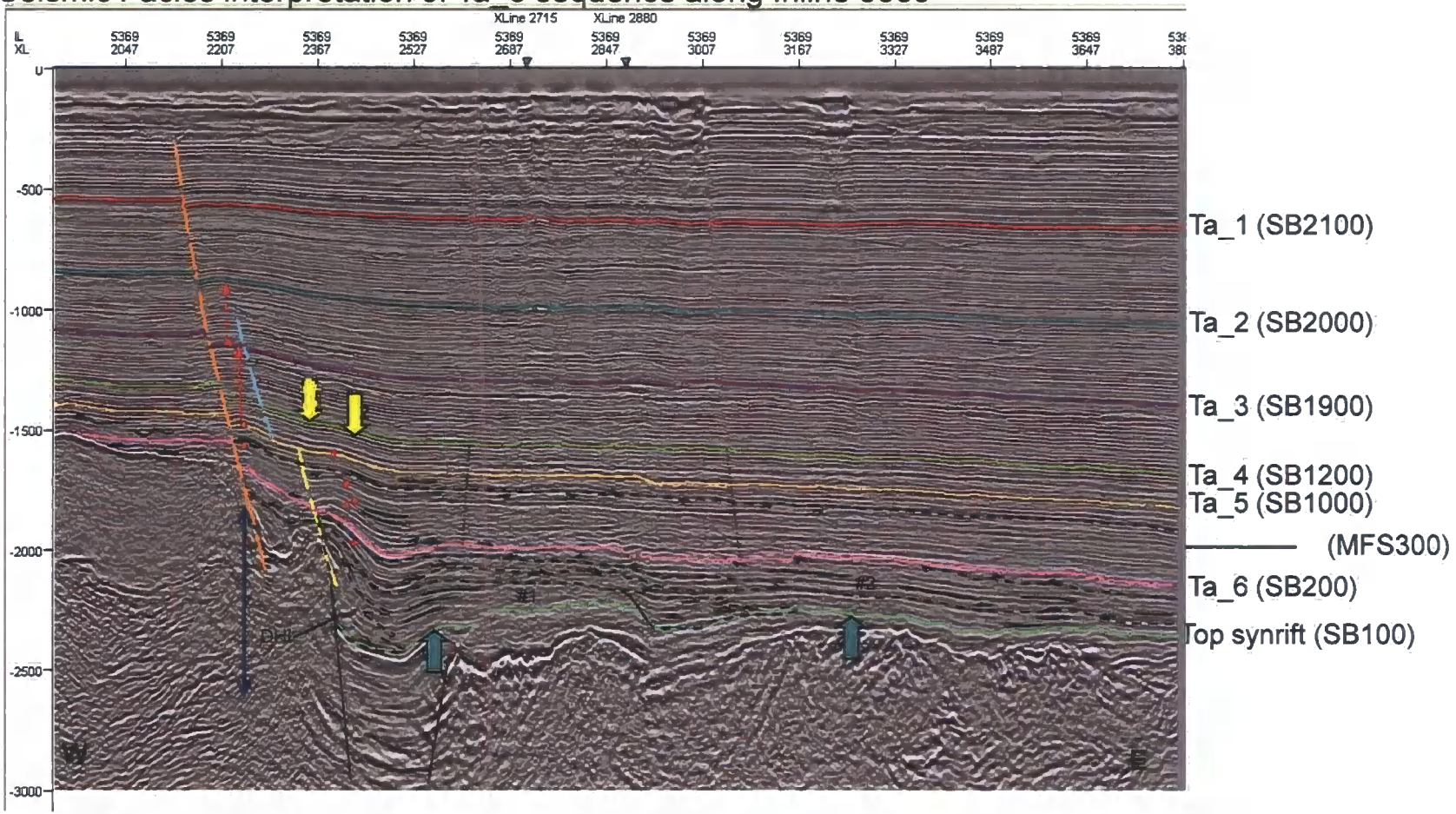

Attachment 10 U-shaped synclinal geometry from top basement top Ta_6 (blue arrow) resultant of sediment sagging which continues occurred during synrift until Ta_6. From basin shape and seismic features, sediment sagging occurred in association with syn-depositional of synrift and Ta_6 sediment in the sub-basin. This interpretation can be demonstrated in a simple sketch model (next figure). Sediment sagging in the sub-basins terminates during Lower E. Miocene (Ta_6) and does not occur again at younger stage on Tenggol Arc, sediment depo-centers of younger intervals shifted to present-day basin centre (East and northeast), sediment sagging should take place in basin center at younger stage as observed by EPIC, 1994. Synrift and Lower Early Miocene sediment depo-centers are in localized sub-basins on west basin margin.

Seismic Facies interpretation of Ta_6 sequence along Inline 5369

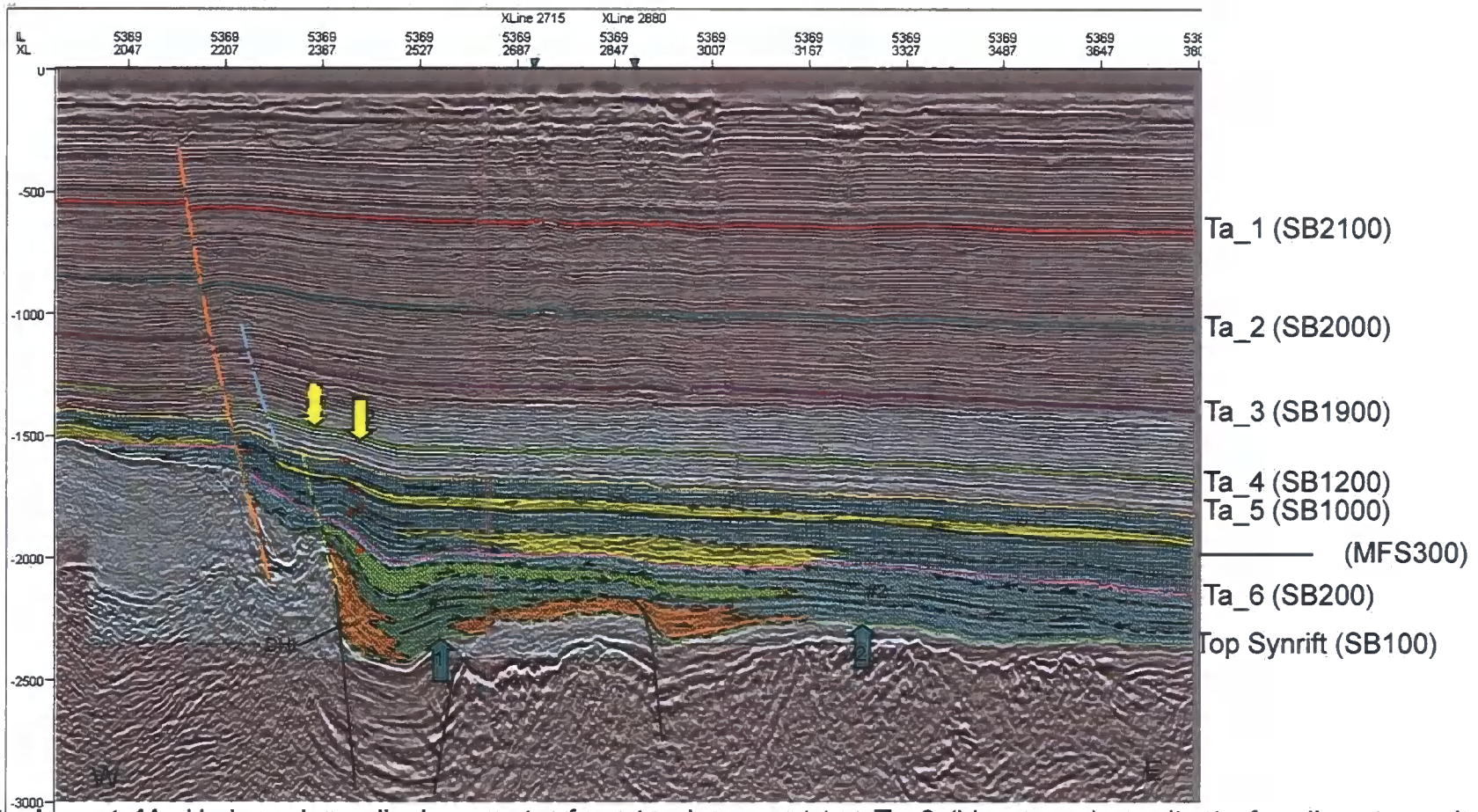

Attachment 11 U-shaped synclinal geometry from top basement top Ta_6 (blue arrow) resultant of sediment sagging which continues occurred during synrift until Ta_6. From basin shape and seismic features, sediment sagging occurred in association with syn-depositional of synrift and Ta_6 sediment in the sub-basin. This interpretation can be demonstrated in a simple sketch model (next figure). Sediment sagging in the sub-basins terminates during Lower E. Miocene (Ta_6) and does not occur again at younger stage on Tenggol Arc, sediment depo-centers of younger intervals shifted to present-day basin centre (East and northeast), sediment sagging should take place in basin center at younger stage as observed by EPIC, 1994. Synrift and Lower Early Miocene sediment depocenters are in localized sub-basins on west basin margin.

Attachment 12

Top Basement Structure Map

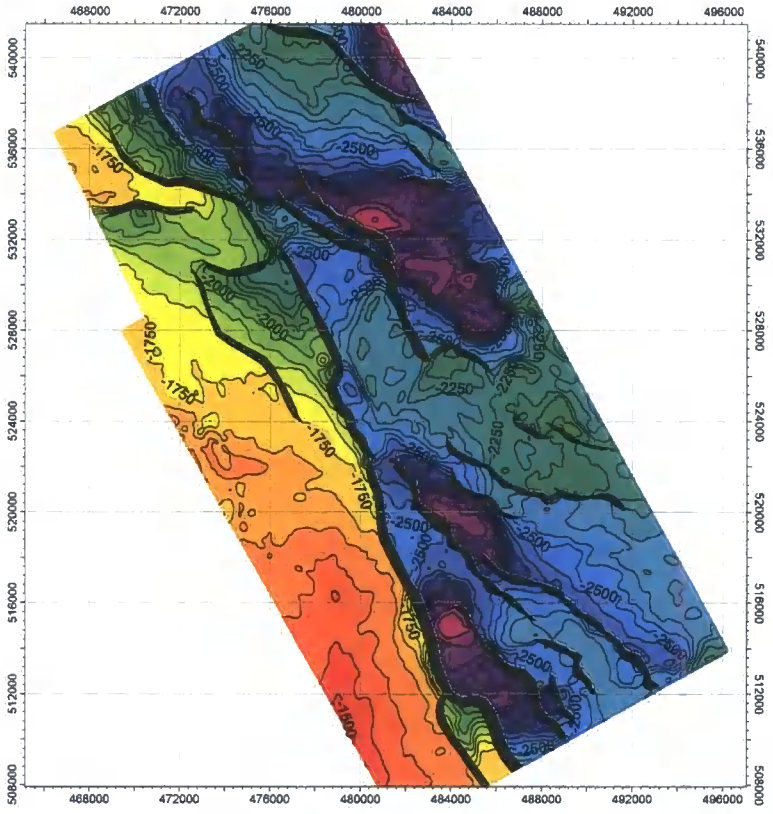

Top Syn-rift Structure Map

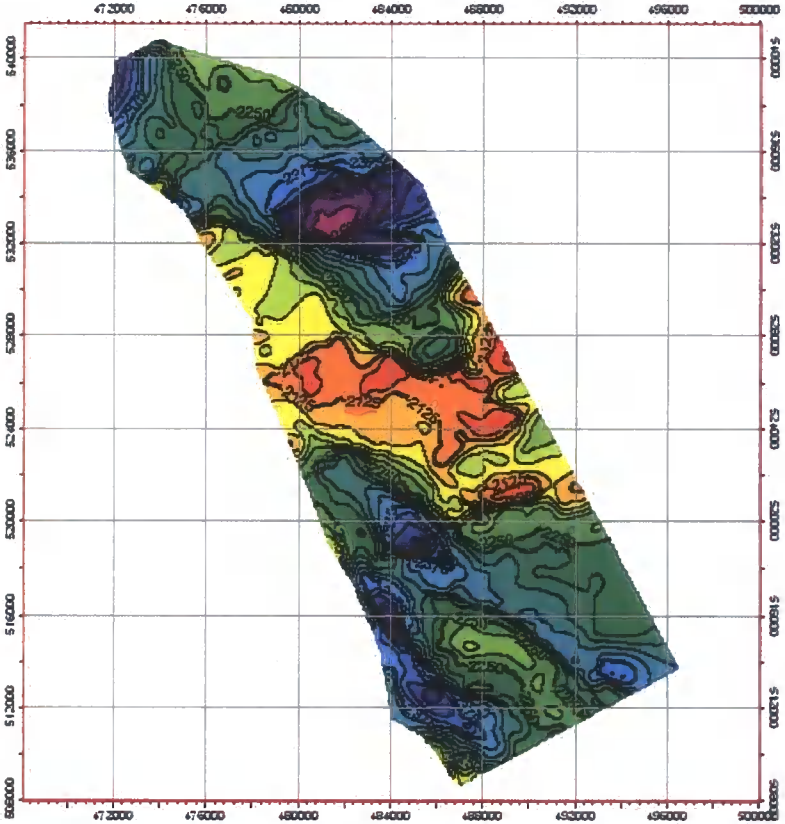

Attachment 13

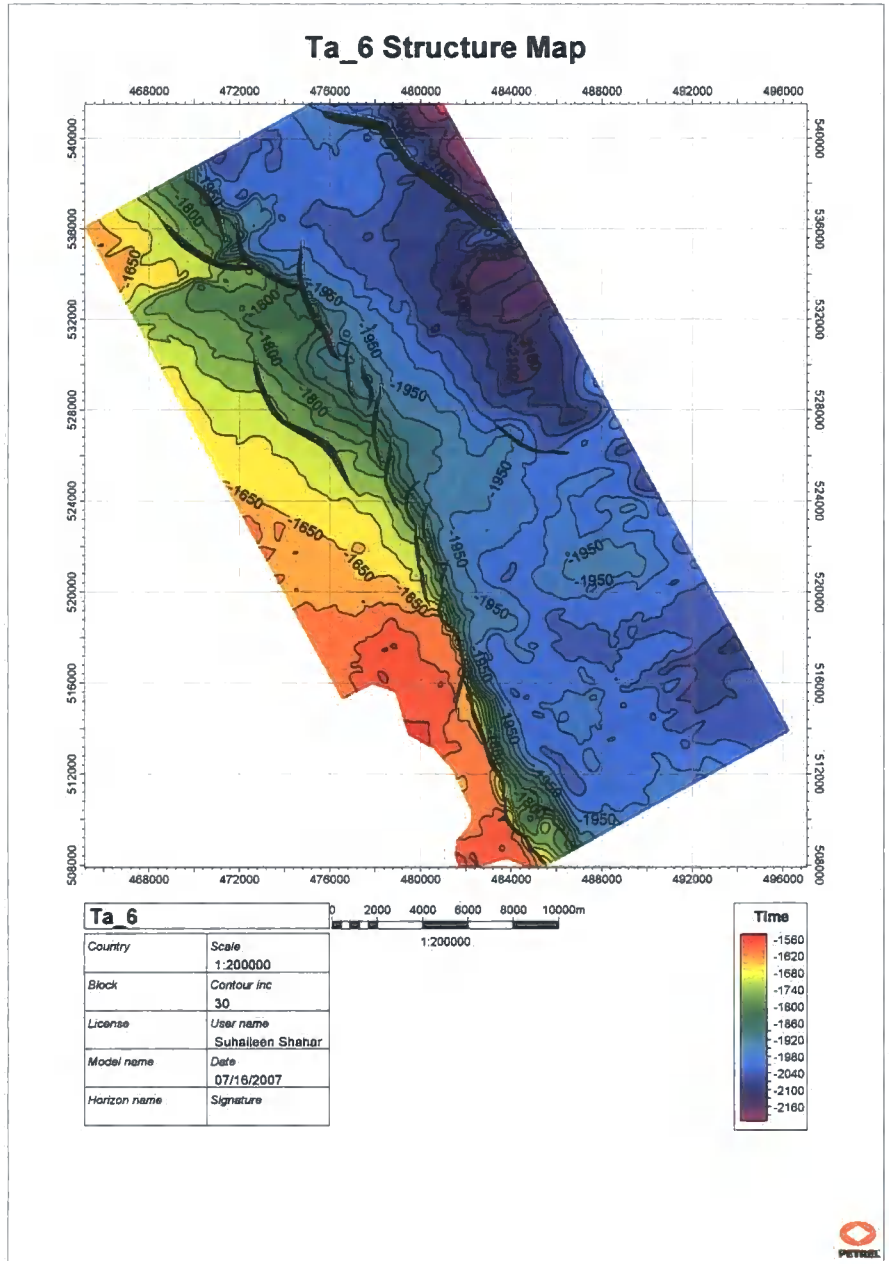

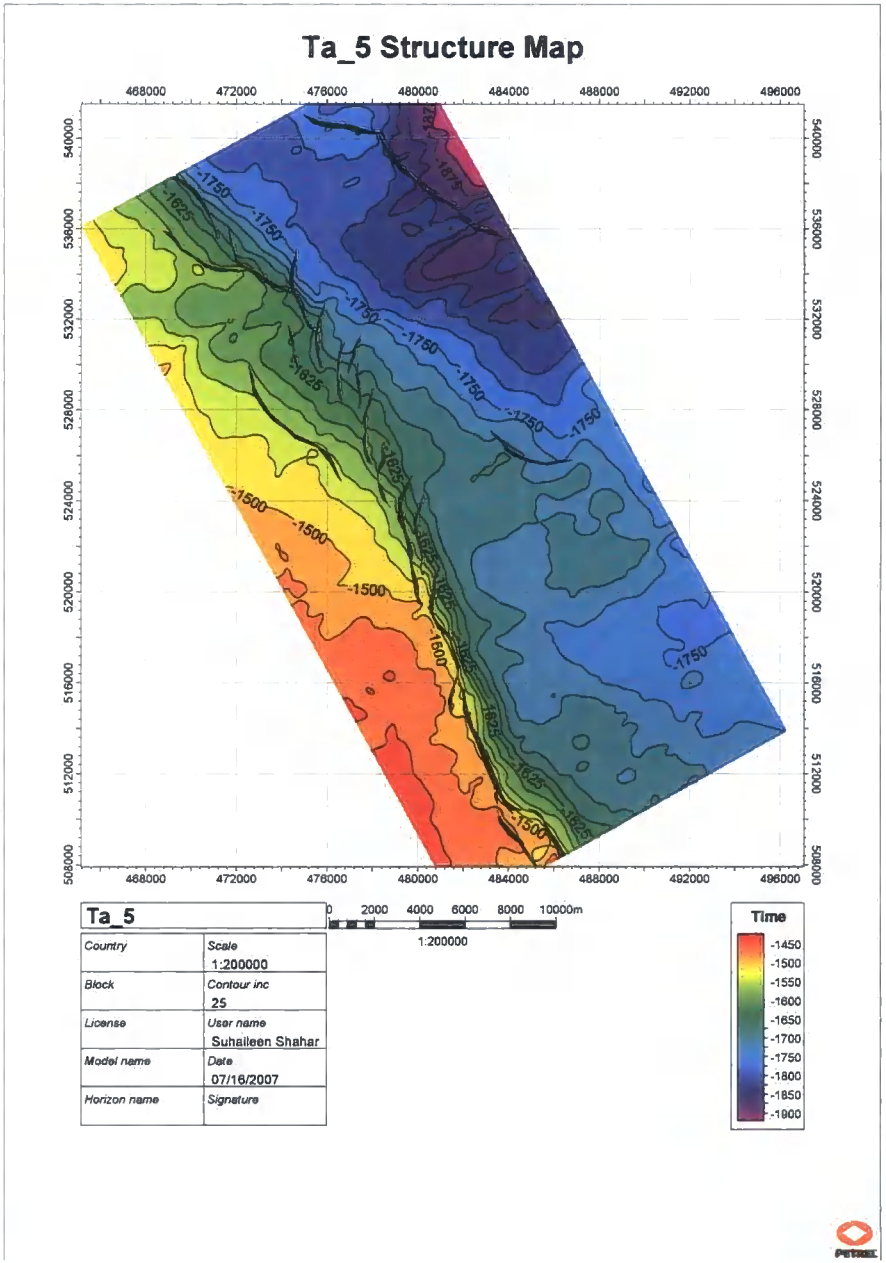

Attachment 14

a)

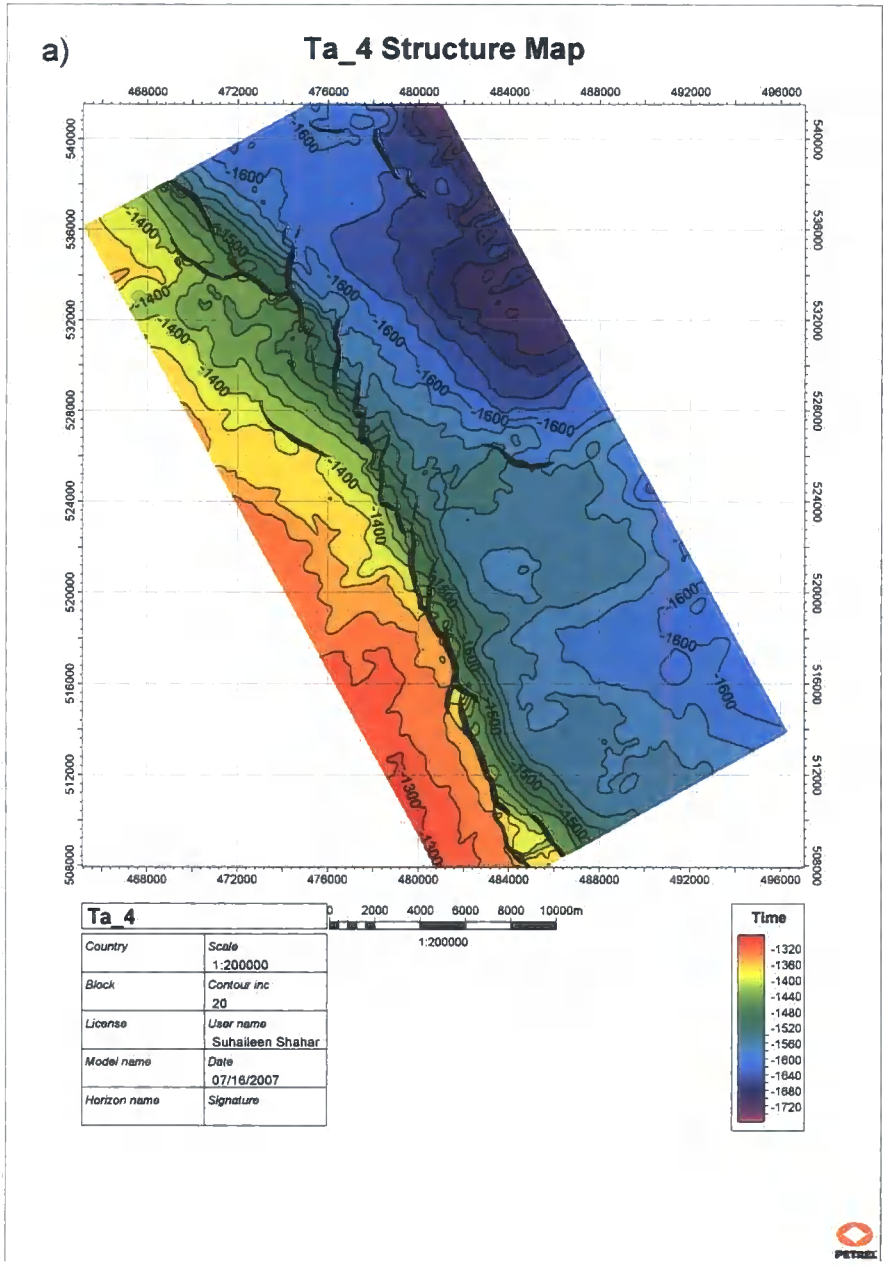

b)

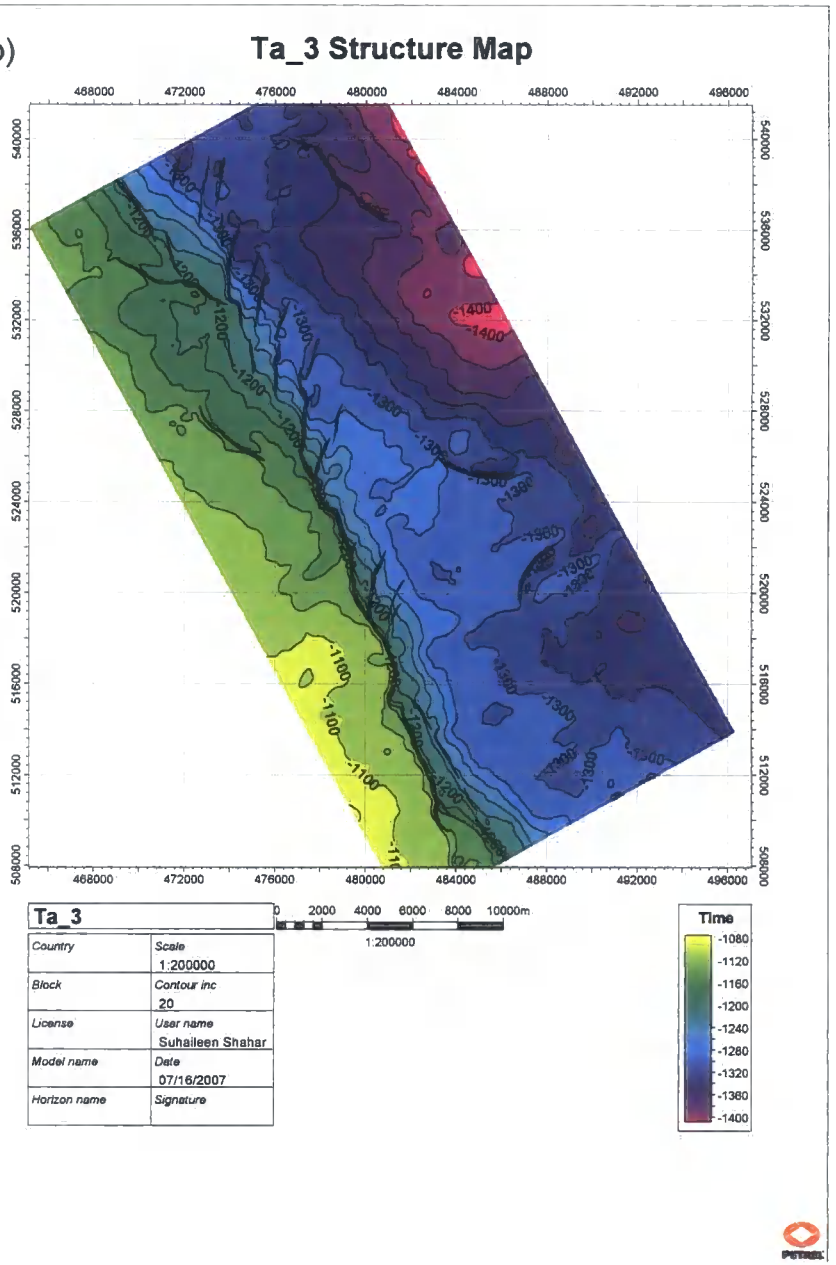

Attachment 15

a)

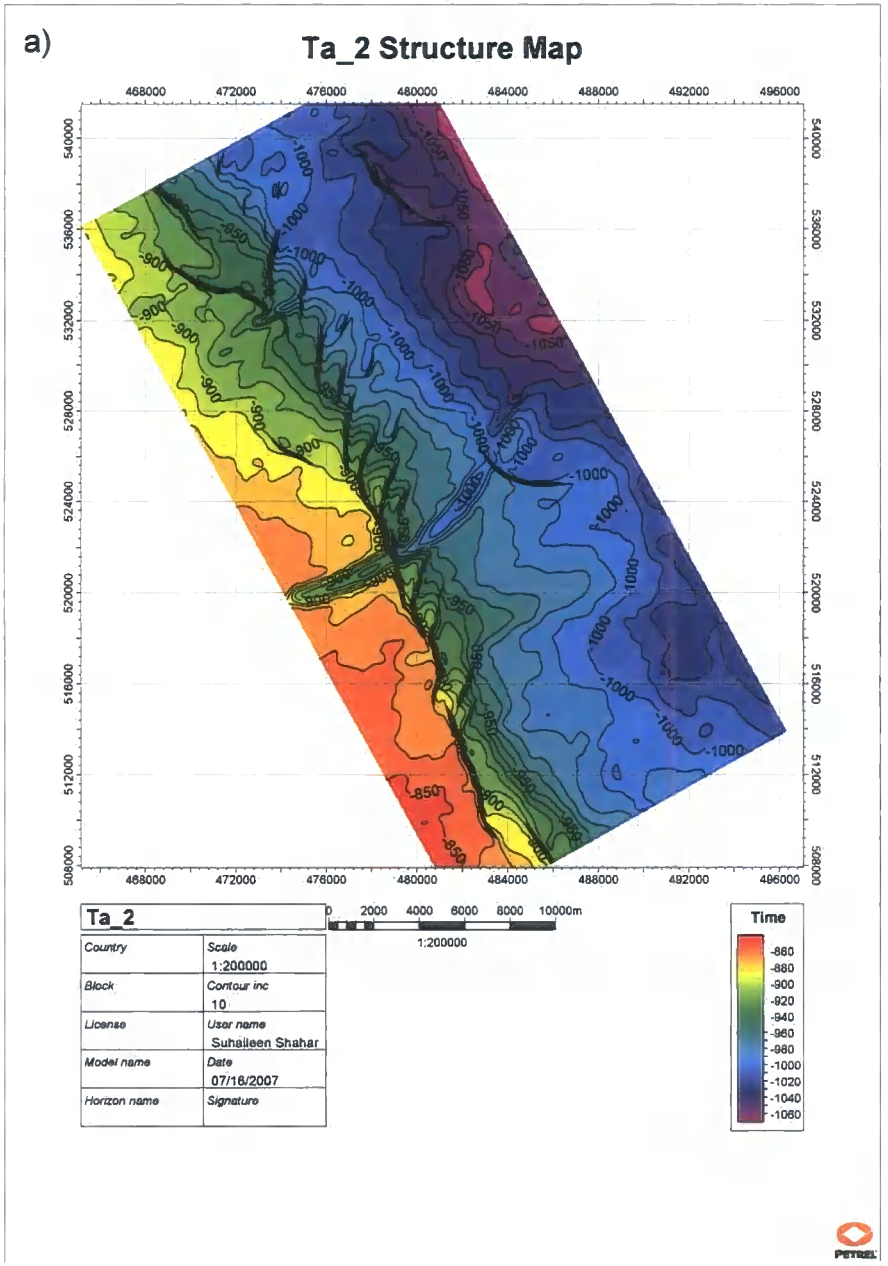

b)

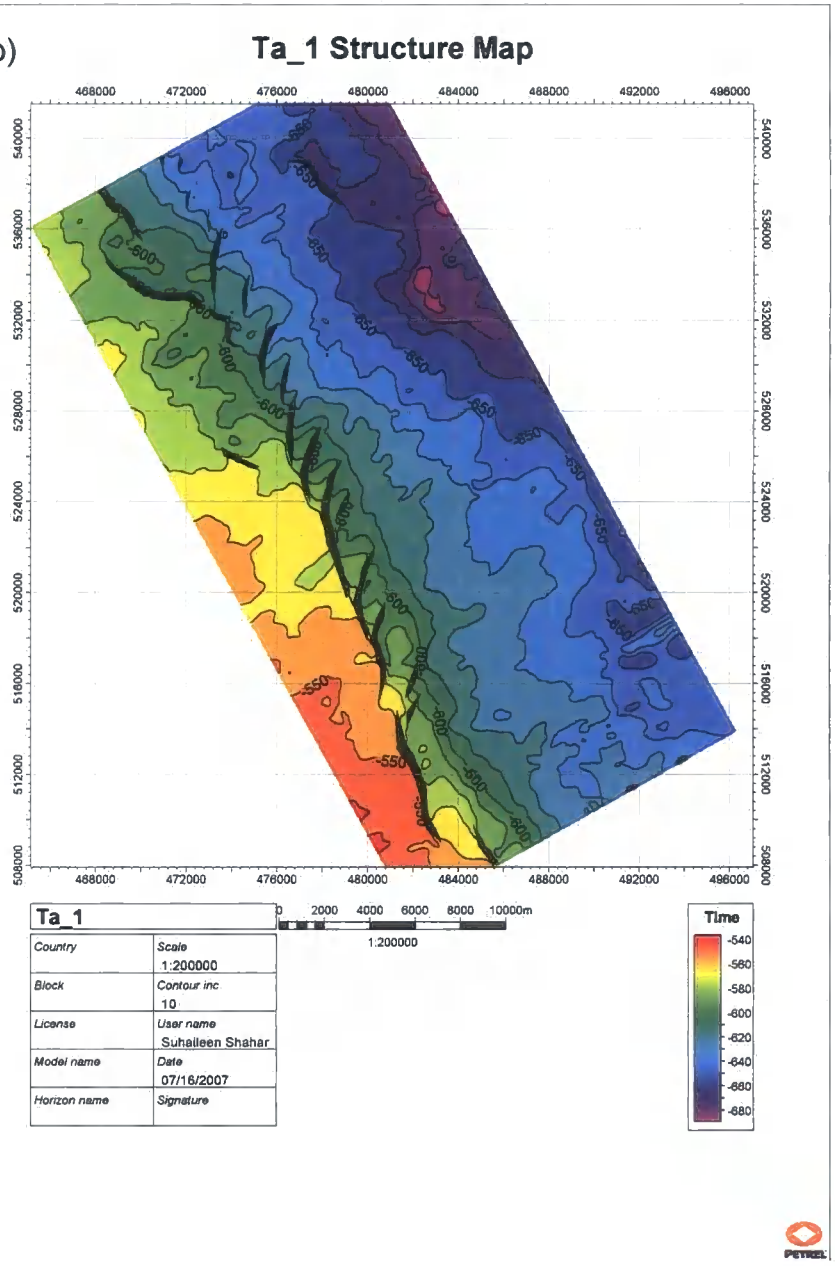

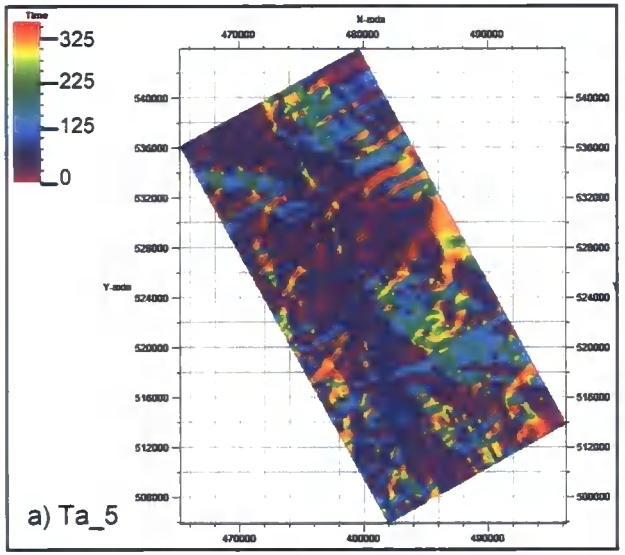

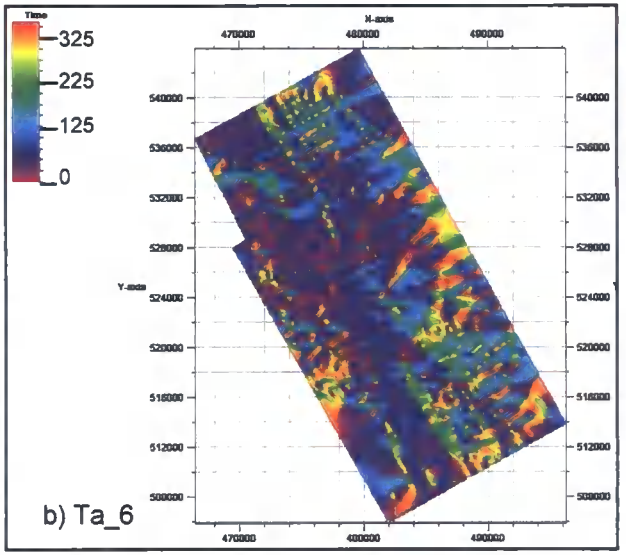

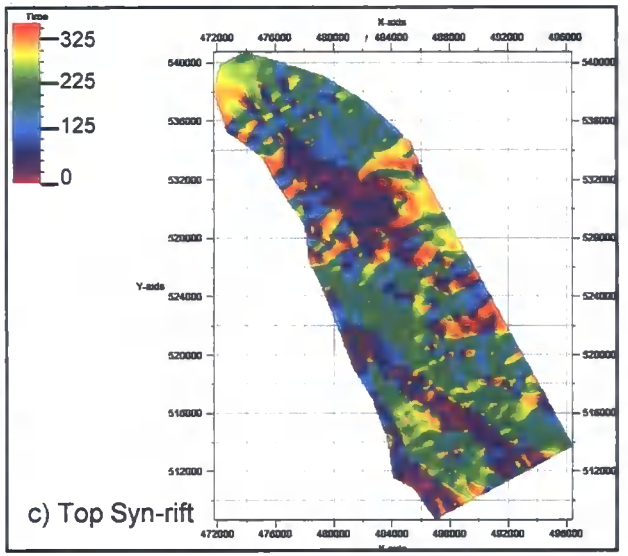

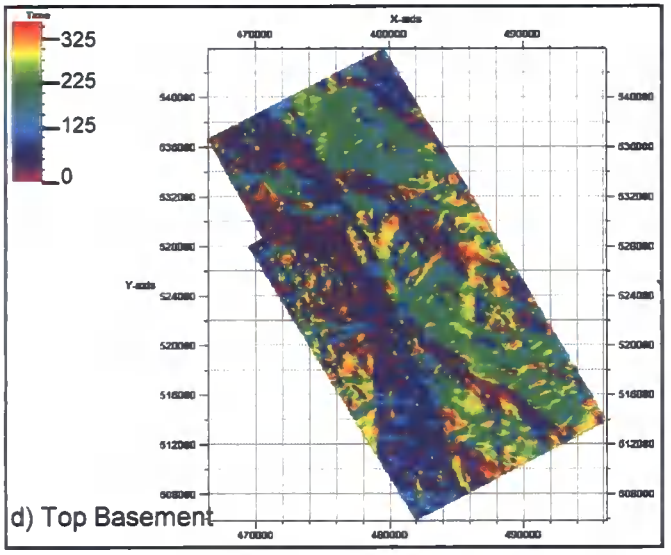

Notes: All azimuth values are apparent values, manipulated from gridding of time horizons.

Attachment 16 show azimuth maps generated along present-day surface of (a) Ta_5, (b) Ta_6, (c) top syn-rift and (d) top basement seismic markers. N-NE dipping surface indicates by magenta, E-SE indicates by light blue and Southerly dipping surface indicates by light green. In general surface topography on Tenggol Arch shows N-NE dipping within Early Miocene strata. Surface topography along (c) top syn-rift and (d) top basement are generally dipping E-SE on the hanging-wall of downthrown block while foot-wall of upthrown block is generally dipping N-NE. The azimuth maps generally illustrates present-day structure trends on each surfaces, where on top basement and top syn-rift show predominantly NNW and NW trending structures. Azimuth maps of Early Miocene strata (Ta_5/Ta_6) hardly show any strong structure trends except slight N-NE trends south of study area (a and b).

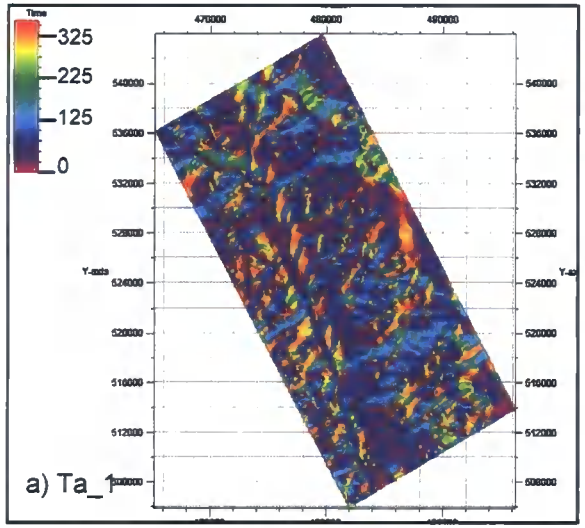

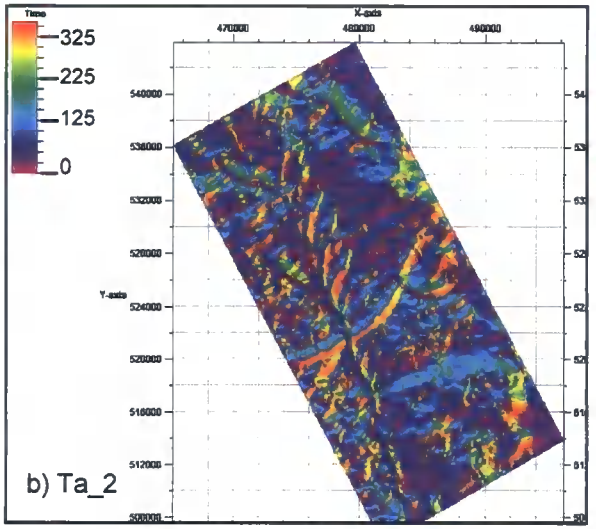

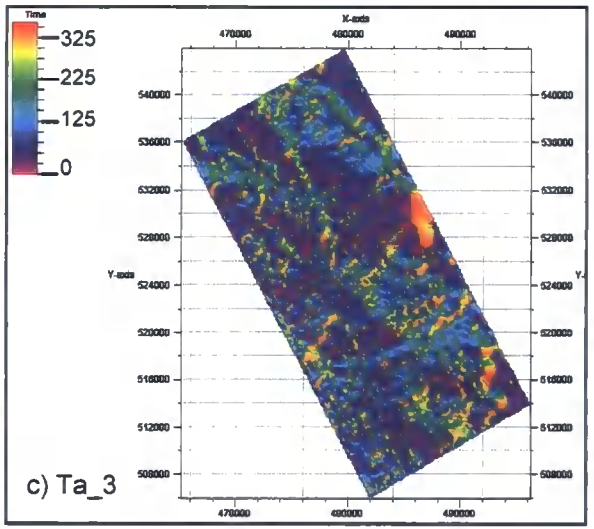

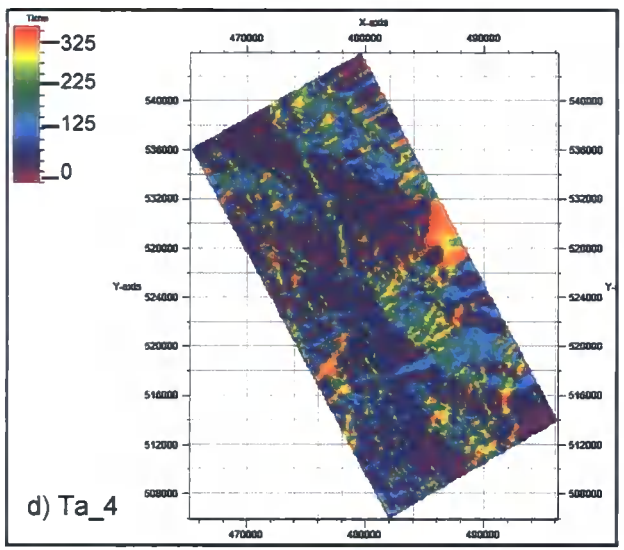

Notes: All azimuth values are apparent values, manipulated from gridding of time horizons.

Attachment 17 show azimuth maps along (a)Ta_1, (b)Ta_2, (c)Ta_3 and (d)Ta_4 represents Middle Miocene to Pliocene age present-day surface topography. In general, surface topography of Miocene strata (Ta_4/Ta_3) dipping E-SE. Pliocene strata (Ta_2/Ta_1) shows generally N-NE dipping surface. General structure trends observed at (b) Ta_2/ (a)Ta_1 (Pliocene) shows NNE structures in NNW trending en-echelon arrangement. (c) Ta_3 and (d)Ta_4 show fairly presence of similar NNE structures as shallow section.

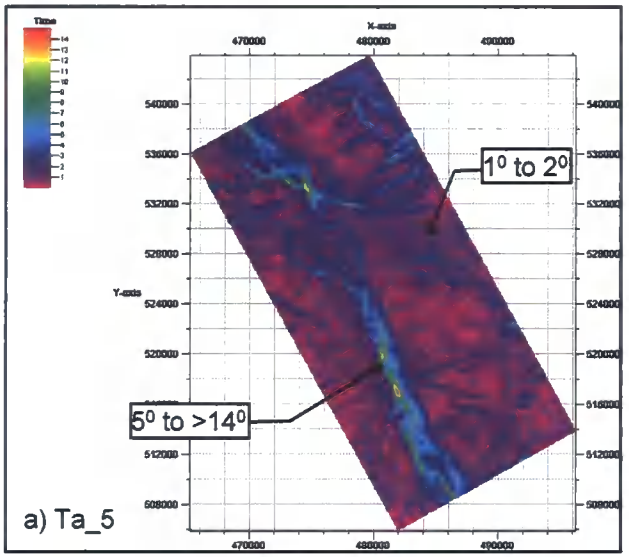

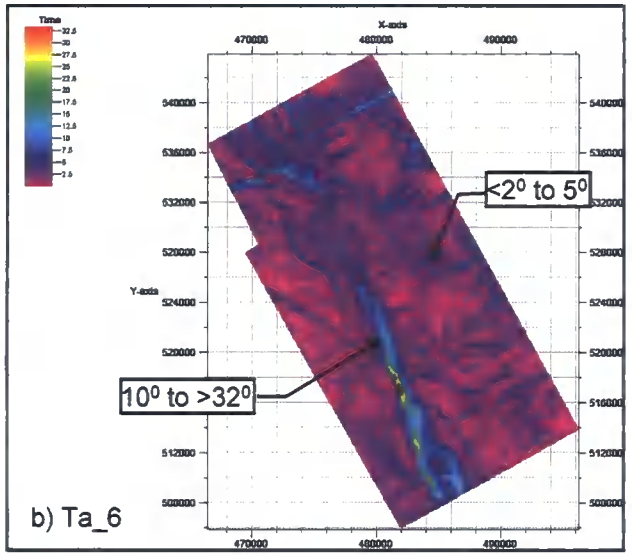

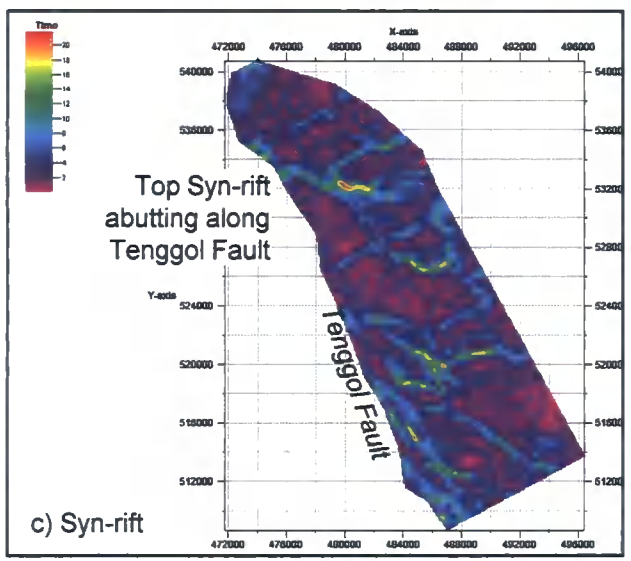

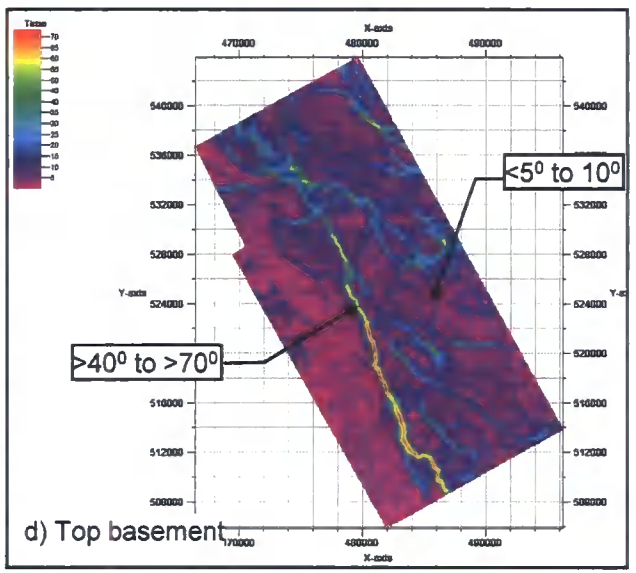

Attachment 18 show dip maps of Early Miocene (a) Ta_5, (b) Ta_6 and (c) top syn-rift and (d) top basement. The dip maps clearly highlights fault pattern corresponds to each surface. Steeply dipping faults are represents by yellow and red attributes and gentle dipping faults represents by light blue attribute. Though dip maps generally highlights faults patterns due to distinct changes in surface dips, however some lineaments does not corresponds to fault traces. Hence, dip maps were utilized as reference to improve some fault trace mapping on time-slices or seismic sections.

Notes: All dips are apparent dips manipulated from gridding of time horizons.

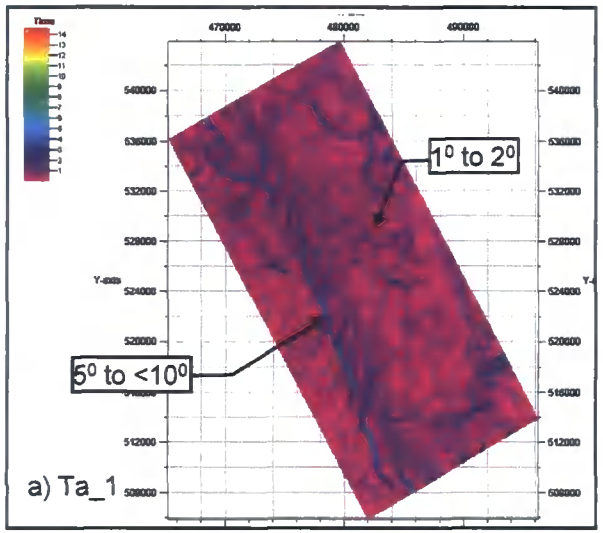

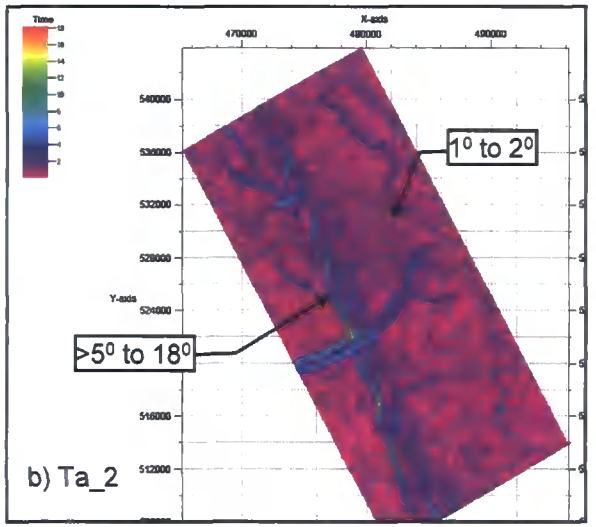

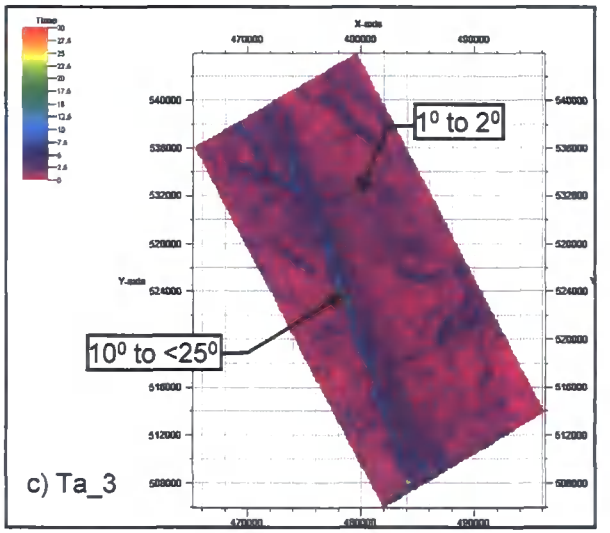

Notes: All dips are apparent dips manipulated from gridding of time horizons.

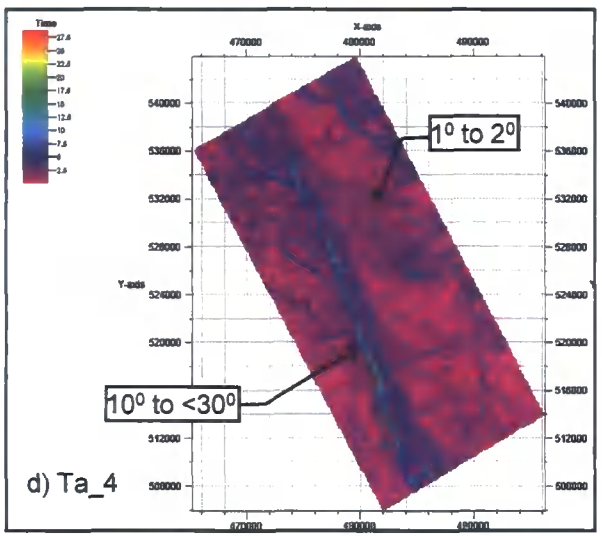

Attachment 19 shows dip maps of Middle Miocene/Late Miocene (Ta_4/Ta_3) and Pliocene (Ta_2/Ta_1) strata. Dip maps of these two strata clearly corresponds to fault pattern on the markers. All surfaces show predominantly N-NE striking faults in en-echelon arrangement which corresponds to N-NW trending major Tenggol Fault. The N_NE striking en-echelon faults are interpreted as repercussion of strike-slip movement along major Tenggol Fault most likely during Late Miocene. During Pliocene, faults on Tenggol Arch has reactivated where normal fault displacements are prevalent along pre-existing N-NE faults. This reactivation has further accentuated faults at Ta_2 (Lower/Upper Pliocene). Most faults continue until Ta_1 and dies-out 50 to 100ms above Ta_1 surface.

Attachment 20 Structure Chronology of Tenggol Arch

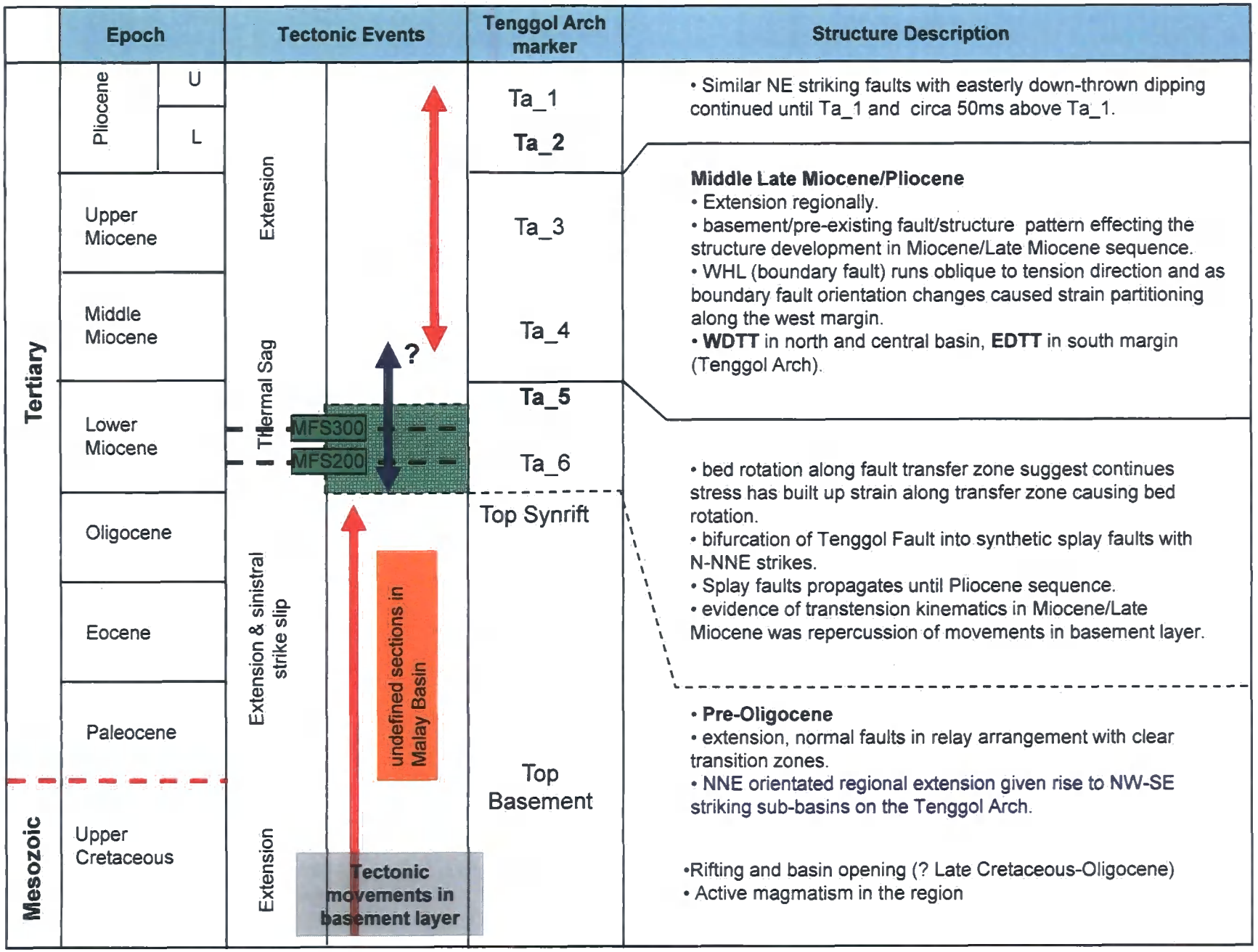

Attachment 21 Facies interpretation based on gamma-ray log pattern

Sedimentary facies and depositional setting	Gamma-ray log pattern	Sedimentary facies and depositional setting	Gamma-ray log pattern
	Funnel-shaped	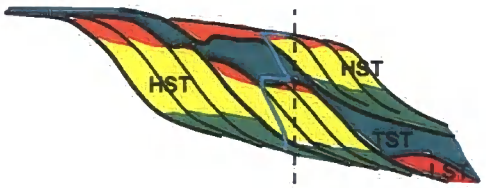	Stacked funnel-shaped
Fluvial coastal-marginal marine, progradational deltaic facies.		Coastal fluvial – marginal marine, deltaic facies.	
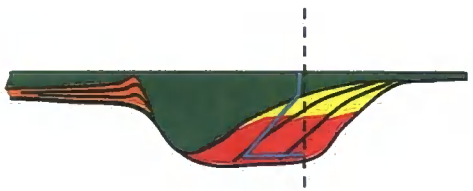	Bell-shaped	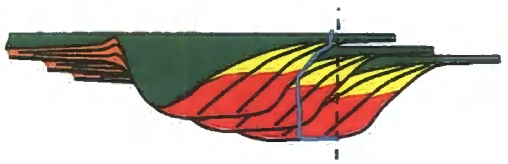	Blocky-shaped
Coastal plains fluvial system, channel with sandy point-bars facies.		Upper coastal fluvial, fluvial system of amalgamated channel facies.	
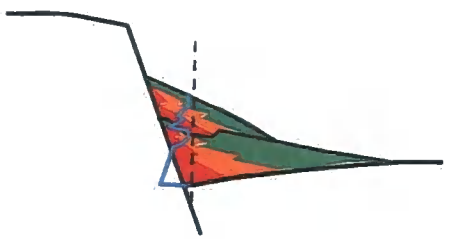	Serrated and cusped-shape	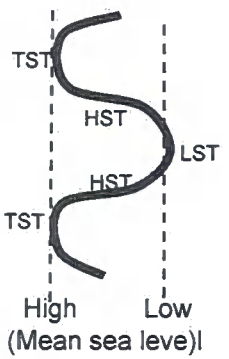	Single sinusoidal eustatic cycle illustrates condition for lowstand system tract (LST), highstand system tract (HST) and transgressive system tract (TST).
Slope deposition, upper coastal plain, alluvial plain facies.			

Attachment 22 sequence stratigraphy concept adapted in this study

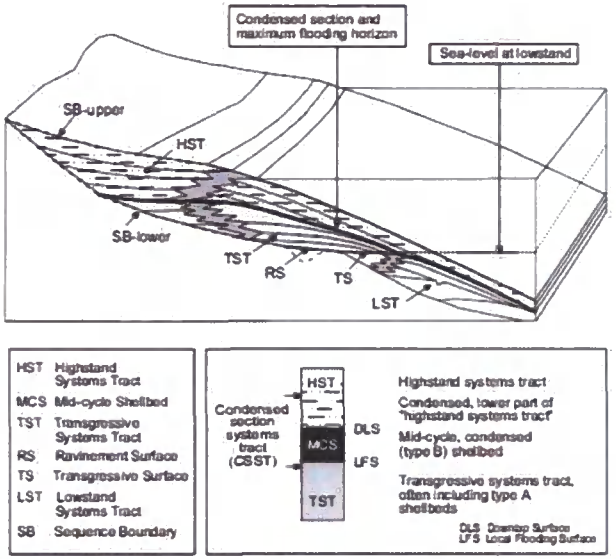

Fig. 1. The conventional sequence stratigraphic model at seismic scale (after Vail et al., 1991), which recognizes a mid-cycle condensed section and maximum flooding surface (= maximum flooding horizon). Inset (bottom right): outcrop scale summary of the mid-cycle condensed section, after Pleistocene examples described by Abbott and Carter (1994).

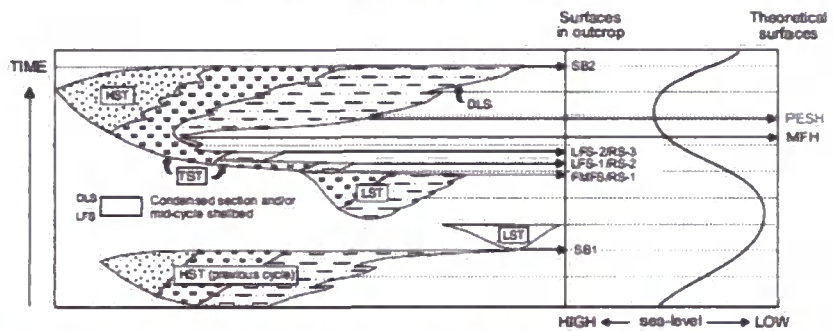

Time-stratigraphic diagram of a sequence deposited during a single sinusoidal eustatic sea-level cycle. Note the *diachronous nature* of the major surfaces which provide the physical stratigraphic framework in each vertical section: the sequence boundaries (SB1, SB2), ravinement surfaces (RS1–3) and first marine and local flooding surfaces (FFS and LFS1–2), and downlap surfaces (DLS). In contrast, the maximum flooding horizon (MFH) and peak eustatic sea-level horizon (PESH) are *theoretical isochronous surfaces* which correspond, respectively, to the level of maximum landward advance of the shoreline and to the peak of the sea-level curve. Particular local flooding surfaces pass into ravinement surfaces near the basin margin.

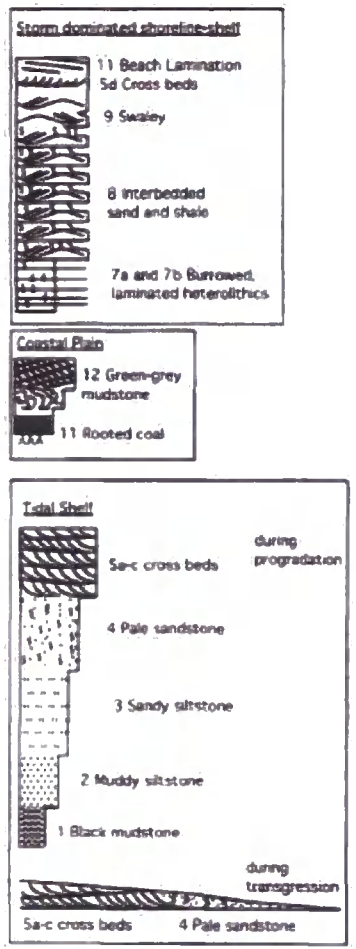

Figure 4 Symbols used to represent facies (1–12) and facies associations on the graphic logs shown in *Figures 6–9*

Attachment 23 Approximate well locations along the Tenggol Fault. Some of these wells are characterised by the intermittent presence of hydrocarbon shows in basement or deepest strata overlying the basement complex.

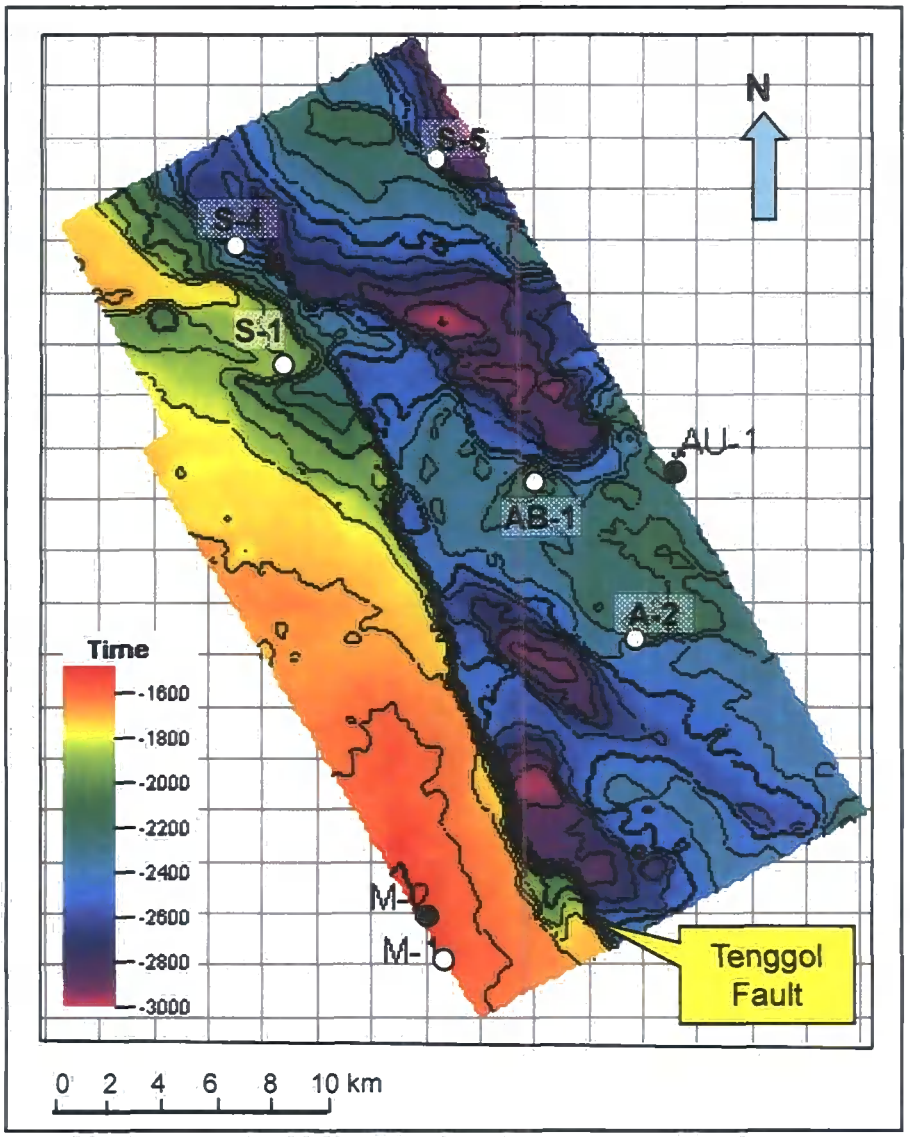

○ Dry in basement or strata overlain the basement

● Oil in basement or strata overlain the basement

Appendix 1

Malay Basin Chronostratigraphic Chart

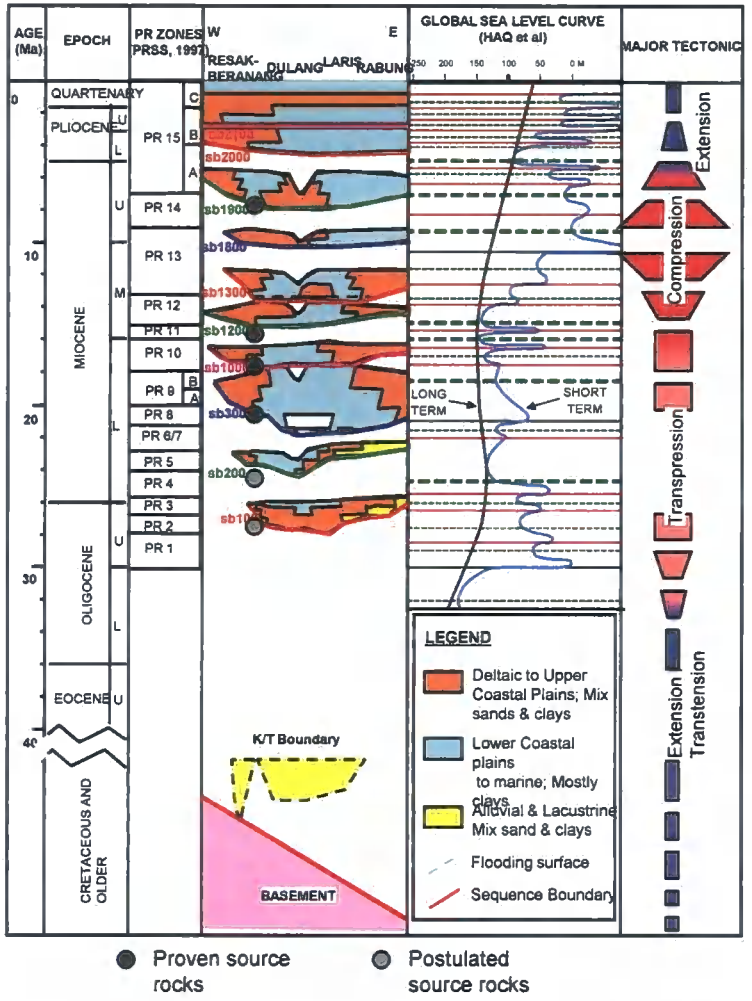

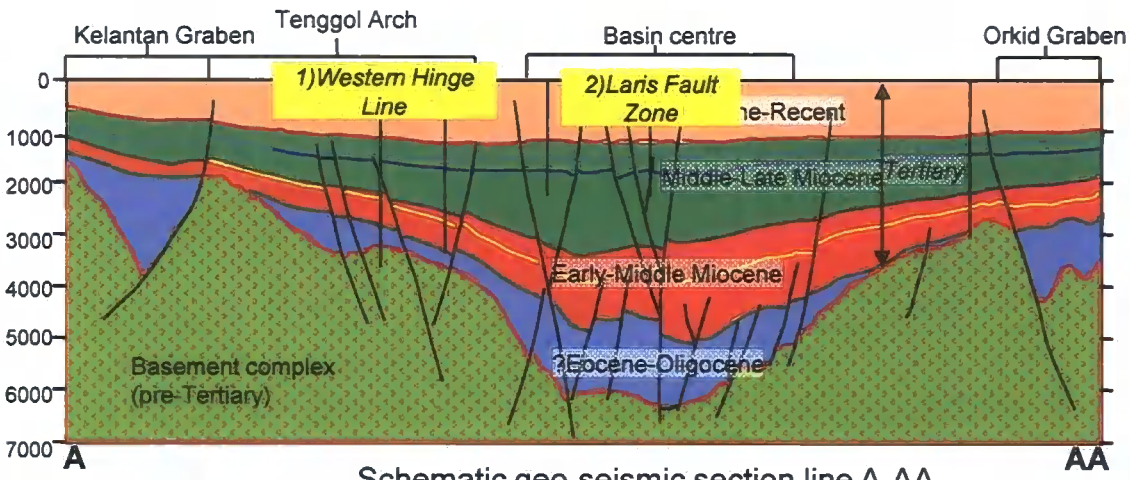

Schematic geo-seismic section line A-AA

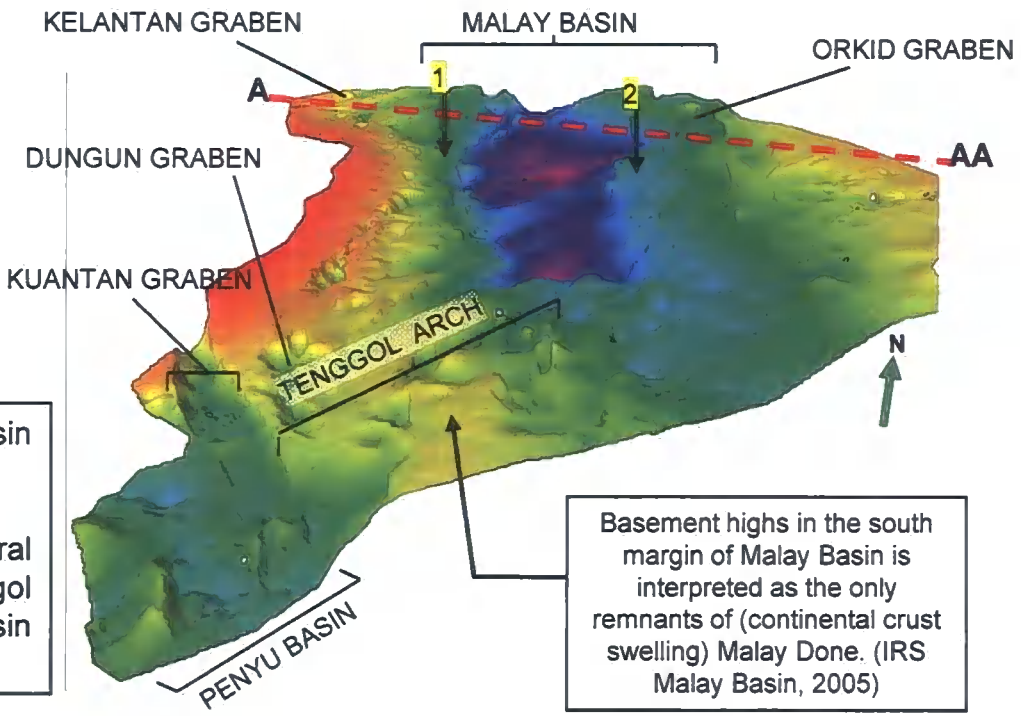

3d grid surface of Top Basement showing Malay Basin architecture and surrounding sub-basins.

Schematic geo-seismic section A-AA shows general stratigraphic scheme of the basin across Tenggol Arch/Terengganu Platform and basin centre. The basin comprises of mainly Middle to Late Tertiary sediment.

Basement highs in the south margin of Malay Basin is interpreted as the only remnants of (continental crust swelling) Malay Done. (IRS Malay Basin, 2005)

Integrated Regional Study of Malay Basin, PCSB 2005

Facies Interpretation of Late Miocene to Early Tertiary (Paleogene) sequence of Malay Basin

Appendix 2

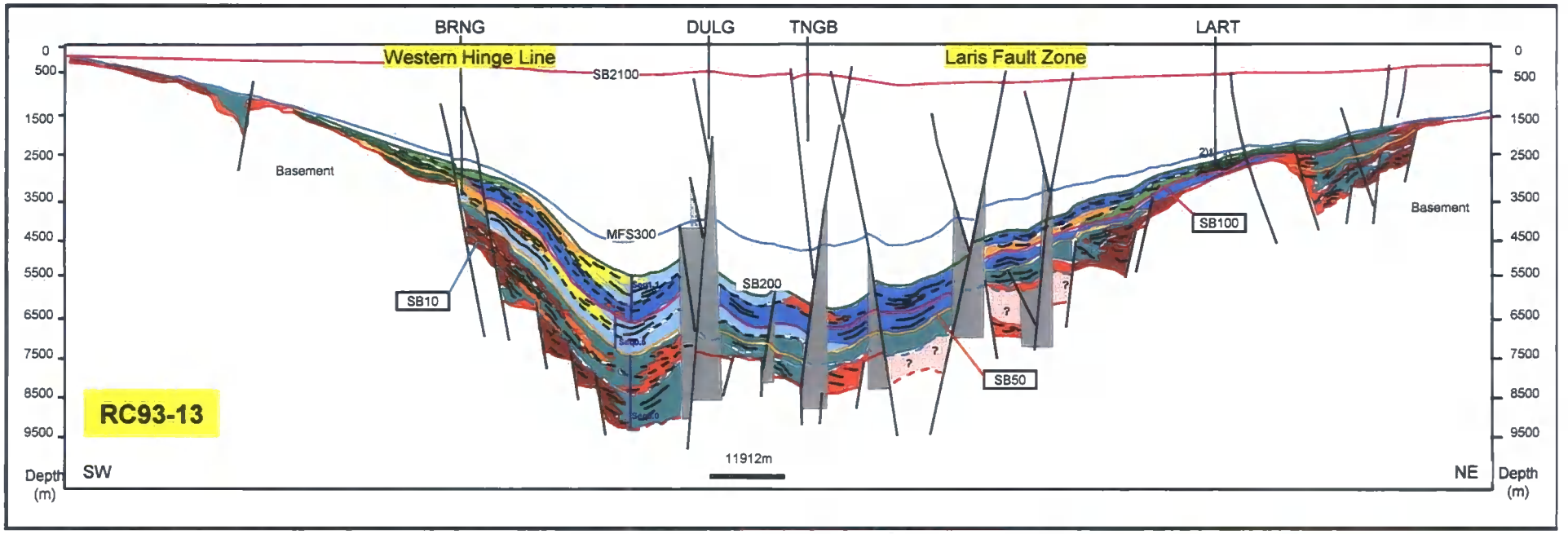

Description of seismic facies shown above are included in Appendix 3a (1/2) and (2/2)

Seismic Basemap

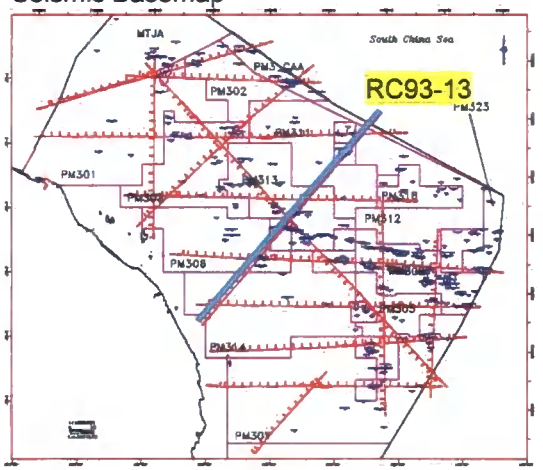

Seismic basemap above show location of 2D regional seismic RC93-13

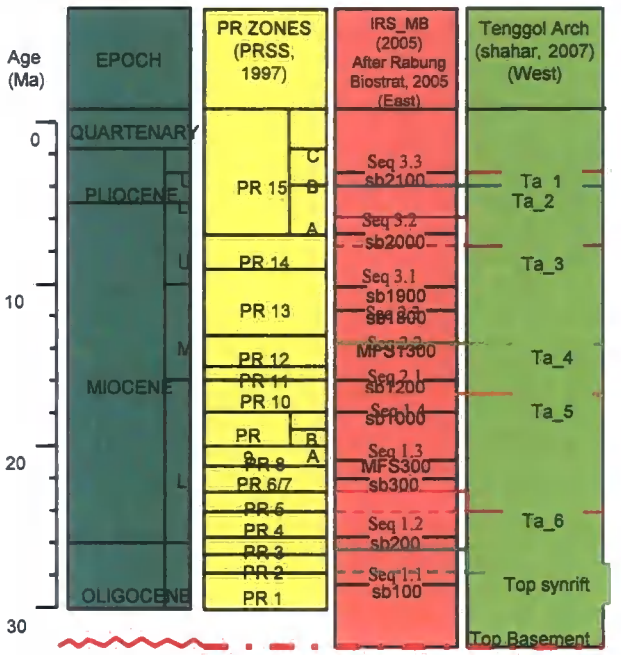

Seismic Facies Description	Interpreted Facies	Interpreted EOD	Remarks
 High amplitude, low frequency discontinues reflector, slightly wavy reflector.	Fluvial system, consists of channel and splay system with interlays of flood plain sediments with high calcareous and carbonaceous content.	Upper coastal plain (UCP), possibly related to slope deposition and associated with restricted lacustrine setting.	**West Belumut-1 and Belumut 1&2** Data: GR/Res/SP, mud log, paleontology/core study of Belumut 1&2 report. **WBLMT-1:** GR pattern indicates series of funnel shaped, coarsening and thickening upward succession. Sand thickness ranges from 2- 4m. **BLMT-1** (Core#2: 4389-4396 ft) and (Core#3: 4815-4842 ft): Sandstone with festoon cross-bedding, truncated ripples, *random* occurrences of grit and pebbles. Barren. 4140-4690 ft: Sandstone and siltstone interbeds, pyrite and siderite are common and roughly 500ft of interval abundant of *siderite oolites.* **BLMT-2** (Core#1: 3702-3709 ft) and (Core#2: 3732-3739 ft): Sandstone, graded sand medium to fine grained, presence of scour marks with fill units, fining upward succession. 3320-3840 ft:: Interval of abundant *siderite oolites.* *Proposed for proper lithofacies study of available cores to determined the EOD.*
 Medium to low amplitude, medium to low frequency, slightly wavy reflector.	Fluvial system, possible consists of channel and splay system with interlays of flood plain sediments.	?Lower coastal plain (LCP).	***Proposed*** *for interpretation update based on any new deep well(s).* *Data required: logs, core, BHI.* *Analysis required: Sedimentary analysis of logs, core and BHI, palyn/foram lithofacies, biostratigraphy study for facies and EOD interpretation. Additional biostrat study for stratigraphic age.*
 High to medium amplitude, medium to low frequency, occasionally discontinues reflector.	Coastal environment, possible consists of tidal sand and flats or deltaic system.	Coastal (COL) environment. Possible with tidal influence.	**Larut-2 (at level (2))** Data: GR, logs, core photographs and sedimentary report. Core #3 (2033-2046m): No lithofacies study. Core photographs indicates sand and shale sequences with abundant of organic materials. Sandstone appears medium to fine grained with cross lamination. Some intervals show high angle cross lamination and bi-directional dips. ***Proposed*** *for detail lithofacies and core description for existing core data to determined the facies and EOD.*
 Medium to high amplitude, medium to low frequency continues parallel to sub-parallel reflector.	Basin margin or deltaic deposits.	COL to Fluvial Inner Neritic (FIN) environment.	**Beranang 6F-18.1** Data: GR/logs, mud logs, biostrat/palyn study (1984). Ditch cuttings: (3275-3303m) Shale: Black- dark gray, moderate hard – hard, fissile, flaky, elongated, non-calcareous, no carbonaceous. Sandstone: Light gray, light brown, fine – very fine grained, predominantly carbonaceous, weakly calcareous, sub angular- sub rounded translucent grains, moderate visual porosity. Siltstone: Dark brownish gray- dark gray, blocky, moderate hard, calcareous, carbonaceous specks.

Seismic Facies Description	Interpreted Facies	Interpreted EOD	Remarks
 Low amplitude, medium to high frequency, continues parallel to sub-parallel reflector.	Shallow marine or possible large lake system, possible consists of middle fan deposits.	Marginal marine/ Holo-inner neritic (HIN).	***Proposed*** *for interpretation update based on any new deep well(s).* *Data required: logs, core, BHI.* *Analysis required: Sedimentary analysis of logs, core and BHI, palyn/foram lithofacies, biostratigraphy study for facies and EOD interpretation. Additional biostrat study for stratigraphic age.*
 High amplitude, low frequency continues parallel reflector.	Open marine/ open lake system. Possible transgressive shale.	?Holo-inner neritic (HIN) – Holo-middle neritic (HMN).	***Proposed*** *for interpretation update based on any new deep well(s).* *Data required: logs, core, BHI.* *Analysis required: Sedimentary analysis of logs, core and BHI, palyn/foram lithofacies, biostratigraphy study for facies and EOD interpretation. Additional biostrat study for stratigraphic age.*
 High to medium amplitude, medium to low frequency, mounded feature.	Open marine/ open lake system. Possible associated with slope deposits such as basin floor fan.	?HIN to HMN.	***Proposed*** *for interpretation update based on any new deep well(s).* *Data required: logs, core, BHI.* *Analysis required: Sedimentary analysis of logs, core and BHI, palyn/foram lithofacies, biostratigraphy study for facies and EOD interpretation. Additional biostrat study for stratigraphic age.*
Lacustrine Setting			
 High to medium amplitude, medium to low frequency, discontinues and occasionally wavy reflector.	Fluvial plain and alluvial fan, high mud flat.	?UCP. Alluvial lacustrine setting.	**Rabung-1** Data: GR/logs, Biostratigraphic study of Rabung-1 (PRSS_2006). **Sample Depth: 2680-2750m** Consistently abundance of `thick-walled' freshwater algae, *Bosedinia* and *Magnastriatites howardii*.
 Medium to low amplitude, medium frequency, sub-parallel reflector.	Fluvial plain of deltaic/ interdeltaic setting.	?UCP. Marginal lacustrine setting.	
 High to medium amplitude, low frequency, discontinues reflector.  High to medium amplitude, medium to low frequency, parallel continues reflector.	Fluvial plain and alluvial fan, high mud flat and lower deltaic plain. Open lake deposits.	?UCP. Alluvial lacustrine setting. ?UCP. Open lacustrine setting.	***Proposed*** *for interpretation update based on any new deep well(s).* *Data required: logs, core, BHI.* *Analysis required: Sedimentary analysis of logs, core and BHI, palyn/foram lithofacies, biostratigraphy study for facies and EOD interpretation. Additional biostrat study for stratigraphic age.*
 Poor data area due to fault shadow.	 Undetermined due to unclear reflector features.		

Tenggol Arch 2004 3D seismic data summary

Acquisition parameters:
Streamer length: 4.8km
Line interval: 75m
Tow length: 6m
Acquisition bin size: 6.25 x 18.75m
Source: Dual sleeves air gun (2000 psi)
Shooting interval: 18.75m
Tow depth: 5m
Sample interval: 2msec
Record length: 6sec
Instrument parameters:
Low cut filter: 2Hz 12db/oct
High cut filter: 206Hz 264db/oct

Pre-Stack Time Migration processing information:
1st velocity grid: 1km x 1km grid
2nd velocity grid: 50m x 500m grid
Final interpolated bin size: 12.5 x 9.375m
Sample interval: 2msec
Record length: 6sec
Low cut filter: 3Hz 18db/oct
Format: SEGY 32 bit floating point
Seismic wavelet: zero phase
Seismic polarity: Low to high density as maximum peak
Resolution: 15m at 1.8 second

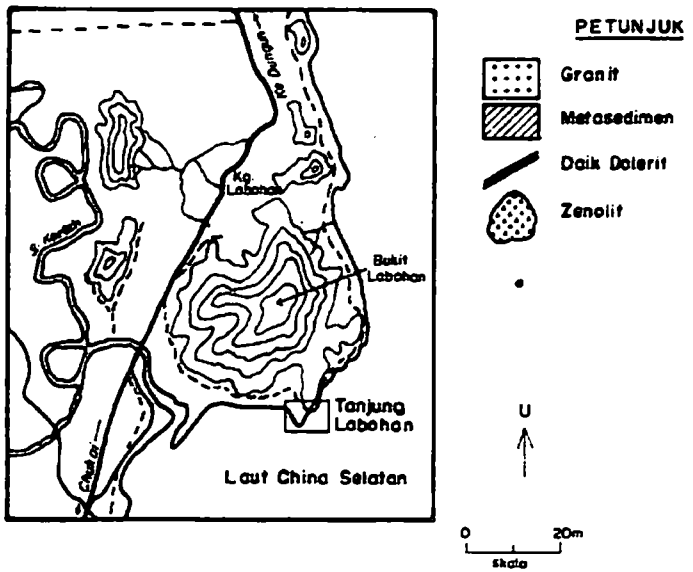

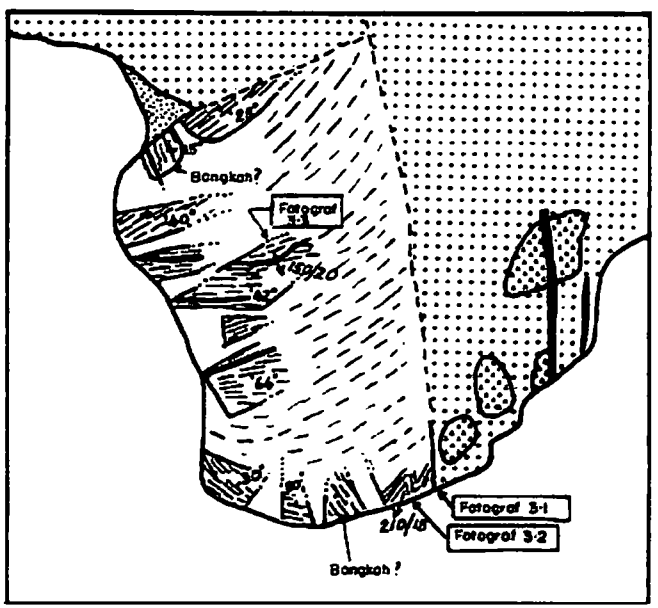

basementOnshore01

Bukit Labohan, a few kilometres South of the Kerteh petroleum complex consists mainly of granitoid in contact with relatively small patches of metasedimentary rocks of probably Carbo-Permian age. Some of the metasedimentary blocks are clearly xenoliths. Contact metamorphic features (hornfels, regular zoning) are present. Intrusions consist of late-plutonic pegmatite and aplite dykes, and post-plutonic dolerite dykes trending N-S and E-W.

These rock associations may be analogous to the basement at Malong-1.

The geology was mapped by Ramlee Abdul Rahman (1990, unpublished).

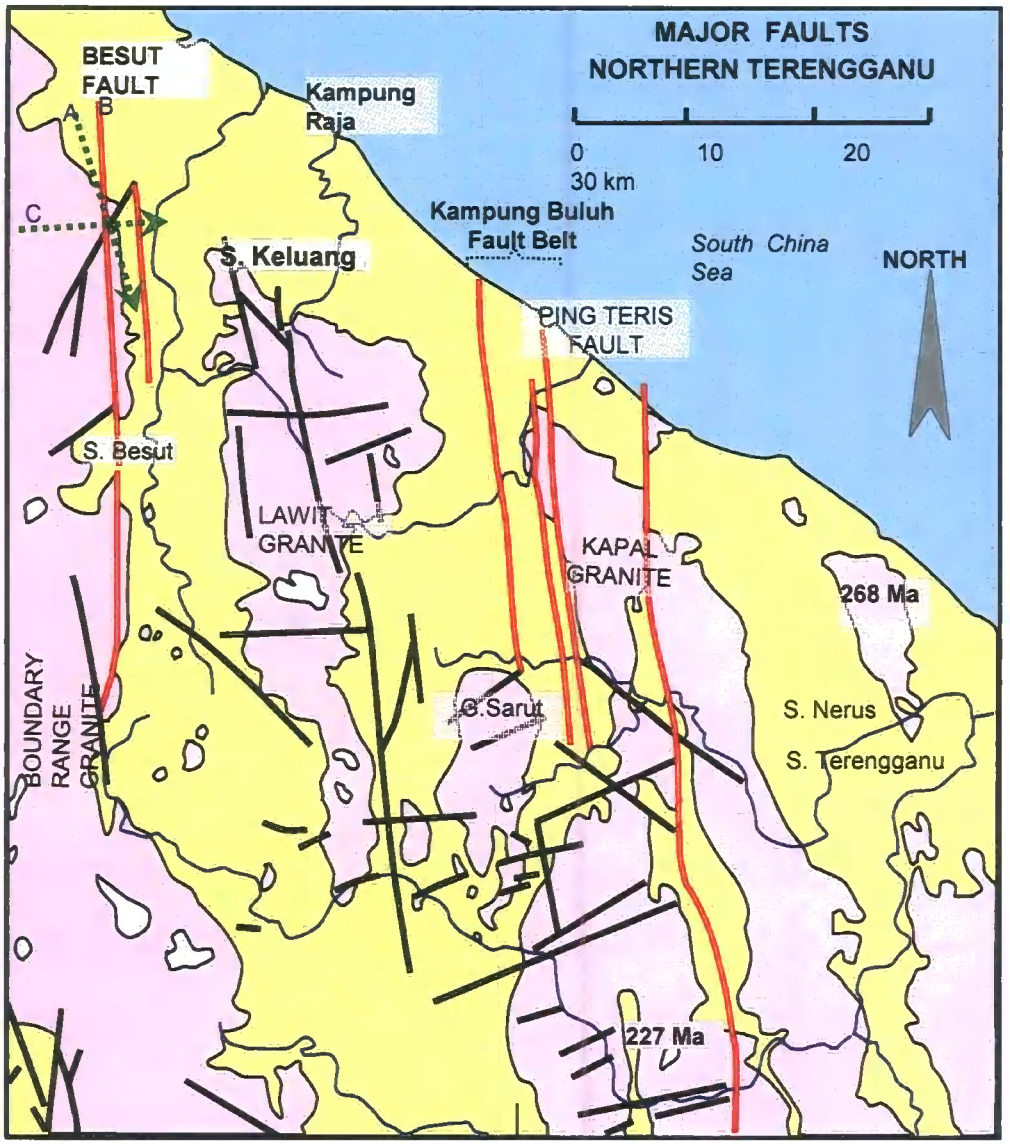

Integrated Regional Study of Malay Basin, PCSB (2005)

Major north-south trending Terengganu faults (Besut, Kampung Buluh Belt, Ping-Teris) extend into the northern Malay basin. 7b. A 25-m wide shear zone through the Boundary Range Granite at QMC quarry (person for scale).

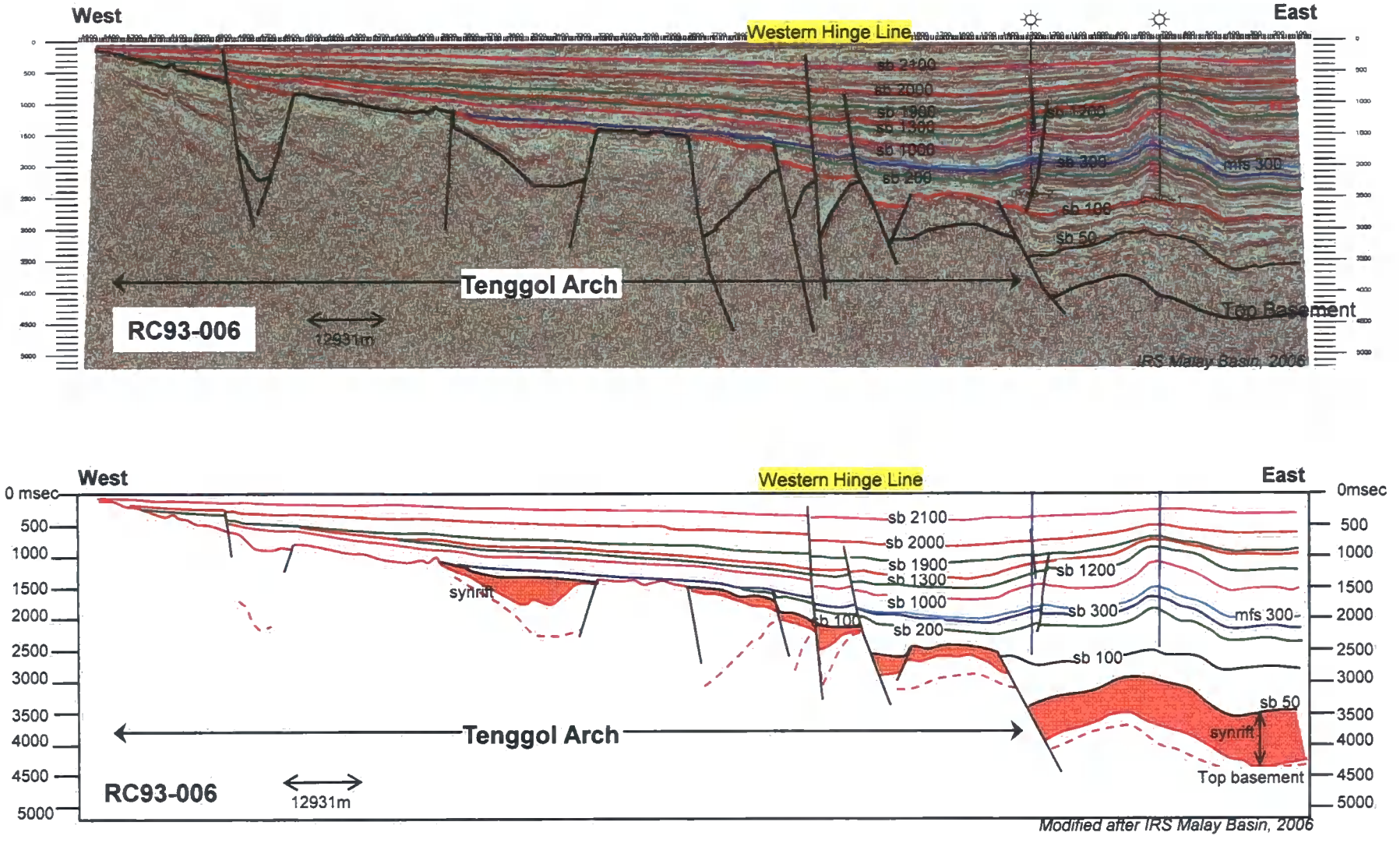

Regional 2D seismic line showing geo-seismic section across Tenggol Arch sb100 relation to top synrift marker on Tenggol Arch. Tertiary package wedging westward overlaying basement highs at western margin. Folding become more prevalent basinward (East).

Antracking parameters for basement section (A) and shallow section (B)

A

Dataset: 1) realized SEGY normalized amplitude (16 bit)

Vertical range: 1500ms to 3000ms (basement level)

Input dataset: 1) structure smoothed cube (8 bit)

2) variance cube (8 bit)

Output dataset: 1) basement Antracking cube (4bit)

Antracking method: Passive antracking

	Variables	Value
1	Initial Ant boundary	11
2	Ant track deviation	2
3	Ant step size	3
4	Illegal steps	2
5	Legal steps	2
6	Stop criteria (%)	10

B

Dataset: 1) realized SEGY normalized amplitude (16 bit)

Vertical range: 500ms to 1550ms (shallow level)

Input dataset: 1) structure smoothed cube (8 bit)

2) variance cube (8 bit)

Output dataset: 1) shallow Antracking cube (4bit)

Antracking method: Passive antracking

	Variables	Value
1	Initial Ant boundary	11
2	Ant track deviation	3
3	Ant step size	3
4	Illegal steps	2
5	Legal steps	2
6	Stop criteria (%)	10

Mesozoic			
Formation	**Age**	**Remarks**	**Reference**
(M14) Lanis conglomerate (Tembeling Group)	?Upper Jurassic to ?Lower Cretaceous	Lithology: conglomeratic sandstone, shale, siltsone with volcanic ash in some part.	Khoo (1975, 1977), Khoo (1983)
(M16) Termus Shale (Tembeling Group)	?Upper Jurassic to Cretaceous	Lithology: reddish shale/mustone, siltstone interbedded with sandstone.	Khoo (1975, 1977)
(M18) Badong conglomerate (Gagau formation)	?Jurassic	Lithology: Reddish conglomerate with subordinate sandstone, siltstone and shale.	Rishworth (1974), Khoo (1983)
(M19) Lotong sandstone (Gagau Group)	Upper Jurassic to Lower Cretaceous	Lithology: sandstone with subordinate volcanics and rare thin lenses of coal.	Rishworth (1974), Khoo (1983)
(M20) Tebak Formation	Upper Jurassic to Lower Cretaceous	Lithology: predominantly arenaceous rocks with minor siltstone and mudstone.	Rajah (1968), Khoo (1983)
Paleozoic (continued)			
(M1) Semanggol Formation	Lower Permian to Upper Triassic	Lithology: Chert, *Rhytmite* and conglomerate member (deep marine turbidite)	Alexander et. al. (1959), Burton (1973a), Kobayashi (1963b), Khoo (1983)
(P29) Belata Formation (P30) Kenny Hill Formation	Carboniferous to Permian	Lithology: argillaceous facies (basal strata) and arenaceous facies (upper strata) with thin chert beds in argillaceous facies. (P29) Sequence of phyllitic shale, mudstone and fine to medium grained sandstone. (30)	Gan (1992), Stauffer (1973), Abdullah Sani (1985)
(P2) Machincang Formation	Cambrian to Lower Ordovician	Sandstone, quartzite and subsidiary conglomerate, siltstone, shale, mudstone and acid tuff.	Jones (1961, 1981), Lee (1983), M. Shafeea Leman (1997)

Extracted from Stratigraphic Lexicon of Malaysia, Special Publication of GSM (2004), Lee C.P., M. Shafeea Leman, Kamaludin Hassan, Bahari Nasib and Rashidah Karim)

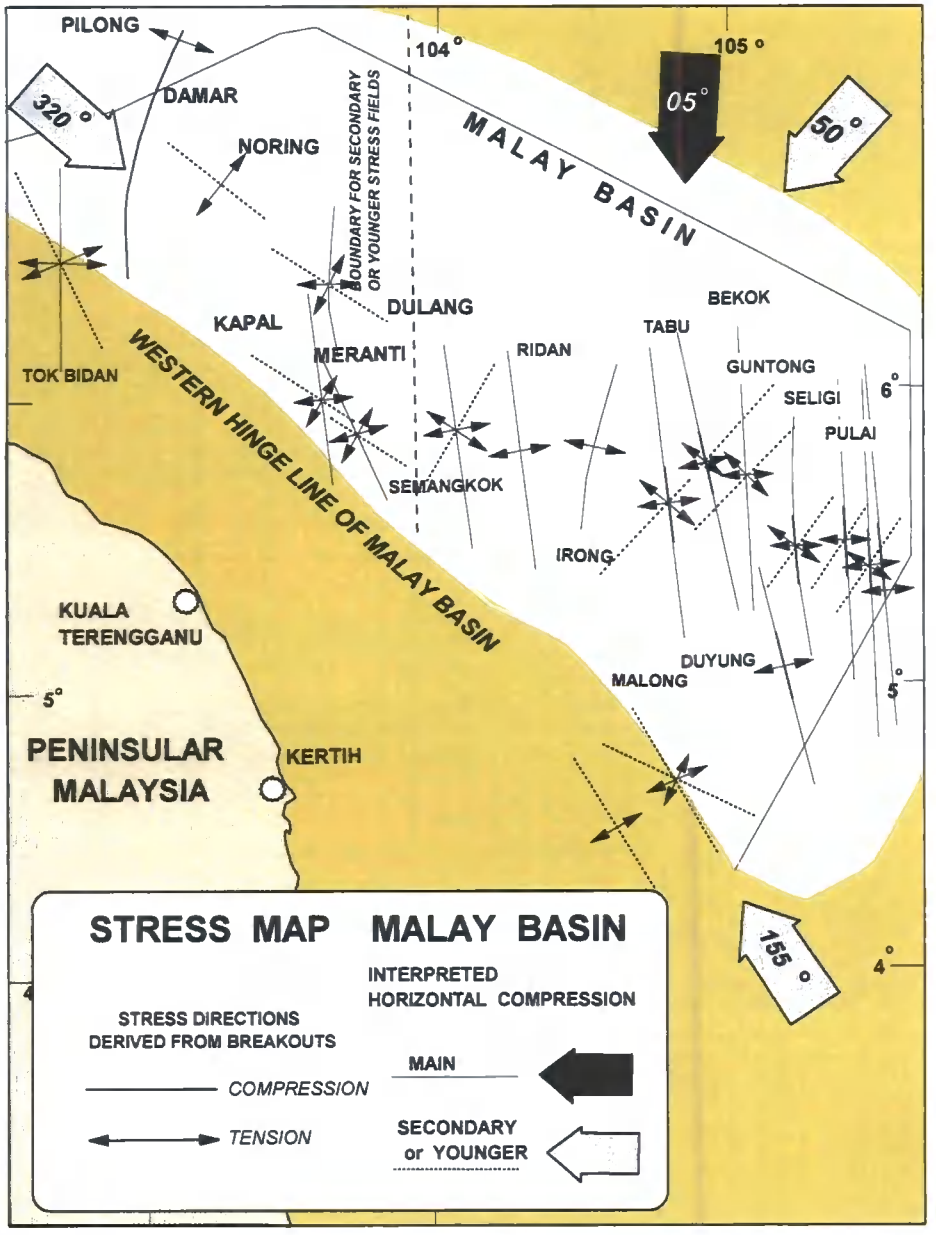

Well-bore breakout analysis

PCSB, 2005

- Primary horizontal compression operates within 05° - 050° sector.

- Potentially pre-existing faults controlled structure trends in NW and SE region (basement highs).

***Tjia & Idrus**, 1994*
*Tectonic implication of well-bore breakouts in Malaysia basins, GSM Bulletin **36**, Dec 1994: pp. 175-186*

Kuala Abang, Terengganu

Overturned to recumbent fold in interfoliated thicker schist and thinner phyllite. Details on the west side include incipient ball-and-pillow structures and flame injections. West vergence is indicated.

Interpretation is by Ibrahim Abdullah (2001)

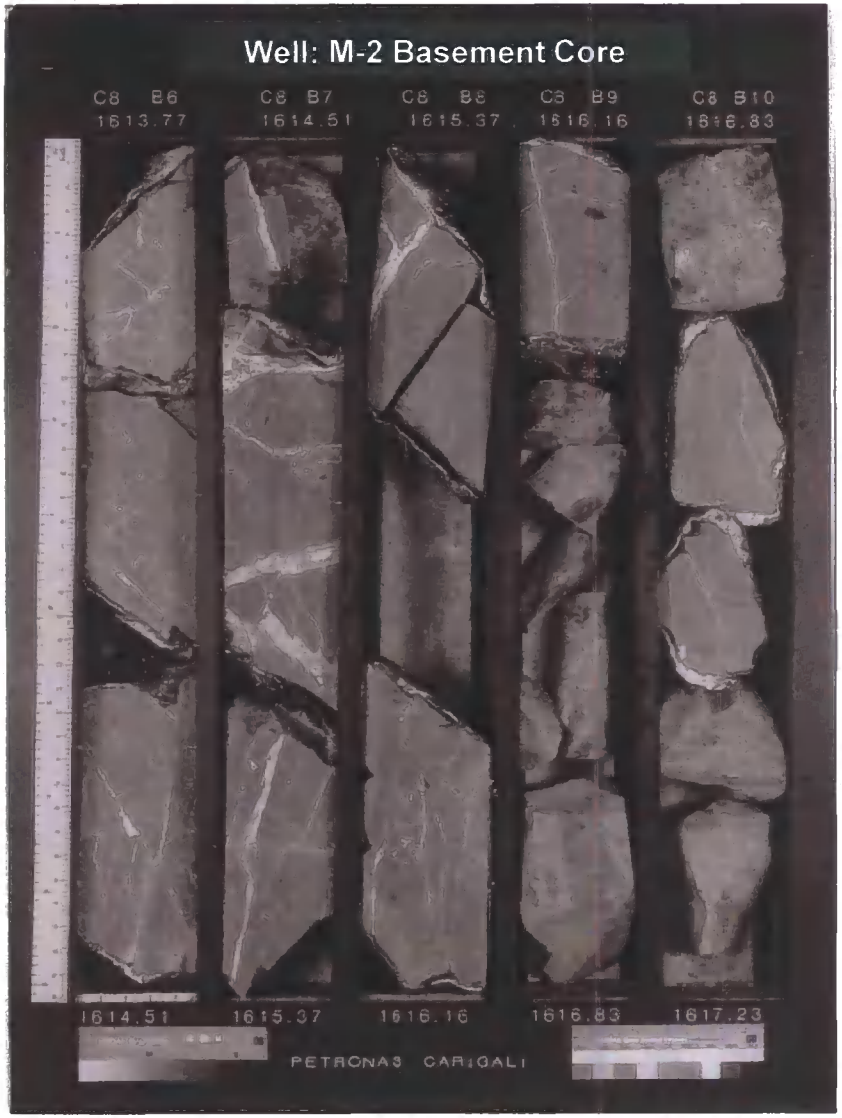

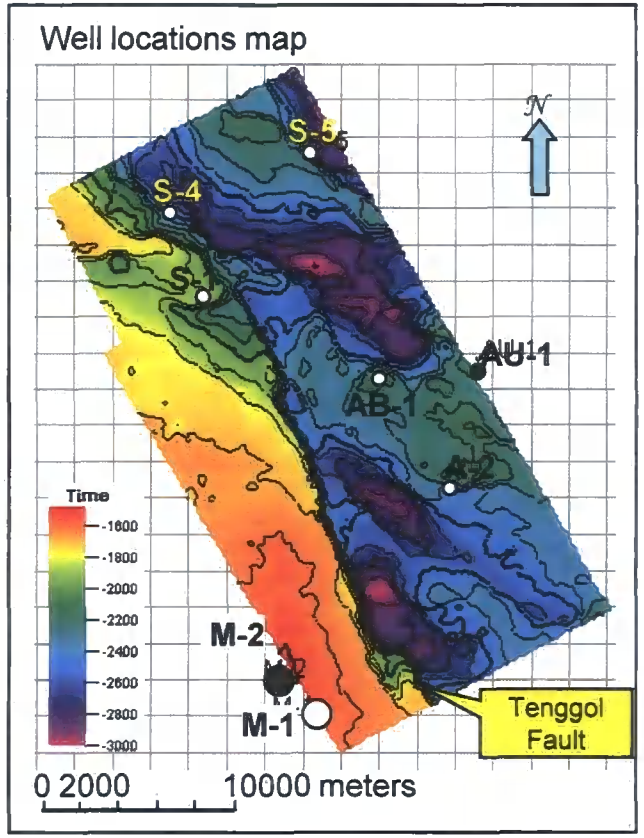

Bore-hole core from basement unit of M-2 well indicates dolerite to andesitic basement rock with present of calcite-filled fractures. Some oil show was reported in the basement of M-2 well however, main reservoirs are mostly in Miocene strata.

a) Late Miocene/Pliocene

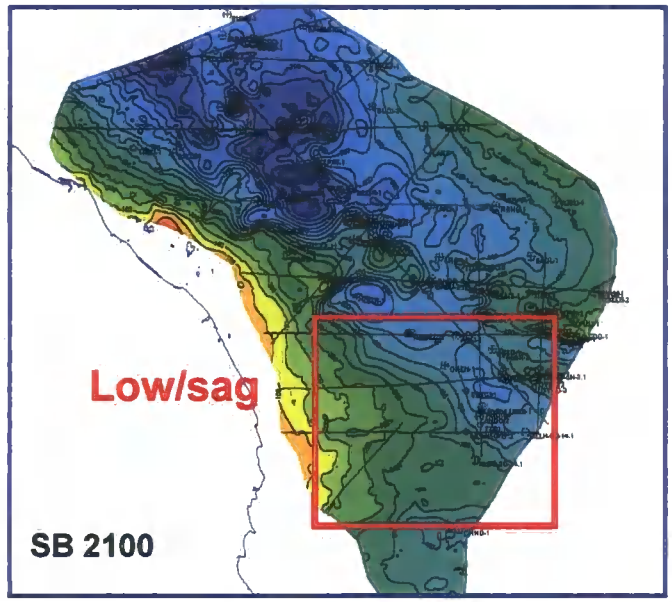

b) Middle Late Miocene

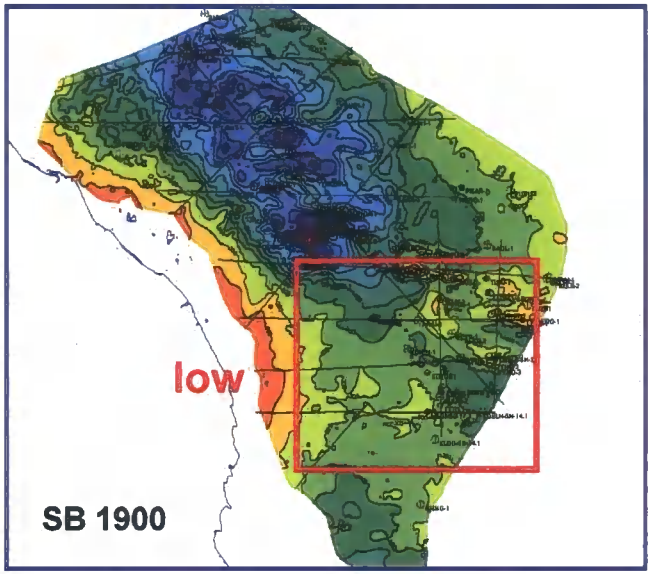

c) Middle Miocene

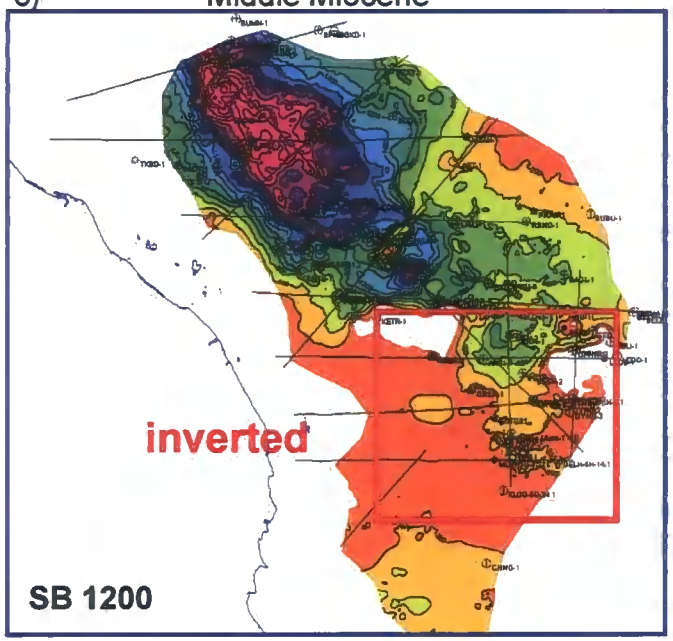

Isochore maps of Malay basin from Middle Miocene (SB1200) to Late Miocene/Pliocene (SB2100) show gradual changed in Malay Basin structure trend from relatively quiescence environment in Middle Miocene (SB1200) to East-West trending tight folds during Middle Late Miocene (SB1900). Folding in central basin is associated with transtension during Miocene-Pliocene time.

Integrated Regional Study of Malay Basin, PCSB, 2005

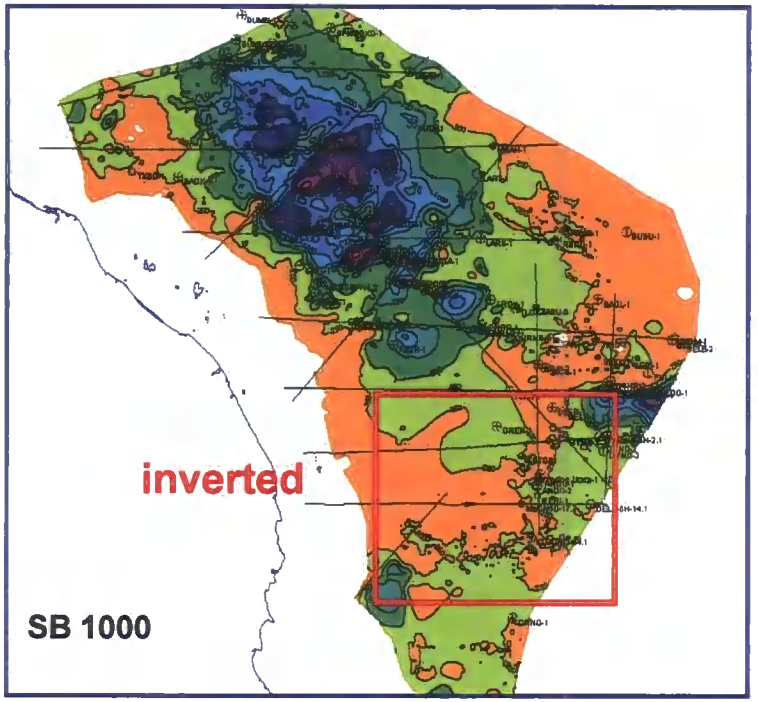

Isochore maps of Malay basin from SB200 (Early Miocene) to Sb1000 (middle Miocene). The maps indicate south margin of Malay Basin was a structure high in Early Miocene followed by widening of the basin. The basin depocentre has moved to the north margin in Middle Miocene, causing uplifting or inverted basement in the south margin of Malay Basin.

Integrated Regional Study of Malay Basin, PCSB, 2005

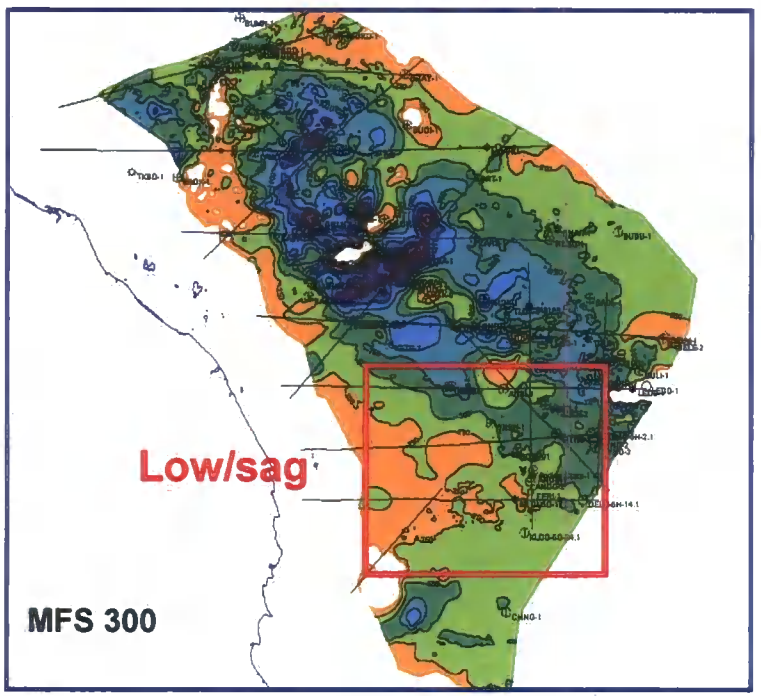

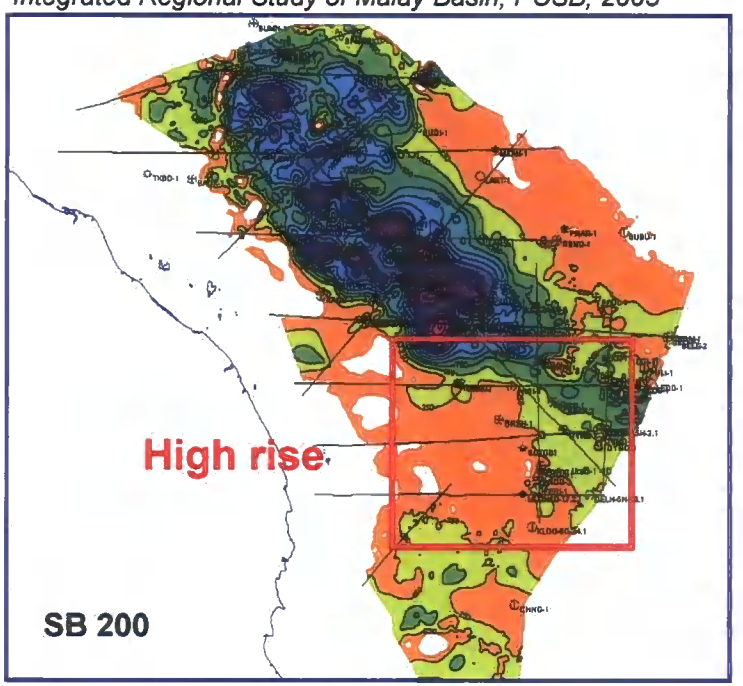

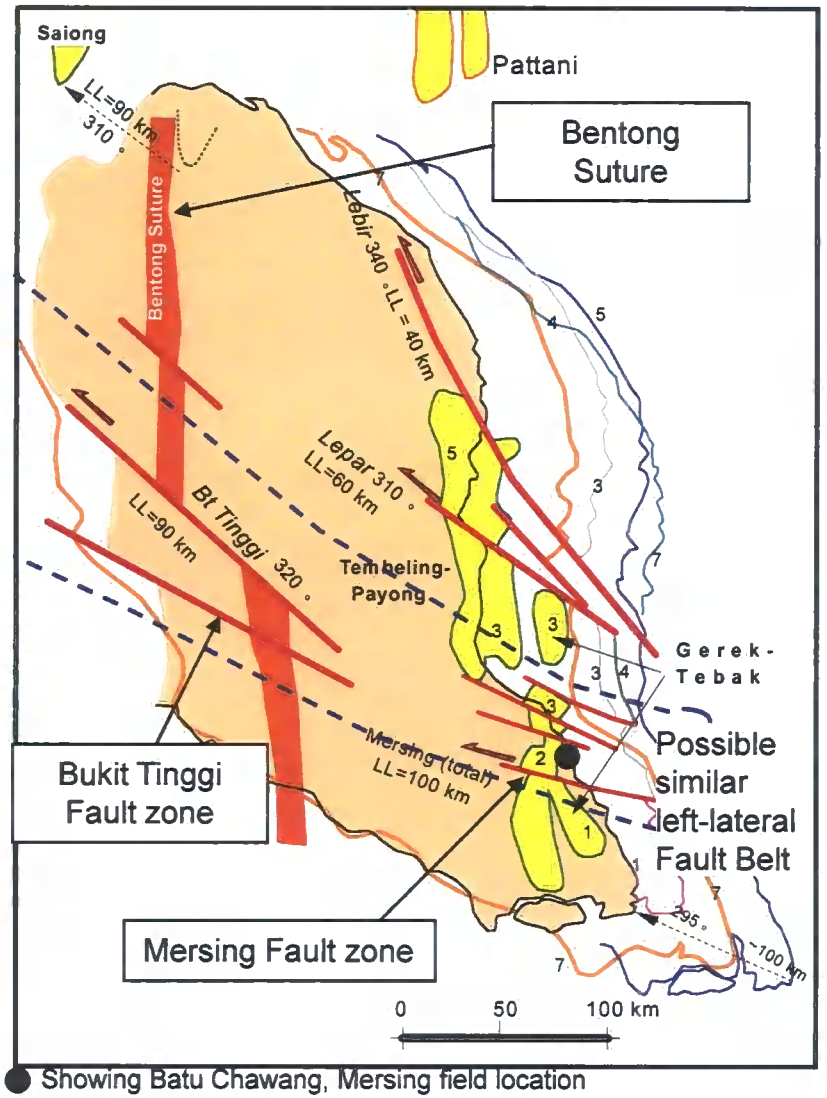

Schematic map of Peninsular Malaysia showing Post-Jurassic/Cretaceous displacement of Bentong Suture (brown polygon) and Tembeling Group (yellow polygon) reached 100 km along Northwest striking major faults.

Extended interpretation of left-lateral displacement along Mersing Fault zone was based on field observation at Batu Chawang, Mersing.

Batu Chawang, Fault showing Left lateral movement.

Appendix 15

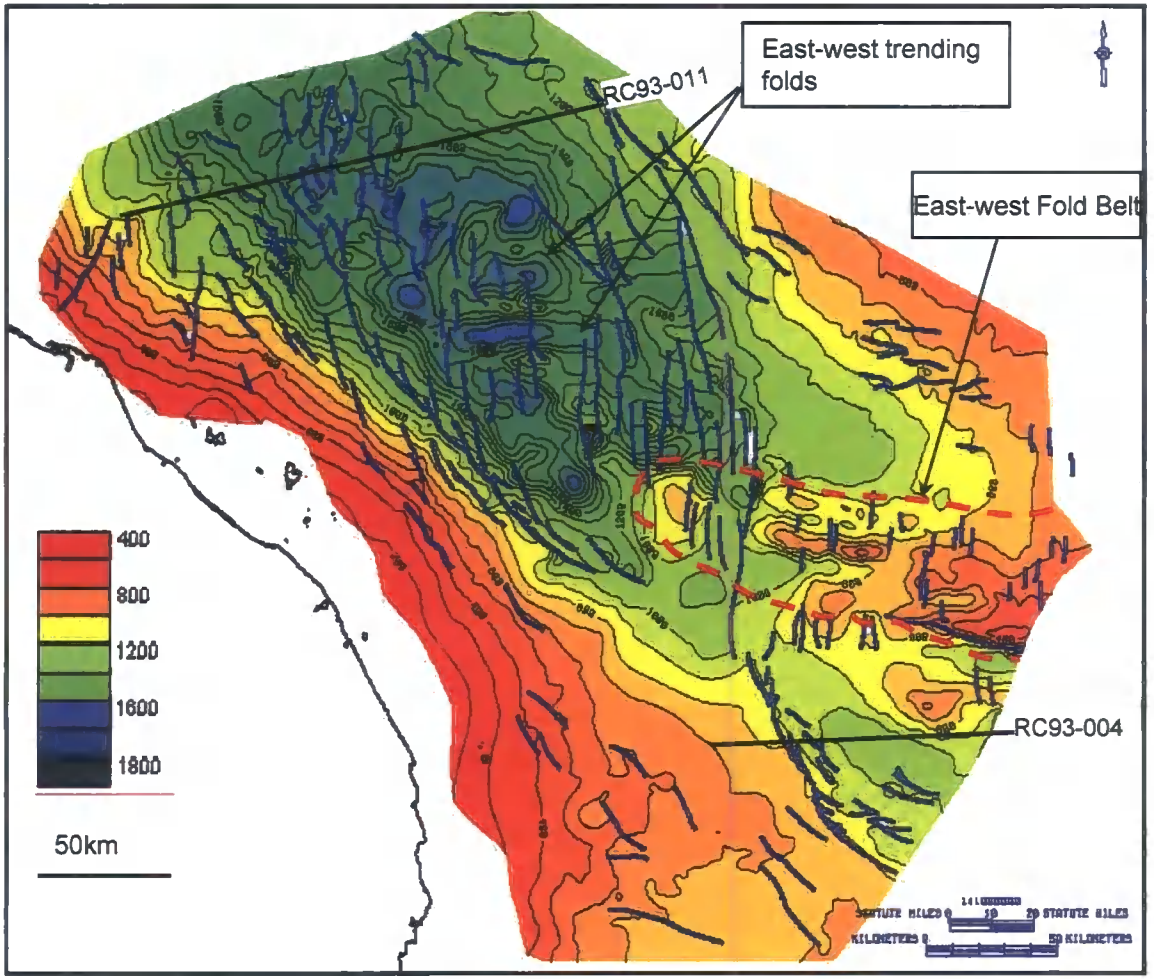

Depth Structure Map - SB1900

2D seismic Line	Marker	Age (IRS, 2005)	Percentage
RC93-004	sb2000	Late Miocene/Pliocene	0.2
	Sb1900	Middle Late Miocene	1.5
	Sb1200	Upper Early Miocene/Middle Miocene	2.5
RC93-011	sb2000	Late Miocene/Pliocene	0
	sb1900	Middle Late Miocene	1
	sb1800	Middle Miocene	0.7

Paleozoic			
Formation	**Age**	**Remarks**	**Reference**
(P32) Panching Lst (Kuantan Group)	Middle Carboniferous	Lithology: Massive, partly recrystallised, fossiliferous limestone	Metcalfe, Idris & Tan (1980)
(P34) Aring Formation	Upper Carboniferous to Lower Triassic	Lithology: Dolomite marble overlain by tuff and calcareous argillite, subordinate interbedded lavas of rhyolite to andesite composition.	Aw (1990)
(P35) Kepis beds	Lower Permian	Lithology: Reddish brown to purplish carbonaceous shales, siltsone, mudstone and rare red sandstone.	Khoo (1973), Loganathan (1993)
(P37) Chuping Lst	Lower Permian to Middle or Upper Triassic	Lithology: Massive, pale colored finely crystalline, pure calcite limestone, fossiliferous and dark grey with chert nodules in basal formation.	Jones (1973, 1981)
(P39) Dohol Formation	Middle Permian	Lithology: Grey carbonaceous shale, siltstone, slate, phyllite and schist. Minor beds of arenite, limestone and volcanics.	Rajah (1986)
(P40) Sri Jaya beds	Upper Middle to Lower Upper Permian	Lithology: pelitic hornfels, slate, metatuff and metasiltstone (Jempul Slate, P40.1), massively bedded and strongly jointed basal marble (Mengapur Lst, P40.2)	Lee (1990)
(P40.1.1) Luit tuffs (Jempul slates)	Permian	Lithology: metavolcanic, mainly crystal-vitric rhyolitic metatuff.	Lee (1990)
(P41) Sedili volcanic	Upper Middle Permian to Middle Triassic	Lithology: Ignimbrite, tuff, agglomerate, lava and volcanic ash varying in composition from rhyolite to rhyodacite and andesite.	Rajah (1986)
(P42) Linggui Formation	Upper Permian	Lithology: Bedded grey carbonaceous shale and sandstone with coglomerate beds.	Rajah (1986)

Extracted from Stratigraphic Lexicon of Malaysia, Special Publication of GSM (2004), Lee C.P., M. Shafeea Leman, Kamaludin Hassan, Bahari Nasib and Rashidah Karim)

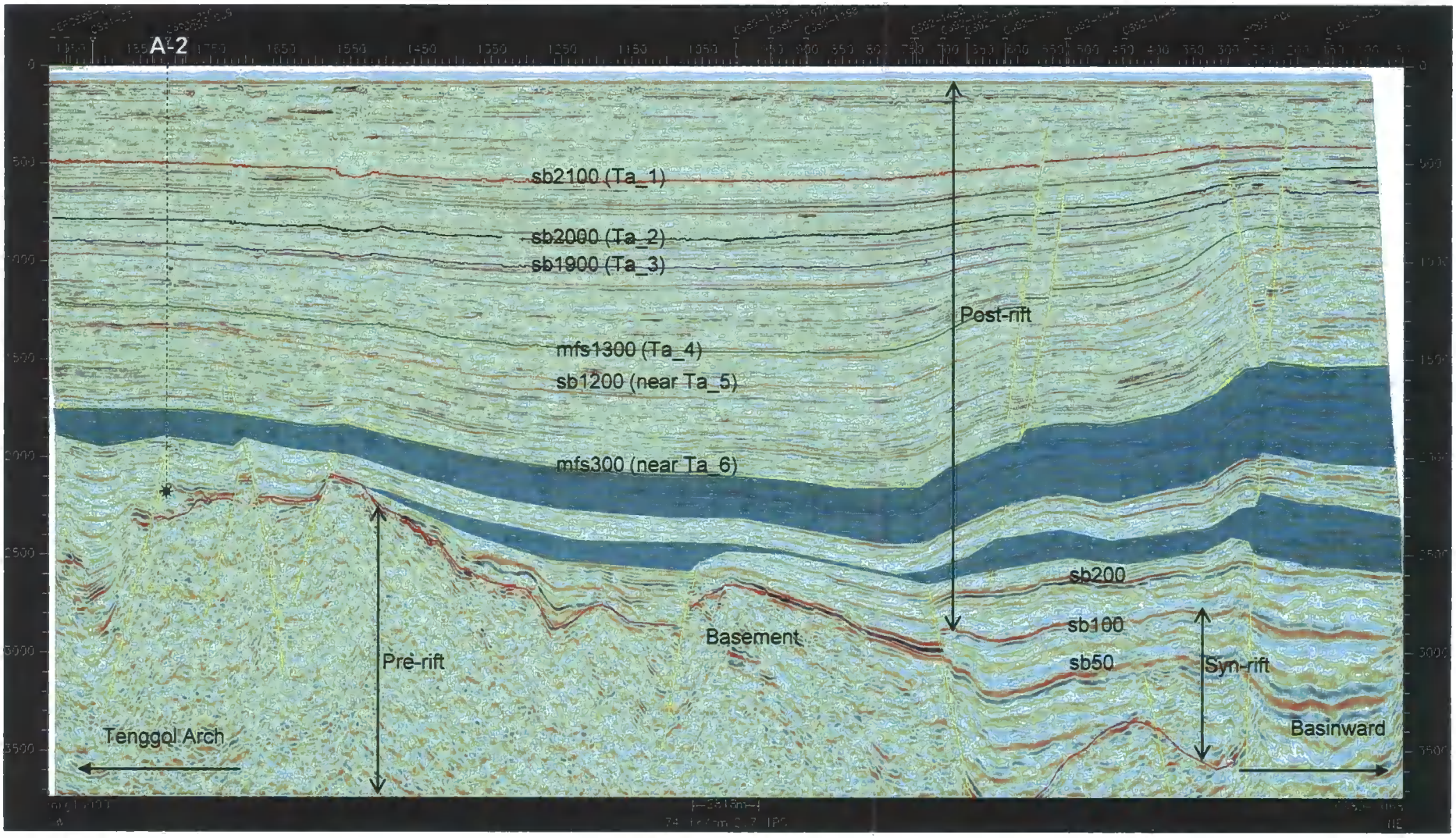

2D Seismic section running SW-NE from edge of Tenggol Arch towards basin centre illustrates the mfs300 and mfs200 shale sequence (shaded green) thickening towards basin centre may provide detachment-like surface that promotes variation in fault pattern and fault dip direction in sequence below (top basement- sb200) from sequence above (sb200-sb2100). (*Seismic data, interpretation and markers from PETRONAS, IRS Malay Basin (2006b)*).